Path Integrals for Optically Driven Quantum Dots: State Preparation Protocols and Combination of Hamiltonian and non-Hamiltonian Dynamics

Von der Universität Bayreuth
zur Erlangung des Grades eines
Doktors der Naturwissenschaften (Dr. rer. nat.)
genehmigte Abhandlung

von

Andreas Barth

geboren in Kirchheimbolanden

Path Integrals for Optically Driven Quantum Dots: State Preparation Protocols and Combination of Hamiltonian and non-Hamiltonian Dynamics

Von der Universität Bayreuth
zur Erlangung des Grades eines
Doktors der Naturwissenschaften (Dr. rer. nat.)
genehmigte Abhandlung

von

Andreas Barth

geboren in Kirchheimbolanden

1. Gutachter: Prof. Dr. V. M. Axt
2. Gutachter: Prof. Dr. S. Kümmel

Tag der Einreichung: 25. Oktober 2016
Tag des Kolloquiums: 15. September 2017

Abstract

Semiconductor quantum dots exhibit many advantageous properties that are highly valued in atomic quantum optics, but in contrast to atoms they can also be easily integrated in solid state devices. This makes these nanostructures very attractive for numerous applications in quantum information processing, quantum cryptography and for the realization of innovative photon sources. The interaction with light is fundamental for almost all these technologies, and thus the diverse characteristics of optically driven quantum dots are nowadays studied across many topical fields of research.

A major challenge from a theoretical point of view is a correct treatment of the coupling of quantum dots to their solid-state environment, which can have a pronounced impact on the driven system dynamics. Of particular importance is the interaction with lattice vibrations of the surrounding semiconductor crystal, because it is always present and often leads to a severe reduction of the maximal available coherence times. This cumulative thesis contributes to the active discussion of the impact of phonons on the dynamics of optically driven quantum dots. More specifically, it deals with an elaborate real-time path-integral method that allows for numerically exact simulations of the system evolution under the influence of the pure dephasing coupling to longitudinal acoustic phonons. As a prominent result, the existing path-integral approach is generalized to account homogeneously for both Hamiltonian and non-Hamiltonian dynamics, making it possible to calculate the effects of both the phonon coupling and additional processes that can be sufficiently described by phenomenological rates. This is an important methodological advancement, parts of which can potentially be carried over to related systems where similar techniques are being used. The generalization of the method removes a significant previous limitation, because on the one hand a number of relevant dissipative processes, like the radiative decay of excited quantum dot states or photon losses of coupled quantum dot cavity systems, could previously not be dealt with when using the path-integral method. On the other hand, many alternative techniques that are able to deal with these processes rely on approximations for either the optical coupling or the phonon interaction and are thus valid only to a limited extent. The extended path-integral formalism presented here combines the exact treatment of the non-Markovian multi-particle phonon coupling of optically driven quantum dots with the flexibility of adding phenomenological dissipation as it is given for example in many master equation approaches. Moreover, this thesis introduces a crucial technical optimization of the method that makes it possible to apply the path-integral approach to situations, like the radiative biexciton cascade, that previously were thought of being inaccessible due to their large numerical cost.

As an important application of the path-integral simulations, this thesis also discusses optical excitation protocols that are targeted at the controlled manipulation of the quantum dot states, which is a necessary prerequisite for many quantum dot based devices. To this end, the discussion first focuses on quantum dot state preparation using adiabatic rapid passage protocols. It is analyzed how the acoustic phonon interaction affects the quality of the preparation and advantages and disadvantages of different excitation schemes targeted at the creation of the biexciton state using frequency-swept picosecond laser pulses are discussed. The second possibility of state preparation that is studied extensively is fundamentally different to previous protocols, as it makes active use of the carrier-phonon interaction and performs the better the stronger the phonon coupling is. This phonon-assisted preparation method is first investigated theoretically and very promising protocols offering a robust, high-fidelity, and fast preparation of both the exciton and biexciton states are proposed. The discussion includes the experimental verification of the proposed schemes using extensive experimental data provided by collaborating groups. In these studies it is explicitly shown that the phonon-assisted preparation of the quantum dot states can be achieved using pulsed laser excitation and a very close agreement between the theory and experimental observations is achieved. Importantly, this exact comparison also allows making general conclusions about the nature of the exciton-phonon coupling with a higher accuracy than it was possible before. The underlying dynamics of the phonon-assisted state preparation is theoretically studied in detail and is found to be best analyzed using the picture of the laser dressed states. It is shown that the preparation process is not only dominated by the phonon-induced relaxation between the dressed states, but that a crucial role can be also attributed to the character of the switch-off phase of the applied laser pulses. The importance of this adiabatic undressing process becomes most obvious when varying the shape of the laser pulse and it is demonstrated that the fidelity of the preparation can be unfavorably reduced when using, e.g., rectangular pulse shapes. This analysis is also extended to the possible case of negative biexciton binding energies and it is analyzed how the target state of the phonon-assisted preparation can be selected by varying the laser energy, the biexciton binding energy and the pulse length. In another study about the phonon-assisted state preparation, the depopulation of an excited quantum state by phonon-induced processes is demonstrated both theoretically and by using photo current measurements provided by experimental collaborators. It is also shown, that by using alternating blue- and red-shifted pulses the quantum dot exciton can be switched on and off making use of the dynamic nature of the phonon coupling, which becomes enhanced by raising the optical excitation intensity.

Finally, this thesis contributes to the topical discussion of QD-microcavity systems in the strong coupling regime. As a main result, it is shown by comparing theoretical simulations with provided experimental data that, despite the detrimental effects of the phonon interaction, strong QD-cavity coupling at increased temperatures can be achieved using QDs which hold the special property of a temperature-dependent light-matter coupling strength.

Kurzfassung

Halbleiter-Quantenpunkte verkörpern zahlreiche positive Eigenschaften, die sich in der Quantenoptik von Atomen als sehr nützlich erwiesen haben, lassen sich darüber hinaus jedoch auch äußerst gut in Festkörper-basierte technologische Anwendungen integrieren. Diese Nanostrukturen eignen sich daher äußerst gut für zahlreiche Einsatzmöglichkeiten in der Quanteninformationsverarbeitung, der Quantenkryptographie und für die Realisierung neuartiger Lichtquellen. Bei so gut wie allen dieser Technologien ist die Wechselwirkung mit Licht von zentraler Bedeutung, weshalb die vielfältigen Eigenschaften von optisch getriebenen Quantenpunkten heutzutage in mehreren hochaktuellen Forschungsgebieten studiert werden.

Eine der größten Herausforderungen aus theoretischer Sicht ist die korrekte Behandlung der Kopplung von Quantenpunkten an ihre Festkörperumgebung, die einen stark ausgeprägten Einfluss auf die getriebene Systemdynamik haben kann. Von spezieller Bedeutung sind hierbei Wechselwirkungen mit den Gitterschwingungen des umgebenden Halbleiterkristalls, da diese immer auftreten und häufig zu einer starken Beschränkung der maximal möglichen Kohärenzzeiten führt. Die vorliegende kumulative Dissertation liefert einen weiteren Beitrag zur aktuellen Diskussion des Phononeinflusses auf die getriebene Quantenpunktdynamik. Im engeren Sinne wird eine aufwändig ausgearbeitete Echtzeit-Pfadintegralmethode, die eine numerisch exakte Simulation der getriebenen Quantenpunktdynamik unter Einflussnahme der rein dephasierenden Kopplung an longitudinal akustische Phononen ermöglicht, weiter erforscht. Als eines der Hauptresultate dieser Arbeit wird der bestehende Pfadintegralzugang so verallgemeinert, dass eine homogene Behandlung von Hamiltonscher und nicht-Hamiltonscher Dynamik ermöglicht wird. Dadurch können die Effekte der Phononkopplung und zusätzliche Prozesse, die in ausreichender Weise durch phänomenologische Ratengleichungen beschrieben werden können, simultan berücksichtigt werden. Dies stellt einen erheblichen methodischen Fortschritt dar, der teilweise auch auf verwandte Systeme, die mit ähnlichen Methoden behandelt werden, übertragbar ist. Die hier gefundene Verallgemeinerung behebt eine starke bestehende Einschränkung der Anwendbarkeit der Methode, da einerseits eine Vielzahl von wichtigen dissipativen Vorgängen, wie z.B. der strahlende Zerfall angeregter Quantenpunktzustände oder Photonverluste gekoppelter Quantenpunkt-Mikroresonator Systeme, bisher nicht mit der Pfadintegralmethode behandelt werden konnten. Andererseits beruhen viele alternative Simulationstechniken, die diese Prozesse einschließen könnten, auf Näherungen der optischen Kopplung oder der Wechselwirkung mit der Phononumgebung und sind daher nur in beschränkten Parameterbereichen gültig. Der hier vorgestellte erweiterte Pfadintegralformalismus vereint die exakte Behandlung der nicht-Markovschen Vielteilchen-Phononkopplung optisch getriebener Quanten-

punkte mit der Möglichkeit phänomenologische Dissipation einzubeziehen, wie es z.B. in vielen Mastergleichungszugängen gegeben ist. Darüber hinaus wird in dieser Arbeit eine technische Optimierung der Pfadintegralmethode vorgestellt, die es ermöglicht den Zugang in Situationen anzuwenden, die aufgrund des hohen numerischen Aufwands bisher noch nicht im Pfadintegralformalismus behandelt werden konnten. Ein wichtiges Beispiel hierfür ist unter anderem die Simulation der strahlenden Quantenpunkt-Biexzitonkaskade.

Eine zentrale Anwendung des Pfadintegralformalismus, die in der vorliegenden Arbeit ausführlich diskutiert wird, liegt in der Analyse von optischen Anregungsprotokollen zur kontrollierten Manipulation des Quantenpunktzustands, die für viele Quantenpunkt-basierte Anwendungen notwendig sind. Diesbezüglich wird zunächst die Präparation des Quantenpunktzustands mittels adiabatisch geführter Dynamik studiert. Dabei wird untersucht welchen Einfluss die Wechselwirkung eines Quantenpunktes mit akustischen Phononen auf die Qualität der Präparation haben kann. Hierbei werden die Vor- und Nachteile verschiedener Anregungsschemata, die auf die Erzeugung des Biexzitonzustands mit Hilfe von pikosekundenlangen Laserpulsen mit zeitabhängiger Frequenzmodulation abzielen, herausgearbeitet. Die zweite Möglichkeit der Zustandspräparation, die im Detail diskutiert wird, unterscheidet sich in grundlegender Weise von bisherigen Protokollen, da die Ladungsträger-Phononkopplung hierbei aktiv ausgenutzt wird und die Qualität der Präparation mit der Stärke der Phonokopplung steigt. Diese sogenannte Phonon-assistierte Methode wird zuerst rein theoretisch untersucht, wobei sehr vielversprechende Schemata, die eine robuste, höchst effiziente und schnelle Präparation der Exzitonzustände und des Biexzitonzustands erlauben, vorgeschlagen werden. Die Diskussion schließt auch die experimentelle Bestätigung dieser Protokolle mit ein, die anhand von umfangreichen von kollaborierenden Gruppen zur Verfügung gestellten Messungen erfolgt. In diesen Studien wird explizit der experimentelle Beweis erbracht, dass eine Phonon-assistierte Präparation des Quantenpunktzustands durch gepulste Laseranregung möglich ist und dass die theoretischen Vorhersagen sehr genau mit den gemessenen Daten übereinstimmen. Ein wichtiger Aspekt dieser genauen Vergleiche zwischen Theorie und Experiment ist auch, dass sie erlauben allgemeine Aussagen über die Natur der Exziton-Phononkopplung in Quantenpunkten in einer Form zu treffen wie es anhand bisheriger Messungen nicht möglich war. Die zugrundelegende Dynamik der Phonon-assistierten Präparation wird ebenfalls im Detail studiert, wobei sich herausstellt, dass diese am besten im Bild der bekleideten Zustände interpretiert werden kann. Es wird gezeigt, dass der Präparationsprozess nicht nur von der viel diskutierten Phonon-induzierten Relaxation zwischen den bekleideten Zuständen bestimmt wird, sondern dass auch der Abschaltvorgang des verwendeten Laserpulses eine wichtige Rolle spielt. Die Bedeutung des Auftretens eines adiabatischen Entkleidungsprozesses wird am besten ersichtlich indem die Pulsform des Lasers variiert wird und es stellt sich heraus, dass sich die Genauigkeit der Präparation deutlich verschlechtern kann, wenn die Pulse sich z.B. einer Rechtecksform nähern. Die Analyse der Phonon-assistierten Präparationsmethode wird ebenfalls auf den möglichen Fall einer negativen Biexzitonbindungsenergie ausgeweitet und es wird untersucht wie der Zielzustand durch eine Variation der Laserenergie, der Biexzitonbindungsenergie und der Pulslänge selektiert werden kann. In einer weiteren Studie wird die Abregung eines vorher präparierten Exzitonzustands durch Phonon-induzierte Prozesse anhand von theoretischen Simulationen

und experimentellen Photostrommessungen, die von einer kollaborierenden Gruppe zur Verfügung gestellt wurden, demonstriert. Es wird auch gezeigt, dass durch die Verwendung von abwechselnden blau- und rot-verschobenen Pulsen ein An- und Abregen des Exzitonzustandes möglich ist und dass die Phonon-assistierte Präparation stark mit der dynamischen Natur der Phononkopplung, die durch die Intensität der optischen Anregung verstärkt werden kann, verknüpft ist.

Schließlich trägt diese Dissertationsschrift auch zur aktuellen Diskussion der starken Kopplung in Quantenpunkt-Mikroresonator Systemen bei. Als eines der Hauptergebnisse wird hierbei durch einen weiteren Vergleich simulierter Ergebnisse mit zur Verfügung gestellten experimentellen Daten gezeigt, dass eine starke Kopplung trotz der schädlich wirkenden Phononeinflüsse auch bei erhöhten Temperaturen auftreten kann. Dies setzt voraus, dass die verwendeten Quantenpunkte die spezielle Eigenschaft einer temperaturabhängigen Licht-Materie Kopplungsstärke aufweisen.

Contents

Part I

Introduction

1 Motivation

Quantum dots (QDs) [1–4] are nanometer sized manufactured structures in semiconductors that confine electrons and holes in all spatial directions. The restricted carrier mobility gives rise to a discrete energy spectrum, that, in principle, can be controlled by the details of the fabrication method. This opportunity to artificially create quantum systems with an atom-like energetic structure embedded in a solid state environment makes QDs highly useful for the development of numerous innovations in technology and continues to inspire active research into the fascinating properties of these special systems.

With respect to technological applications, QDs are for example proposed candidates for the implementation of qubits [5–9]. Qubits are the basic units of information in quantum computation [10, 11], which holds out the prospect of, e.g., very efficient data searches [12]. There are many more systems that are being discussed as possible qubits, like ions trapped in electromagnetic fields [13] or isolated electron spins associated with the nitrogen vacancy center in diamond [14], but so far it remains unclear which of these systems will be best suited to fulfill the difficult requirements for constructing a quantum computer [15]. Furthermore, the optical transitions between the discrete QD states can be exploited to realize triggered sources of single photons [16–22] and entangled photon pairs [23–29], which are also highly useful for quantum information processing [30] and are needed for quantum cryptography [31, 32]. Additional possible uses of QDs can be found, e.g., in the topical fields of nano lasers [33–35], display technology [36] and even in medical research, where QDs are used as biological markers [37, 38].

In the majority of these and other technological applications a detailed knowledge of the *optically driven* behavior of a single QD is required. QDs are thus typically studied under external excitation by a laser field or in terms of a coupling to quantized field modes of a surrounding optical cavity. An important result of these studies is the experimental verification of a resonant coherent response that manifests itself in, e.g., Rabi oscillations between the QD levels [39–42] or an anti-crossing of the dispersion relations of the cavity mode and an excited QD state [43, 44]. For a profound understanding of the QD dynamics and the influence of different system properties and excitation conditions it is also highly desirable to find a functional theoretical description of these systems. In this respect, simulations of the time-dependent evolution of the QD state allow deep insights into the complex dynamics of QDs and can be used to explain and predict experimental observations. This thesis focuses on both the theoretical calculation of the driven QD dynamics and the comparison with experimental data.

An important difference between atoms and QDs, that are often seen as artificial

counterparts of atoms, is that QDs are intrinsically affected by their solid state surrounding and thus can often not be treated as isolated systems. On the one hand, such environmental interactions lead to a dephasing of the QD states and can spoil any kind of coherent dynamics that many applications rely on. On the other hand, such dissipative processes in QDs can also provide a fantastic opportunity to study fundamental aspects of open quantum systems [45, 46], and in some rare cases can even be of direct practical use [47–49], which we shall also see here. For strongly confined QDs, as they are discussed in this thesis, a major contribution to the environment coupling is given by the interaction with lattice vibrations of the semiconductor crystal, i.e. acoustic phonons. Amongst many other effects, the phonon coupling can lead to a damping of resonantly driven Rabi oscillations [50, 51] or an enhanced QD-cavity coupling for cavities that are detuned from the QD transition [52]. Further dissipative processes that can play an important role include the radiative decay of excited QD states, which is due to a coupling to external electromagnetic field modes [53], or tunneling effects, where electrons and holes are absorbed by an external voltage [41].

Calculating the driven QD dynamics under the influence of environmental interactions is generally not an easy task. This is especially true when the important pure dephasing coupling to acoustic phonons [54, 55] is considered. An exact modeling of this coupling involves a microscopic treatment of an infinite number of phonon modes and due to the non-Markovian nature of this coupling it cannot be fully captured by rate descriptions. Typically, such an interacting many-particle system [56] is not exactly solvable and instead can only be dealt with by using approximative methods. However, for a certain class of system-bath type models it has been found that despite this complexity the dynamics can be calculated in a numerically exact way using an elaborate real-time path-integral method [57, 58]. This elegant and highly practical approach takes into account the influence of the surrounding via so called influence functionals [59] and yields the dynamics in terms of a reduced system where the environmental degrees of freedom have been traced out. The method has also been successfully applied to account for the phonon coupling of optically driven QDs [50, 60, 61] and, notably, does not require further approximations to the model commonly used for these systems.

So far, a major drawback of the path-integral method for QDs has been that it did not allow for a homogenous inclusion of any kind of non-Hamiltonian contributions to the equations of motion. Most importantly, this prohibited a phenomenological treatment of additional interactions between the QD and the environment, except in a very restricted border case [62]. This is problematic, because many of the environmental couplings, like the radiative decay, are very hard to include in a strictly Hamiltonian way. Therefore, in practice the path-integral approach has been mostly limited to account only for the phonon coupling and so far could not be used to deal with any other relaxation processes relevant for QDs in many important situations. This stands in sharp contrast to many other methods like, e.g., master equation approaches [63], where environmental effects that can be sufficiently described by simple rate equations can be easily incorporated next to the phonon coupling. One of the most important achievements of this thesis is a reformulation of the path-integral approach that lifts this restriction and thus drastically extends the range of applicability of the method. The modification makes it possible to calculate the driven QD dynamics under the combined

influence of the phonon coupling and other relaxation processes without restricting the accessible parameter range and thus allows for very detailed theoretical studies and a close comparison with corresponding experiments.

Besides the new possibility to combine Hamiltonian and non-Hamiltonian dynamics when using the path-integral approach, another important accomplishment of this thesis is a technical optimization of the method that under certain conditions makes it possible to deal with systems that are considerably larger than the maximum of four electronic levels that previously could be dealt with [64, 65]. An important class of systems that fulfill these conditions are QDs coupled to quantized cavity modes, where many product states between the QD levels and the Fock states of the cavity mode need to be considered. It is assumed that this technical advancement will pave the way for a complete microscopic investigation of the influence of the phonon coupling on systems that previously have been out of reach when using the path-integral approach. The most prominent example, which is also briefly discussed in this thesis, is the biexciton decay cascade of a QD that is most interesting due to the possible creation of polarization entangled photon pairs.

Many QD-based devices rely on a specific manipulation of QD states, which is often achieved by pulsed laser excitation. The different optical control protocols can be roughly distinguished by the chosen laser energy. Non-resonant pumping schemes, like excitation above the band gap or p-shell excitation, require subsequent relaxation processes, that follow the excitation by the laser pulse, to obtain the desired state. In contrast, resonant or almost resonant schemes involve laser energies that are very close to the lowest QD transition and, for example, can be advantageous for the production of photons as they can provide a considerably higher photon indistinguishability [21, 29, 66]. A large part of this thesis deals with this latter kind of optical state preparation schemes for QDs where a special emphasis lies on the role of the acoustic phonon interaction. This includes a study of the effects of the carrier-phonon coupling on adiabatic rapid passage protocols for biexciton state preparation. While adiabatic rapid passage is commonly known for state manipulation in atomic systems, in the present work also a novel method that is specific to QDs is presented in detail. This new phonon-assisted method makes active use of the phonon coupling and works the better the stronger the coupling is, which stands in sharp contrast to other protocols where the phonon-induced dephasing is considered to be detrimental to the fidelity of the state preparation. The state manipulation process is studied extensively using numerical calculations and the obtained QD state is also analyzed using different experimental observations provided by collaborating research groups. The measurements are closely reproduced by according simulations and verify the practical applicability of the phonon-assisted method. The dynamical behavior during the preparation is also studied in depth in terms of the dressed state picture. The detailed analysis reveals an interesting multi-phase character of the dynamics that makes it possible to explain how phonon-assisted state manipulation can be achieved on the timescale of ultra fast pulses.

This work also contributes to the topical discussion of temperature effects on strong coupling phenomena in QD-cavity systems [67, 68]. By analyzing an extensive set of photoluminescence spectra of strongly coupled QD-micropillars, it is found that the phonon-induced decoherence, which is typically assumed to prevent strong coupling at

elevated temperatures, can be overcompensated by a temperature-dependent increase of the light-matter coupling strength. This latter property is attributed to a unique characteristic of the confinement potential of the QDs used in the measurements.

The present cumulative dissertation is organized as follows. Part I gives an introduction to the publications belonging to this thesis. It provides some common background, explains the relation between the presented articles and summarizes the most important results. After a brief motivation in Chapter 1 the model used for a single optically driven semiconductor QD is presented in Chapter 2 along with the necessary theoretical background. Chapter 3 introduces the numerical path-integral method that is used throughout this work along with the modifications that make it possible to combine Hamiltonian and non-Hamiltonian dynamics while keeping the exact treatment of the phonon coupling. Chapter 3 also discusses some important technical advances of the method, some future applications and a brief comparison with perturbative methods. The following two chapters introduce the publications dealing with state preparation (Chapter 4) and temperature-dependent effects of QDs embedded in a microcavity (Chapter 5). Finally, Part II collects the nine papers belonging to this thesis.

2 Optically driven semiconductor quantum dots

The three-dimensional confinement of charge carriers in a QD can be achieved in a variety of ways [2, 3]. One particularly widespread method, that is especially useful to produce defect-free samples for QD-based devices and that allows a strong electronic confinement, is the self-assembly Stranski-Krastanov growth technique [69–71]. Using this method, a smaller band gap material, such as InAs, is deposited on a clean substrate of a larger band gap material with a small lattice mismatch, such as GaAs. This is typically achieved using molecular beam epitaxy and initially leads to the growth of a thin wetting layer. In the process, the lattice mismatch builds up to an increasing strain and eventually induces the assembly of small nanometer sized islands of the smaller band gap material. These islands, which minimize the energy in the layer similar to the formation of water drops on a surface, form the QDs. To confine the carriers also in the growth direction the QD layer is finally capped by an additional epitaxial film of the wider band gap material. Some important properties such as the thickness of the wetting layer or the energy and size distribution of the QDs can be influenced by the details of the manufacturing process and the chosen material composition.

In this thesis such self-assembled GaAs-based InAs QDs with a strong confinement potential, that leads to a clear energetic separation of the electronic levels, provide the foundation for the theoretical modeling. Similar to an atom, the discrete states of a QD are connected by optical transitions obeying the spin selection rules. The QD dynamics is also affected by the unavoidable phonon coupling of the surrounding crystal and, possibly, by additional interactions with the environment. Here, the Hamiltonian of an optically driven QD is written generically as

$$\widehat{H} = \widehat{H}_{\text{dot-light}} + \widehat{H}_{\text{dot-ph}}. \tag{2.1}$$

The first contribution $\widehat{H}_{\text{dot-light}}$ describes the electronic structure of the QD including the optical coupling and is introduced in Section 2.1. Section 2.2 reviews $\widehat{H}_{\text{dot-light}}$ in the so called dressed state picture, which is frequently used in this thesis. The second term in Eq. (2.1) given by $\widehat{H}_{\text{dot-ph}}$ represents the phonon environment and the QD-phonon interaction and is introduced in Section 2.3. Further possible QD-environment interactions are accounted for in an approximative, non-Hamiltonian way by direct phenomenological modifications of the equations of motion and are briefly reviewed in Section 2.4.

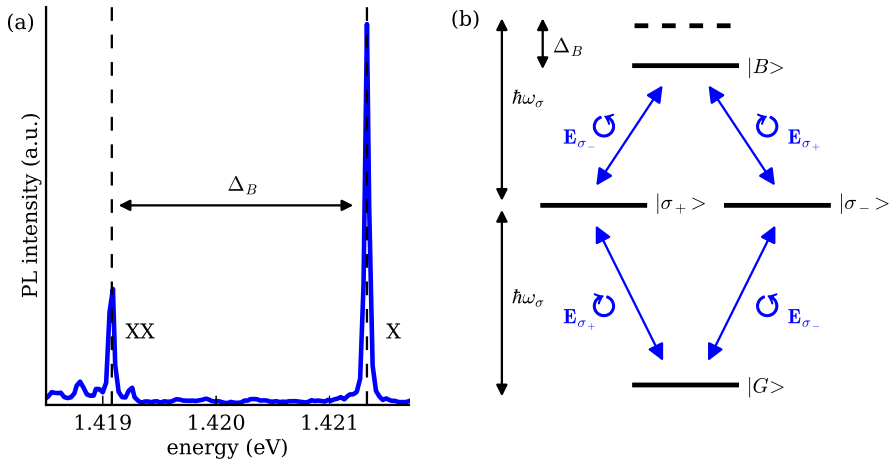

Figure 2.1: (a) Photoluminescence (PL) emission spectrum of a single QD under non-resonant above band gap excitation (1.51 eV) taken from Ref. [73] with the kind permission of the authors. The two peaks correspond to the optical transitions from the biexciton state $|B\rangle$ to the exciton states $|\sigma_\pm\rangle$ (labeled by XX) and the transitions from the exciton states to the ground state $|G\rangle$ (labeled by X), respectively. The spectral peaks are separated by the biexciton binding energy Δ_B. (b) Energy level diagram of the four QD states, which are optically coupled by the circularly polarized components of a laser field $\mathbf{E}_{\sigma_\pm}$ (illustrated by the left- and right-rotating arrows). The biexciton binding energy Δ_B is equal to the distance between the energy of the biexciton state $|B\rangle$ and twice the amount of the exciton energy $\hbar\omega_\sigma$.

Electronic few level model and optical driving

Different to bulk semiconductors, the strong electronic confinement in QDs leads to a clear energetic separation of the single particle states. Therefore, an optical excitation that is close to the transition energy between the topmost valence band and the lowest conduction band states can yield a maximum number of two electron-hole pairs with different spin configurations due to Pauli's exclusion principle. In the limit of strong confinement the Coulomb interaction between the electrons and holes does not lead to a mixing of different single particle states, but only leads to an adjustment of the resulting energies [72]. The relevant electronic states of an optically driven QD are thus typically written in terms of the excited electron-hole pairs, which are referred to as excitons. These include the optically active exciton states $|\sigma_+\rangle$ and $|\sigma_-\rangle$, the biexciton state $|B\rangle$, where both these excitons are present, and the ground state $|G\rangle$ without any electron-hole pairs. The excitonic states $|\sigma_\pm\rangle$ differ in the configurations of the electron spin σ and the angular momentum of the hole state m, which is given by $(\sigma, m) = (+1/2, -3/2)$ and $(-1/2, +3/2)$, respectively. There exist other possible excitonic states, such as charged excitons, dark exciton states, that do not couple to an external light field due to the spin selection rule, and excitations that involve energetically higher lying single particle states. For the optical excitations discussed in this thesis, these additional states can be safely neglected.

A typical photoluminescence emission spectrum of a strongly confined single QD can be seen in Fig. 2.1(a). The sharp peaks labeled as 'X' and 'XX' are due to photons that are emitted from the exciton to ground state and biexciton to exciton transitions,

respectively. As it appears, the biexciton energy is below the combined energy of the two exciton states. This energetic difference, called the biexciton binding energy Δ_{B}, originates from the Coulomb interaction between the electrons and holes and, like here, is typically on the order of a few meV. Interestingly, the biexciton binding energy can have a positive or negative sign depending on the QD geometry [4].

Considering these properties, the QD-light Hamiltonian can be written in the basis of the four states $|G\rangle$, $|\sigma_+\rangle$, $|\sigma_-\rangle$ and $|B\rangle$ as

$$\widehat{H}_{\text{dot-light}} = \sum_{\nu} \hbar\omega_\nu |\nu\rangle\langle\nu| + \hbar\omega_{\text{ex}}\big(|\sigma_+\rangle\langle\sigma_-| + |\sigma_-\rangle\langle\sigma_+|\big) + \sum_{\nu,\nu'} \hbar M_{\nu\nu'} |\nu\rangle\langle\nu'|. \tag{2.2}$$

The first term accounts for the energies $\hbar\omega_\nu$ of the four basis states that are indexed by ν. The energies strongly depend on the details of the confinement potential and, as already mentioned, are also affected by the Coulomb interaction. However, for the purpose of this thesis it is sufficient to treat the energies simply as input parameters to the model. The biexciton energy can be expressed as $\hbar\omega_B = 2\hbar\omega_\sigma - \Delta_B$ with $\hbar\omega_\sigma = \hbar\omega_{\sigma_+} = \hbar\omega_{\sigma_-}$, and the ground state energy $\hbar\omega_G$ is set to zero. The relative values of the energies are shown in the schematic energy level diagram in Fig. 2.1(b). The second term in Eq. (2.2) represents a possible exchange interaction $\hbar\omega_{\text{ex}}$ between the exciton levels that is typically on the order of only a few tens of μeV. For the studies in this thesis the exchange interaction plays a very minor role and with a single exception in Section 3.4 it is neglected.

The matrix elements $M_{\nu\nu'}$ in the last term in Eq. (2.2) describe optical transitions that are due to external light. The following presentation will first focus on the coupling to a classical field as, for example, it is realized by an intense laser pulse. The modeling of the interaction of a QD with a quantized field mode, that is also relevant for this thesis, is presented thereafter. To describe the interaction with laser light, it is useful to split the electric field vector into its two circularly polarized components. These are denoted by $\mathbf{E}_{\sigma_\pm}$ and couple separately to the QD transitions due to the spin selection rules, as it is also indicated in Fig. 2.1(b). When the common dipole and rotating wave approximations are employed, the only non-vanishing elements of the coupling matrix are given by

$$M_{G\sigma_+} = M^*_{\sigma_+ G} = M_{\sigma_- B} = M^*_{B\sigma_-} = \frac{1}{2} f_{\sigma_+}(t) e^{i\omega_L t} \tag{2.3}$$

$$M_{G\sigma_-} = M^*_{\sigma_- G} = M_{\sigma_+ B} = M^*_{B\sigma_+} = \frac{1}{2} f_{\sigma_-}(t) e^{i\omega_L t}, \tag{2.4}$$

where ω_L denotes the central frequency of the laser and the quantities $f_{\sigma_\pm}(t)$, which are referred to as field strengths, are defined by

$$-\mathbf{d}\cdot\mathbf{E}_{\sigma_\pm} = \frac{\hbar}{2} f_{\sigma_\pm}(t) e^{-i\omega_L t}. \tag{2.5}$$

The dipole matrix element $\mathbf{d}$ is assumed to be equal for all transitions as it is justified in the limit of small QDs with a strong confinement [74, 75]. Experimentally, it is very challenging to control the exact field strength that is applied at a given time. Therefore, the so called pulse area α, which is proportional to the much more accessible square

root of the laser power, is frequently used throughout this thesis. The pulse area for a pulsed excitation is defined by

$$\alpha = \int_{-\infty}^{\infty} f(t)dt, \tag{2.6}$$

where $f(t)$ denotes the total field strength $f(t) = f_{\sigma_+}(t) + f_{\sigma_-}(t)$. The pulse area is typically given in units of π.

There are two limiting cases for the polarization of the laser that are worth mentioning. First, if one of the circularly polarized components $\mathbf{E}_{\sigma_\pm}$ vanishes, and in case the size of $\hbar\omega_{\text{ex}}$ is negligible, the model reduces to a driven two-level system consisting of the ground state and a single exciton state. For resonant excitation this system performs well known Rabi oscillations between the two levels [76] and the Rabi frequency is given by the field strength f. Second, for linearly polarized light, i.e. $f_{\sigma_+} = f_{\sigma_-}$, the model reduces to an effective three-level system. In this case, only one of the linear combinations $|X_H\rangle$ (H for horizontal) and $|X_V\rangle$ (V for vertical), defined by the relation

$$|\sigma_\pm\rangle = \frac{1}{\sqrt{2}}\big(|X_H\rangle \pm i|X_V\rangle\big), \tag{2.7}$$

can be optically addressed, while the other decouples from the system dynamics.

Some studies in this thesis also deal with QDs that are kept within a small optical cavity [43], which makes a quantized description of the light field necessary. In the simplest case, the photon modes are energetically well separated and the QD only couples to a single cavity mode. Under these conditions the QD can again be modeled as a two-level system comprising the QD ground state $|G\rangle$ and an exciton state $|X\rangle$ that corresponds to the polarization of the cavity mode. The light-matter interaction of the QD-cavity system is described by the Jaynes-Cummings Hamiltonian

$$\widehat{H}_{JC} = \hbar\omega_X|X\rangle\langle X| + \hbar\omega_c\hat{a}^\dagger\hat{a} + \hbar g\big(\hat{a}^\dagger|G\rangle\langle X| + \hat{a}|X\rangle\langle G|\big), \tag{2.8}$$

where again the dipole and rotating wave approximations have been applied. The symbols $\hbar\omega_c$ and $\hbar\omega_X$ denote the energy of the cavity mode and the exciton state, respectively. The destruction and creation operators $\hat{a}$ and $\hat{a}^\dagger$ correspond to the photons within the cavity mode and g is the light-matter coupling strength that depends on both QD and cavity properties. In the rotating wave approximation the optical coupling only allows a coherent exchange of energy between the QD and the cavity mode, but not the creation of additional photons. If initially only a single excitation of the QD-cavity system is present, the Hamiltonian can therefore be rewritten in the basis spanned by the states $|X\rangle$, now representing the exciton state without additional photons, and $|P\rangle$, representing the QD ground state with a single photon inside the cavity. In this basis the QD-light Hamiltonian reads

$$\widehat{H}_{\text{dot-light}} = \hbar\omega_X|X\rangle\langle X| + \hbar\omega_c|P\rangle\langle P| + \hbar g\big(|P\rangle\langle X| + |X\rangle\langle P|\big). \tag{2.9}$$

Dressed state picture

The optically driven QD dynamics can often be best interpreted using the so called dressed state picture [77]. The dressed states can be thought of as the bare QD states

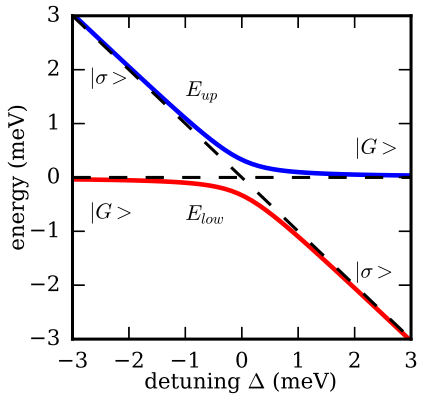

Figure 2.2: Dressed state energies of the two-level system as a function of the detuning Δ for a fixed field strength $f = 1.0$ ps^{-1} (red and blue). It can be seen that the light-matter interaction induces an anti-crossing at resonance. For large absolute values of the detuning where $\hbar f << |\Delta|$, the dressed states correspond to the bare QD states $|G\rangle$ and $|\sigma\rangle$ in the rotating frame, the energies of which are shown by the dashed black lines. The bare QD states that correspond to the dressed states in this limit are indicated by the labels in the figure.

that are additionally *dressed*, i.e. modified, by the light-matter interaction, and are thus also called laser dressed states or photon dressed states. Formally, the dressed states are defined as the eigenstates of the coupled light-matter Hamiltonian [c.f. Eq. (2.2)] in the frame rotating with the laser frequency ω_L. Here, the dressed states will be briefly introduced for the abovementioned two-level case, in which a QD is driven by a constant circularly polarized laser field. The two-level case will suffice to demonstrate the most important properties of the dressed states.

After the transformation to the rotating frame, the coupled QD-light Hamiltonian [c.f. Eq. (2.2)] reads for the two-level system

$$\widehat{H}^{\text{2LS}}_{\text{dot-light}} = -\Delta|\sigma\rangle\langle\sigma| + \frac{\hbar f}{2}(|G\rangle\langle\sigma| + |\sigma\rangle\langle G|), \tag{2.10}$$

where $|\sigma\rangle$ represents the exciton state that matches the selection rules for the polarization of the laser field, i.e. $|\sigma\rangle = |\sigma_+\rangle$ or $|\sigma\rangle = |\sigma_-\rangle$ depending on the polarization. The laser is detuned from the QD transition by the energy $\Delta = \hbar\omega_L - \hbar\omega_\sigma$. A straightforward calculation of the eigenstates of $\widehat{H}^{\text{2LS}}_{\text{dot-light}}$ yields the dressed states

$$|\psi_{\text{up}}\rangle = +\cos(\theta)|G\rangle + \sin(\theta)|\sigma\rangle \tag{2.11a}$$
$$|\psi_{\text{low}}\rangle = -\sin(\theta)|G\rangle + \cos(\theta)|\sigma\rangle \tag{2.11b}$$

with the corresponding energies

$$E_{\text{up/low}} = \frac{1}{2}(-\Delta \pm \hbar\Omega). \tag{2.12}$$

The laser coupling leads to a mixing of the bare states, which can be quantified by the mixing angle θ, that is defined by the relation

$$\tan(\theta) = \frac{\hbar f}{\Delta + \hbar\Omega}. \tag{2.13}$$

The symbol Ω denotes the so called Rabi frequency

$$\hbar\Omega = \sqrt{(\hbar f)^2 + \Delta^2}, \tag{2.14}$$

which increases for larger driving strengths and detunings. The dressed state energies are illustrated in Fig. 2.2, where they are shown as a function of the detuning forming the so called adiabatic branches. It can be seen that for large absolute values of the detuning, where the light-matter interaction has a negligible effect, the dressed state energies are equal to the energies of the bare QD states in the rotating frame. The splitting of the dressed state energies at resonance, the Rabi splitting, is given by $\hbar f$. Notably, the adiabatic branches connect different QD states due to the anti-crossing that occurs at resonance. This finding is essential for adiabatic rapid passage protocols, that are discussed in Section 4.3. For the studies in this thesis it is also important to note that the *character* of the dressed states, which is determined by the admixture of the different QD states to the dressed states, is defined by the instantaneous field strength and the detuning of the laser, and thus can be time-dependent. This as well has important consequences for the state preparation protocols discussed in Chapter 4.

Interaction with the phonon environment

The strong electronic confinement in QDs also has a pronounced impact on the nature of the carrier-phonon interaction. While in extended semiconductors the electronic energies can be redistributed between different states by phonon-induced transitions, such inelastic phonon scattering is strongly suppressed in QDs, where typically the phonon energies do not match the large energy gap between the electronic levels. This energetic mismatch is often called the *phonon bottleneck* and implies that in QDs, compared to bulk semiconductors or quantum wells, phonon related decoherence is almost exclusively related to elastic scattering processes. Such elastic carrier-phonon interactions do not change the electronic occupations, but can have a strong influence on the phase relations between the QD states, which is referred to as *pure dephasing* and represents the dominant decoherence mechanism in strongly confined QDs [54–56, 78]. Importantly, the phonon scattering always takes place and thus represents a lower bound for the decoherence in QDs.

The pure dephasing model has been successfully applied to optically driven QDs many times and is able to reproduce a number of experimentally observed features. These include, the renormalization of the Rabi frequency of coherently driven QDs [79], a driving strength dependent damping of Rabi oscillations [50, 51, 80–83] and the broadening of the Mollow sidebands in resonance fluorescence spectra of a QD embedded in a microcavity [84, 85]. For GaAs-based QDs, as they are discussed here, the major coupling mechanism between excitons and the solid state environment is given by the coupling to longitudinal acoustic phonons via the deformation potential [78], and is therefore also considered in this thesis. Other types of phonon coupling, like the piezoelectric coupling to acoustic phonons [86] or a coupling to optical phonon modes, are neglected.

The Hamiltonian describing the phonon modes and the QD-phonon interaction can be written as

$$\widehat{H}_{\text{dot-ph}} = \hbar \sum_{\mathbf{q}} \left\{ \omega_{\mathbf{q}} b_{\mathbf{q}}^{\dagger} b_{\mathbf{q}} + \sum_{\nu} n_{\nu} \left(\gamma_{\mathbf{q}}^{*} b_{\mathbf{q}} + \gamma_{\mathbf{q}} b_{\mathbf{q}}^{\dagger} \right) |\nu\rangle\langle\nu| \right\}, \tag{2.15}$$

where the operator $b_{\mathbf{q}}^{\dagger}$ ($b_{\mathbf{q}}$) creates (destroys) a longitudinal acoustic phonon with wave vector $\mathbf{q}$ and energy $\hbar\omega_{\mathbf{q}} = \hbar c_s|\mathbf{q}|$ with c_s denoting the longitudinal sound velocity, n_ν is the number of electron-hole pairs of the ν-th QD state, and $\gamma_{\mathbf{q}}$ is the phonon coupling constant of the $\mathbf{q}$-th phonon mode. The phonon coupling being proportional to the number of electron-hole pairs is again a consequence of the strong electronic confinement. Due to the similarity of the lattice properties of the QD and the surrounding material it is usually justified to assume bulk phonon modes. Not surprisingly, $\widehat{H}_{\text{dot-ph}}$ is diagonal in the electronic subspace, which reflects the pure dephasing type of the coupling.

A very useful quantity to describe details of the phonon coupling is the spectral density

$$J(\omega) = \sum_{\mathbf{q}} |\gamma_{\mathbf{q}}|^2 \delta(\omega - \omega_{\mathbf{q}}), \tag{2.16}$$

that is often used for a parametric description of the phonon coupling in the form

$$J(\omega) = \alpha\omega^3 \exp(-\omega^2/\omega_c^2), \tag{2.17}$$

where α scales the coupling strength and ω_c defines the high frequency cut-off [63]. A microscopic expression for $J(\omega)$, that is used in this thesis and many previous works [61, 87], can be obtained using the standard bulk form of the deformation potential coupling for $\gamma_{\mathbf{q}}$ that in the envelope function approximation is modified by an additional form factor reflecting the wave function of the confined electron and hole states [78]. In most cases the phonon related influence on the QD dynamics can be sufficiently described assuming spherically symmetric QDs with a harmonic confinement potential, which yields Gaussian ground state wave functions for electrons and holes, and implies

$$J(\omega) = \frac{\omega^3}{4\pi^2\rho\hbar c_s^5}\left(D_e \exp(-\frac{\omega^2 a_e^2}{4c_s^2}) - D_h \exp(-\frac{\omega^2 a_h^2}{4c_s^2})\right)^2. \tag{2.18}$$

Here, ρ is the mass density and $D_{e(h)}$ denote the deformation potential constants of electrons and holes that are taken from the literature [78, 88]. The quantities $a_{e(h)}$ represent the electronic confinement lengths of electrons and holes and roughly correspond to the QD radius that is typically chosen to be $3-5$ nm for the calculations in this thesis in accordance with experimental observations. Importantly, it can be seen that in both Eqs. (2.17) and (2.18) $J(\omega)$ scales as ω^3 for small ω. This expresses the *super-ohmic* character of the phonon-coupling. Compared to ohmic and sub-ohmic couplings, which for low frequencies scale as ω^a with $a \leq 1$, a super-ohmic coupling is characterized by non-exponential, typically only partial relaxations that exhibit a variety of non-Markovian dynamical effects [45, 89].

In the presence of external optical driving, the elastic phonon scattering can have a significant impact on the occupations of the QD states, despite the pure dephasing nature of the phonon coupling. This can be best understood by employing the dressed state picture. For example, in the two-level case described in Section 2.2 it can be seen that the optical coupling leads to finite excitonic contributions to both dressed states [c.f. Eq. (2.11)], and thus both dressed states are coupled to the phonon environment. Because the energetic splitting between the dressed states is often close to typical phonon

energies, phonon-induced transitions between the dressed states are possible via phonon emission and absorption processes. The energetic difference between the dressed states is very different to the splitting between the bare QD states, because the dressed states are defined in the rotating frame and thus include the laser energy. It should be noted that at low temperatures phonon emission is dominant and therefore the phonon coupling effectively leads to a relaxation towards the lower dressed state. This has far reaching consequences that will be discussed in much more detail in Chapter 4 and *pubs 2-8*.

Further environmental interactions

Besides the phonon coupling, there are many other environmental interactions that can induce dephasing and relaxation processes which affect the driven QD dynamics. Important examples are charge fluctuations in the surrounding material [90] and interactions with the radiation field [54, 91, 92], that can lead to an exponential decay of the exciton or biexciton state, as it is for example discussed in *pub 1* of this thesis. Additionally, in *pub 7* and *pub 8* an electronic tunneling effect, which is due to an externally applied bias voltage needed for photo current measurements [41], plays a central role as it also limits the exciton life time. For coupled QD-cavity systems an important effect is also the loss of cavity photons caused by imperfections of the optical cavity [53], as it is considered in *pub 1* and *pub 9* of the present work. Different to the non-Markovian phonon coupling, most of these processes can be reasonably described by phenomenological rate equations and often do not necessarily require a detailed microscopic description. Therefore, they are not explicitly included in the Hamiltonian in Eq. (2.1), but instead will be separately incorporated in the resulting equations of motion in Section 3.2.

3 Simulation of the quantum dot dynamics using path-integrals

Based on the modeling in the previous chapter, in the present work the dynamics of a single QD is simulated for a number of different optical excitation conditions and taking into account various couplings to the environment. The theoretical calculations turn out to be highly useful to systematically study the complex dynamical behavior of QDs and to predict or explain experimental observations. Section 3.1 outlines the equations of motion that need to be solved and explains the fundamental ideas of a sophisticated numerical technique [57, 58, 61, 93] that is based on the path-integral formalism [59, 94, 95]. This technique is used to calculate the driven QD dynamics throughout this thesis and in the following is simply referred to as the path-integral method. Section 3.2 introduces an important extension of the method that allows the inclusion of non-Hamiltonian dynamics within the formalism and is established in *pub 1*. Some significant technical advancements that further increase the applicability of the path-integral approach are presented in Section 3.3. Section 3.4 briefly discusses two examples of systems that based on the progress described in this chapter can be studied in detail using the path-integral technique in the future.

Path-integral formalism for driven quantum dots

In this section the path-integral formalism is introduced for systems where the environment purely consists of the phonon subsystem while other environmental interactions are disregarded. How this restriction can be lifted in certain situations will be discussed in Section 3.2. The state of the combined system comprising the optically coupled QD and the phonon environment can be expressed using the statistical operator $\hat{\rho}$. The time-evolution of this operator is determined by the Liouville von-Neumann equation

$$\frac{d}{dt}\hat{\rho} = \frac{1}{i\hbar}[\widehat{H}, \hat{\rho}], \tag{3.1}$$

with the Hamiltonian $\widehat{H} = \widehat{H}_{\text{dot-light}} + \widehat{H}_{\text{dot-ph}}$ given in Eq. (2.1), and appropriate initial conditions.

Finding a closed expression for the solution of this equation is only possible in a very few special situations. Even when the QD is described as a two-level system and the phonon coupling is disregarded, the possibly time-dependent optical driving term in $\widehat{H}_{\text{dot-light}}$ allows an analytical solution only in some rare cases [76, 96]. While the optical driving of the finite number of QD states can relatively easily be accounted for using

standard numerical techniques, the phonon coupling described by $\widehat{H}_{\text{dot-ph}}$ represents a much bigger obstacle, because it requires the treatment of a coupling to an infinite number of harmonic oscillators, c.f. Eq. (2.15). In the presence of the phonon coupling analytical solutions are only known for delta pulse excitations [97, 98] or an undriven QD, in which case the system reduces to the so called independent boson model [56, 63]. To deal with the many degrees of freedom when calculating the driven QD dynamics in situations that go beyond these border cases, a variety of approximative approaches, that either treat the phonon coupling or the optical driving perturbatively, have been developed [63, 80, 99–103]. While some of these methods are highly elaborate and allow for very accurate simulations, they are typically only valid in a limited parameter range where the assumptions of the underlying approximations are reasonably fulfilled. Special care must be taken when using Markovian descriptions as it is known that the pure dephasing phonon coupling induces non-Markovian features, such as a non-monotonic temperature dependence of the initial decay of the optical polarization after ultrafast excitation [88, 104], non-Lorentzian line shapes in photoluminescence spectra [55, 78, 105], and phonon sidebands in resonance fluorescence emission [106].

A unique possibility to derive a numerical exact solution of Eq. (3.1), that does not require approximations to the model defined by $\widehat{H}$, is given by the path-integral methodology presented in this section. The path-integral method has been frequently applied to calculate the phonon influence on the dynamics of two and four-level models of QDs coupled to a classical laser field [29, 50, 60, 61, 64, 65, 77, 87, 107] as well as for the case of a two-level system coupled to a quantized cavity mode [62, 107]. Notably, it exactly reproduces all non-Markovian features of the phonon coupling, takes into account arbitrary multi-phonon processes, and is applicable in a very wide parameter range including weak and strong optical driving, low and high temperatures, and an enhanced phonon coupling strength. The path-integral approach therefore provides an excellent tool for theoretical studies of optically driven QDs and is especially useful to benchmark perturbative approaches and to explore new parameter ranges, where less accurate techniques come to their limits.

The path-integral technique provides a numerical iteration scheme, that allows the calculation of the QD dynamics in terms of the reduced density matrix, where the phonon degrees of freedom have been traced out. This is achieved by an extensive iterative summation over different system configurations at each time step and will be explained in the following. To employ the method, it is important that the system under study can be divided into an inner system, with a relatively small finite dimension N, and environmental degrees of freedom that can influence the dynamics of the inner system, but will be traced out at the end. In the present case the inner system comprises the optically driven QD system, described by $\widehat{H}_{\text{dot-light}}$, while the phonon subsystem represents the environment. For example, the N inner system states can be given solely by the QD states as in Eq. (2.2), in which case N typically equals two, three or four depending on which of the excitonic states are optically active. Alternatively, the inner system might also include a finite number of photon states as in Eq. (2.9). Under these conditions the path-integral approach can solve Eq. (3.1) yielding the dynamics in terms of the N-dimensional reduced density matrix

$$\hat{\tilde{\rho}} = \text{Tr}_{\text{ph}}\left(\hat{\rho}\right), \tag{3.2}$$

where $\mathrm{Tr}_{\mathrm{ph}}$ denotes the trace over all phonon variables. The diagonal elements of the reduced density matrix represent the probabilities for the QD to be prepared in one of the basis states with an arbitrary configuration of the phonon subsystem. These probabilities are referred to as *occupations* and are frequently used to describe the QD dynamics in this thesis. At the initial time t_0, it is assumed that the statistical operator is given by the product state

$$\hat{\rho}(t_0) = \hat{\tilde{\rho}}(t_0) \otimes \hat{\rho}_{\mathrm{th}}, \tag{3.3}$$

i.e. that the phonon environment is in a thermal equilibrium at temperature T described by $\hat{\rho}_{\mathrm{th}}$, while the inner system is prepared in an arbitrary state expressed by $\hat{\tilde{\rho}}(t_0)$. The time axis is discretized by equally spaced grid points $t_l = t_0 + l\Delta t$ with the time step size Δt and the target of the calculations is the reduced density matrix at the n-th time step $\hat{\tilde{\rho}}(t_n)$. Formally, this quantity can be obtained by propagating the initial density matrix using the time evolution operator for the whole system and taking the trace over the phonon degrees of freedom, which can be written as

$$\hat{\tilde{\rho}}(t_n) = \mathrm{Tr}_{\mathrm{ph}}\left(\widehat{U}_{\mathrm{sys}}^{t_0,t_n}\hat{\rho}(t_0)(\widehat{U}_{\mathrm{sys}}^{t_0,t_n})^{\dagger}\right). \tag{3.4}$$

The time evolution operator is given by

$$\widehat{U}_{\mathrm{sys}}^{t_0,t_n} = \mathcal{T}\exp\left(-\frac{i}{\hbar}\int_{t_0}^{t_n}\widehat{H}dt\right), \tag{3.5}$$

where $\mathcal{T}$ denotes the time ordering. Using the path-integral method this expression is evaluated by first splitting the time evolution into several time steps of length Δt, yielding

$$\widehat{U}_{\mathrm{sys}}^{t_0,t_n} = \widehat{U}_{\mathrm{sys}}^{t_{n-1},t_n} \cdot \ldots \cdot \widehat{U}_{\mathrm{sys}}^{t_0,t_1}, \tag{3.6}$$

which is correct in linear order of Δt. The validity of this numerical approximation can be easily controlled by performing the simulations for different choices of Δt [61]. Inserting unity operators $\sum_\nu |\nu\rangle\langle\nu|$ of the inner system at each time step then gives

$$\widehat{U}_{\mathrm{sys}}^{t_0,t_n} = \sum_{\nu_0,\ldots,\nu_n} |\nu_n\rangle\langle\nu_n|\widehat{U}_{\mathrm{sys}}^{t_{n-1},t_n}|\nu_{n-1}\rangle \cdot \ldots \cdot \langle\nu_1|\widehat{U}_{\mathrm{sys}}^{t_0,t_1}|\nu_0\rangle\langle\nu_0|, \tag{3.7}$$

where each of the $n+1$ indices ν_l cycles through the N states of the inner system. Keeping the linear accuracy in Δt, the time evolution operators for the different time steps can be split into a phonon related and a phonon-free part, yielding

$$\widehat{U}_{\mathrm{sys}}^{t_{l-1},t_l} = \widehat{U}_{\mathrm{ph}}\widehat{U}_{\mathrm{free}}^{t_{l-1},t_l}. \tag{3.8}$$

Here, the phonon related evolution operator, which is the same at each time step, is given by

$$\hat{U}_{\mathrm{ph}} = \exp\left(-\frac{i}{\hbar}\hat{H}_{\text{dot-ph}}\Delta t\right), \tag{3.9}$$

while the phonon-free part of the dynamics is described by

$$\widehat{U}_{\mathrm{free}}^{t_{l-1},t_l} = \mathcal{T}\exp\left(-\frac{i}{\hbar}\int_{t_{l-1}}^{t_l}\widehat{H}_{\text{dot-light}}dt\right). \tag{3.10}$$

By exploiting the fact that due to its pure dephasing character the phonon coupling is diagonal in the inner system and writing

$$\widehat{U}_{\nu_l} = \langle \nu_l | \widehat{U}_{\mathrm{ph}} | \nu_l \rangle \tag{3.11}$$

as well as

$$M_{\nu_{l-1},\nu_l} = \langle \nu_l | \widehat{U}_{\mathrm{free}}^{t_{l-1},t_l} | \nu_{l-1} \rangle, \tag{3.12}$$

the separation of the phonon related and the phonon-free dynamics given by Eq. (3.8) yields the following expression for the total time evolution operator

$$\widehat{U}_{\mathrm{sys}}^{t_0,t_n} = \sum_{\nu_0,\ldots,\nu_n} \widehat{U}_{\nu_n} \cdot \ldots \cdot \widehat{U}_{\nu_1} M_{\nu_{n-1},\nu_n} \cdot \ldots \cdot M_{\nu_0,\nu_1} |\nu_n\rangle\langle\nu_0|. \tag{3.13}$$

Finally, inserting Eq. (3.13) into Eq. (3.4) yields

$$\bar{\rho}_{\nu_n\mu_n} = \sum_{\substack{\nu_0,\ldots,\nu_{n-1} \\ \mu_0,\ldots,\mu_{n-1}}} \bar{\rho}_{\nu_0\mu_0} \exp(S_{\nu_n\ldots\nu_1}^{\mu_n\ldots\mu_1}) \prod_{l=1}^{n} \mathcal{M}_{\nu_l\mu_l}^{\nu_{l-1}\mu_{l-1}}, \tag{3.14}$$

where

$$\bar{\rho}_{\nu_l\mu_l} = \langle \nu_l | \hat{\bar{\rho}}(t_l) | \mu_l \rangle \tag{3.15}$$

denotes the (ν_l, μ_l)-th entry of the reduced density matrix at the l-th time step and the symbol

$$\mathcal{M}_{\nu_l\mu_l}^{\nu_{l-1}\mu_{l-1}} = M_{\nu_{l-1},\nu_l} M_{\mu_{l-1},\mu_l}^{*} \tag{3.16}$$

has been introduced. Each contribution to the summation in Eq. (3.14) is associated with one of N^{2n} possible choices for the $2n$ variables $(\nu_0, \mu_0), ..., (\nu_{n-1}, \mu_{n-1})$, that are referred to as *paths* and can be roughly interpreted as possible trajectories through the configuration space of the inner system at the different time steps t_l leading from the initial state $\bar{\rho}_{\nu_0\mu_0}$ to the final state $\bar{\rho}_{\nu_n\mu_n}$. The symbol

$$\exp(S_{\nu_n\ldots\nu_1}^{\mu_n\ldots\mu_1}) = \mathrm{Tr}_{\mathrm{ph}} \left(\widehat{U}_{\nu_n} \cdot \ldots \cdot \widehat{U}_{\nu_1} \hat{\rho}_{\mathrm{ph}} \widehat{U}_{\nu_1}^{\dagger} \cdot \ldots \cdot \widehat{U}_{\nu_n}^{\dagger} \right) \tag{3.17}$$

represents the exponential of the so called phonon influence functional $S_{\nu_n\ldots\nu_1}^{\mu_n\ldots\mu_1}$, which captures all phonon related effects. It is usually straightforward to evaluate the matrix elements M_{ν_{l-1},ν_l} associated with the phonon-free dynamics, because of the small dimension of the inner system. The calculation of the influence functional $S_{\nu_n\ldots\nu_1}^{\mu_n\ldots\mu_1}$ is much more involved, but can be performed analytically without further approximations by rewriting the expression as a path-integral over the phonon degrees of freedom and exploiting the fact that the phonons are given as a collection of harmonic oscillators, which yields Gaussian integrals. This is described in detail in Ref. [61]. According to these calculations, the influence functional reads

$$\begin{aligned} S_{\nu_n\ldots\nu_1}^{\mu_n\ldots\mu_1} = \sum_{l=1}^{n} \sum_{l'=1}^{l} \Big(& - K_{\nu_{l'}\nu_l}(t_l - t_{l'}) - K_{\mu_l\mu_{l'}}^{*}(t_l - t_{l'}) \\ & + K_{\nu_l\mu_{l'}}^{*}(t_l - t_{l'}) + K_{\nu_{l'}\mu_l}(t_l - t_{l'}) \Big), \end{aligned} \tag{3.18}$$

and depends on the current and previous time steps $t_1, ..., t_n$, which makes it possible to account for a finite phonon memory time and thus allows non-Markovian dynamics. The memory kernels

$$K_{\nu_l\mu_{l'}}(\tau) = 2n_{\nu_l}n_{\mu_{l'}}\int_0^\infty d\omega\frac{J(\omega)}{\omega^2}\times \\ (1-\cos(\omega\Delta t))\left(\coth(\frac{\hbar\omega}{2k_BT})\cos(\omega\tau) - i\sin(\omega\tau)\right) \quad (3.19)$$

and

$$K_{\nu_l\mu_l}(0) = n_{\nu_l}n_{\mu_l}\int_0^\infty d\omega\frac{J(\omega)}{\omega^2}\times \\ \left(\coth(\frac{\hbar\omega}{2k_BT})(1-\cos(\omega\Delta t)) + i\sin(\omega\Delta t) - i\omega\Delta t\right) \quad (3.20)$$

are defined entirely by the initial temperature T, the spectral density of the phonon coupling $J(\omega)$ and the number of electron-hole pairs of the different states n_ν, c.f. Section 2.3.

Quite obviously, the summation in Eq. (3.14) quickly becomes unfeasible due to the large number of summands even for a relatively small number of time steps n and a small dimension of the inner system N. This problem can be partly circumvented by exploiting the fact that the memory kernels, Eq. (3.19), quickly approach zero after a few picoseconds, which reflects the finite phonon memory time specific to acoustic phonons [61]. By limiting the system memory to a small number of n_c time steps and applying the so called augmented density matrix algorithm [57, 58], the numerical effort of the calculations can be reduced from N^{2n} to N^{2n_c} [61]. Notably, this means that the numerical cost no longer depends on the total number of simulated time steps and it is thus also possible to deal with long-time studies of the QD dynamics [64, 77]. On the other hand, the augmented density matrix approach increases the memory consumption of the numerical calculations, which is determined by the chosen number of memory steps n_c. Due to the large computational cost, it is very important to arrive at a highly efficient numerical implementation of Eq. (3.14), especially when dealing with systems where $N > 2$. A possibility to drastically reduce the number of required paths, that even allows dealing with values of $N > 4$ in certain situations, has been established in the context of this thesis, as described in Section 3.3.

It should be noted that the clear separation between the phonon related and the phonon-free part of the dynamics expressed by Eq. (3.14) is essential for the inclusion of non-Hamiltonian dynamics within the path-integral approach that is presented in the following section.

Inclusion of non-Hamiltonian dynamics

As discussed in Section 2.4, in some situations the phonon coupling does not provide the only relevant relaxation mechanism, but for a realistic simulation of the QD dynamics further processes must be considered. For example, the radiative decay of the exciton

states involves the coupling to a continuum of external optical field modes that would have to be included in a complete model. This and other interactions, which different to the pure dephasing coupling to acoustic phonons induce direct transitions between the QD states, can so far not be included on a microscopic level when using the path-integral method. However, quite often a phenomenological description of environmental relaxation processes is appropriate and therefore a treatment on this approximate level can be sufficient. Formally, this can be achieved by extending the Liouville von-Neumann equation, Eq. (3.1), by additional modifications of the statistical operator $\hat{\rho}$ on the right hand side. This can be expressed generically by a Liouville space operator [108], denoted by $\mathcal{L}[\cdot]$, and yields a generalized dynamical equation for the system, which reads

$$\frac{d}{dt}\hat{\rho} = \frac{1}{i\hbar}[\widehat{H}, \hat{\rho}] + \mathcal{L}[\hat{\rho}]. \tag{3.21}$$

Here, we assume that $\mathcal{L}[\cdot]$ does not act on the phonon degrees of freedom, but only on the subsystem consisting of the QD and photon states, that is described by $\widehat{H}_{\text{dot-light}}$. Different to the commutator expression defined by the Hamiltonian on the right hand side of Eq. (3.21), $\mathcal{L}[\cdot]$ does not necessarily induce a unitary evolution of $\hat{\rho}$, and is thus referred to as a non-Hamiltonian contribution to the dynamical equation. For example, a well known choice for $\mathcal{L}[\cdot]$, which maintains important properties of the statistical operator, such as a constant trace of $\hat{\rho}$, is given by the so called Lindblad form [46]

$$\mathcal{L}[\hat{\rho}] = \frac{1}{2}\sum_i \gamma_i(t)\left(2\hat{A}_i\hat{\rho}\hat{A}_i^\dagger - \hat{A}_i^\dagger\hat{A}_i\hat{\rho} - \hat{\rho}\hat{A}_i^\dagger\hat{A}_i\right). \tag{3.22}$$

In this expression the symbols $\hat{A}_i$ represent operations acting on the states of the QD-light subspace and the factors γ_i denote according relaxation rates.

While the path-integral method so far allowed for a complete treatment of the Hamiltonian part of Eq. (3.21), i.e. the inherently complex QD-phonon interaction under optical driving, it has previously not been possible to additionally account for the non-Hamiltonian contributions $\mathcal{L}[\cdot]$. This might be rather unexpected, especially because $\mathcal{L}[\cdot]$ is assumed to leave the phonon degrees of freedom invariant and thus only acts on a relatively small set of states. Taking into account Markovian relaxation rates between a finite number of states typically does not provide a serious obstacle for numerical calculations of the system dynamics when using other methods than the path-integral approach. However, as shown above, the path-integral method relies on a representation in terms of the unitary time-evolution operator and therefore previous applications of the method were restricted to purely Hamiltonian dynamics. Here, it should be noted that a hybrid approach, which uses the numerically exact path-integral solution of Eq. (3.1) as input parameter for a system of rate equations that accounts for the non-Hamiltonian part of the dynamics in Eq. (3.21), was developed in Ref. [62]. This method has been utilized to study the competition between the radiative decay of the exciton state, cavity losses, and phonon-induced pure dephasing in a coupled QD-cavity system [62] and is also used to deal with cavity losses in *pub 9*. However, because this approach is strongly restricted to resonant QD-cavity couplings and also prohibits a time-dependent light-matter coupling, it can often not be applied.

As a key result of this work, in *pub 1* the path-integral method is generalized, now making it possible to treat the Hamiltonian and non-Hamiltonian contributions

in Eq. (3.21) on an equal footing, which allows a numerically exact simulation of the QD dynamics including phenomenological relaxation processes. This important advancement greatly improves the applicability of the method and is for example utilized in *pub 7* and *pub 8* yielding a very close agreement with experimental data that would not have been possible without the generalization of the formalism. It is worth mentioning here that, as it is discussed in *pub 1*, the modifications of the path-integral method are applicable not only to QDs, but to any few-level system with a pure dephasing coupling to a collection of harmonic oscillators.

In the following, the central idea of the extension to non-Hamiltonian dynamics is briefly explained. A more rigorous derivation of the extended formalism can be found in *pub 1*. As already mentioned, one of the difficulties of the treatment of the phenomenological contributions in Eq. (3.21) lies in the fact that the path-integral method is based on a special representation of the unitary time evolution operator, which does not involve any kind of non-Hamiltonian dynamics. However, the derivation of the path-integral formalism presented in the previous section allows the important observation that in the final formula for the iteration scheme, Eq. (3.14), the phonon-free evolution is entirely captured by the factors

$$\mathcal{M}_{\nu_l\mu_l}^{\nu_{l-1}\mu_{l-1}} = \langle\nu_l|\widehat{U}_{\text{free}}^{t_{l-1},t_l}|\nu_{l-1}\rangle\langle\mu_{l-1}|(\widehat{U}_{\text{free}}^{t_{l-1},t_l})^\dagger|\mu_l\rangle, \tag{3.23}$$

which are determined independently of the phonon coupling by the transition matrix elements of the phonon-free evolution operator $\widehat{U}_{\text{free}}^{t_{l-1},t_l}$ [c.f. Eqs. (3.10) and (3.16)]. In a more abstract way, the factors $\mathcal{M}_{\nu_l\mu_l}^{\nu_{l-1}\mu_{l-1}}$ can thus be obtained by calculating the phonon-free evolution of the reduced density matrix between the $(l-1)$-th and the l-th time step, starting with $|\nu_{l-1}\rangle\langle\mu_{l-1}|$ as initial state. Therefore, a more general definition of these factors, which allows the inclusion of phenomenological relaxation processes, can be

$$\mathcal{M}_{\nu_l\mu_l}^{\nu_{l-1}\mu_{l-1}} = \langle\nu_l|\mathcal{M}_{t_{l-1}}\left[|\nu_{l-1}\rangle\langle\mu_{l-1}|\right]|\mu_l\rangle, \tag{3.24}$$

where $\mathcal{M}_{t_{l-1}}[|\nu_{l-1}\rangle\langle\mu_{l-1}|]$ is the solution of the phonon-free equation of motion

$$\frac{d}{dt}\hat{\rho} = \frac{1}{i\hbar}[\hat{H}_{\text{dot-light}}, \hat{\rho}] + \mathcal{L}[\hat{\rho}] \tag{3.25}$$

at time $t = t_l$ with the initial condition $\hat{\rho}(t_{l-1}) = |\nu_{l-1}\rangle\langle\mu_{l-1}|$. As shown in *pub 1*, this generalization combined with the clear separation of the phonon related and the phonon-free part of the QD evolution achieved in the previous section are the core of the inclusion of non-Hamiltonian dynamics within the path-integral formalism.

To verify the applicability of the new formalism, *pub 1* carefully compares the simulations with some known results obtained using alternative techniques. The article first discusses the comparison with a driven two-level QD under the influence of the radiative decay of the exciton state. For this system there exist analytical results in the absence of the phonon interaction, which can be exactly reproduced by the generalized path-integral formalism when the phonon coupling is disabled. It is also verified that the new method works correctly when the coupling to acoustic phonons is included by comparing it with a weak-coupling theory [63], which treats the phonon coupling up to second order and is valid at low temperatures. A very close match between the two methods is

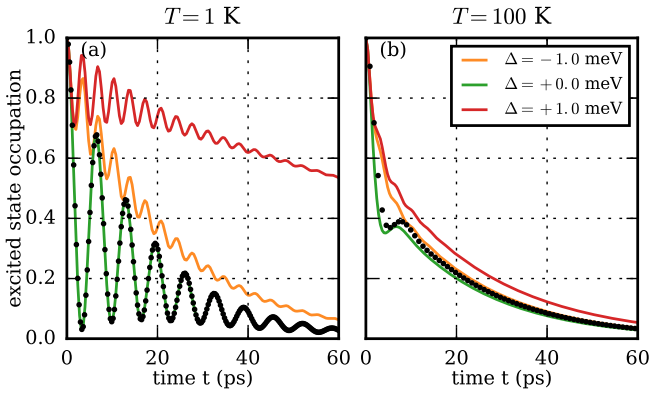

Figure 3.1: Comparison of the time-dependent excited state occupation of a QD coupled to a leaky cavity mode for different detunings between the cavity mode and the QD transition as indicated. The simulations are performed using the extended path-integral formalism (solid lines) and the hybrid approach (black dots). For resonant coupling (green) both methods yield very similar results, while the path-integral simulations also allow the analysis of detuned QD-cavity couplings (red and orange), which is not possible using the hybrid method. This figure is adapted from *pub 1*.

found in the range of validity of the weak-coupling theory, and partly even for increased temperatures. Moreover, it is shown that the path-integral method is able to identify the limits of this approximative method, which turn out to become best visible for detuned excitations and high temperatures. Subsequently, the path-integral approach is compared with the hybrid method mentioned at the beginning of this section [62] for the case of a QD resonantly coupled to a leaky optical cavity mode. This is shown in Fig. 3.1, where the excited state occupation of the system is plotted as a function of time for different temperatures and different detunings between the cavity mode and the QD transition. For a resonant QD-cavity coupling (solid green lines), which is also accessible by the hybrid method (black dots), pronounced Rabi oscillations, that are damped due to the combined influence of photon losses and the phonon-induced decoherence, are visible and both methods yield very similar results. For off-resonant couplings, a clearly visible asymmetry between positive (solid red lines) and negative (solid orange lines) detunings appears at low temperatures [panel (a)], which almost vanishes at high temperatures [panel (b)]. This effect is due to the fact that at low temperatures phonon emission processes are more frequent than phonon absorption processes. Importantly, the results of the extended path-integral formalism are fully in line with previous calculations addressing the same situation that used a polaron-transform master equation approach to account for the phonon coupling [109].

Overall, the comparison shows that the generalized path-integral approach reliably reproduces known results, which indicates the correctness of the derived formalism. This provides a solid foundation for further studies using the method, like the investigation of combined cavity and phonon-effects on the biexciton cascade, which is briefly discussed in the final section of this chapter.

Technical optimizations

In the context of this thesis, the numerical path-integral simulations used at the department for quantum theory of condensed matter led by Prof. Axt at Universität Bayreuth have also been substantially enhanced on a technical level. In this respect, a considerable improvement of the runtime and memory efficiency of the simulations, that, e.g., makes it possible to account for longer phonon memory times or a smaller time step, has been achieved through various optimizations, like, e.g., caching strategies, parallelization and a more efficient path representation. This has been shown to be of great help for example for the extensive parameter studies that were taken out to arrive at the results presented in *pub 2* and *pub 3*. However, the most important advancement in this regard is a drastic reduction of the numerical cost of the simulations for systems where multiple states are identical in terms of the phonon coupling. For example, in the exciton-biexciton system the phonon coupling is identical for both exciton states, because the number of electron-hole pairs n_ν equals one for both states, c.f. Eq. (2.15). This symmetry makes it possible to partially contract the augmented density matrix in each time step and by this strongly reduce its dimensionality and the number of required paths. More precisely, the numerical effort of the path-integral method can be reduced from N^{2n_c} to $N^2M^{2(n_c-1)}$, where M is the number of states that are different with respect to the phonon coupling. For example, in the exciton-biexciton system, where $N = 4$ and $M = 3$, this means a reduction of the number of required paths of 90% for a typical value of $n_c = 5$. This significant improvement paves the way for the application of the path-integral method to systems that could otherwise not be handled, as will be described in the following section.

Potential further applications of the method

The technical optimizations mentioned in the previous section not only allow for more efficient simulations that make it possible to, e.g., analyze larger sets of different parameters, but also enable the utilization of the path-integral method for systems that previously were numerically far too demanding. To this end, the improvements are especially useful for systems where a QD is coupled to one or more quantized cavity modes. In this case, there can be multiple basis states with equal QD configurations and different photon numbers. Because the phonon coupling does not depend on the number of photons, these states are affected equally by the phonon interaction and the abovementioned optimization can be very beneficial, as M can be considerably smaller than N.

Of particular importance in this class of systems is the model of a QD coupled to two linearly polarized orthogonal cavity modes. This system attracts a lot of interest, because the decay of the biexciton state and the resulting photon emission can lead to the generation of polarization entangled photon pairs [23, 25–29, 110]. The typical dynamics of the biexciton cascade can be briefly described as follows. Starting from the biexciton state $|B\rangle$ and an empty cavity, the emission of a horizontally or vertically polarized photon, which is absorbed by the corresponding cavity mode, from the QD leads to a transition of the QD to one of the exciton states $|X_H\rangle$ or $|X_V\rangle$, c.f. Eq. (2.7). Besides the possible reabsorption of the photon, the emission of a second photon can

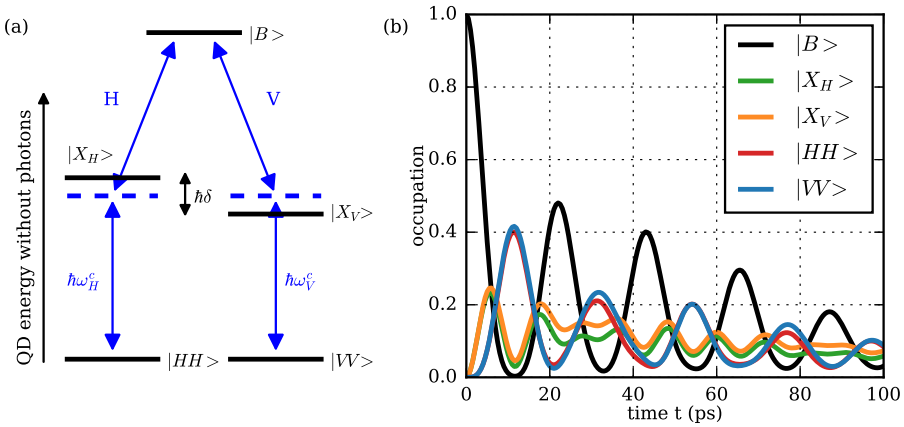

Figure 3.2: (a) Schematic energy level diagram of a QD coupled to two linearly polarized cavity modes as it is relevant for the simulation of the biexciton cascade. The illustration ignores the photon energies. $|B\rangle$ represents the state where the QD is prepared in the biexciton state and the cavity modes are empty. $|X_H\rangle$ and $|X_V\rangle$ denote the exciton states that are coupled to the horizontally (H) or vertically (V) polarized cavity mode (illustrated by the blue arrows) with a single photon, while $|HH\rangle$ and $|VV\rangle$ represent the QD ground state with two horizontally (HH) or vertically (VV) polarized photons excited in the cavity. The exciton states are split by an energy $\hbar\delta = 0.1$ meV and the energies of the cavity modes $\hbar\omega^c_{H/V}$ are tuned halfway between the exciton states as indicated by the dashed blue lines. The biexciton binding energy Δ_B is set to zero. (b) Time-dependent occupations of the five states assuming that the system is initially prepared in the state $|B\rangle$, the light-matter coupling strength of both cavity modes equals $\hbar g = 0.1$ meV, the cavity loss rate is $\kappa = 0.01$ ps^{-1} and the temperature is chosen to be $T = 10$ K.

induce the transition of the QD to the ground state leaving behind two photons in either the horizontally or vertically polarized cavity mode. Here, these two states are denoted by $|HH\rangle$ and $|VV\rangle$, respectively. The situation is illustrated in the energy level diagram in Fig. 3.2(a) and a more detailed description of this commonly used model for the biexciton dynamics can be found in the literature [110–112]. For the production of entangled photon pairs the system ideally gets prepared in a maximally entangled superposition state, such as

$$|\Psi\rangle = \frac{1}{\sqrt{2}}\left(|HH\rangle + |VV\rangle\right), \tag{3.26}$$

at the end of the relaxation process. The equivalence of both relaxation paths is decisive for the degree of entanglement and for example a finite energetic splitting between the exciton states $\hbar\delta$, which can arise due to the exchange interaction [c.f. Section 2.1], can be harmful in this context [25].

While previous implementations of the path-integral method would not have allowed to calculate the dynamics of the biexciton cascade including the phonon interaction, because of the very high computational cost of this five-level system, this has now become feasible due to the technical progress described in the previous section. The new possibility to include non-Hamiltonian dynamics in the path-integral simulations is also very important when studying the biexciton cascade, because it allows to consider phe-

nomenological cavity photon losses, which practically always play a fundamental role in experiments dealing with QD-cavity systems. As a short proof of principle, Figure 3.2(b) shows the time-dependent evolution of the occupations of the five QD-cavity states mentioned above for a finite splitting between the exciton states. The system performs strongly damped Rabi-like oscillations, where the damping is due to the combined effect of the phonon coupling and the cavity losses. It is worth noting that a small deviation between the occupations of the states $|HH\rangle$ and $|VV\rangle$, as well as between the occupations of the exciton states $|X_H\rangle$ and $|X_V\rangle$, is visible. Similar to the asymmetry between positive and negative detunings in Fig. 3.1(a), this is due to the unequal probabilities of phonon emission and phonon absorption at low temperatures [113]. In the absence of the phonon coupling these deviations do not occur, because in the present calculations the exciton energies are chosen to be symmetrically detuned from the cavity mode frequency, c.f. Fig. 3.2(a). Because the path-integral method not only yields the occupations shown here, but the complete reduced density matrix, it should be possible to make conclusions about the temperature-dependent phonon-impact on the degree of entanglement of the two-photon states. Notably, this has not been achieved so far in such a rigorous way as given by the path-integral approach.

Besides the important example of the biexciton cascade dynamics, another interesting model that might be worth studying using the path-integral method in the future is a QD-cavity system driven by an external laser field [85, 114, 115]. Importantly, the laser driving leads to the excitation of additional cavity photons and therefore the possible photon number of the created states is only limited by photon losses of the cavity. Due to this large number of different states that are involved in the dynamics of the light-matter subsystem, it has previously been thought of as impossible to treat this model using the path-integral method. However, by exploiting again the fact that the phonon coupling is independent of the photon number, and thereby drastically reducing the number of relevant paths, simulations including a few tens and up to a hundred photons should now be within reach.

4 State preparation

This chapter deals with different protocols that can be used to manipulate the QD state by means of optical excitation, as it is discussed in *pubs 2-8*. Such controlled state preparation is a key ingredient for many QD-based devices and, as it will be seen in the following, studying these schemes allows deep insights into the complex laser driven dynamics of QDs and their interaction with the phonon environment.

A relatively simple way of state preparation, that is being used frequently, is off-resonant excitation, where the laser energy is chosen above the band gap energy, like in Fig. 2.1. In this case a preparation of the excited QD states is achieved via incoherent relaxation processes of the excited carriers into the lower lying QD states. While this can be realized using very short pulses on the femtosecond scale, a very important drawback of this method is that it leads to timing jitter of the photons that are emitted when the QD relaxes back to the ground state [116, 117]. Thus, this method is clearly inferior to protocols that make use of resonant excitation of the QD, if the creation of indistinguishable photons is the goal [21, 29]. A resonant excitation leads to Rabi oscillations between the QD levels, that can be exploited for state preparation if the laser intensity and the pulse length are chosen such that by the end of the optical excitation the occupation of the desired QD state is maximal [41, 118]. As the required intensity depends on the optical dipole moment of the driven transition, which is typically not known very well, the exact pulse parameters often have to be found empirically making it hard to achieve precise state manipulations. A preparation of the exciton and biexciton states that is robust against fluctuations of the pulse intensity can be achieved by protocols relying on adiabatic rapid passage, which are the topic of Section 4.1. Sections 4.2 - 4.4 extensively discuss an innovative method that also allows a robust preparation, but different to adiabatic rapid passage schemes makes active use of the phonon coupling.

Adiabatic rapid passage protocols for biexciton preparation

State preparation protocols relying on adiabatic rapid passage (ARP) [100, 113, 119–123] can be realized by chirped laser pulses, where the laser frequency is swept through the QD resonance during the pulse. As demonstrated in Section 2.2 for the two-level case, changing the detuning between the laser energy and the QD transition strongly affects the character of the laser dressed states. Depending on the sign of the detuning, this can imply that a given dressed state is more ground state or more exciton-like. In fact, this can be exploited to induce a complete inversion of the initial QD state, if the system evolves along one of the adiabatic branches during the pulse [119]. An adia-

batic evolution can be expected, if the pulse envelope and the laser frequency change slowly compared to the instantaneous Rabi frequency [124]. However, as described in Section 2.3, the ideal evolution along the adiabatic branches can be spoiled by phonon-induced transitions between the dressed states. This has been identified as the major mechanism to reduce the preparation fidelity, i.e. the achieved occupation of the target state, in ARP protocols for QDs in the two-level case [100, 113, 121].

In *pub 2* these theoretical considerations are extended to the case of the exciton-biexciton system. By means of two different optical excitation protocols, the preparation fidelity of the biexciton is studied as a function of the pulse parameters, the biexciton binding energy, and for different temperatures using path-integral simulations that account for the coupling to acoustic phonons. The first protocol uses a linearly polarized frequency-swept laser pulse that at its maximum is chosen to be in resonance with the two-photon transition of the QD, i.e. the laser energy is equal to half the energy of the ground state to biexciton transition. The second protocol uses two simultaneous, circularly polarized, and frequency-swept pulses that are tuned to be in resonance with the ground state to exciton and exciton to biexciton transition, respectively. It is shown that both schemes can yield a robust and high fidelity preparation of the biexciton state at low temperatures. However, towards higher temperatures the fidelity becomes worse, which as in the two-level case can be traced back to phonon-induced transitions between the dressed states taking place during the adiabatic evolution. Interestingly, for both protocols the preparation fidelity also depends on the sign of the chirp already in the phonon-free case, which is explained in the article. Depending on the situation, either of the two protocols can be favorable. For example the two-color scheme can yield a slightly higher preparation fidelity and requires a lower pulse area threshold especially for large biexciton binding energies, while the two-photon resonance scheme is generally simpler to realize and keeps the QD transitions laser free.

Phonon-assisted state preparation

The phonon-induced transitions between the laser dressed states, which are a major obstacle for the realization of a high fidelity preparation when using ARP protocols, are for the first time recognized as the foundation of a fundamentally new method for QD state preparation in *pub 3*. This technique is the topic of the present and the two following sections. In the ideal case of ARP, a time-dependent detuning is used to transform the system along a single adiabatic branch, which leads to the preparation of the target state. Phonon-induced transitions to the other branches lead to deviations from this ideal behavior and thus mean a loss of occupation of the desired state. In contrast, the protocol proposed in *pub 3* uses a constant detuning of the laser pulse meaning that the character of the dressed states at the beginning and the end of the pulse, where the field strength approaches zero, is the same. In fact, the target state is actively reached by means of transitions to energetically lower lying branches, which are due to the acoustic phonon interaction and ultimately lead to a thermal distribution in the dressed state basis. If the energetic separation of the dressed states is sufficiently large or the temperature is sufficiently low, such a thermalization practically leads to a pure population of the lowest dressed state, which, as discussed in *pub 3*, can be exploited to reach the desired state with a very high preparation fidelity. In this sense, the phonon

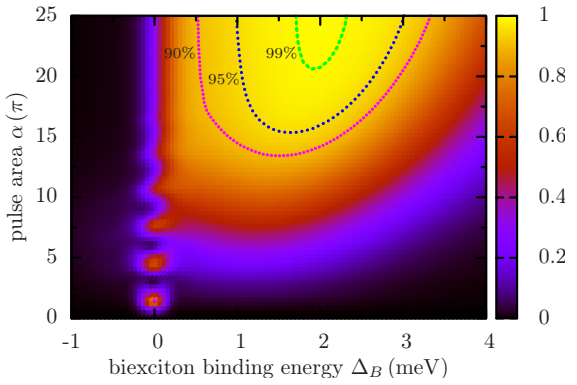

Figure 4.1: Occupation of the biexciton state resulting from a linearly polarized Gaussian pulse with $\tau = 15$ ps FWHM as a function of the biexciton binding energy Δ_B and the pulse area α. The laser energy is chosen resonant to the ground state to exciton transition. The temperature is set to $T = 4$ K. As it can be seen by the dashed lines, there are pronounced regions of high-fidelity biexciton preparation above 90%. This figure is taken from *pub 3*.

coupling is used actively for the QD state preparation, which is therefore referred to as phonon-assisted preparation, and is conceptually very different to ARP protocols, where the phonon environment is a hindrance.

In *pub 3* the phonon-assisted state preparation method is first discussed for the two-level case using circularly polarized light to create the exciton state. The simulations show that an almost perfect inversion towards the exciton state is possible within about 15 ps by exciting the QD with a strong, positively detuned pulse that needs to exceeds a certain pulse area threshold. The requirement for a sufficiently large pulse area can be understood by considering that the phonon-induced equilibration needs to complete within the time frame of the pulse. An efficient relaxation requires an energetic splitting between the dressed states close to the most prominent phonon energies, i.e. close to the maximum of the phonon spectral density in Eq. (2.18), and is thus not realized if the laser intensity is too weak. On the other hand it is found that once the threshold is exceeded, the resulting exciton occupation is robust against variations of the pulse area and, on the range of a few meV, is also robust for different detunings. The preparation fidelity only decreases again for very large pulse areas when the phonon environment gets out of resonance due to the increasing Rabi splitting.

Publication 3 also discusses the important case of biexciton state preparation using a linearly polarized laser pulse, that is resonant to the ground state to exciton transition. Figure 4.1 shows the obtained biexciton occupation as a function of the biexciton binding energy Δ_B and the pulse area. Not surprisingly, Rabi rotations can be seen for $\Delta_B = 0$, as the excitation is completely resonant in this case. For positive values of Δ_B, however, the energy of the biexciton state is lowered and thus the laser is positively detuned from the exciton to biexciton transition. This leads to a broad phonon sideband feature, similar to the one found in the two-level case, indicating the possibility of the creation of a very high biexciton population. Importantly, for negative biexciton binding energies no such preparation is possible, as in this case the thermal dressed state distribution does not lead to a considerable occupation of the biexciton state.

The theoretical proposal of the phonon-assisted state preparation method in *pub 3* has immediately attracted a lot of attention from different experimental physics groups, which resulted in *pubs 4* and *5* of this thesis as well as Ref. [48]. The reason for the large interest in the new protocol is that the new method not only relies on a highly interesting physical mechanism, but also offers several practical advantages over other

state preparation schemes, such as the already mentioned robustness against variations of the different pulse parameters and a relatively simple practical implementation. From an experimental point of view, there are several challenges that have to be dealt with to demonstrate the proposed phonon-assisted manipulation of the QD state. Naturally, samples of strongly confined QDs that are expected to show a sufficiently strong coupling to acoustic phonons are needed, because the phonon-induced relaxation is of fundamental importance for this method. However, typical samples do not contain a single QD, but rather an ensemble of many different QDs that can have, e.g., different transition energies and dipole moments. Measurements on such an ensemble can make it hard to draw clear conclusions about the state manipulation process as the resulting signal will be a superposition of many slightly different contributions. Therefore, it is very desirable to find a subregion of the sample where the energy distribution of the different QDs is sufficiently sparse such that it is feasible to select a single QD from the spectrum. Ideally, it is not only possible to optically address a single QD, but the phonon sideband of the QD should also be free from signals that are due to neighboring QDs. The next requirement for a conclusive experimental analysis of the phonon-assisted state preparation protocol is the possibility to repetitively excite the QD with controlled picosecond pulses that are stable regarding their pulse shape, intensity and central frequency. A minimal time-bandwidth product of the pulses is also highly advantageous to exclude the influence of ARP effects. For a systematic study, the laser frequency needs to be adjustable in small steps in the range of a few meV around the QD resonance. Moreover, to exceed the threshold for an optimal state preparation, which can be rather large, usually a very strong laser intensity must be realized, which at resonance allows several Rabi rotations. It should be noted that, in principle, phonon-assisted QD state manipulation can also be achieved using continuous wave excitation (cw), but in this case the heating of the sample will typically lead to additional complications. Finally, there must be a way to measure or know the QD state before and after the optical excitation to quantify the impact of the laser pulse.

All these difficult needs could be sufficiently fulfilled in the measurements of *pub 4* and *pub 5*, which present independent experimental evidence for the theoretically proposed phonon-assisted state manipulation effects. Both publications show the results of a very close collaboration between theoretical and experimental groups, where the theoretical considerations were carefully adjusted to the exact experimental situations. The measurements presented in *pub 4* were realized by a group around J. H. Quilter at the Department of Physics and Astronomy at the University of Sheffield in England, while the experiments leading to *pub 5* were performed by S. Bounouar and M. Müller at the Institut für Halbleiteroptik und Funktionelle Grenzflächen at Universität Stuttgart. Similar studies were also published in Ref. [48] by a group around P. L. Ardelt.

The goal of the project resulting in *pub 4* was to demonstrate that in a strongly confined QD an exciton population can be generated by a strong, positively detuned laser pulse, as it can be expected in view of the theoretical results in *pub 3*. In the measurements, the QD state was detected by a photo current absorption technique that prior to this project has already been successfully used to study acoustic phonon effects on resonant and off-resonant Rabi rotations of single QDs [51, 79, 125]. This absorption method yields an electric signal proportional to the number of electron-hole pairs within

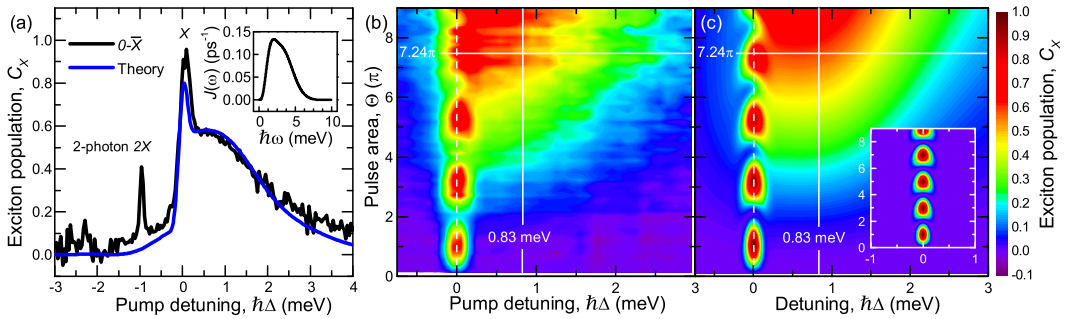

Figure 4.2: Comparison between photo current measurements and path-integral calculations targeted at optically driven phonon-assisted exciton preparation, taken with kind permission by the authors from *pub 4*. (a) Exciton occupation for different detunings at a fixed pulse area $\alpha = 7.24\pi$. The inset shows the phonon spectral density $J(\omega)$ used for the calculations. (b) Experimental data for different values of the pulse area and the detuning and (c) corresponding path-integral calculations. The inset in panel (c) shows the results of the calculations in case the phonon-induced dephasing is disregarded. The comparison clearly identifies the phonon coupling as the main cause of the partial QD inversion seen at positive detunings and increased pulse areas.

the sample and is thus sensitive to the QD state. To differentiate between the signals coming from different QDs within the sample, a two-pulse pump-probe technique was employed. This method first uses an off-resonant and circularly polarized pump pulse to initiate the phonon-assisted state preparation. The achieved exciton population is then probed by applying a resonant π-pulse that inverts the QD. Importantly, the dipole moment of the QD must be significantly larger than the dipole moments of neighboring QDs with similar transition energies, such that the probe pulse practically only affects the QD under study. This is achieved by carefully selecting an appropriate QD from the sample. By comparing the photo current signal with the signal that is gained if no probe pulse is applied, a reliable measurement of the influence of the pump pulse on the QD state becomes possible. The pump-probe technique was performed for both co- and cross-polarizations of the probe pulse in *pub 4*. As described in the article, this allows to extract the exciton population of a single QD created by the pump pulse in three different ways. These methods take into account the contributions to the photo current signal that are due to the population of the exciton and the biexciton states and also consider an exponential decay of the excitonic occupations that is caused by the external bias voltage. Figure 4.2(b) presents the exciton population extracted from the co-polarized two-pulse measurements of *pub 4* as a function of the detuning from the exciton transition and the pulse area of the pump pulse. The experimental data clearly shows resonant Rabi rotations and, most importantly, a pronounced phonon sideband at positive detunings and larger pulse areas. This feature would not be expected without the phonon coupling, as it can be seen from the inset in panel (c), and verifies the theoretical prediction of the phonon-assisted exciton preparation by blue-shifted laser pulses stated in *pub 3*.

For a quantitative comparison with the theory it is necessary to make valid assumptions about the different system parameters entering the model. In the measurements

of *pub 4* a very detailed control of the optical setup was achieved such that important properties of the pulses, like the central frequency as well as the temporal and spectral width, could be taken directly from the measurements. Some of the other parameters such as the mass density and the speed of sound of the QD material are well known and can be found in the literature. However, some quantitative aspects determining the strength of the phonon coupling, like the details of the confinement potential and the exact deformation potential coupling constants for electrons and holes, are very hard to estimate. The layer thickness of the QD sample provides an upper bound for the vertical confinement lengths of electrons and holes, but does not yet allow a sufficiently exact estimation of these parameters. Even if the confinement lengths were known approximately, one still would have to make an assumption about the shape of the confinement potential. Similarly, so far only the energetic difference between the deformation potential coupling constants for electrons and holes, but not their absolute values, are accessible by measurements [54, 78, 88, 126]. Regardless of these properties, that can be very specific to the material or can even strongly deviate between different QDs, all relevant features of the QD-phonon interaction that enter the calculations are captured by the spectral density of the phonon coupling $J(\omega)$, c.f. Eq. (2.18). In the absence of further information about the system parameters, this function needs to be used as fitting parameter when comparing the theoretical predictions with the experimental data. Notably, the spectral dependence of the exciton occupation in Fig. 4.2(a) allows for a much more detailed estimation of $J(\omega)$ than it was previously possible by only looking at the resonant Rabi rotations [79]. In *pub 4* the function $J(\omega)$ was modeled by Eq. (2.18) using the confinement lengths of electrons and holes $a_e(h)$ as fitting parameters. The spectral density obtained by this fitting procedure can be seen in the inset of Fig. 4.2(a) and yields a very close agreement between the theory and the measurements. The simulations correctly reproduce the characteristic roll-off of the exciton occupation towards large positive detunings as well as the pulse area threshold, that has to be exceeded to reach a significant exciton occupation.

While *pub 4* is targeted at the phonon-assisted preparation of the exciton state, the combined experimental and theoretical study presented in *pub 5* deals with the creation of the biexciton state. The investigations are motivated by the fact that a resonant preparation of the biexciton and the subsequent relaxation can lead to the emission of photons with a very high degree of indistinguishability [21, 29]. Because of this property, the light emitted in such a resonance fluorescence setup is highly suitable for the realization of sources of single photons or entangled photon pairs. The preparation can be achieved by driving the QD via the two-photon resonance, as it has been demonstrated by the experimentalists in Stuttgart in an earlier study [29]. Another advantage of this method is that for a finite biexciton binding energy the QD transitions can be kept laser-free when using the two-photon resonance excitation method. In *pub 5* it is analyzed if these properties still hold for a phonon-assisted preparation process that is initiated by an intense, linearly polarized, picosecond laser pulse that is tuned slightly above the two-photon resonance.

The biexciton occupation is measured by recording the time-integrated intensity of the radiative emission belonging to the biexciton to exciton transition, which follows the creation of the biexciton state. The obtained signal is shown as a function of the

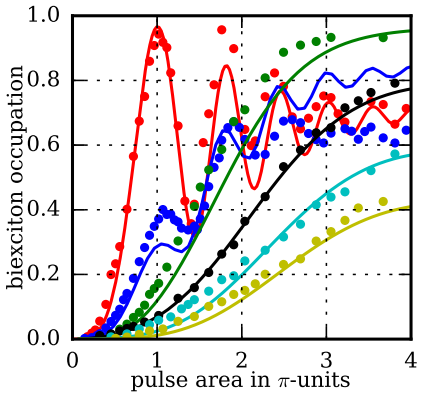

Figure 4.3: Biexciton occupation obtained by a slightly chirped 13 ps pulse using the two-photon resonance method (red) and the phonon-assisted state preparation protocol. The data is shown as a function of the pulse area for different detunings Δ between the laser energy and the two-photon resonance (red: $\Delta = 0.0$ meV, blue: 0.08 meV, green: 0.65 meV, black: 1.13 meV, cyan: 1.30 meV, and olive: 1.46 meV). The solid lines show path-integral calculations, while the colored dots represent experimental observations taken from *pub 5* with the kind permission of the authors.

applied pulse area by the colored dots in Fig. 4.3, while the solid lines show the results of corresponding path-integral simulations, which directly calculate the biexciton occupation yielded by the initiating pulse. In contrast to the definition of the pulse area in Eq. (2.6), in the two-photon excitation scenario a "π-pulse" is often associated with a pulse that yields the first maximum of the resonant Rabi rotations. The measured intensity signal is normalized such that it fits the simulated π-pulse maximum. The overall increase of the mean value of the resonant oscillations (red) is caused by a finite chirp of the laser pulses that is due to details of the optical setup and has also been accounted for in the according simulations. The QD size, i.e. the electronic confinement length, is not precisely known for the samples used in the measurements and is therefore used as a fitting parameter in the calculations. It can be seen that when the QD is excited exactly at the two-photon resonance, i.e. when the detuning equals $\Delta = 0$ meV (red), the pulse area needs to be chosen very close to 1π to realize a high-fidelity preparation of the biexciton state. In contrast, for positively detuned excitations, the data in Fig. 4.3 clearly demonstrates a very high occupation of the biexciton state around $\Delta = 0.65$ meV (green), that is robust against changes of the pulse area for large pulse areas above 3π. This would not be expected without the phonon coupling, because the excitation is off-resonant. The simulations verify that the chirp of the pulses plays a minor role for the occupation of the biexciton for detuned excitations. In fact, the biexciton occupation is not very sensitive to variations of the exact laser frequency for larger detunings and can therefore be purely attributed to phonon-assisted processes. The data in *pub 5* thus provides important evidence that the phonon-assisted preparation protocol can be applied in practice for the creation of the biexciton state and the close match between the measurements and the simulations further confirms the applicability of the theoretical QD model. Notably, the excitation method used in *pub 5* is different to the one discussed in *pub 3*, where the ground state to exciton transition is driven resonantly to prepare the biexciton state.

Beyond the demonstration of the phonon-assisted preparation of the biexciton state, *pub 5* also discusses the influence of the pulse length on the achieved biexciton population. In agreement with the theoretical predictions, it is demonstrated by the measurements that a reduced pulse length can lead to a reduction of the probability for the

creation of the biexciton state, which is due to an incomplete phonon-induced relaxation during the pulse. Another significant result of *pub 5* is that the coherence time of the generated photons is found to be practically equal to the coherence time that is observed if the QD is brought to the biexciton state by applying a resonant π-pulse. While this is not further investigated by theoretical considerations in *pub 5*, it is of very high importance for the practicability of the phonon-assisted method.

In summary, *pubs 3-5* theoretically and experimentally proof the practical possibility of a robust and high-fidelity phonon-assisted preparation of excitonic QD states, which can be made more efficient by increasing the QD-phonon coupling strength. An enhanced phonon coupling can for example be achieved by reducing the vertical extension of the used QDs [87]. The following two sections take a much closer look at the temporal behavior of the QD states during the optical excitation and deal with the possibility to delete a previously existing exciton state by making active use of phonon-assisted processes.

Influence of adiabatic undressing on phonon-assisted state preparation

The results presented so far clearly show that phonon-assisted QD state manipulation is possible using pulsed excitation on a picosecond timescale. However, the phonon-induced relaxation within the dressed state basis, that has been identified as the key driver of the preparation process in *pubs 3-5*, does, by itself, not provide an entirely satisfactory explanation of the observed effects if the preparation is realized with a very high fidelity within a very short time. In fact, corresponding path-integral calculations show that there exists a tradeoff situation between a short timescale and a high fidelity of the preparation if only the phonon-induced relaxation is considered. Therefore, *pub 6*, which is presented in this section, closely analyzes the temporal evolution of the QD during the preparation in order to arrive at a complete understanding of the phonon-assisted preparation process, that also covers the case of a fast high fidelity preparation.

To simplify the discussion, *pub 6* first considers the QD two-level model introduced in Chapter 2 and assumes that the QD is initially prepared in its ground state before it is excited by a positively detuned laser pulse. The analysis reveals that besides the previously discussed relaxation between the dressed states also the temporal evolution of the dressed states itself is directly related to the achieved preparation fidelity. This is studied quantitatively by simulating the driven QD dynamics for different pulse shapes. Since the detuning of the optical pulse is assumed to be constant in *pub 6*, the envelope of the laser pulse directly determines the temporal evolution of the dressed states, as it can be seen for example from Eqs. (2.11)-(2.14). The resulting evolution of the QD state is illustrated exemplarily for rectangular pulses with variable switch-on and switch-off times τ in Fig. 4.4. The pulse envelopes are plotted in panel (a), and the QD state is shown in terms of the occupations of the energetically lower lying dressed state $|\psi_{\mathrm{low}}\rangle$ in panel (b) and the exciton state in panel (c). The calculations indicate that before the switch-off of the pulses at $t = 20$ ps the phonon-induced relaxation is practically finished and the QD is prepared in the lower dressed state, c.f. panel (b). However, as it can be seen in panel (c), this still corresponds to an exciton occupation

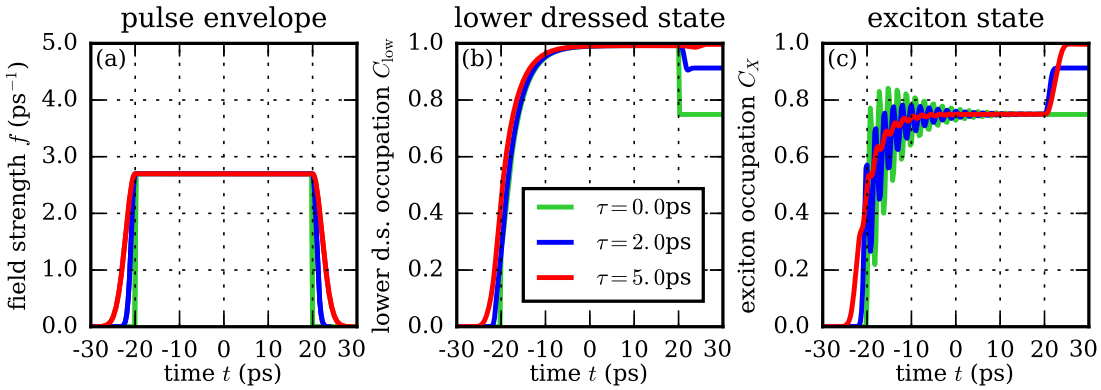

Figure 4.4: (a): Pulse envelope of rectangular pulses with different switch-on and switch-off times, that are modeled by the first and second half of a Gaussian function with FWHM τ, respectively. (b): Time-dependent occupation of the energetically lower lying dressed state during the interaction of a QD with a circularly polarized laser pulse with detuning $\Delta = 1.0$ meV. (c): Time-dependent exciton occupation during the pulse. The temperature is set to $T = 1$ K. This figure is adapted from *pub 6*.

that is below 0.8. Compared to an instantaneous switch-off time of $\tau = 0$ ps, that does not induce a further change of the exciton occupation (green), a smoother switch-off (red) yields a drastic further increase of the exciton occupation. This is of significant importance for a high fidelity preparation on a short timescale. As explained in detail in *pub 6*, the increase occurring at the end of the pulse is a consequence of the adiabatic transformation of the dressed states back towards the bare QD states, that takes place as the pulse envelope is smoothly reduced to zero. In analogy to the dressing of the QD states induced by the laser pulse, in *pub 6* this process is referred to as *undressing*. Importantly, the undressing needs to happen slow enough such that the predominantly occupied lower dressed state is transformed to the desired exciton state adiabatically. This is for example not fully realized if the switch-off time is chosen to be $\tau = 2$ ps, which only leads to a partial increase, but not a perfect exciton occupation, as it is shown by the blue line in Fig. 4.4(c). In contrast to the switch-off time, the switch-on time is not as crucial for the final exciton population, even though a non-adiabatic dressing process leads to an initial occupation of both dressed states, that becomes best visible by the Rabi oscillations of the green curve in Fig. 4.4(c).

Another interesting aspect of the phonon-assisted state preparation process discussed in *pub 6* is that the incoherent phonon scattering leads to a restoration of coherence that is initially lost. This is illustrated in the article using the so called Bloch sphere that is commonly used to visualize the configuration space of a two-level system [76]. It is shown that the trajectory of the two-level system takes a way through the middle of the Bloch sphere towards the opposite pole during the preparation. This is rather uncommon, because typically a coherent dynamics leads to a trajectory that either goes along the surface of the sphere or ends inside the sphere as a consequence of irreversible decoherence processes.

Based on the new and clear understanding of the phonon-assisted state preparation method, *pub 6* also discusses the more complex exciton-biexciton system. To this end,

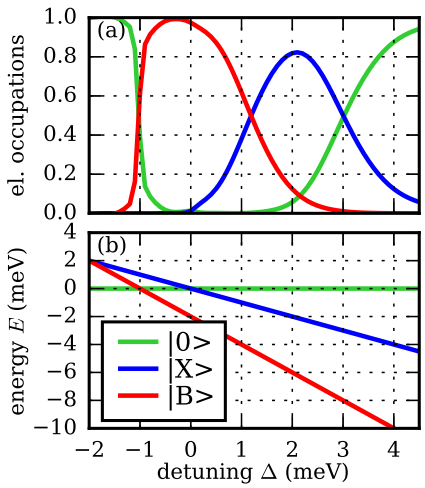

Figure 4.5: (a): Occupations of the ground state (green), the exciton state (blue), and the biexciton state (red) after optical excitation with a linearly polarized Gaussian pulse with a temporal FWHM of 20 ps and a pulse area of 20π, as a function of the detuning of the laser from the ground state to exciton transition Δ. The biexciton binding energy of the QD is $\Delta_B = 2.0$ meV and the temperature is set to $T = 1$ K. (b): Corresponding energies of the QD states in the rotating frame. This figure is adapted from *pub 6*.

the QD state resulting from an intense, linearly polarized Gaussian pulse is analyzed systematically for different choices of the laser frequency. Notably, this analysis is different to the one carried out in *pub 3*, where a similar dependence on the biexciton binding energy is discussed. Interestingly, it is found that, when starting from the ground state, both the exciton and the biexciton can be prepared by phonon-assisted processes, and the target state can be selected by choosing the detuning, the pulse length and the biexciton binding energy. This is exemplarily illustrated in Fig. 4.5(a), where the populations of the QD states reached after the optical excitation are plotted as a function of the detuning from the ground state to exciton transition for a fixed pulse length and a fixed biexciton binding energy $\Delta_B = 2.0$ meV. The biexciton occupation shows a pronounced maximum around $\Delta = 0$ meV, while the exciton population becomes maximal around $\Delta = 2$ meV and at even higher detunings the QD remains in the ground state. The analysis in *pub 6* shows that, provided the undressing process is adiabatic, the target state is determined by two factors. These are given by the order of the QD energies in the frame rotating with the laser frequency, and by how far the phonon-induced relaxation between the photon-dressed states proceeds during the time window that is set by the duration of the pulse. The energies of the QD states in the rotating frame are shown in Fig. 4.5(b), where it can be seen that for all detunings $\Delta > -\Delta_B/2 = -1$ meV the biexciton state (red) is the energetically lowest state, which therefore at first sight is expected to get prepared predominantly. For increased detunings $\Delta > 0$ meV however, the energetic splittings become larger, and thus the phonon coupling no longer leads to a complete thermalization of the dressed states for the given pulse. This results in the preparation of the ground state or the exciton, instead of the biexciton state, c.f. panel (a), and shows that in the exciton-biexciton system also an incomplete relaxation can lead to a useful preparation of one of the QD states. Another important finding is that it is possible to realize a phonon-assisted preparation of the biexciton state also in case of a negative biexciton binding energy, which has not yet been recognized in *pub 3*. This can be achieved by choosing the optical excitation frequency slightly above the two-photon resonance as shown in *pub 6*.

In summary, *pub 6* represents an important contribution to the discussion of the phonon-assisted state preparation protocol, which gives a clear explanation of the un-

derlying dynamics, emphasizes the importance of an adiabatic undressing process and makes new predictions, like the possibility to select the target state via different pulse and QD parameters, that might inspire future experiments.

Further aspects of the phonon-assisted preparation process

This section presents some further findings about the phonon-assisted state preparation method, that have been worked out in the context of this thesis. For example, *pub 1* analyzes the phonon-assisted inversion of a continuously driven two-level QD system taking into account the radiative decay of the exciton state. It turns out that there can be a competition between this decay, which drives the QD towards the ground state, and the phonon-assisted preparation process of the exciton state. Because both the phonon-induced relaxation and the influence of the radiative decay depend on the driving strength, there occurs an interesting non-monotonic dependence of the stationary exciton occupation that is reached towards long times under positively detuned excitation.

While *pubs 3-6* discuss the phonon-assisted transition of a QD from the ground state to an excited state using a strong blue-shifted laser pulse, *pub 7* and *pub 8* deal with the inverse process, in which the QD is driven back to the ground state making active use of the phonon coupling. It is shown by both experiments and theoretical calculations that such a phonon-assisted depopulation of the exciton state is possible for negatively detuned, i.e. red-shifted, excitations in a relatively broad spectral range of a few meV. Since the transition of the QD to the ground state is accompanied by the emission of a photon, the emission process is termed LA-phonon-assisted stimulated emission (LAPSE). In addition, *pub 8* investigates the temperature dependence and the coherence properties of an exciton state created via the phonon-assisted protocol and discusses the possibility to switch the exciton state on and off by using subsequent blue- and red-shifted pulses. The results presented in *pub 7* and *pub 8* have been worked out in collaboration with a group of experimentalists around A. J. Brash and F. Liu at the Department of Physics and Astronomy at the University of Sheffield in England.

In *pub 7* the QD is first brought to the exciton state by applying a resonant, circularly polarized π-pulse, and subsequently an intense red-shifted control pulse is applied to initiate the phonon-assisted depopulation of the exciton state. This experiment is performed using various delay times between the pulses as well as different frequencies and intensities of the control pulse. The QD state is detected using the same electric absorption technique as in *pub 4* yielding a time-integrated photo current signal. The absorption leads to a finite probability for the electron-hole pair excited by the first pulse to tunnel out of the QD before the arrival of the control pulse. This induces an exponential decay of the exciton occupation between the two pulses and has a significant impact on the QD dynamics, because the tunneling time is on the order of the timescale of the dynamics induced by the laser and the phonon coupling. For a complete theoretical description of the driven QD dynamics it is therefore necessary to take into account not only the optical driving and the coupling to the phonon environment, but also the influence of the tunneling relaxation. This is especially true for the time-resolved measurements, where the exciton occupation after the control pulse

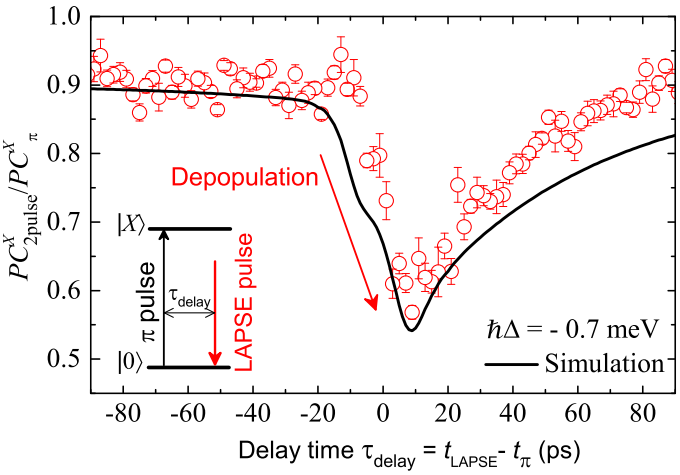

Figure 4.6: Time-dependent photo current measurement of the LAPSE process. The red circles show the time-integrated and normalized experimental photo current signal of a two pulse experiment, where a QD is first inverted by a resonant π-pulse and then de-excited by a red-shifted control pulse after a delay time τ_{delay} (c.f. the level diagram). The phonon-assisted depopulation of the exciton state becomes visible by the sharp decrease of the signal for small delay times. The solid black line shows the results of corresponding path-integral simulations, that phenomenologically account for the tunneling relaxation which is due to an external bias voltage. This figure is taken from *pub 7* with the kind permission by the authors.

is studied as a function of the delay time and the pulses might strongly overlap for short delays. The lifetime of the created hole is much longer than that of the electron [127, 128] and in fact is much longer than the averaging time of the time-integrated photo current measurements. Therefore, the tunneling process can be described by an incoherent phenomenological transition of the exciton state to a stable third state $|h\rangle$, where the electron has tunneled out and only the hole remains within the QD. The hole state $|h\rangle$ is not coupled to the optical field due to the spin selection rules and the Pauli blocking of the remaining hole. Incorporating this additional process in the path-integral calculations for the dynamics of the optically driven QD is made possible by the methodical advancement that enables a combined treatment of Hamiltonian and non-Hamiltonian dynamics within the path-integral method described in *pub 1*.

Fig. 4.6 shows the photo current signal as a function of the delay time between the pulses including negative delay times, where the control pulse is applied before the π-pulse. The signal is normalized to the photo current obtained by a single π-pulse as it is described in *pub 7*. The sharp decrease of the signal for small positive delays indicates the depopulation of the QD state on a timescale of about 20 ps. The theoretically predicted results for the measured signal, which are shown by the black solid line, are in very good agreement with the measurements and provide a strong indication for the validity of the modeling and the correct incorporation of the non-Hamiltonian dynamics within the path-integral formalism. In *pub 7*, the LAPSE-process is also studied for different detunings and a fixed delay time of the control pulse. The corresponding data shows a broad spectral feature that indicates the depopulation of the exciton state in full agreement with the theory.

In a similar experiment that addresses the LAPSE process in *pub 8*, the initial inversion of the QD is achieved by phonon-assisted processes using a strong blue-shifted pulse instead of the resonant π-pulse. This demonstrates a purely phonon-assisted switching between the ground and the exciton state, which offers the advantage of not requiring any resonant excitation of the QD. The measured results are again in a good agreement with the path-integral simulations. Moreover, in *pub 8* the phonon-assisted exciton preparation protocol is analyzed for different temperatures. An increased temperature has two different effects on the QD dynamics. First, it increases the efficiency of the phonon-induced relaxation. Second, at higher temperatures phonon absorption processes become more frequent and thus the upper dressed state is occupied with a larger probability when a thermal distribution is reached. This typically implies a reduced occupation of the exciton state for increased temperatures. However, in the measurements it is found that the exciton occupation becomes larger for rising temperatures. In agreement with corresponding simulations, this can be traced back to the relatively small pulse area used in the experiments. A small driving strength prevents a complete thermalization within the dressed state basis and thus the temperature-induced enhancement of the relaxation rate, and not the altered thermal distribution, is decisive for the final exciton occupation. This is also related to the fact that the phonon coupling becomes dynamically enhanced by the optical driving, which is termed as dynamic vibronic coupling (DVC) in *pub 8*. Finally, *pub 8* shows experimentally that the exciton state prepared by the phonon-assisted process is incoherent, i.e. the phase of the exciton is not determined by the phase of the laser and concludes that the process is spin-preserving.

The studies of these different aspects and parameter dependencies of the phonon-assisted state manipulation process provide further evidence that a solid understanding of the underlying dynamics has been achieved. The inclusion of phenomenological tunneling effects in *pub 7* and *pub 8* and the comparison with the corresponding experimental data serves as an excellent confirmation of the functionality of the extended path-integral formalism presented in *pub 1*.

5 Temperature dependence of strong coupling in dot-cavity systems

The strong coupling regime in cavity quantum electrodynamics (cQED) [129] is characterized by a reversible energy exchange between an optical cavity mode and an atom-like emitter. Compared to the weak coupling regime, such a coherent interaction is possible if the light-matter coupling strength exceeds the influence of dephasing processes like irreversible spontaneous emission and photon losses of the reflective cavity. The realization of strongly coupled cQED systems is important for many applications in quantum information processing [30, 130, 131], including quantum networks [132, 133] and quantum computation [10, 134], and offers the excellent possibility to study fundamental aspects of quantum physics like the quantum-classical boundary [135, 136].

While early studies were focused on free atoms, today strongly coupled systems can also be integrated in the solid-state environment using QDs [43, 44, 137–139], which is highly desirable in view of the abovementioned applications. This advancement has become possible mostly due to drastic improvements of the quality factors and the decreased volume of modern optical cavities [140, 141]. The reduced cavity loss rates also imply that the phonon-induced dephasing, which is inevitable in a crystal surrounding, plays an increasingly important role for the achievement of the strong coupling regime. Especially at elevated temperatures, where the phonon coupling becomes more efficient, this dephasing can diminish the timescale in which a coherent exchange of energy between the emitter and the cavity is possible. To make practical use of cQED systems, it is therefore crucial to gain a profound understanding of the temperature dependence of strong coupling effects.

The occurrence of strong coupling leads to an anti-crossing of the energy levels of the excited emitter state and the interacting cavity mode, which is formally analogous to the anti-crossing of the laser dressed states shown in Fig. 2.2. The anti-crossing can be quantified by the energetic difference of the coupled eigenstates at resonance, the so called vacuum Rabi splitting (VRS) [142]. In different theoretical studies [67, 107, 143, 144] it has been found that the phonon-interaction of QDs is expected to result in a temperature-dependent decrease of the VRS and can eventually lead to a transition to the weak coupling regime, where no VRS can be measured. The temperature-dependent reduction of the VRS is directly related to the well known phonon-induced renormalization of the Rabi frequency of laser-driven QDs [79–81]. The

experimental verification of a decreasing VRS is complicated by additional temperature dependences of the cavity mode energy and the excitonic transition of the QD, but nonetheless, could be largely realized [68, 145, 146]. Notably, in Ref. [146] an increased range of temperatures has been investigated by tuning the QD in resonance with the cavity mode using an external electric field, which made it possible to show the decrease of the VRS up to the transition to the weak coupling regime at about 40 K.

The studies presented in *pub 9* make further contributions to this active discussion of the temperature dependence of strong coupling effects. The investigations have been realized in collaboration with the experimental group led by Prof. Reitzenstein at Technische Universität Berlin, which provided a comprehensive set of experimental data containing the VRS of a very large number of strongly coupled QDs at different temperatures. In these measurements it was not possible to keep a single QD in resonance in an extended temperature range. Therefore a statistical approach, that uses the recorded VRS of QDs with similar properties at different temperatures, is applied to analyze the QD ensemble. By utilizing this method, it is shown that due to a peculiarity of the QDs under study, which is related to their large lateral extension, the phonon-induced decrease of the VRS can be overcompensated by an increase of the light-matter coupling strength at higher temperatures. This finding is supported by extensive theoretical calculations, which account for both phonon-induced pure dephasing and cavity losses. The simulations assume a temperature-dependent optical coupling strength that is directly taken from measurements. Because the extension of the path-integral formalism to non-Hamiltonian dynamics presented in *pub 1* was not available at the time of these studies, the photon losses are taken into account using the hybrid approach introduced in Ref. [62] and discussed in Section 3.2. As a major result of *pub 9*, the overcompensation of the phonon-induced decrease of the VRS is identified as a rare mechanism that allows strong coupling of QD-cavity systems in an unexpectedly large temperature range. This can considerably increase the applicability of these systems and has not been anticipated before.

Bibliography

[1] L. Jacak, P. Hawrylak and A. Wójs. *Quantum dots* (Springer, Berlin, 1998).

[2] D. Bimberg, M. Grundmann and N.N. Ledencov. *Quantum dot heterostructures* (Wiley, Chichester, 1999).

[3] F. Rossi (Ed.). *Semiconductor macroatoms* (Imperial College Press, London, 2005).

[4] P. Michler. *Single Semiconductor Quantm Dots* (Springer, Berlin, 2009).

[5] D. Loss and D.P. DiVincenzo. *Quantum computation with quantum dots.* Phys. Rev. A **57**, 120–126 (1998).

[6] E. Biolatti, R.C. Iotti, P. Zanardi and F. Rossi. *Quantum information processing with semiconductor macroatoms.* Phys. Rev. Lett. **85**, 5647 (2000).

[7] X.Q. Li, Y.W. Wu, D. Steel, D. Gammon, T.H. Stievater, D.S. Katzer, D. Park, C. Piermarocchi and L.J. Sham. *An all-optical quantum gate in a semiconductor quantum dot.* Science **301**, 809 (2003).

[8] M. Veldhorst, J.C.C. Hwang, C.H. Yang, A.W. Leenstra, B. de Ronde, J.P. Dehollain, J.T. Muhonen, F.E. Hudson, K.M. Itoh, A. Morello and A.S. Dzurak. *An addressable quantum dot qubit with fault-tolerant control fidelity.* Nature Nanotechnology **9**, 981 (2014).

[9] Y. Kodriano, E.R. Schmidgall, Y. Benny and D. Gershoni. *Optical control of single excitons in semiconductor quantum dots.* Semicond. Sci. Technol. **29**, 053001 (2014).

[10] M.A. Nielsen and I. Chuang. *Quantum computation and quantum information* (Cambridge University Press, Cambridge, 2000).

[11] J. Jones. *Quantum information, computation and communication* (Cambridge Univ. Press, Cambridge, 2012).

[12] L.K. Grover. *Quantum Mechanics Helps in Searching for a Needle in a Haystack.* Phys. Rev. Lett. **79**, 325–328 (1997).

[13] J.I. Cirac and P. Zoller. *Quantum Computations with Cold Trapped Ions.* Phys. Rev. Lett. **74**, 4091–4094 (1995).

[14] M.V.G. Dutt, L. Childress, L. Jiang, E. Togan, J. Maze, F. Jelezko, A.S. Zibrov, P.R. Hemmer and M.D. Lukin. *Quantum Register Based on Individual Electronic and Nuclear Spin Qubits in Diamond.* Science **316**, 1312–1316 (2007).

[15] T.D. Ladd, F. Jelezko, R. Laflamme, Y. Nakamura, C. Monroe and J.L. O'Brien. *Quantum computers.* Nature **464**, 45 (2010).

[16] P. Michler, A. Kiraz, C. Becher, W.V. Schoenfeld, P. Petroff, L.D. Zhang, E. Hu and A. Imamoğlu. *A quantum dot single-photon turnstile device.* Science **290**, 2282 (2000).

[17] D. Press, S. Götzinger, S. Reitzenstein, C. Hofmann, A. Löffler, M. Kamp, A. Forchel and Y. Yamamoto. *Photon antibunching from a single quantum-dot-microcavity system in the strong coupling regime.* Phys. Rev. Lett. **98**, 117402 (2007).

[18] A. Ulhaq, S. Weiler, S.M. Ulrich, R. Roßbach, M. Jetter and P. Michler. *Cascaded single-photon emission from the Mollow triplet sidebands of a quantum dot.* Nature Photonics **6**, 238 (2012).

[19] K.D. Jöns, P. Atkinson, M. Müller, M. Heldmaier, S.M. Ulrich, O.G. Schmidt and P. Michler. *Triggered indistinguishable single photons with narrow line widths from site-controlled quantum dots.* Nano Lett. **13**, 126 (2013).

[20] Y.M. He, Y.J. Wei, D. Wu, M. Atatüre, C. Schneider, S. Höfling, M. Kamp, C.Y. Lu and J.W. Pan. *On-demand semiconductor single-photon source with near-unity indistinguishability.* Nature Nanotech. **8**, 213–217 (2013).

[21] Y.J. Wei, Y.M. He, M.C. Chen, Y.N. Hu, Y. He, D. Wu, C. Schneider, M. Kamp, S. Höfling, C.Y. Lu and J.W. Pan. *Deterministic and robust generation of single photons from a single quantum dot with 99.5% indistinguishability using adiabatic rapid passage.* Nano Letters **14**, 6515–6519 (2014).

[22] D. Heinze, D. Breddermann, A. Zrenner and S. Schumacher. *A quantum dot single-photon source with on-the-fly all-optical polarization control and timed emission.* Nature Comm. **6**, 8473 (2015).

[23] O. Benson, C. Santori, M. Pelton and Y. Yamamoto. *Regulated and entangled photons from a single quantum dot.* Phys. Rev. Lett. **84**, 2513–2516 (2000).

[24] E. Moreau, I. Robert, L. Manin, V. Thierry-Mieg, J.M. Gérard and I. Abram. *Quantum cascade of photons in semiconductor quantum dots.* Phys. Rev. Lett. **87**, 183601 (2001).

[25] T.M. Stace, G.J. Milburn and C.H.W. Barnes. *Entangled two-photon source using biexciton emission of an asymmetric quantum dot in a cavity.* Phys. Rev. B **67**, 085317 (2003).

[26] R. Stevenson, R.J. Young, P. Atkinson, K. Cooper, D.A. Ritchie and A.J. Shields. *A semiconductor source of triggered entangled photon pairs.* Nature **439**, 179 (2006).

[27] N. Akopian, N.H. Lindner, E. Poem, Y. Berlatzky, J. Avron, D. Gershoni, B.D. Gerardot and P.M. Petroff. *Entangled photon pairs from semiconductor quantum dots.* Phys. Rev. Lett. **96**, 130501 (2006).

[28] A. Dousse, J. Suffczyński, A. Beveratos, O. Krebs, A. Lemaître, I. Sagnes, J. Bloch, P. Voisin and P. Senellart. *Ultrabright source of entangled photon pairs.* Nature **466**, 217 (2010).

[29] M. Müller, S. Bounouar, K.D. Jöns, M. Glässl and P. Michler. *On-demand generation of indistinguishable polarization-entangled photon pairs.* Nature Photonics **8**, 224–228 (2014).

[30] D. Bouwmeester, A.K. Ekert and A. Zeilinger. *The physics of quantum information* (Springer, Berlin, 2000).

[31] A.K. Ekert. *Quantum cryptography based on bell theorem.* Phys. Rev. Lett. **67**, 661 (1991).

[32] N. Gisin, G. Ribordy, W. Tittel and H. Zbinden. *Quantum cryptography.* Rev. Mod. Phys. **74**, 145 (2002).

[33] D. Bimberg. *Quantum dots for lasers, amplifiers and computing.* J. Phys. D: Appl. Phys. **38**, 2055 (2005).

[34] S. Strauf and F. Jahnke. *Single quantum dot nanolaser.* Laser and Photonics Reviews **5**, 607–633 (2011).

[35] J. Ohtsubo. *Semiconductor lasers* (Springer, Berlin, 2013).

[36] Q. Sun, Y. Wang, L. Li, D. Wang, T. Zhu, J. Xu, C. Yang and Y. Li. *Bright, multicoloured light-emitting diodes based on quantum dots.* Nature Photonics **1**, 717–722 (2007).

[37] X. Wu, H. Liu, J. Liu, K.N. Haley, J.A. Treadway, J.P. Larson, N. Ge, F. Peale and M.P. Bruchez. *Immunofluorescent labeling of cancer marker Her2 and other cellular targets with semiconductor quantum dots.* Nature Biotechnology **21**, 41–46 (2003).

[38] I.L. Medintz, H.T. Uyeda, E.R. Goldman and H. Mattoussi. *Quantum dot bioconjugates for imaging, labelling and sensing.* Nature Materials **4**, 435–446 (2005).

[39] T.H. Stievater, X. Li, D.G. Steel, D. Gammon, D.S. Katzer, D. Park, C. Piermarocchi and L.J. Sham. *Rabi oscillations of excitons in single quantum dots.* Phys. Rev. Lett. **87**, 133603 (2001).

[40] H. Kamada, H. Gotoh, J. Temmyo, T. Takagahara and H. Ando. *Exciton Rabi oscillation in a single quantum dot.* Phys. Rev. Lett. **87**, 246401 (2001).

[41] A. Zrenner, E. Beham, S. Stufler, F. Findeis, M. Bichler and G. Abstreiter. *Coherent properties of a two-level system based on a quantum-dot photodiode.* Nature **418**, 612 (2002).

[42] P. Borri, W. Langbein, S. Schneider, U. Woggon, R.L. Sellin, D. Ouyang and D. Bimberg. *Rabi oscillations in the excitonic ground-state transition of InGaAs quantum dots.* Phys. Rev. B **66**, 081306 (2002).

[43] J.P. Reithmaier, G. Sek, A. Löffler, C. Hofmann, S. Kuhn, S. Reitzenstein, L.V. Keldysh, V.D. Kulakovskii, T.L. Reinecke and A. Forchel. *Strong coupling in a single quantum dot-semiconductor microcavity system.* Nature **432**, 197 (2004).

[44] E. Peter, P. Senellart, D. Martrou, A. Lemaître, J. Hours, J.M. Gérard and J. Bloch. *Exciton-Photon Strong-Coupling Regime for a Single Quantum Dot Embedded in a Microcavity.* Phys. Rev. Lett. **95**, 067401 (2005).

[45] U. Weiss. *Quantum dissipative systems* (World Scientific, Singapore, 1999).

[46] H.P. Breuer and F. Petruccione. *The theory of open quantum systems* (Oxford University Press, Oxford, 2002).

[47] S. Hughes and H.J. Carmichael. *Phonon-mediated population inversion in a semiconductor quantum-dot cavity system.* New Journal of Physics **15**, 053039 (2013).

[48] P.L. Ardelt, L. Hanschke, K.A. Fischer, K. Müller, A. Kleinkauf, M. Koller, A. Bechtold, T. Simmet, J. Wierzbowski, H. Riedl, G. Abstreiter and J.J. Finley. *Dissipative preparation of the exciton and biexciton in self-assembled quantum dots on picosecond time scales.* Phys. Rev. B **90**, 241404 (2014).

[49] K. Müller, K.A. Fischer, A. Rundquist, C. Dory, K.G. Lagoudakis, T. Sarmiento, Y.A. Kelaita, V. Borish and J. Vučković. *Ultrafast Polariton-Phonon Dynamics of Strongly Coupled Quantum Dot-Nanocavity Systems.* Phys. Rev. X **5**, 031006 (2015).

[50] A. Vagov, M.D. Croitoru, V.M. Axt, T. Kuhn and F.M. Peeters. *Nonmonotonic field dependence of damping and reappearance of Rabi oscillations in quantum dots.* Phys. Rev. Lett. **98**, 227403 (2007).

[51] A.J. Ramsay, A.V. Gopal, E.M. Gauger, A. Nazir, B.W. Lovett, A.M. Fox and M.S. Skolnick. *Damping of exciton (Rabi) rotations by acoustic phonons in optically excited InGaAs/GaAs quantum dots.* Phys. Rev. Lett. **104**, 017402 (2010).

[52] S. Ates, S.M. Ulrich, A. Ulhaq, S. Reitzenstein, A. Löffler, S. Höfling, A. Forchel and P. Michler. *Non-resonant dot-cavity coupling and its potential for resonant single-quantum-dot spectroscopy.* Nature Photonics **3**, 724 (2009).

[53] H.J. Carmichael. *Statistical Methods in Quantum Optics 1: Master Equations and Fokker-Planck Equations* (Springer, Berlin, 1999).

[54] T. Takagahara. *Theory of exciton dephasing in semiconductor quantum dots.* Phys. Rev. B **60**, 2638 (1999).

[55] L. Besombes, K. Kheng, L. Marsal and H. Mariette. *Acoustic phonon broadening mechanism in single quantum dot emission.* Phys. Rev. B **63**, 155307 (2001).

[56] G.D. Mahan. *Many-particle physics* (Plenum Press, New York, 1990).

[57] N. Makri and D. Makarov. *Tensor propagator for iterative quantum time evolution of reduced density matrices. I. Theory.* J. Chem. Phys. **102**, 4600 (1995).

[58] N. Makri and D. Makarov. *Tensor propagator for iterative quantum time evolution of reduced density matrices. II. Numerical methodology.* J. Chem. Phys. **102**, 4611 (1995).

[59] R.P. Feynman and F. Vernon. *The theory of a general quantum system interacting with a linear dissipative system.* Ann. Phys. (NY) **24**, 118 (1963).

[60] A. Vagov, M.D. Croitoru, V.M. Axt, T. Kuhn and F.M. Peeters. *High pulse area undamping of Rabi oscillations in quantum dots coupled to phonons.* Phys. Status Solidi B **243**, 2233 (2006).

[61] A. Vagov, M.D. Croitoru, M. Glässl, V.M. Axt and T. Kuhn. *Real-time path integrals for quantum dots: Quantum dissipative dynamics with superohmic environment coupling.* Phys. Rev. B **83**, 094303 (2011).

[62] A. Vagov, M. Glässl, M.D. Croitoru, V.M. Axt and T. Kuhn. *Competition between pure dephasing and photon losses in the dynamics of a dot-cavity system.* Phys. Rev. B **90**, 075309 (2014).

[63] A. Nazir and D.P.S. McCutcheon. *Modelling exciton–phonon interactions in optically driven quantum dots.* Journal of Physics: Condensed Matter **28**, 103002 (2016).

[64] M. Glässl, M.D. Croitoru, A. Vagov, V.M. Axt and T. Kuhn. *Impact of dark superpositions on the relaxation dynamics of an optically driven exciton-biexciton quantum dot system.* Phys. Rev. B **85**, 195306 (2012).

[65] M. Glässl and V.M. Axt. *Polarization dependence of phonon influences in exciton-biexciton quantum dot systems.* Phys. Rev. B **86**, 245306 (2012).

[66] F. Troiani, J.I. Perea and C. Tejedor. *Analysis of the photon indistinguishability in incoherently excited quantum dots.* Phys. Rev. B **73**, 035316 (2006).

[67] P. Kaer, T.R. Nielsen, P. Lodahl, A.P. Jauho and J. Mørk. *Non-Markovian model of photon-assisted dephasing by electron-phonon interactions in a coupled quantum-dot-cavity system.* Phys. Rev. Lett. **104**, 157401 (2010).

[68] Y.J. Wei, Y. He, Y.M. He, C.Y. Lu, J.W. Pan, C. Schneider, M. Kamp, S. Höfling, D.P.S. McCutcheon and A. Nazir. *Temperature-Dependent Mollow Triplet Spectra from a Single Quantum Dot: Rabi Frequency Renormalization and Sideband Linewidth Insensitivity.* Phys. Rev. Lett. **113**, 097401 (2014).

[69] D. Leonard, M. Krishnamurthy, C.M. Reaves, S.P. Denbaars and P.M. Petroff. *Direct formation of quantum sized dots from uniform coherent islands of InGaAs on GaAs surfaces.* Applied Physics Letters **63**, 3203–3205 (1993).

[70] J.Y. Marzin, J.M. Gérard, A. Izraël, D. Barrier and G. Bastard. *Photoluminescence of Single InAs Quantum Dots Obtained by Self-Organized Growth on GaAs.* Phys. Rev. Lett. **73**, 716–719 (1994).

[71] Q. Xie, A. Madhukar, P. Chen and N.P. Kobayashi. *Vertically Self-Organized InAs Quantum Box Islands on GaAs(100).* Phys. Rev. Lett. **75**, 2542–2545 (1995).

[72] S. Schmitt-Rink, D.A.B. Miller and D.S. Chemla. *Theory of the linear and nonlinear optical properties of semiconductor microcrystallites.* Phys. Rev. B **35**, 8113 (1987).

[73] S. Bounouar, M. Müller, A.M. Barth, M. Glässl, V.M. Axt and P. Michler. *Phonon-assisted robust and deterministic two-photon biexciton preparation in a quantum dot.* Phys. Rev. B **91**, 161302 (2015).

[74] T. Takagahara. *Biexciton states in semiconductor quantum dots and their nonlinear optical properties.* Phys. Rev. B **39**, 10206–10231 (1989).

[75] G. Bacher, R. Weigand, J. Seufert, V.D. Kulakovskii, N.A. Gippius, A. Forchel, K. Leonardi and D. Hommel. *Biexciton versus Exciton Lifetime in a Single Semiconductor Quantum Dot.* Phys. Rev. Lett. **83**, 4417–4420 (1999).

[76] L. Allen and J.H. Eberly. *Optical resonance and two-level atoms* (John Wiley and Sons, New York, 1975).

[77] M. Glässl, A. Vagov, S. Lüker, D.E. Reiter, M.D. Croitoru, P. Machnikowski, V.M. Axt and T. Kuhn. *Long-time dynamics and stationary nonequilibrium of an optically driven strongly confined quantum dot coupled to phonons.* Phys. Rev. B **84**, 195311 (2011).

[78] B. Krummheuer, V.M. Axt and T. Kuhn. *Theory of pure dephasing and the resulting absorption lineshape of semiconductor quantum dots.* Phys. Rev. B **65**, 195313 (2002).

[79] A.J. Ramsay, T.M. Godden, S.J. Boyle, E.M. Gauger, A. Nazir, B.W. Lovett, A.M. Fox and M.S. Skolnick. *Phonon-induced Rabi-frequency renormalization of optically driven single InGaAs/GaAs quantum dots.* Phys. Rev. Lett. **105**, 177402 (2010).

[80] J. Förstner, C. Weber, J. Danckwerts and A. Knorr. *Phonon-assisted damping of Rabi oscillations in semiconductor quantum dots.* Phys. Rev. Lett. **91**, 127401 (2003).

[81] A. Krügel, V.M. Axt, T. Kuhn, P. Machnikowski and A. Vagov. *The role of acoustic phonons for Rabi oscillations in semiconductor quantum dots.* Appl. Phys. B **81**, 897 (2005).

[82] P. Machnikowski and L. Jacak. *Resonant nature of phonon-induced damping of Rabi oscillations in quantum dots.* Phys. Rev. B **69**, 193302 (2004).

[83] L. Monniello, C. Tonin, R. Hostein, A. Lemaitre, A. Martinez, V. Voliotis and R. Grousson. *Excitation-Induced Dephasing in a Resonantly Driven* InAs/GaAs *Quantum Dot.* Phys. Rev. Lett. **111**, 026403 (2013).

[84] S.M. Ulrich, S. Ates, S. Reitzenstein, A. Löffler, A. Forchel and P. Michler. *Dephasing of triplet-sideband optical emission of a resonantly driven InAs/GaAs quantum dot inside a microcavity.* Phys. Rev. Lett. **106**, 247402 (2011).

[85] C. Roy and S. Hughes. *Phonon-dressed Mollow triplet in the regime of cavity quantum electrodynamics: Excitation-induced dephasing and nonperturbative cavity feeding effects.* Phys. Rev. Lett. **106**, 247403 (2011).

[86] B. Krummheuer, V.M. Axt, T. Kuhn, I. D'Amico and F. Rossi. *Pure dephasing and phonon dynamics in GaAs- and GaN-based quantum dot structures: Interplay between material parameters and geometry.* Phys. Rev. B **71**, 235329 (2005).

[87] M. Glässl, M.D. Croitoru, A. Vagov, V.M. Axt and T. Kuhn. *Influence of the pulse shape and the dot size on the decay and reappearance of Rabi rotations in laser driven quantum dots.* Phys. Rev. B **84**, 125304 (2011).

[88] A. Vagov, V.M. Axt, T. Kuhn, W. Langbein, P. Borri and U. Woggon. *Nonmonotonous temperature dependence of the initial decoherence in quantum dots.* Phys. Rev. B **70**, 201305 (2004).

[89] A.J. Leggett, S. Chakravarty, A.T. Dorsey, M.P.A. Fisher, A. Garg and W. Zwerger. *Dynamics of the dissipative two-state system.* Rev. Mod. Phys. **59**, 1 (1987).

[90] T. Itakura and Y. Tokura. *Dephasing due to background charge fluctuations.* Phys. Rev. B **67**, 195320 (2003).

[91] P. Borri, W. Langbein, S. Schneider, U. Woggon, R.L. Sellin, D. Ouyang and D. Bimberg. *Ultralong dephasing time in InGaAs quantum dots.* Phys. Rev. Lett. **87**, 157401 (2001).

[92] M. Bayer and A. Forchel. *Temperature dependence of the exciton homogeneous linewidth in InGaAs/GaAs self-assembled quantum dots.* Phys. Rev. B **65**, 041308 (2002).

[93] N. Makri and D. Makarov. *Path-integrals for dissipative systems by tensor multiplication - condensed-phase quantum dynamics for arbitrarily long-time.* Chem. Phys. Lett. **221**, 482 (1994).

[94] R.P. Feynman and A.R. Hibbs. *Quantum mechanics and path integrals* (McGraw-Hill, New York, 1965).

[95] H. Kleinert. *Path integrals in quantum mechanics, statistics, polymer physics, and financial markets* (World Scientific, Singapore, 2006).

[96] E. Barnes and S. Das Sarma. *Analytically Solvable Driven Time-Dependent Two-Level Quantum Systems.* Phys. Rev. Lett. **109**, 060401 (2012).

[97] A. Vagov, V.M. Axt and T. Kuhn. *Electron-phonon dynamics in optically excited quantum dots: Exact solution for multiple ultrashort laser pulses.* Phys. Rev. B **66**, 165312 (2002).

[98] V.M. Axt, P. Machnikowski and T. Kuhn. *Reducing decoherence of the confined exciton state in a quantum dot by pulse-sequence control.* Phys. Rev. B **71**, 155305 (2005).

[99] A. Krügel, V.M. Axt and T. Kuhn. *Back action of nonequilibrium phonons on the optically induced dynamics in semiconductor quantum dots.* Phys. Rev. B **73**, 035302 (2006).

[100] A. Debnath, C. Meier, B. Chatel and T. Amand. *Chirped laser excitation of quantum dot excitons coupled to a phonon bath.* Phys. Rev. B **86**, 161304 (2012).

[101] P. Kaer, P. Lodahl, A.P. Jauho and J. Mørk. *Microscopic theory of indistinguishable single-photon emission from a quantum dot coupled to a cavity: The role of non-Markovian phonon-induced decoherence.* Phys. Rev. B **87**, 081308 (2013).

[102] N. Renaud and F.C. Grozema. *Cooperative biexciton generation and destructive interference in coupled quantum dots using adiabatic rapid passage.* Phys. Rev. B **90**, 165307 (2014).

[103] R. Manson, K. Roy-Choudhury and S. Hughes. *Polaron master equation theory of pulse-driven phonon-assisted population inversion and single-photon emission from quantum-dot excitons.* Phys. Rev. B **93**, 155423 (2016).

[104] A. Vagov, V.M. Axt and T. Kuhn. *Impact of pure dephasing on the nonlinear optical response of single quantum dots and dot ensembles.* Phys. Rev. B **67**, 115338 (2003).

[105] E. Peter, J. Hours, P. Senellart, A. Vasanelli, A. Cavanna, J. Bloch and J.M. Gérard. *Phonon sidebands in exciton and biexciton emission from single GaAs quantum dots.* Phys. Rev. B **69**, 041307 (2004).

[106] D.P.S. McCutcheon. *Optical signatures of non-Markovian behavior in open quantum systems.* Phys. Rev. A **93**, 022119 (2016).

[107] M. Glässl, L. Sörgel, A. Vagov, M.D. Croitoru, T. Kuhn and V.M. Axt. *Interaction of a quantum-dot cavity system with acoustic phonons: Stronger light-matter coupling can reduce the visibility of strong coupling effects.* Phys. Rev. B **86**, 035319 (2012).

[108] S. Mukamel. *Principles of nonlinear optical spectroscopy.* 1st edn. (Oxford University Press, New York, 1995).

[109] P. Kaer, T.R. Nielsen, P. Lodahl, A.P. Jauho and J. Mørk. *Microscopic theory of phonon-induced effects on semiconductor quantum dot decay dynamics in cavity QED.* Phys. Rev. B **86**, 085302 (2012).

[110] F. Troiani, J.I. Perea and C. Tejedor. *Cavity-assisted generation of entangled photon pairs by a quantum-dot cascade decay.* Phys. Rev. B **74**, 235310 (2006).

[111] A. Carmele and A. Knorr. *Analytical solution of the quantum-state tomography of the biexciton cascade in semiconductor quantum dots: Pure dephasing does not affect entanglements.* Phys. Rev. B **84**, 075328 (2011).

[112] M.B. Harouni. *Phonon impacts on entangled photon pair generation from the biexciton cascade in a quantum dot: phonon coherent state representation.* Laser Physics **24**, 115202 (2014).

[113] S. Lüker, K. Gawarecki, D.E. Reiter, A. Grodecka-Grad, V.M. Axt, P. Machnikowski and T. Kuhn. *Influence of acoustic phonons on the optical control of quantum dots driven by adiabatic rapid passage.* Phys. Rev. B **85**, 121302 (2012).

[114] C. Roy and S. Hughes. *Polaron master equation theory of the quantum-dot Mollow triplet in a semiconductor cavity-QED system.* Phys. Rev. B **85**, 115309 (2012).

[115] F. Hargart, M. Müller, K. Roy-Choudhury, S.L. Portalupi, C. Schneider, S. Höfling, M. Kamp, S. Hughes and P. Michler. *Cavity-enhanced simultaneous dressing of quantum dot exciton and biexciton states.* Phys. Rev. B **93**, 115308 (2016).

[116] E.B. Flagg, S.V. Polyakov, T. Thomay and G.S. Solomon. *Dynamics of Nonclassical Light from a Single Solid-State Quantum Emitter.* Phys. Rev. Lett. **109**, 163601 (2012).

[117] T. Huber, A. Predojević, D. Föger, G. Solomon and G. Weihs. *Optimal excitation conditions for indistinguishable photons from quantum dots.* New Journal of Physics **17**, 123025 (2015).

[118] S. Stufler, P. Machnikowski, P. Ester, M. Bichler, V.M. Axt, T. Kuhn and A. Zrenner. *Two photon Rabi oscillations in a single InGaAs quantum dot.* Phys. Rev. B **73**, 125304 (2006).

[119] E.R. Schmidgall, P.R. Eastham and R.T. Phillips. *Population inversion in quantum dot ensembles via adiabatic rapid passage.* Phys. Rev. B **81**, 195306 (2010).

[120] C.M. Simon, T. Belhadj, B. Chatel, T. Amand, P. Renucci, A. Lemaître, O. Krebs, P.A. Dalgarno, R.J. Warburton, X. Marie and B. Urbaszek. *Robust quantum dot exciton generation via adiabatic passage with frequency-swept optical pulses.* Phys. Rev. Lett. **106**, 166801 (2011).

[121] K. Gawarecki, S. Lüker, D.E. Reiter, T. Kuhn, M. Glässl, V.M. Axt, A. Grodecka-Grad and P. Machnikowski. *Dephasing in the adiabatic rapid passage in quantum dots: Role of phonon-assisted biexciton generation.* Phys. Rev. B **86**, 235301 (2012).

[122] A. Debnath, C. Meier, B. Chatel and T. Amand. *High-fidelity biexciton generation in quantum dots by chirped laser pulses.* Phys. Rev. B **88**, 201305 (2013).

[123] R. Mathew, E. Dilcher, A. Gamouras, A. Ramachandran, H.Y.S. Yang, S. Freisem, D. Deppe and K.C. Hall. *Subpicosecond adiabatic rapid passage on a single semiconductor quantum dot: Phonon-mediated dephasing in the strong-driving regime.* Phys. Rev. B **90**, 035316 (2014).

[124] J.S. Melinger, S.R. Gandhi, a. Hariharan, D. Goswami and W.S. Warren. *Adiabatic population transfer with frequency-swept laser pulses.* J. Chem. Phys. **101**, 6439–6454 (1994).

[125] A.J. Ramsay, T.M. Godden, S.J. Boyle, E.M. Gauger, A. Nazir, B.W. Lovett, A.V. Gopal, A.M. Fox and M.S. Skolnick. *Effect of detuning on the phonon induced dephasing of optically driven InGaAs/GaAs quantum dots.* J. Appl. Phys. **109**, 102415 (2011).

[126] P.E. Selbmann, M. Gulia, F. Rossi, E. Molinari and P. Lugli. *Coupled free-carrier and exciton relaxation in optically excited semiconductors.* Phys. Rev. B **54**, 4660–4673 (1996).

[127] A.J. Ramsay, S.J. Boyle, R.S. Kolodka, J.B.B. Oliveira, J. Skiba-Szymanska, H.Y. Liu, M. Hopkinson, A.M. Fox and M.S. Skolnick. *Fast Optical Preparation, Control, and Readout of a Single Quantum Dot Spin.* Phys. Rev. Lett. **100**, 197401 (2008).

[128] A.J. Brash, L.M.P.P. Martins, F. Liu, J.H. Quilter, A.J. Ramsay, M.S. Skolnick and A.M. Fox. *High-fidelity initialization of long-lived quantum dot hole spin qubits by reduced fine-structure splitting.* Phys. Rev. B **92**, 121301 (2015).

[129] S. Haroche and J. Raimond. *Exploring the quantum* (Oxford University Press, Oxford, 2006).

[130] S.B. Zheng and G.C. Guo. *Efficient Scheme for Two-Atom Entanglement and Quantum Information Processing in Cavity QED.* Phys. Rev. Lett. **85**, 2392–2395 (2000).

[131] H. Kim, R. Bose, T.C. Shen, G.S. Solomon and E. Waks. *A quantum logic gate between a solid-state quantum bit and a photon.* Nature Physics **7**, 373–377 (2013).

[132] J.I. Cirac, P. Zoller, H.J. Kimble and H. Mabuchi. *Quantum state transfer and entanglement distribution among distant nodes in a quantum network.* Phys. Rev. Lett. **78**, 3221 (1997).

[133] A. Reiserer and G. Rempe. *Cavity-based quantum networks with single atoms and optical photons.* Rev. Mod. Phys. **87**, 1379–1418 (2015).

[134] A. Imamoğlu, D.D. Awschalom, G. Burkard, D.P. DiVincenzo, D. Loss, M. Sherwin and A. Small. *Quantum Information Processing Using Quantum Dot Spins and Cavity QED.* Phys. Rev. Lett. **83**, 4204–4207 (1999).

[135] M. Brune, F. Schmidt-Kaler, A. Maali, J. Dreyer, E. Hagley, J. Raimond and S. Haroche. *Quantum Rabi oscillation: a direct test of field quantization in a cavity.* Phys. Rev. Lett. **76**, 1800 (1996).

[136] J.M. Raimond, M. Brune and S. Haroche. *Manipulating quantum entanglement with atoms and photons in a cavity.* Rev. Mod. Phys. **73**, 565–582 (2001).

[137] T. Yoshie, A. Scherer, J. Hendrickson, G. Khitrova, H.M. Gibbs, G. Rupper, C. Ell, O.B. Shchekin and D.G. Deppe. *Vacuum Rabi splitting with a single quantum dot in a photonic crystal nanocavity.* Nature **432**, 200–203 (2004).

[138] K. Hennessy, A. Badolato, M. Winger, D. Gerace, M. Atatüre, S. Gulde, S. Fält, E.L. Hu and A. Imamoğlu. *Quantum nature of a strongly coupled single quantum dot cavity system.* Nature **445**, 896 (2007).

[139] P. Lodahl, S. Mahmoodian and S. Stobbe. *Interfacing single photons and single quantum dots with photonic nanostructures.* Rev. Mod. Phys. **87**, 347–400 (2015).

[140] K. Aoki, D. Guimard, M. Nishioka, M. Nomura, S. Iwamoto and Y. Arakawa. *Coupling of quantum-dot light emission with a three-dimensional photonic-crystal nanocavity.* Nature Photonics **2**, 688–692 (2008).

[141] C. Schneider, P. Gold, S. Reitzenstein, S. Höfling and M. Kamp. *Quantum dot micropillar cavities with quality factors exceeding 250,000.* Applied Physics B **122**, 1–6 (2016).

[142] G. Khitrova, H.M. Gibbs, M. Kira, S.W. Koch and A. Scherer. *Vacuum Rabi splitting in semiconductors.* Nature Physics **2**, 81 (2006).

[143] I. Wilson-Rae and A. Imamoğlu. *Quantum dot cavity-QED in the presence of strong electron-phonon interactions.* Phys. Rev. B **65**, 235311 (2002).

[144] F. Milde, A. Knorr and S. Hughes. *Role of electron-phonon scattering on the vacuum Rabi splitting of a single-quantum dot and a photonic crystal nanocavity.* Phys. Rev. B **78**, 035330 (2008).

[145] Y. Ota, S. Iwamoto, N. Kumagai and Y. Arakawa. *Impact of electron-phonon interactions on quantum-dot cavity quantum electrodynamics.* arXiv:0908.0788 (2009).

[146] A. Laucht. *Semiconductor Quantum Optics with Tailored Photonic Nanostructures* (Walter Schottky Institut, Technische Universität München, 2011).

Acknowledgment

Foremost, I would like to thank my advisor **Prof. Martin Axt**, who has constantly supported me by taking his time for many great discussions and sharing with me his broad experience in scientific research. His clear explanations have helped me to progress many times and his profound understanding of physics and his deep passion to truly gain new knowledge have been a continuous source of inspiration.

I also had the pleasant opportunity to collaborate with many other researchers that I would like to thank. **Martin Gläßl** made every effort to introduce me to the research projects and methodology related to laser-driven quantum dots discussed in our group. He has also been a very good tutor during my years as a physics student. I also want to thank **Lutz Sörgel** for all the nice and helpful discussions we had during our studies, **Andre Brand** who has been a great office colleague the last years, **Alexei Vagov** for his collaboration in the path-integral projects and all other present and former members of our group for the enjoyable and friendly atmosphere. I am also thankful for the very kind collaboration, the interesting discussions and the excellent measurements performed by my experimental colleagues **Prof. Stephan Reitzenstein**, **Anna Musial** and **Max Strauß** from TU Berlin, **John Quilter**, **Feng Liu** and **Alistair Brash** from the University of Sheffield and **Prof. Peter Michler**, **Samir Bounouar** and **Markus Müller** from the University of Stuttgart. I am grateful for the collaboration with the team from University of Münster especially **Prof. Tilmann Kuhn**, **Doris Reiter** and **Sebastian Lüker** and the trusted technical support by **Markus Hilt** at the University of Bayreuth. I also acknowledge the financial support by the Deutsche Forschungsgemeinschaft via Project No. AX 17/7-1.

Finally, I would like to thank my family and my girlfriend for their love and endless support without which this thesis could certainly not have been realized.

Erklärung

Hiermit versichere ich an Eides statt, dass ich die vorliegende Arbeit selbständig verfasst und keine anderen als die angegebenen Quellen und Hilfsmittel verwendet habe.

Weiterhin erkläre ich hiermit, dass ich bisher keinen anderweitigen Promotionsversuch unternommen habe und Hilfe von gewerblichen Promotionsberatern bzw. -vermittlern weder bisher in Anspruch genommen habe noch künftig in Anspruch nehmen werde.

Bayreuth, den 22. Oktober 2017

Andreas Barth

Part II

Publications

List of included publications as referred to in this thesis:

pub 1 A. M. Barth, A. Vagov and V. M. Axt,
Phys. Rev. B **94**, 125439 (2016):
Path-integral description of combined Hamiltonian and non-Hamiltonian dynamics in quantum dissipative systems.

pub 2 M. Glässl, A. M. Barth, K. Gawarecki, P. Machnikowski, M. D. Croitoru, S. Lüker, D. E. Reiter, T. Kuhn and V. M. Axt,
Phys. Rev. B **87**, 085303 (2013):
Biexciton state preparation in a quantum dot via adiabatic rapid passage: comparison between two control protocols and impact of phonon-induced dephasing.

pub 3 M. Glässl, A. M. Barth and V. M. Axt,
Phys. Rev. Lett. **110**, 147401 (2013):
Proposed Robust and High-Fidelity Preparation of Excitons and Biexcitons in Semiconductor Quantum Dots Making Active Use of Phonons.

pub 4 J. H. Quilter, A. J. Brash, F. Liu, M. Glässl, A. M. Barth, V. M. Axt, A. J. Ramsay, M. S. Skolnick and A. M. Fox,
Phys. Rev. Lett. **114**, 137401 (2015):
Phonon-Assisted Population Inversion of a Single InGaAs/GaAs Quantum Dot by Pulsed Laser Excitation.

pub 5 S. Bounouar, M. Müller, A. M. Barth, M. Glässl, V. M. Axt and P. Michler,
Phys. Rev. B **91**, 161302(R) (2015):
Phonon-assisted robust and deterministic two-photon biexciton preparation in a quantum dot.

pub 6 A. M. Barth, S. Lüker, A. Vagov, D. E. Reiter, T. Kuhn and V. M. Axt,
Phys. Rev. B **94**, 045306 (2016):
Fast and selective phonon-assisted state preparation of a quantum dot by adiabatic undressing.

pub 7 F. Liu, L. M. P. Martins, A. J. Brash, A. M. Barth, J. H. Quilter, V. M. Axt, M. S. Skolnick and A. M. Fox,
Phys. Rev. B **93**, 161407(R) (2016):
Ultrafast depopulation of a quantum dot by LA-phonon-assisted stimulated emission.

pub 8 A. J. Brash, L. M. P. P. Martins, A. M. Barth, F. Liu, J. H. Quilter, M. Glässl, V. M. Axt, A. J. Ramsay, M. S. Skolnick and A. M. Fox,
J. Opt. Soc. Am. B **33**, C115-C122 (2016):
Dynamic vibronic coupling in InGaAs quantum dots [Invited].

pub 9 C. Hopfmann, A. Musial, M. Strauß, A. M. Barth, M. Glässl, A. Vagov, M. Strauß, C. Schneider, S. Höfling, M. Kamp, V. M. Axt and S. Reitzenstein,
Phys. Rev. B **92**, 245403 (2015):
Compensation of phonon-induced renormalization of vacuum Rabi splitting in large quantum dots: Towards temperature-stable strong coupling in the solid state with quantum dot-micropillars.

Summary of my contributions to the publications

The articles *pubs 1-9* were published in close collaboration with my coauthors. Here, I briefly summarize my contributions to these articles.

I developed the idea of the inclusion of non-Hamiltonian dynamics within the path-integral approach in *pub 1*, elaborated the formalism and implemented the generalized simulations. I also wrote the manuscript and answered the referee reports taking into account the comments from my coauthors.

My most important contribution to *pub 2* was a significant performance improvement of the existing implementation of the four-level path-integral simulations, which made it possible to perform very comprehensive parameter studies in a relatively short time. I was also involved in the discussion about how the results should be best presented and in proofreading the manuscript. This also applies for *pub 3*, where I was additionally responsible for the analysis and the simulations of the exciton-biexciton system, which led to the corresponding figure in the article.

I was the main correspondent for the theoretical part of the projects resulting in *pubs 4, 5, 7* and *9*, which all were regularly discussed with the experimental collaborators for about 9 - 18 months. In these projects I was responsible for the theoretical calculations and the necessary extensions of the theory, like the inclusion of tunneling effects in *pub 7*, and additionally helped to a large extent in interpreting the experimental observations in view of the simulated results. I was also involved in writing the manuscripts and the supplemental material and in answering the reports in the peer-review process.

In *pub 6*, I used the idea of the two-phase character of the phonon-assisted state preparation, which originates from my colleagues from Münster, to create the first draft of the manuscript including all calculations and figures. I completed the manuscript and the answers to the referee reports with the help of the comments from my coauthors.

In *pub 8*, I contributed all theoretical calculations and was involved in the discussion about the phase relations between the pulses in the figure that shows the phonon-assisted excitation and de-excitation process.

Publication 1

Path-integral description of combined Hamiltonian and non-Hamiltonian dynamics in quantum dissipative systems

A. M. Barth, A. Vagov and V. M. Axt

Physical Review B **94**, 125439 (2016)

DOI: 10.1103/PhysRevB.94.125439

PHYSICAL REVIEW B **94**, 125439 (2016)

Path-integral description of combined Hamiltonian and non-Hamiltonian dynamics in quantum dissipative systems

A. M. Barth,* A. Vagov, and V. M. Axt
Institut für Theoretische Physik III, Universität Bayreuth, 95440 Bayreuth, Germany
(Received 1 July 2016; revised manuscript received 5 September 2016; published 26 September 2016)

We present a numerical path-integral iteration scheme for the low-dimensional reduced density matrix of a time-dependent quantum dissipative system. Our approach simultaneously accounts for the combined action of a microscopically modeled pure-dephasing-type coupling to a continuum of harmonic oscillators representing, e.g., phonons, and further environmental interactions inducing non-Hamiltonian dynamics in the inner system represented, e.g., by Lindblad-type dissipation or relaxation. Our formulation of the path-integral method allows for a numerically exact treatment of the coupling to the oscillator modes and moreover is general enough to provide a natural way to include Markovian processes that are sufficiently described by rate equations. We apply this new formalism to a model of a single semiconductor quantum dot which includes the coupling to longitudinal acoustic phonons for two cases: (a) external laser excitation taking into account a phenomenological radiative decay of the excited dot state and (b) a coupling of the quantum dot to a single mode of an optical cavity taking into account cavity photon losses.

DOI: 10.1103/PhysRevB.94.125439

I. INTRODUCTION

Practically every quantum system experiences some kind of coupling to its environment and in many cases a realistic modeling requires the inclusion of quantum dissipative processes [1,2]. Such interactions with the environment typically lead to a decay of quantum mechanical coherence within the subsystem of interest that is known as decoherence or dephasing and often affects the dynamics in a non-negligible way. When the system-bath coupling becomes strong or when the environmental correlation decay becomes slow, it can be insufficient to treat the environment as a constant entity simply acting on the system but instead the reaction of the external degrees of freedom to the system dynamics also has to be considered. Accounting for these non-Markovian effects in a complete and correct way is not an easy task as besides the system dynamics also the finite bath-memory has to be incorporated in the equations of motion. A powerful and widely used method that allows such an exact treatment is provided by the path-integral approach [3–6], which exactly takes into account the environment excitations via the so-called influence functionals for the degrees of freedom of the quantum system [7]. This formalism has been applied in a variety of fields of both physics and chemistry such as energy transfer dynamics [8–16], Landau-Zener transitions [17,18], quantum mechanical Brownian motion [19], and semiconductor quantum dots with and without optical driving [20–25]. Moreover, it has been applied to systems with bosonic and fermionic baths [26,27], Ohmic and super-Ohmic [23] environments and can also be used to include multiple baths. However, in some cases the path-integral approach becomes impractical, because depending on the type of environmental interaction the influence functional cannot always be obtained easily. On the other hand, a completely microscopic description of the environment is not always necessary because many dissipative processes are well known to be correctly described in the Markov limit and a simplified or even parametric treatment of the environment is sufficient. In these cases a realistic modelling is usually achieved by simply adding phenomenological non-Hamiltonian contributions to the equations of motion of the reduced system as it is done, e.g., in the Lindblad formalism [2].

In this paper, we show that in a new generalized formulation the framework of the path-integral method allows to treat such non-Hamiltonian dynamics on equal footing with the Hamiltonian part of the equations of motion and can therefore also be used for models that describe some parts of the environment by phenomenological rates, while fully accounting for all non-Markovian effects induced by other couplings. This is not obvious, because the path-integral method usually relies on describing the dynamics in terms of the time-evolution operator, which yields purely Hamiltonian dynamics. More specifically here we present the path-integral formalism for a finite dimensional system that exhibits arbitrary non-Hamiltonian relaxation and a coupling to an arbitrary number of microscopic harmonic oscillator modes that is of the pure-dephasing type, i.e., the coupling does not induce transitions between the finite basis states. After defining the model and establishing our new formalism in Sec. II we apply it to a strongly confined semiconductor quantum dot coupled to a continuum of longitudinal acoustic phonons in Sec. III. The new method allows for an unbiased study of the interplay of the carrier-phonon coupling with the presence of radiative decay that is due to external field modes even in the regime of high temperatures and strong driving that is presented in Sec. III A. By exemplarily comparing the path-integral calculations with a Markovian master equation we also show that the new formalism can serve as an important benchmark tool. In Sec. III B, we then study the dynamics of a quantum dot coupled to a single photon mode inside a microcavity and compare the results with a previously developed hybrid approach. Finally, Sec. IV summarizes and concludes the paper.

*andreas.barth@uni-bayreuth.de

II. MODEL AND NUMERICAL METHOD

Our generic model consists of a few level system with a pure-dephasing type coupling to a continuum of harmonic oscillators. Further interactions between the few level system and the environment can be accounted for by additional non-Hamiltonian contributions to the equations of motion. The dynamics of the statistical operator for the total system consisting of the N states of the few level system belonging to the subspace $\mathcal{H}_N$ and the oscillatory modes belonging to the subspace $\mathcal{H}_{\rm osc}$ is given by the dynamical equation

$$\frac{d}{dt}\hat{\rho} = \frac{1}{i\hbar}\{\hat{H},\hat{\rho}\}_- + \mathcal{L}[\hat{\rho}], \tag{1}$$

where $\{.,.\}_-$ denotes the commutator. The Hamiltonian

$$\hat{H} = \hat{H}_N + \hat{H}_{\rm osc} \tag{2}$$

consists of an arbitrary N-dimensional time-dependent Hamiltonian $\hat{H}_N$ acting only on the N states $\{|\nu\rangle\} \in \mathcal{H}_N$ and

$$\hat{H}_{\rm osc} = \hbar\sum_j \omega_j \hat{b}_j^\dagger \hat{b}_j + \hbar\sum_{\nu j}\left(\gamma_j^\nu \hat{b}_j^\dagger + \gamma_j^{\nu *}\hat{b}_j\right)|\nu\rangle\langle\nu|, \tag{3}$$

which describes the interaction with the harmonic oscillators. Here, the symbol γ_j^ν denotes the coupling constant for the coupling between the state $|\nu\rangle$ and the bosonic mode j with energy $\hbar\omega_j$ that is created (destroyed) by $\hat{b}_j^\dagger$ ($\hat{b}_j$). Note that for simplicity, we treat the mode index j as being discrete even though the presented formalism can account for an arbitrary number of modes. The pure-dephasing type of the coupling often dominates for systems where the states of the few level system are energetically well separated such that inter-state transitions induced by the bosonic modes can be neglected.

While we denote Hilbert space operators with "hat" signs, the operator $\mathcal{L}[\hat{\rho}]$ appearing in Eq. (1) represents a Liouville space operator [28], i.e., a linear mapping between such operators, that allows the inclusion of non-Hamiltonian dynamics. In the following, we indicate such Liouville operators by putting the Hilbert space operator they act on into square brackets for clarity. Here, $\mathcal{L}[\hat{\rho}]$ is assumed to keep the parts of $\hat{\rho}$ belonging to the subspace $\mathcal{H}_{\rm osc}$ invariant and to only act on the few level system $\mathcal{H}_N$. We further assume that while $\mathcal{L}[\cdot]$ can be time-dependent, for simplicity it should be local in time. In principle, it would be possible to relax this assumption. However, depending on the memory depth of $\mathcal{L}[\cdot]$, this could increase the total memory time and thus the numerical cost of the path integral algorithm. Moreover, in many cases it is advisable to require certain conditions for the operator $\mathcal{L}[\cdot]$ such that important physical properties of the density matrix are preserved. All of these conditions mentioned above are enforced when $\mathcal{L}[\cdot]$ has the so called Lindblad form [2]

$$\mathcal{L}[\hat{\rho}] = \sum_i \gamma_i(t)\left(\hat{A}_i\hat{\rho}\hat{A}_i^\dagger - \frac{1}{2}\{\hat{\rho},\hat{A}_i^\dagger\hat{A}_i\}_+\right), \tag{4}$$

where the operators $\hat{A}_i$ represent operations within $\mathcal{H}_N$, the factors $\gamma_i(t)$ denote possibly time-dependent relaxation rates, and $\{.,.\}_+$ is the anticommutator. However, we would like to stress that the presented formalism does not depend on $\mathcal{L}[\cdot]$ to have this specific form.

Initially, the system is assumed to be in a product state of the states $\{|\nu\rangle\}$ and a thermal distribution of the oscillator modes $\hat{\rho}_{\rm th}$, i.e.,

$$\hat{\rho}(t=t_0) = \hat{\tilde{\rho}}(t=t_0)\otimes\hat{\rho}_{\rm th}. \tag{5}$$

The reduced density matrix of the N level subsystem

$$\hat{\tilde{\rho}}(t) = {\rm Tr}_{\rm osc}(\hat{\rho}(t)) \tag{6}$$

is obtained by tracing out all the degrees of freedom belonging to the subspace $\mathcal{H}_{\rm osc}$. In the following, we will derive a discretized representation of $\hat{\tilde{\rho}}(t)$ that is applicable for numerical calculation and does not require further approximations to the model given above.

A. Derivation of the path-integral solution

We start by separating the right-hand side of the master equation Eq. (1) into two Liouville operators $\mathcal{L}_N[\cdot]$ and $\mathcal{L}_{\rm osc}[\cdot]$ that are given by

$$\mathcal{L}_N[\hat{\rho}] = \frac{1}{i\hbar}\{\hat{H}_N,\hat{\rho}\}_- + \mathcal{L}[\hat{\rho}], \tag{7}$$

$$\mathcal{L}_{\rm osc}[\hat{\rho}] = \frac{1}{i\hbar}\{\hat{H}_{\rm osc},\hat{\rho}\}_-, \tag{8}$$

and write the master equation as

$$\frac{d}{dt}\hat{\rho} = \mathcal{L}_N[\hat{\rho}] + \mathcal{L}_{\rm osc}[\hat{\rho}]. \tag{9}$$

Keeping the accuracy linear in a small time step Δt the propagation of the statistical operator to a time $t+\Delta t$ can be performed by applying $\mathcal{L}_N[\cdot]$ and $\mathcal{L}_{\rm osc}[\cdot]$ subsequently and we can write

$$\hat{\rho}(t+\Delta t) = \hat{U}\mathcal{M}_t[\hat{\rho}(t)]\hat{U}^\dagger + \mathcal{O}(\Delta t^2). \tag{10}$$

Here, we have used the fact that the dynamics described by $\mathcal{L}_{\rm osc}[\cdot]$ is purely Hamiltonian and therefore can be expressed in terms of the time evolution operator

$$\hat{U} = \exp\left(-\frac{i}{\hbar}\hat{H}_{\rm osc}\Delta t\right). \tag{11}$$

Further, we have introduced the time-ordered operator

$$\mathcal{M}_t[\cdot] = \mathcal{T}\exp\left(\int_t^{t+\Delta t}\mathcal{L}_N dt'\right)[\cdot], \tag{12}$$

which acts as a generalized time evolution operator that describes the evolution of the few level system including the non-Hamiltonian part of the dynamics in the absence of the oscillator coupling from time t to $t+\Delta t$. Importantly, the representation of these operators in terms of the matrix exponentials fulfills the necessary conservation requirements at each time step, such as a unitary evolution for the Hamiltonian dynamics.

We can now use the relation Eq. (10) recursively to find an expression for the statistical operator at time t starting from the initial time t_0. By inserting several identity operators $\sum_\nu |\nu\rangle\langle\nu|$ acting on $\mathcal{H}_N$ at different time steps $t_l = t_0 + l\Delta t$, where the summation $\sum_\nu$ runs over all states of the few level system, we

arrive at a discretized representation

$$\hat{\rho}_{\nu_n\mu_n} = \sum_{\substack{\nu_0\ldots\nu_{n-1}\\ \mu_0\ldots\mu_{n-1}}} \hat{U}_{\nu_n}\ldots\hat{U}_{\nu_1}\hat{\rho}_{\nu_0\mu_0}\hat{U}^{\dagger}_{\mu_1}\ldots\hat{U}^{\dagger}_{\mu_n} \prod_{l=1}^{n}\mathcal{M}^{\nu_{l-1}\mu_{l-1}}_{\nu_l\mu_l} \tag{13}$$

for the matrix elements of the statistical operator, which we denote by

$$\hat{\rho}_{\nu_l\mu_l} = \langle\nu_l|\hat{\rho}(t_l)|\mu_l\rangle. \tag{14}$$

We have written

$$\hat{U}_{\nu} = \langle\nu|\hat{U}|\nu\rangle \tag{15}$$

for the diagonal elements of the time-evolution operator $\hat{U}$ that are operators acting on the subspace $\mathcal{H}_{\rm osc}$ and also introduced the symbol

$$\mathcal{M}^{\nu_{l-1}\mu_{l-1}}_{\nu_l\mu_l} = \langle\nu_l|\mathcal{M}_t[|\nu_{l-1}\rangle\langle\mu_{l-1}|]|\mu_l\rangle, \tag{16}$$

which represents the matrix elements of the operator that results when $\mathcal{M}_t$ is applied to the canonical basis operator $|\nu_{l-1}\rangle\langle\mu_{l-1}|$.

We can now use the results of previous work [23] where using a path-integral method and a representation of the oscillatory modes in terms of coherent states the trace over the oscillators for an operator of the same form as the one in Eq. (13) has been performed. Tracing out in this way the oscillator degrees of freedom we finally obtain the elements of the reduced density matrix $\bar{\rho}$ at the nth time step

$$\bar{\rho}_{\nu_n\mu_n} = \mathrm{Tr}_{\rm osc}\left(\hat{\rho}_{\nu_n\mu_n}\right) = \sum_{\substack{\nu_0\ldots\nu_{n-1}\\ \mu_0\ldots\mu_{n-1}}} \bar{\rho}_{\nu_0\mu_0}\exp\left(S^{\mu_n\ldots\mu_1}_{\nu_n\ldots\nu_1}\right)\prod_{l=1}^{n}\mathcal{M}^{\nu_{l-1}\mu_{l-1}}_{\nu_l\mu_l}, \tag{17}$$

where all summations run over the N states of $\mathcal{H}_{\mathcal{N}}$ and the influence functional $S^{\mu_n\ldots\mu_1}_{\nu_n\ldots\nu_1}$ incorporates the memory of the oscillator modes in the dynamics of the few-level system. For simplicity, here, we only give the expression for the influence functional for the special case where the coupling constants γ^{ν}_j are all either purely real or purely imaginary. A more general representation for the influence functional that does not make use of this assumption can be found in Ref. [23]. The functional reads

$$S^{\mu_n\ldots\mu_1}_{\nu_n\ldots\nu_1} = \sum_{l=1}^{n}\sum_{l'=1}^{l} S_{\nu_l\nu_{l'}\mu_l\mu_{l'}} \tag{18}$$

with

$$S_{\nu_l\nu_{l'}\mu_l\mu_{l'}} = -K_{\nu_{l'}\nu_l}(t_l - t_{l'}) - K^{*}_{\mu_l\mu_{l'}}(t_l - t_{l'}) + K^{*}_{\nu_l\mu_{l'}}(t_l - t_{l'}) + K_{\nu_{l'}\mu_l}(t_l - t_{l'}) \tag{19}$$

and the memory kernels

$$K_{\nu_l\mu_{l'}}(\tau) = 2\int_0^{\infty} d\omega\frac{J_{\nu_l\mu_{l'}}(\omega)}{\omega^2}(1-\cos(\omega\Delta t)) \times\left[\coth\left(\frac{\hbar\omega}{2k_BT}\right)(\cos(\omega\tau)) - i\sin(\omega\tau)\right] \tag{20}$$

and

$$K_{\nu_l\mu_l}(0) = \int_0^{\infty} d\omega\frac{J_{\nu_l\mu_l}(\omega)}{\omega^2}\times\left[\coth\left(\frac{\hbar\omega}{2k_BT}\right) \times(1-\cos(\omega\Delta t)) + i\sin(\omega\Delta t) - i\omega\Delta t\right] \tag{21}$$

where we have introduced the spectral density

$$J_{\nu\mu}(\omega) = \sum_j \gamma^{\nu}_j\gamma^{\mu *}_j\delta(\omega-\omega_j). \tag{22}$$

It should be noted that the last term in Eq. (21) induces a polaronic shift of the energy levels of the few-level system.

B. Evaluation of the path-integral expression

Obtaining the reduced density matrix at the nth time step from Eq. (17) requires the summation over N^{2n} single contributions, which quickly becomes unfeasible even for very small N. Each of the single summands represents a possible *path*, i.e., a trajectory through the subspace $\mathcal{H}_N\otimes\mathcal{H}_N$ given by the configurations at each time-step $(\nu_n,\mu_n)\ldots(\nu_1,\mu_1)$, which is the reason that the summation scheme is called a numerical path-integration method. To efficiently use this expression also for the iteration over many time-steps it is necessary to exploit the finite memory time of the system of oscillator modes that is reflected by a finite decay time of the memory kernels [Eqs. (20) and (21)]. This allows a truncation of the influence functional $S^{\mu_n\ldots\mu_1}_{\nu_n\ldots\nu_1}$, efficiently making it only depend on the states of the n_c most recent time-steps $(\nu_n,\mu_n)\ldots(\nu_{n-n_c+1},\mu_{n-n_c+1})$. Such a truncation can be exploited by combining the path-integral method with the augmented density matrix approach [4,5], which applies also in the present case when including non-Hamiltonian dynamics. The augmented density matrix can be thought of as a $2n_c$ dimensional tensor of weights for the different possible configurations of the most recent n_c time steps and can be calculated iteratively in each time step following the relation

$$\rho^{\mu_n\ldots\mu_{n-n_c+1}}_{\nu_n\ldots\nu_{n-n_c+1}} = \mathcal{M}^{\nu_{n-1}\mu_{n-1}}_{\nu_n\mu_n} \times\sum_{\substack{\nu_{n-n_c}\\ \mu_{n-n_c}}}\exp\left(S^{\mu_n\ldots\mu_{n-n_c}}_{\nu_n\ldots\nu_{n-n_c}}\right)\rho^{\mu_{n-1}\ldots\mu_{n-n_c}}_{\nu_{n-1}\ldots\nu_{n-n_c}}. \tag{23}$$

This explicit iteration yields a numerical effort that is linear in the total number of time steps and requires the calculation and storage of only N^{2n_c} (compared to N^{2n}) weights and thus removes the restriction to a limited number of iteration steps in Eq. (17) that we mentioned above.

The decay time of the memory kernels is determined by the spectral density of the harmonic oscillator coupling $J(\omega)$, which can be classified by its low-frequency behavior into sub-Ohmic coupling where $J(\omega)\sim\omega^a$ with $a<1$ as $\omega\to 0$, Ohmic coupling where $a=1$ and super-Ohmic coupling where $a>1$. The Ohmic case marks the borderline between a sub-Ohmic environment inducing exponential relaxations and the super-Ohmic case which is characterized by non-exponential typically only partial relaxations that entail a variety of non-Markovian dynamical effects [3]. The presented formalism can also deal with the latter super-Ohmic case [23] that is realized in the examples in this article for the coupling of acoustic phonons in a crystal solid where $a=3$.

Finally, we would like to note that the inclusion of non-Hamiltonian dynamics in Eq. (1) does not increase the required memory depth n_c compared to the case of purely Hamiltonian dynamics as long as the former part of the dynamics does not involve a memory time that is longer than the one induced by the harmonic oscillator coupling. Here, this is obviously fulfilled as the operator $\mathcal{L}[\cdot]$ in Eq. (1) is assumed to be local in time. Notably, this also means that the numerical cost is practically not increased by adding non-Hamiltonian contributions.

III. APPLICATION: DYNAMICS OF A SEMICONDUCTOR QUANTUM DOT

In this section, we utilize the extended path-integral formalism to calculate the dynamics of an optically coupled strongly confined semiconductor quantum dot (QD) and also compare the results with those of some established methods. For circularly polarized light with a central frequency close to the excitonic resonance, a QD can be described for many purposes in good approximation as a two-level system consisting of the crystal ground-state $|0\rangle$ and an exciton state $|X\rangle$ with energy $\hbar\omega_X$ given by the Hamiltonian

$$\hat{H}_{\mathrm{QD}} = \hbar\omega_X |X\rangle\langle X|. \tag{24}$$

Apart from the optically induced coherent dynamics which we will describe specifically in the corresponding two subsections also the coupling to the lattice vibrations of the surrounding solid state material needs to be taken into account. For the strongly confined GaAs-based QD considered here the deformation potential coupling to longitudinal acoustic (LA) phonons represents the predominant impact of the phonon environment [29] and has the same form as Eq. (3) where the index j refers to the wave vector $\mathbf{q}$ of the LA phonon modes. The coupling constants $\gamma_{\mathbf{q}}^{\nu}$ are given by $\gamma_{\mathbf{q}}^{0} = 0$ for the ground state and $\gamma_{\mathbf{q}}^{1} = \gamma_{\mathbf{q}}^{e} - \gamma_{\mathbf{q}}^{h}$ for the exciton state with

$$\gamma_{\mathbf{q}}^{e(h)} = \Psi^{e(h)}(\mathbf{q}) \frac{|\mathbf{q}| D_{e(h)}}{\sqrt{2V\rho\hbar\omega_{\mathbf{q}}}} \tag{25}$$

being the coupling constants for the electron (e) and hole (h) coupling to the $\mathbf{q}$ phonon mode. Here, the form factors $\Psi^{e(h)}$ are assumed to be spherically symmetric and Gaussian as applies for a parabolic confinement potential and the deformation potential constants $D_e = 7.0$ eV and $D_h = -3.5$ eV, the mass density $\rho = 5370$ kg/m^3 as well as the sound velocity $c_s = 5110$ m/s for GaAs are taken from the literature [30]. The mode volume V simply represents a normalization constant for the summation over the phonon modes in Eq. (3). The spectral density of the phonon coupling given in Eq. (22) is only nonvanishing for $\nu = \mu = 1$ and in this case reads

$$J_{11}(\omega) = \frac{\omega^3}{4\pi^2\rho\hbar c_s^5}\left(D_e e^{-\omega^2 a_e^2/(4c_s^2)} - D_h e^{-\omega^2 a_h^2/(4c_s^2)} 77\right)^2, \tag{26}$$

where the sound velocity enters via the linear phonon dispersion relation $\omega_{\mathbf{q}} = c_s|\mathbf{q}|$ and $a_{e(h)}$ denote the root mean square of the Gaussian wave function extensions of the electron and hole, respectively. Here we set $a_e = 4.0$ nm, which can be interpreted as the QD radius and set a_e/a_h to 1.15.

We would like to point out that there have been many suggestions to simulate the QD dynamics under the influence of the carrier-phonon interaction outlined above including correlation expansions [31,32], analytical solutions for delta excitation [33], an exact diagonalization approach [34], quantum jump approaches [35] and various forms of master equations [36–42] some of which account for contributions of arbitrarily high order in the dot-phonon coupling with the help of the polaron transformation [22,43–46]. This variety of methods is also a result of the many different optical excitation scenarios that are discussed for QDs which can range from weak cavity couplings to strong pulsed laser excitation. The path integral approach presented here provides a numerical scheme that allows to deal with all of these situations without introducing further approximations to the model formulated above.

A. Laser-driven quantum dot with radiative decay

As a first example for an application of our new method we consider the QD dynamics that is driven by an external laser field and affected by both the phonon-induced relaxation and the radiative decay of the exciton state that reduces the exciton lifetime. As the radiative decay is known to be reasonably described as a Markov process in a good approximation it can be included by a Lindblad contribution to the master equation. In the rotating frame, the contribution to the Hamiltonian for the laser driven QD reads after applying the common dipole and rotating wave approximations

$$\hat{H}_{\text{dot-light}} = \tfrac{1}{2}\hbar f(t)\big(|0\rangle\langle X| + |X\rangle\langle 0|\big) - \Delta|X\rangle\langle X|, \tag{27}$$

where $f(t)$ is the envelope function of the laser field referred to as field strength and Δ is the detuning of the laser from the polaron-shifted exciton resonance. The radiative decay of the exciton state is treated as a phenomenologically damping rate accounted for by a Lindblad type operator in the form of Eq. (4) with a single transition $\hat{A}_1 = |0\rangle\langle X|$ and a corresponding damping rate γ (cf. Ref. [45]).

Figure 1 shows the time-dependent exciton occupation of the QD under resonant and off-resonant cw excitation as indicated. In the absence of the phonon interaction (left column) our computational scheme exactly reproduces known analytical results exhibiting damped Rabi oscillations. For off-resonant excitation [cf. panel (c)], of course, the amplitude of the oscillations is reduced and the Rabi frequency is increased as can be seen in Fig. 1(c). The radiative decay also influences the stationary exciton occupation for $\gamma > 0$, which is given by [47]

$$C_{X,\text{noph.}}^{\infty} = \frac{f^2}{2f^2 + \gamma^2 + (2\Delta/\hbar)^2} \tag{28}$$

and decreases from its maximum value of 0.5 with an increasing damping rate and an increasing detuning. This simple application without the phonon interaction serves as a proof of principle that the formalism presented here correctly incorporates non-Hamiltonian dynamics of Lindblad-type within the framework of the path-integral method.

In the other limiting case where $\gamma = 0$, but the phonon coupling is included the results obtained from the presented formalism coincide with previous path-integral calculations [23]

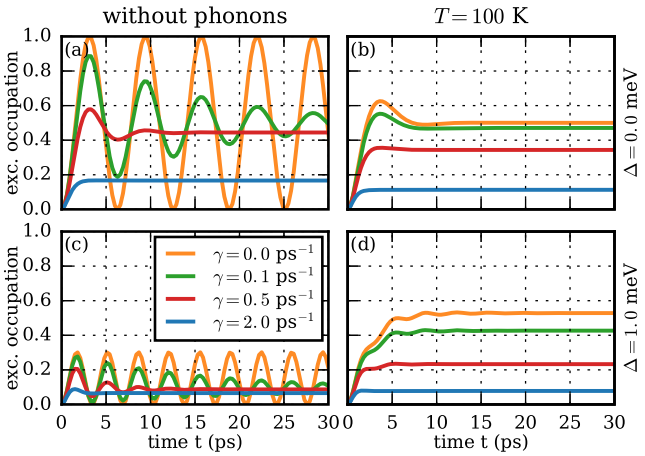

FIG. 1. Time-dependent exciton occupation C_X of a QD calculated by the path-integral formalism for constant driving with field strength $f = 1.0\,\mathrm{ps}^{-1}$ for resonant [(a) and (b)] and detuned [(c) and (d)] excitation ($\Delta = 1.0$ meV) for different values of the radiative decay rate (see legend). Left column: without phonon interaction, right column: including phonon interaction at temperature $T = 100\,\mathrm{K}$ in addition to the radiative decay.

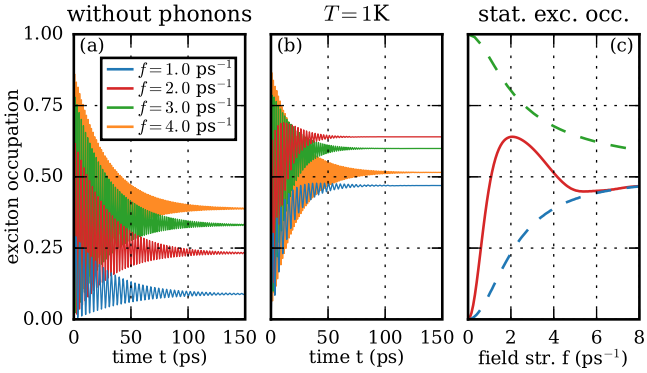

FIG. 2. Time-dependent exciton occupation C_X of a QD for off-resonant ($\Delta = 1.0$ meV) cw excitation for different field strengths (see legend) including radiative decay ($\gamma = 0.05\,\mathrm{ps}^{-1}$) without the phonon-interaction (a) and including phonons at temperature $T = 1\,\mathrm{K}$ (b). (c) Stationary exciton occupation reached at long times when only the phonon interaction is present (green, dashed), when only the radiative decay is present (blue, dashed) and when both relaxation mechanisms are present (red, solid).

that did not yet allow to account for any non-Hamiltonian dynamics. This can be seen explicitly from the orange curve for $\gamma = 0$ in the right column of Fig. 1 where calculations that include the phonon coupling for a temperature of $T = 100$ K are shown. As known from previous simulations at such high temperatures the Rabi oscillations are almost completely damped by the phonon scattering.

As for the radiative damping also the phonon coupling strongly affects the stationary value of the exciton occupation that is reached at long times. It can be seen that for fixed γ the stationary value C_X^∞ is slightly decreased by the phonon coupling for resonant excitation while it is increased for off-resonant excitation. The reason for this is that while the radiative decay always drives the QD towards the ground state and thus away from the exciton, off-resonant excitation with positive detuning enables phonon-assisted transitions between the laser dressed states that yield a higher exciton occupation [41,46,48–53]. As it can be seen in Fig. 1, this feature prevails when the phonon induced relaxation between photon dressed states is combined with the radiative decay of the exciton state discussed here.

Figure 2 shows the combined influence of the radiative decay and the phonon-interaction by plotting the time-dependent exciton occupation under positively detuned cw excitation for different field strengths as indicated. Without the phonon interaction [panel (a)] the stationary exciton occupation that is reached at long times C_X^∞ always stays below 0.5 and rises with increasing field strength as it was expected from Eq. (28). Interestingly, when including the phonon scattering [panel (b)] the stationary exciton occupation no longer depends on the field strength in a monotonic way. To analyze this in more detail, we have plotted C_X^∞ as a function of the field strength in Fig. 2(c) (red, solid) together with corresponding results for the two limiting cases where only the phonon scattering (dashed, green) or only the radiative decay (dashed, blue) has been accounted for. In case of the complete dynamic, there is a clear maximum around $f = 2.0\,\mathrm{ps}^{-1}$ and a local minimum around $f = 5.0\,\mathrm{ps}^{-1}$ and overall the full model predicts very different features compared to the two limiting cases. This behavior originates from the combination effects between the radiative decay and the phonon-induced relaxation as will be explained in the following. For very small field strengths, e.g., below $f = 0.5\,\mathrm{ps}^{-1}$, the timescale of the phonon-induced relaxation [54] is long compared to the radiative decay rate and therefore one might expect the phonon coupling to play a subordinate role. However, in this regime, the QD state targeted by the phonon-induced relaxation has an especially strong excitonic character [24], which without radiative decay would result in an exciton occupation near one towards very long times [54]. This can be seen by the dashed green line where the exciton occupation approaches one in the limit $f \to 0^+$, but of course, in the absence of any optical coupling, i.e., at exactly $f = 0$, the system remains in its ground state. When the radiative decay is included a remainder of this strong effect is still visible and thus leads to a clear difference between the results with (red, solid) and without phonons (blue, dashed) even for low field strengths. For larger values of f the phonon-induced relaxation becomes more effective yielding a steep increase of C_X^∞ and values well above 0.5 that would not be expected from the radiative decay alone. Beyond the maximum at $f = 2.0\,\mathrm{ps}^{-1}$, C_X^∞ decreases again as the QD state targeted by the phonon relaxation becomes less excitonic in character and even more importantly the phonon-coupling becomes less efficient again because the phonon environment is too sluggish to follow the rapid dynamics of the QD [21,55]. At very large $f > 5.0\,\mathrm{ps}^{-1}$ the phonon coupling no longer has a significant impact on C_X^∞ and the stationary exciton occupation is almost entirely dominated by the radiative decay resulting in a local minimum and a subsequent slow increase towards 0.5. It is worth noting that the nonmonotonic dependence of the damping of the Rabi oscillations that is due to the phonon

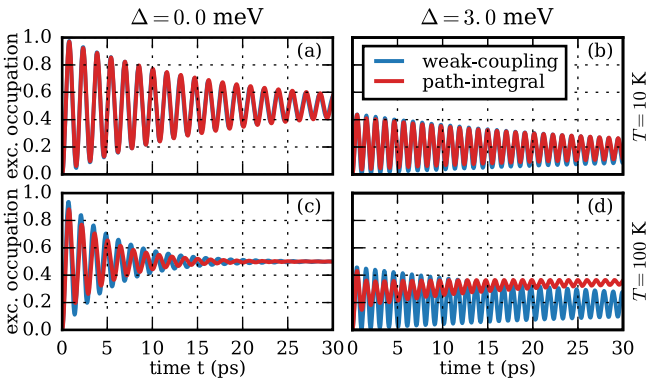

FIG. 3. Comparison of the time-dependent exciton occupation of a QD for resonant (left) and detuned (right) cw excitation calculated by the path-integral method (red) and the weak coupling theory (blue). The radiative decay rate has been set to $\gamma = 0.05\ \mathrm{ps}^{-1}$ and a relatively high field strength of $f = 4.0\ \mathrm{ps}^{-1}$ was chosen.

coupling persists under the influence of the radiative decay as it can be seen from Fig. 2(b).

A strong advantage of the numerical path-integral method is that because of the exact treatment of the model discussed here it can be used to benchmark perturbative approaches and explore their range of validity. To this end, we have compared our results with those of a Markovian master equation that treats the phonon coupling up to second order which we took from the literature [42] and that also allows an inclusion of the radiative exciton decay considered here. Figure 3(a) shows the damped Rabi oscillations of the exciton occupation under constant resonant excitation by a strong electric field ($f = 4.0\ \mathrm{ps}^{-1}$) under the influence of the phonon coupling ($T = 10$ K) and the radiative decay ($\gamma = 0.05\ \mathrm{ps}^{-1}$). As it can be expected at such low temperatures the weak-coupling theory (blue) works very well and the predicted dynamics of the exciton occupation is practically identical with those of the path-integral method (red), which indicates that in this parameter range non-Markovian effects and multiphonon processes that the weak-coupling theory cannot capture are of minor importance. Notably, the close match between the two methods is an important further verification of the correctness of the presented path-integral algorithm with Lindblad-type relaxation. When raising the temperature to $T = 100$ K, cf. Fig. 3(c), some differences between the results of the path-integral calculations and the weak-coupling theory become visible. The phonon-induced damping is slightly underestimated by the weak-coupling theory and also there is a slight discrepancy of the predicted Rabi frequency renormalization between the two methods. However, considering the very high temperature, the Master equation still yields reasonable results. This is due to the strong driving chosen here while for slower driving it is well known that the weak coupling theory can not account for the strong Rabi frequency renormalization [22] and even can yield unphysical results at very high temperatures [42]. For off-resonant excitation, the path-integral calculations again practically coincide with those obtained from the Master equation approach at $T = 10$ K [panel (b)]. However, at higher temperatures, cf. Fig. 3(d), strong differences between the two approaches become visible. The phonon-induced damping is clearly underestimated by the weak-coupling theory and even more important the stationary exciton occupation at long times predicted by the weak-coupling theory is considerably lower than the value predicted by the path-integral calculations. The regime of strong driving at elevated temperatures is especially difficult to deal with in the Master equation approach. Because the path-integral method does not rely on any approximations regarding the order of the phonon coupling or the optical driving that it accounts for and is only limited by the errors introduced by the discretization of the time axis, it provides an important benchmark. Most importantly, the regime of strong driving must be considered when simulating pulsed excitation scenarios in which high field strengths can be reached and that are often required to reproduce experimental results.

B. QD coupled to a single cavity mode

Another system that can be described within the combined Lindblad and path-integral method is a QD inside an optical cavity. Here, we assume that the quantized cavity photon modes are sufficiently separated in frequency such that only a single mode effectively couples to the QD. Further, we assume that the system can be described in the single-photon limit where only states with zero or one cavity photon have to be considered. Besides the coupling to LA phonons that is independent of the cavity coupling also photon losses that are due to imperfections of the cavity mirrors are highly relevant for the system dynamics. Similar to the previous examples we model the dynamics of the QD consisting of two electronic levels coupled to the cavity mode and the phonon subsystem in an exact Hamiltonian way while we attribute the cavity losses to the part of the environment that is described by rate equations. In the rotating frame the Hamiltonian for the QD coupled to the cavity mode is described via the Jaynes-Cummings model and reads after applying the common dipole and rotating wave approximations

$$\hat{H}_{\text{dot-cav}} = \hbar g(|P\rangle\langle X| + |X\rangle\langle P|) - \Delta|X\rangle\langle X|, \quad (29)$$

where g is the light-matter coupling strength, Δ is the detuning of the cavity-mode from the polaron-shifted exciton resonance, and the two-level electronic basis of the QD-cavity system consists of the state $|P\rangle$ with the QD in the ground-state and one cavity photon and the exciton state $|X\rangle$ without a cavity photon. Only $|X\rangle$ couples to the phonon enivironment and the coupling is the same as in the previous examples. The photon losses of the cavity are modelled by a relaxation with rate κ from $|P\rangle$ to the state where the QD is in its ground-state and no photon is present $|G\rangle$ which is accounted for by a Lindblad contribution to the equation of motion for the reduced density matrix [45] by setting $\hat{A}_1 = |G\rangle\langle P|$ in Eq. (4).

Figure 4 shows the occupation of the excited state $|X\rangle$ as a function of time for a system initially prepared in the excited state for a cavity-loss rate $\kappa = 0.1\ \mathrm{ps}^{-1}$ at two different temperatures for resonant and off-resonant coupling (see caption). For resonant coupling we can see Rabi oscillations with a decreasing amplitude, which can be attributed to the cavity losses. Similar oscillations can also be seen for off-resonant coupling, but in this case a positive detuning (red) leads to a strongly increased exciton decay time compared

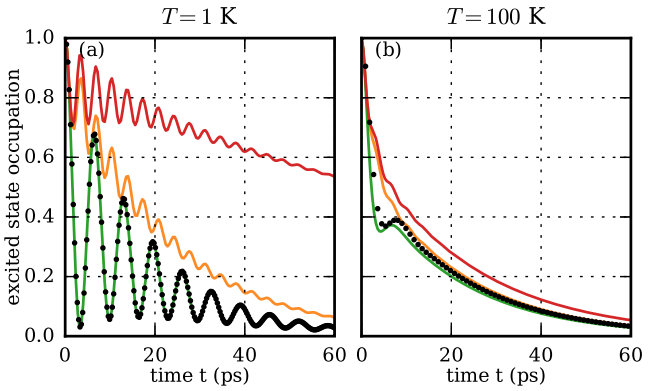

FIG. 4. Time-dependent occupation of the excited state C_X of a QD inside a cavity for resonant (green) and off-resonant (red: $\Delta = 1.0$ meV, orange: $\Delta = -1.0$ meV) coupling. The black dots show the results of a hybrid approach that is only applicable in the resonant case (see text). (Left) $T = 1$ K. (Right) $T = 100$ K. $\kappa = 0.1$ ps^{-1}.

to a negative detuning (orange). This asymmetry has already been discussed in Ref. [45] and is due to the fact that at low temperatures phonon emission process dominate absorption processes, and in fact at a higher temperature (right panel), this asymmetry disappears. Here we have chosen to repeat these kind of calculations to show that temperatures as high as $T = 100$ K can easily be accessed using the path-integral approach, which is hard to reach with other methods. Previously, the present model of a QD-cavity system has also been treated by a hybrid approach [56], which requires the knowledge of the phonon-induced Rabi-frequency renormalization and the strength of the phonon-induced damping in the absence of cavity losses. These input parameters can be gained by analyzing the damped oscillations of the excited state occupation in a lossless cavity occurring for constant resonant coupling as it can be calculated using the path-integral formalism in its previous formulation [23,57]. In the hybrid approach this input is then combined with an *a posteriori* phenomenological treatment of the cavity losses. Thus, even though this way the damping and the frequency renormalization are calculated in a nonperturbative way, the hybrid approach does not yet treat the cavity losses and the phonon coupling on equal footing as the combined Lindblad and path-integral approach does. Moreover, the derivation of the hybrid approach in Ref. [56] made explicit use of special properties that are only fulfilled for constant resonant excitation. Therefore the present work also drastically extends the parameter range accessible with the path-integral approach if one needs to include the effects of cavity losses, which in many cases play a crucial role for the system dynamics. Here, we have compared the results obtained from the hybrid approach for resonant excitation, shown as black dots in Fig. 4, with the path-integral method for both temperatures. For low temperatures the results are identical, while at higher temperature small deviations become visible. Similar to our previous comparison with the weak-coupling theory also here the path-integral method serves as an excellent benchmark to explore the limits of the applicability of less rigorous methods.

IV. CONCLUSIONS

We have presented an extension to the numerical path-integral formalism previously used to calculate the reduced density matrix of a time-dependent few level system coupled to a set of harmonic oscillator modes that allows a natural and systematic inclusion of non-Hamiltonian dynamics within the path integral framework. Our combined method shows a way how to go beyond the representation of the path-integral formalism that relies on using the time-evolution operator and thus can be used to add arbitrary linear operations acting on the reduced density matrix to the equations of motion. We applied this new method to an optically coupled semiconductor quantum dot (QD) where the coupling to longitudinal acoustic phonons is treated nonperturbatively for different optical excitation conditions and different environmental effects that are described in the Markov limit by corresponding phenomenological rates. The combined Lindblad and path-integral method turns out to be a highly valuable tool for the treatment of optically coupled QDs with strong phonon interaction and similar quantum dissipative systems for a number of reasons. First of all, it allows to treat the deformation potential coupling to longitudinal acoustic phonons, which has been identified as the major decoherence mechanism in strongly confined QDs, in a numerically exact way that includes multiphonon processes and all non-Markovian effects. This makes it possible to explore the regimes of arbitrarily strong QD-phonon coupling and both low and high temperatures in a nonperturbative way. Here, it is worth noting that within the path integral approach higher temperatures are actually easier to deal with as the memory time becomes shorter and thus less memory steps are needed while the scope of some approximate methods that explicitly truncate the phonon subspace is restricted to lower temperatures. Besides the phonon coupling also the optical excitation can be chosen arbitrarily as the formalism is able to deal with both weak and strong driving, constant and pulsed excitation and also rapid changes of the excitation parameters that can prevent an adiabatic evolution of the coupled light-matter system. This also includes situations with chirped excitation or with multiple overlapping pulses of different frequency where the introduction of a suitable basis of photon-dressed states as needed by some schemes becomes nonobvious as the rotating frames naturally associated with each pulse differ. Moreover, the method can be used to calculate all elements of the reduced density matrix in the original frame of reference which not only gives access to the QD occupations, but also to the coherences of the reduced system. The inclusion of processes described by rate equations within the path-integral formalism that is made possible by the present work allows taking into account other loss channels that are relevant in typical experimental situations involving QDs. For example, the presented method has already been successfully used to include electron tunneling effects in photocurrent measurements using off-resonant two-pulse and two-color excitation [58,59].

In our first application, we discussed the combined effects of the radiative decay and the phonon scattering on the driven stationary nonequilibrium state of a two-level QD for both resonant and off-resonant excitation showing that there is a nonmonotonic dependence of the stationary exciton

occupation on the driving strength. This is not expected in both limiting cases where either the dot phonon interaction or the radiative decay provide the only environment coupling. So far no unbiased approach was formulated for studying such combination effects. We then used the path-integral results to explore the range of validity of a weak-coupling method that treats the phonon coupling perturbatively and found for strong driving in the regime of detuned excitation at high temperatures significant deviations between the two methods while otherwise the weak-coupling theory works well over wide parameter ranges. Finally, we applied our new formalism to the case of a QD coupled to a single cavity mode and analyzed the exciton lifetime that is limited due to photon losses of the cavity for different detunings of the optical mode from the QD resonance at low and very high temperatures. The combined Lindblad and path-integral method has also been used as a benchmark to test a previously developed hybrid approach that was limited to resonant excitation.

ACKNOWLEDGMENTS

A.M.B. and V.M.A. gratefully acknowledge the financial support from Deutsche Forschungsgemeinschaft via the Project No. AX 17/7-1.

[1] U. Weiss, *Quantum Dissipative Systems*, 2nd ed. (World Scientific, Singapore, 1999).
[2] H. P. Breuer and F. Petruccione, *The Theory of Open Quantum Systems*, 1st ed. (Oxford University Press, Oxford, 2002).
[3] A. J. Leggett, S. Chakravarty, A. T. Dorsey, M. P. A. Fisher, A. Garg, and W. Zwerger, Rev. Mod. Phys. **59**, 1 (1987).
[4] N. Makri and D. Makarov, J. Chem. Phys. **102**, 4600 (1995).
[5] N. Makri and D. Makarov, J. Chem. Phys. **102**, 4611 (1995).
[6] N. Makri, J. Chem. Phys. **141**, 134117 (2014).
[7] R. P. Feynman and F. Vernon, Ann. Phys. (NY) **24**, 118 (1963).
[8] P. Nalbach, A. Ishizaki, G. R. Fleming, and M. Thorwart, New J. Phys. **13**, 063040 (2011).
[9] P. Nalbach and M. Thorwart, J. Chem. Phys. **132**, 194111 (2010).
[10] P. Nalbach, J. Eckel, and M. Thorwart, New J. Phys. **12**, 065043 (2010).
[11] J. Eckel, J. H. Reina, and M. Thorwart, New J. Phys. **11**, 085001 (2009).
[12] M. Thorwart, J. Eckel, J. H. Reina, P. Nalbach, and S. Weiss, Chem. Phys. Lett. **478**, 234 (2009).
[13] P. Nalbach, A. J. A. Achner, M. Frey, M. Grosser, C. Bressler, and M. Thorwart, J. Chem. Phys. **141**, 044304 (2014).
[14] H. Kim, O. Choi, and E. Sim, J. Phys. Chem. C **114**, 20394 (2010).
[15] J. Lee, O. Choi, and E. Sim, J. Phys. Chem. Lett. **3**, 714 (2012).
[16] X.-T. Liang, W.-M. Zhang, and Y.-Z. Zhuo, Phys. Rev. E **81**, 011906 (2010).
[17] P. Nalbach and M. Thorwart, Phys. Rev. Lett. **103**, 220401 (2009).
[18] S. Javanbakht, P. Nalbach, and M. Thorwart, Phys. Rev. A **91**, 052103 (2015).
[19] M. Thorwart, P. Reimann, and P. Hänggi, Phys. Rev. E **62**, 5808 (2000).
[20] M. Thorwart, J. Eckel, and E. R. Mucciolo, Phys. Rev. B **72**, 235320 (2005).
[21] A. Vagov, M. D. Croitoru, V. M. Axt, T. Kuhn, and F. M. Peeters, Phys. Rev. Lett. **98**, 227403 (2007).
[22] D. P. S. McCutcheon, N. S. Dattani, E. M. Gauger, B. W. Lovett, and A. Nazir, Phys. Rev. B **84**, 081305(R) (2011).
[23] A. Vagov, M. D. Croitoru, M. Glässl, V. M. Axt, and T. Kuhn, Phys. Rev. B **83**, 094303 (2011).
[24] M. Glässl, A. Vagov, S. Lüker, D. E. Reiter, M. D. Croitoru, P. Machnikowski, V. M. Axt, and T. Kuhn, Phys. Rev. B **84**, 195311 (2011).
[25] M. Glässl, A. M. Barth, and V. M. Axt, Phys. Rev. Lett. **110**, 147401 (2013).
[26] D. Segal, A. J. Millis, and D. R. Reichman, Phys. Rev. B **82**, 205323 (2010).
[27] L. Simine and D. Segal, J. Chem. Phys. **138**, 214111 (2013).
[28] S. Mukamel, *Principles of Nonlinear Optical Spectroscopy*, 1st ed. (Oxford University Press, New York, 1995).
[29] B. Krummheuer, V. M. Axt, and T. Kuhn, Phys. Rev. B **65**, 195313 (2002).
[30] B. Krummheuer, V. M. Axt, T. Kuhn, I. D'Amico, and F. Rossi, Phys. Rev. B **71**, 235329 (2005).
[31] J. Förstner, C. Weber, J. Danckwerts, and A. Knorr, Phys. Rev. Lett. **91**, 127401 (2003).
[32] A. Krügel, V. M. Axt, and T. Kuhn, Phys. Rev. B **73**, 035302 (2006).
[33] A. Vagov, V. M. Axt, and T. Kuhn, Phys. Rev. B **66**, 165312 (2002).
[34] P. Kaer, P. Lodahl, A.-P. Jauho, and J. Mork, Phys. Rev. B **87**, 081308 (2013).
[35] N. Renaud and F. C. Grozema, Phys. Rev. B **90**, 165307 (2014).
[36] A. Nazir, Phys. Rev. B **78**, 153309 (2008).
[37] A. J. Ramsay, A. V. Gopal, E. M. Gauger, A. Nazir, B. W. Lovett, A. M. Fox, and M. S. Skolnick, Phys. Rev. Lett. **104**, 017402 (2010).
[38] P. Kaer, T. R. Nielsen, P. Lodahl, A. P. Jauho, and J. Mørk, Phys. Rev. Lett. **104**, 157401 (2010).
[39] A. Debnath, C. Meier, B. Chatel, and T. Amand, Phys. Rev. B **86**, 161304 (2012).
[40] P. R. Eastham, A. O. Spracklen, and J. Keeling, Phys. Rev. B **87**, 195306 (2013).
[41] P.-L. Ardelt, L. Hanschke, K. A. Fischer, K. Müller, A. Kleinkauf, M. Koller, A. Bechtold, T. Simmet, J. Wierzbowski, H. Riedl, G. Abstreiter, and J. J. Finley, Phys. Rev. B **90**, 241404 (2014).
[42] A. Nazir and D. P. S. McCutcheon, J. Phys. Condens. Matter **28**, 103002 (2016).
[43] D. P. S. McCutcheon and A. Nazir, New J. Phys. **12**, 113042 (2010).
[44] C. Roy and S. Hughes, Phys. Rev. B **85**, 115309 (2012).
[45] P. Kaer, T. R. Nielsen, P. Lodahl, A.-P. Jauho, and J. Mørk, Phys. Rev. B **86**, 085302 (2012).
[46] R. Manson, K. Roy-Choudhury, and S. Hughes, Phys. Rev. B **93**, 155423 (2016).

[47] R. Loudon, *The Quantum Theory of Light*, 2nd ed. (Oxford Science Publications, Oxford, 1973).
[48] M. Glässl, M. D. Croitoru, A. Vagov, V. M. Axt, and T. Kuhn, Phys. Rev. B **84**, 125304 (2011).
[49] S. Hughes and H. J. Carmichael, New J. Phys. **15**, 053039 (2013).
[50] M. Glässl, A. M. Barth, K. Gawarecki, P. Machnikowski, M. D. Croitoru, S. Lüker, D. E. Reiter, T. Kuhn, and V. M. Axt, Phys. Rev. B **87**, 085303 (2013).
[51] D. E. Reiter, T. Kuhn, M. Glässl, and V. M. Axt, J. Phys. Condens. Matter **26**, 423203 (2014).
[52] J. H. Quilter, A. J. Brash, F. Liu, M. Glässl, A. M. Barth, V. M. Axt, A. J. Ramsay, M. S. Skolnick, and A. M. Fox, Phys. Rev. Lett. **114**, 137401 (2015).
[53] S. Bounouar, M. Müller, A. M. Barth, M. Glässl, V. M. Axt, and P. Michler, Phys. Rev. B **91**, 161302 (2015).
[54] A. M. Barth, S. Lüker, A. Vagov, D. E. Reiter, T. Kuhn, and V. M. Axt, Phys. Rev. B **94**, 045306 (2016).
[55] A. J. Ramsay, T. M. Godden, S. J. Boyle, E. M. Gauger, A. Nazir, B. W. Lovett, A. M. Fox, and M. S. Skolnick, Phys. Rev. Lett. **105**, 177402 (2010).
[56] A. Vagov, M. Glässl, M. D. Croitoru, V. M. Axt, and T. Kuhn, Phys. Rev. B **90**, 075309 (2014).
[57] M. Glässl, L. Sörgel, A. Vagov, M. D. Croitoru, T. Kuhn, and V. M. Axt, Phys. Rev. B **86**, 035319 (2012).
[58] F. Liu, L. M. P. Martins, A. J. Brash, A. M. Barth, J. H. Quilter, V. M. Axt, M. S. Skolnick, and A. M. Fox, Phys. Rev. B **93**, 161407(R) (2016).
[59] A. J. Brash, L. M. P. P. Martins, A. M. Barth, F. Liu, J. H. Quilter, M. Glässl, V. M. Axt, A. J. Ramsay, M. S. Skolnick, and A. M. Fox, J. Opt. Soc. Am. B **33**, C115 (2016).

Publication 2

Biexciton state preparation in a quantum dot via adiabatic rapid passage: Comparison between two control protocols and impact of phonon-induced dephasing

M. Glässl, A. M. Barth, K. Gawarecki, P. Machnikowski, M. D. Croitoru, S. Lüker, D. E. Reiter, T. Kuhn and V. M. Axt,

Physical Review B **87**, 085303 (2013)

DOI: 10.1103/PhysRevB.87.085303

Biexciton state preparation in a quantum dot via adiabatic rapid passage: Comparison between two control protocols and impact of phonon-induced dephasing

M. Glässl,[1,*] A. M. Barth,[1] K. Gawarecki,[2,3] P. Machnikowski,[2] M. D. Croitoru,[1] S. Lüker,[3] D. E. Reiter,[3] T. Kuhn,[3] and V. M. Axt[1]

[1]*Institut für Theoretische Physik III, Universität Bayreuth, 95440 Bayreuth, Germany*

[2]*Institute of Physics, Wrocław University of Technology, 50-370 Wrocław, Poland*

[3]*Institut für Festkörpertheorie, Universität Münster, 48149 Münster, Germany*

(Received 4 October 2012; revised manuscript received 6 January 2013; published 8 February 2013)

We investigate theoretically under what conditions a stable and high-fidelity preparation of the biexciton state in a quantum dot can be realized by means of adiabatic rapid passage in the presence of acoustic phonon coupling. Our analysis is based on a numerically complete real-time path-integral approach and comprises two different schemes of optical driving using frequency-swept (chirped) pulses. We show that depending on the size of the biexciton binding energy, resonant two-photon excitations or two-color schemes can be favorable. It is demonstrated that the carrier-phonon interaction strongly affects the efficiency of both protocols and that a robust preparation of the biexciton is restricted to positive chirps and low temperatures. A considerable increase of the biexciton yield can be achieved realizing temperatures below 4 K.

DOI: 10.1103/PhysRevB.87.085303 PACS number(s): 78.67.Hc, 42.50.Ct, 03.65.Yz, 63.20.kk

I. INTRODUCTION

Realizing an on-demand source of entangled photon pairs is crucial for many innovative applications in quantum information science[1] and quantum optics.[2] Related applications comprise quantum computation,[3] quantum teleportation,[4] or quantum key distribution[5] as well as tests of fundamental aspects of quantum mechanics. A very promising scheme to generate polarization entangled photon pairs is to use the radiative decay of the biexciton state (consisting of two electron-hole pairs) in a semiconductor quantum dot (QD).[6,7] Problems related to the fine-structure splitting of the intermediate exciton states have largely been overcome,[8,9] and recently, impressive experiments have reported the realization of ultrabright sources by coupling a photonic molecule to a single QD.[10]

A necessary precondition for an efficient use of the biexciton decay cascade is a robust preparation of the biexciton state. In principle, an inversion of the QD from the ground to the biexciton state is possible by driving the system with a transform-limited laser pulse of constant frequency, that is resonant to half of the ground-state biexciton transition frequency.[11,12] The drawback of this Rabi-flopping scheme is that it requires a very detailed knowledge of the system parameters such as the transition dipole moments as well as a very precise control of the field intensity in order to ensure the desired inversion. Recalling that these requirements are often only insufficiently fulfilled, it seems that a more practical way to realize a stable and high-quality preparation of the biexciton state is the use of optical driving schemes that rely on adiabatic rapid passage (ARP) and use frequency-swept (chirped) pulses. The basic idea underlying such schemes, which are stable with respect to intensity changes of the laser field, is to drive the system adiabatically along an eigenstate of the coupled light-matter Hamiltonian, whereby the character of the state changes during the pulse via a level anticrossing. Recently, experimental studies by Wu *et al.*[13] and Simon *et al.*[14] that aimed to prepare the single exciton state by means of ARP have proven the applicability of an earlier proposed theoretical protocol[15] and demonstrated a stable generation of the exciton state, which in the ARP regime only slightly depended on the applied pulse area. However, the efficiency reported in these experiments stayed below the ideal case, and most recent theoretical calculations gave compelling evidence that this reduction can be attributed to the coupling of the QD to acoustic phonons.[16–19] It has been demonstrated that acoustic phonons lead to a drastic deterioration of the exciton generation for negative values of the chirp, while an efficient preparation can be achieved for positive chirps, where the phonon influence is restricted to phonon absorption processes that become unlikely at low temperatures.[16] The reported drastic changes compared to the ideal scheme in the absence of the carrier-phonon interaction[15] emphasize the necessity to study the influence of the unavoidable coupling of carriers to acoustic phonons on other schemes relying on ARP in order to fully characterize their true potential.

In this paper, we discuss two different ARP-based protocols aiming at an inversion of the QD to the biexciton state and give a comprehensive analysis of the phonon impact on these schemes. In the first protocol, the QD is driven by a single linearly polarized chirped pulse, where the frequency at the pulse maximum is resonant to half of the ground-state biexciton transition as first suggested by Hui and Liu.[20] In the second scheme, the QD is driven by two circularly polarized chirped pulses, which at the pulse maxima are resonant to the ground-state exciton and to the exciton biexciton transition, respectively. For both protocols, the evolution of the system along an adiabatic branch is more complex than for two-level schemes. For example, in contrast to the two-level case, ARP is here sensitive to the sign of the chirp even without taking the carrier-phonon interaction into account. Therefore, it is *a priori* unclear to what extent the efficiency is affected by the coupling to acoustic phonons. It turns out, however, that similar to the results reported in Ref. 16 for the inversion to the exciton state, an efficient preparation of the biexciton is restricted to positive chirps and low temperatures. Quite significant differences between both investigated protocols

arise for moderate and large values of the biexciton binding energy Δ, as the pulse area threshold that has to be exceeded in order to ensure a purely adiabatic evolution rises strongly with Δ for the first scheme, whereas it is independent of Δ for the second protocol. Above the respective ARP thresholds, the biexciton occupation depends slightly on the pulse area in a nonmonotonic way.

This paper is organized as follows. In Sec. II we outline the model and comment briefly on the real-time path-integral method that is used for our numerical simulations. The latter are presented in Sec. III, where Sec. III A analyzes the phonon impact on the two-photon resonance scheme, while Sec. III B deals with the phonon influence on the two-color protocol and compares the efficiency of both schemes. Finally, Sec. IV concludes the paper.

II. THEORY

We consider an optically driven strongly confined GaAs QD coupled to a continuum of acoustic phonons. Our model Hamiltonian is defined by $H = H_{\text{dot,las}}^{\text{circ/lin}} + H_{\text{dot,ph}}$, where the first term describes the electronic structure of the QD and the coupling to a laser of either circular or linear polarization, while the second term represents the carrier-phonon coupling. For excitations involving circularly σ_+ as well as circularly σ_- polarized pulses, we account for four light-coupled states: the ground state $|G\rangle$, the two single-exciton states $|\sigma_\pm\rangle$, and the biexciton state $|B\rangle$. In this basis, $H_{\text{dot,las}}^{\text{circ}}$ reads

$$\begin{aligned} H_{\text{dot,las}}^{\text{circ}} &= \hbar\omega_0(|\sigma_+\rangle\langle\sigma_+| + |\sigma_-\rangle\langle\sigma_-|) + (2\hbar\omega_0 - \Delta)|B\rangle\langle B| \\ &\quad + \frac{\hbar}{2}[f^{\sigma_+}(t)\,(|\sigma_+\rangle\langle G| + |B\rangle\langle\sigma_-|) + \text{H.c.}] \\ &\quad + \frac{\hbar}{2}[f^{\sigma_-}(t)\,(|\sigma_-\rangle\langle G| + |B\rangle\langle\sigma_+|) + \text{H.c.}]\,, \end{aligned} \tag{1}$$

where $f^{\sigma_\pm}(t) = 2\mathbf{M}\cdot\mathbf{E}_{\sigma_\pm}^{(+)}(t)/\hbar$, with $\mathbf{E}_{\sigma_\pm}^{(+)}$ being the positive frequency component of the $\sigma_\pm$ circularly polarized light field and $\mathbf{M}$ denoting the transition dipole element. $\hbar\omega_0$ defines the ground-state exciton transition energy, and Δ represents the biexciton binding energy. Electron-hole exchange interactions that result in a direct coupling between the single exciton states are neglected, which is well justified for the picosecond time scale considered here and a sufficiently small fine-structure splitting (within 10 μeV for the strongest chirps studied here). For linearly polarized excitations, it is advantageous to introduce the single-exciton state $|X\rangle = (|\sigma_+\rangle + |\sigma_-\rangle)/\sqrt{2}$, which allows us to apply a model with only three levels.[11,21] $H_{\text{dot,las}}^{\text{lin}}$ is then given by

$$\begin{aligned} H_{\text{dot,las}}^{\text{lin}} &= \hbar\omega_0|X\rangle\langle X| + (2\hbar\omega_0 - \Delta)|B\rangle\langle B| \\ &\quad + [\hbar f^{\text{lin}}(t)/2\,(|X\rangle\langle G| + |B\rangle\langle X|) + \text{H.c.}], \end{aligned} \tag{2}$$

with $f^{\text{lin}}(t) = 2\mathbf{M}\cdot\mathbf{E}_{\text{lin}}^{(+)}(t)/\hbar$ and $\mathbf{E}_{\text{lin}}^{(+)}$ denoting the positive frequency component of the linearly polarized electric field.

In this work, we will concentrate on optical driving by chirped Gaussian pulses. These frequency-swept pulses can be obtained from transform-limited Gaussian pulses of the form

$$f_0(t) = \frac{A}{\sqrt{2\pi\tau_0^2}}\exp\left(-\frac{t^2}{2\tau_0^2}\right)\exp(-i\omega t), \tag{3}$$

with the original pulse area A, the pulse duration τ_0, and the central frequency ω. Here, the polarization label used in Eqs. (1) and (2) has been suppressed for simplicity. Applying a Gaussian chirp filter[22] with the chirp coefficient α transforms $f_0(t)$ into

$$f(t) = \frac{A}{\sqrt{2\pi\tau_0\tau}}\exp\left(-\frac{t^2}{2\tau^2}\right)\exp\left(-i\omega t - i\frac{at^2}{2}\right), \tag{4}$$

where $\tau = \sqrt{\alpha^2/\tau_0^2 + \tau_0^2}$ characterizes the chirped pulse length and $a = \alpha/(\alpha^2 + \tau_0^4)$ is the frequency chirp rate. In the following, we will use pulses of different polarizations and central frequencies. Details will be given in Sec. III.

The carrier-phonon coupling is treated in terms of the independent Boson model.[23] Concentrating on the deformation potential coupling to longitudinal acoustic (LA) phonons, which has been shown to provide the dominant dephasing mechanism in GaAs QDs,[24–26] $H_{\text{dot,ph}}$ reads

$$H_{\text{dot,ph}} = \sum_{\mathbf{q}}\hbar\omega_{\mathbf{q}}\,b_{\mathbf{q}}^\dagger b_{\mathbf{q}} + \sum_{\mathbf{q},\nu}\hbar n_\nu(g_{\mathbf{q}}b_{\mathbf{q}} + g_{\mathbf{q}}^* b_{\mathbf{q}}^\dagger)|\nu\rangle\langle\nu|. \tag{5}$$

The operator $b_{\mathbf{q}}^\dagger$ ($b_{\mathbf{q}}$) creates (annihilates) a LA phonon with wave vector $\mathbf{q}$ and energy $\hbar\omega_{\mathbf{q}} = \hbar c_s q$, where $c_s = 5110$ m/s is the longitudinal sound velocity. n_ν denotes the number of excitons present in state $|\nu\rangle$, and $g_{\mathbf{q}} = (g_{\mathbf{q}}^{\text{e}} - g_{\mathbf{q}}^{\text{h}})$ represents the exciton-phonon coupling constant that is given as the difference between the electron-phonon and hole-phonon coupling constants,

$$g_{\mathbf{q}}^{\text{e(h)}} = \Psi^{e(h)}(\mathbf{q})D_{e(h)}\sqrt{\frac{q}{2V\rho\hbar c_s}}, \tag{6}$$

where V is the sample volume, $D_e = -14.6$ eV and $D_h = -4.8$ eV denote the deformation potential coupling constants of electrons and holes, and $\rho = 5370\,\text{kg/m}^3$ is the material density. $\Psi^{e(h)}$ represents the form factor of the carriers confined in the QD. For simplicity, we assume a spherical harmonic oscillator confinement, leading to

$$\Psi^{e(h)}(\mathbf{q}) = \exp\left(-q^2a_{e(h)}^2/4\right). \tag{7}$$

We choose an electron confinement length of $a_e = 3$ nm and set $a_h = 0.87a_e$. As we are interested in the dynamics on time scales of some tens of picoseconds, we neglect further relaxation processes that take place on longer time scales such as radiative decay, which is known to evolve on a nanosecond time scale.[27]

To analyze the combined carrier-phonon dynamics, we use a numerically exact real-time path-integral approach that accounts fully for all non-Markovian effects and arbitrary multiphonon processes. This allows us to study the phonon influence on the driven dynamics at arbitrary temperatures and in parameter ranges where approximate methods come to their limits.[28] A detailed description of the formalism is given in Ref. 29. Additional comments on the challenges that are faced within the path-integral approach when accounting for more than two electronic levels can be found in Ref. 21.

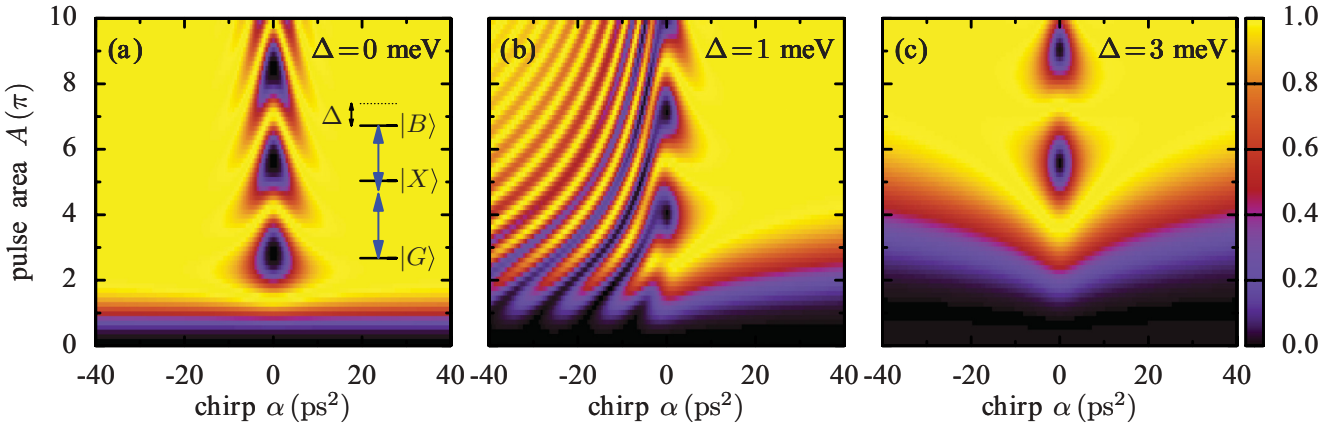

FIG. 1. (Color online) Final biexciton occupation after a linearly polarized and frequency-swept Gaussian pulse with $\tau_0 = 2$ ps as a function of the original pulse area A and the chirp α for biexciton binding energies of (a) $\Delta = 0$, (b) 1, and (c) 3 meV in the absence of the carrier-phonon coupling. The central frequency (at zero chirp) is chosen such that the two-photon process is resonant to the ground-state biexciton transition [cf. inset in (a)].

III. RESULTS

In this section, we shall compare two protocols allowing for the preparation of the biexciton state by means of ARP and analyze how the presence of acoustic phonons affects these schemes. For our calculations, we apply chirps ranging from $\alpha = -40$ to $+40$ ps^2 and choose an original pulse length of $\tau_0 = 2$ ps in order to use parameters similar to those in recent experiments that reported on a robust quantum-dot exciton generation via ARP.[13,14]

A. Two-photon resonance ARP scheme

Let us first concentrate on a two-photon resonance ARP scheme that uses one linearly polarized pulse. The central frequency of this pulse is chosen such that for zero chirp the two-photon process is resonant to the ground-state biexciton transition, i.e., $\omega = \omega_0 - \Delta/(2\hbar)$, as schematically sketched in the inset of Fig. 1(a).

To provide a reference for the phonon influence on the efficiency of this protocol, Fig. 1 shows the final biexciton occupation after the pulse as a function of the original pulse area A and the chirp coefficient α for different values of the biexciton binding energy Δ, neglecting the exciton-phonon coupling. For zero chirp, the biexciton occupation depends sensitively on the pulse intensity and performs Rabi rotations between the ground and the biexciton state with a Rabi period that strongly depends on the biexciton binding energy.[11] In contrast, for large enough positive chirps, an ideal and robust biexciton preparation, which is insensitive to small variations of the pulse area, can be achieved provided that the applied pulse area exceeds the ARP threshold. The latter rises significantly with increasing Δ and shows for finite Δ also a considerable dependence on the strength of the chirp. Interestingly, the situation is different for negative chirps: for $\alpha < 0$, a stable biexciton preparation can be only achieved for almost vanishing or large enough biexciton binding energies [cf. Figs. 1(a) and 1(c)] and fails for moderate values of Δ, as can be exemplarily seen from Fig. 1(b) for $\Delta = 1$ meV, where for $\alpha < 0$ a stripelike pattern forms. This dependence of the dynamics on the sign of the chirp contrasts to the widely studied ARP protocols for the generation of the exciton state[13–16] and has to be taken into account also in situations where one expects the influence of phonons to be negligible.

The results shown in Fig. 1 as well as the phonon impact that will be studied below can be most easily understood by analyzing the system evolution in the dressed-state picture, i.e., by considering the instantaneous eigenstates and eigenenergies that are obtained by diagonalizing the combined light-matter Hamiltonian $H^{\rm lin}_{\rm dot,las}$. The corresponding eigenenergies are plotted in Fig. 2 as a function of time for $\alpha = 20$ ps^2 and different values of the original pulse area A as well as of the biexciton binding energy Δ together with the corresponding pulse envelope functions (shaded areas). Long before and long after the pulse maximum, it is possible to identify the instantaneous eigenstates with the electronic ground state $|G\rangle$, the single-exciton state $|X\rangle$, and the biexciton state $|B\rangle$, as is indicated in Fig. 2. During the pulse, the character of the eigenstates changes. For example, the lowest branch, which can initially be identified with $|G\rangle$, eventually transforms into $|B\rangle$. It is precisely this transformation that allows a stable biexciton preparation within the two-photon resonance ARP scheme for positive values of α when the condition for adiabatic passage is fulfilled, i.e., when the change in the frequency and the change in the amplitude of the pulse are slow compared to the Rabi frequency.[30] In this case the system evolves along a single branch and passes all anticrossings. Obviously, both conditions are better fulfilled for higher pulse areas (corresponding to higher Rabi frequencies), which can be nicely seen from Fig. 2 by comparing the left and the right columns, which show the branches for $A = 2\pi$ and $A = 6\pi$, respectively: the splitting of the anticrossings considerably increases with rising A. By comparing the different rows of Fig. 2 it can also be seen that for a given pulse area, the anticrossings become narrower for larger biexciton binding energies, explaining the rising threshold for ARP with increasing Δ, as shown in Fig. 1. While for $A = 2\pi$ and $\Delta = 0$ meV [cf. Fig. 2(a)] the splitting of the central anticrossing at $t = 0$ is large enough to ensure an adiabatic

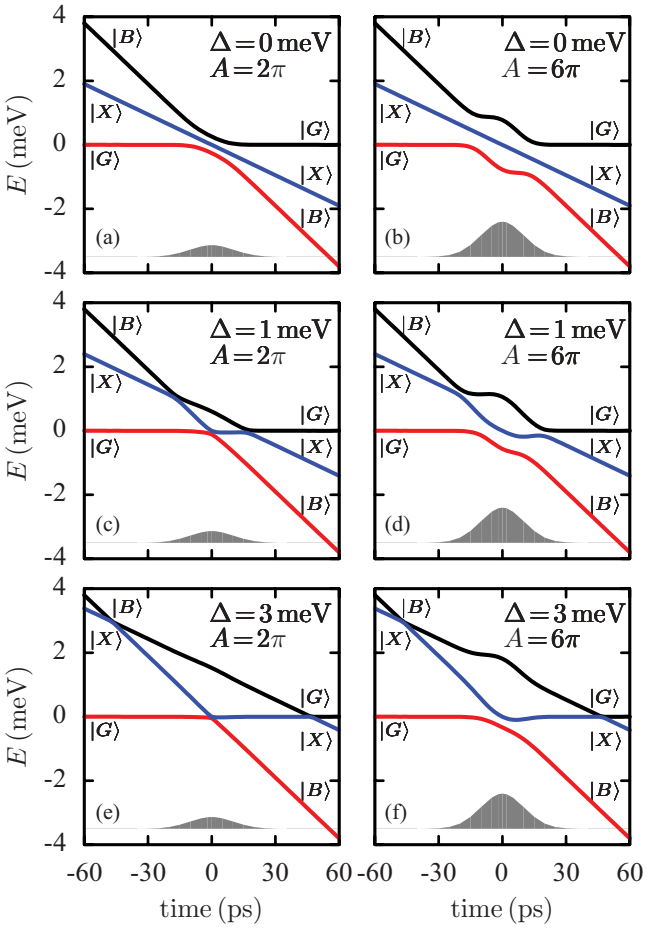

FIG. 2. (Color online) Adiabatic spectral branches of the laser-driven QD system for the two-photon resonance ARP scheme for $\tau_0 = 2$ ps, $\alpha = 20$ ps^2, and pulse areas and biexciton binding energies as indicated. The evolution for $\alpha = -20$ ps^2 can be read off the plots by following the branches from the right to the left. The gray shaded areas represent the pulse envelope functions, which have been shifted downwards for clarity.

passage resulting in the preparation of the biexciton state [cf. Fig. 1(a)], the situation is different for larger Δ. When the anticrossing becomes too narrow [cf. Figs. 2(c) and 2(e)], the chirp rate is no longer small compared to the spacing between the branches, the condition for ARP is violated, and the system does not evolve along a single branch.

Considering negative chirps, the situation is slightly more complex. For $\alpha = -20$ ps^2, the system evolution along the instantaneous eigenstates can easily be derived from Fig. 2 by reading the plots from the right to the left (i.e., by replacing the time t by $-t$). Obviously, a transformation from $|G\rangle$ into $|B\rangle$ is here possible by following the uppermost branch. To understand why this transformation fails at intermediate Δ, as seen in Fig. 1(b), let us concentrate on the right column of Fig. 2, showing the branches for $A = 6\pi$, where for finite chirps a robust preparation of the biexciton is reached for $\Delta = 0$ as well as for $\Delta = 3$ meV [cf. Figs. 1(a) and 1(c)]. In Fig. 2(b), for $\Delta = 0$, one passes two anticrossings along the upper branch that are wide enough to guarantee that the system evolves completely adiabatically. For $\Delta = 3$ meV, as

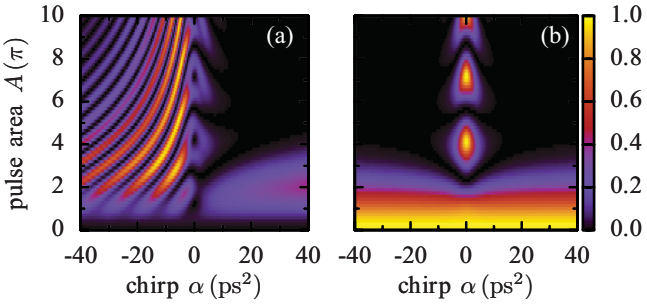

FIG. 3. (Color online) Final (a) exciton and (b) ground-state occupation after a linearly polarized and frequency-swept Gaussian pulse with $\tau_0 = 2$ ps as a function of the original pulse area A and the chirp α for $\Delta = 1$ meV in the absence of the carrier-phonon coupling.

shown in Fig. 2(f), both anticrossings are very narrow, and the system jumps nonadiabatically two times from one branch to another branch instead of following the anticrossings; i.e., here, the evolution is characterized by two crossings. However, both crossings together and in combination with the fact that the level spacing between the two lower branches at $t = 0$ is still wide enough to ensure that this anticrossing is passed adiabatically result again in the preparation of the biexciton. For $\Delta = 1$ meV [cf. Fig. 2(d)], the anticrossings between the two upper branches are narrower than for $\Delta = 0$ meV but are still considerably wider than for $\Delta = 3$ meV. As a consequence, when reaching these anticrossings, the system does neither evolve completely adiabatically (via pure anticrossings) nor purely nonadiabatically (via pure crossings), and a Rabi-like behavior is realized instead of a robust preparation of the biexciton, giving rise to the stripelike pattern, as seen in Fig. 1(b) for $\alpha < 0$. However, as the central anticrossing between the two lowest branches at $t = 0$ is quite wide and passed fully adiabatically, the lowest branch, which finally transforms into $|G\rangle$, is not occupied at all, and the Rabi-like behavior is restricted to the subspace spanned by $|X\rangle$ and $|B\rangle$. The latter is illustrated is Fig. 3, where the occupations of the single-exciton state and the ground state are shown as functions of A and α: while the exciton occupation shows for finite α a stripe pattern that corresponds to that seen in Fig. 1(b), the ground-state occupation does not show such a structure at all and remains unoccupied for high pulse areas. Finally, the details of the stripe pattern can be explained as follows. The fringes which develop from the occupation maxima or minima of the usual Rabi rotations that are realized at $\alpha = 0$ decline for rising chirps because of two reasons: first, with increasing chirp the effective pulse area exceeds more and more the original pulse area [as can be seen by comparing Eqs. (3) and (4)], and second, the Rabi period decreases with increasing detuning.[31] This leads to an increased number of occupation maxima or minima compared to $\alpha = 0$. The attenuation of the stripe pattern in the range of high pulse areas and large chirps is due to an increasing splitting between the upper spectral branches that leads to a more and more adiabatic evolution.

Next, we shall include the carrier-phonon interaction. The final biexciton occupation after the pulse as a function of the original pulse area A and the chirp coefficient α at a temperature of $T = 4$ K for the same biexciton binding energies as considered in Fig. 1 is shown in Figs. 4(a)–4(c).

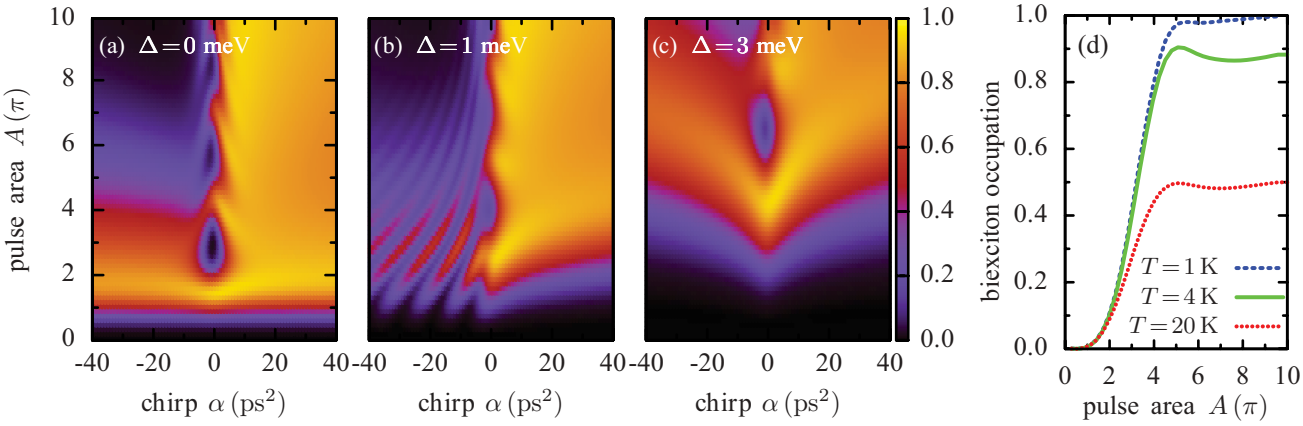

FIG. 4. (Color online) Final biexciton occupation after a linearly polarized and frequency-swept Gaussian pulse with $\tau_0 = 2$ ps within the two-photon resonance ARP scheme. In (a)–(c) the occupation of the biexciton is shown as a function of the original pulse area A and the chirp α for biexciton binding energies of (a) $\Delta = 0$, (b) 1, and (c) 3 meV at $T = 4$ K. In (d) the final occupation is plotted as a function of the original pulse area A for $\Delta = 2$ meV and a chirp of $\alpha = 20$ ps^2 at different temperatures.

Compared to the ideal evolution in the absence of acoustic phonons there are similarities as well as obvious differences. As in the phonon-free case the ARP threshold in the pulse area rises with increasing biexciton binding energies, and for $\Delta = 1$ meV and negative chirps, the stripelike pattern discussed above is still visible. However, it is clearly seen that within the full model, the efficiency of the protocol does now strongly depend on the sign of the chirp, regardless of the size of the biexciton binding energy. While for positive chirps a rather stable biexciton generation is reached, negative chirps result in general in very low occupations of the biexciton state, in particular at high-pulse areas. To understand this difference, one should recall that for a positive chirp, the adiabatic evolution follows the lowest adiabatic branch (cf. Fig. 2). Phonon-mediated transitions to one of the other two branches, which spoil the purely adiabatic evolution and hamper the preparation of the biexciton state, are, for $\alpha > 0$, thus only possible via phonon absorption processes. At 4 K the latter are rather weak, and hence there is a perceivable but small deterioration of the protocol efficiency compared to the phonon-free case. For negative chirps, in contrast, the adiabatic evolution of the system follows the uppermost branch, and transitions to one of the lower branches are possible by phonon emission processes, which dominate at low temperatures. As a consequence, the population of the upper branch is drastically reduced over the course of time, and an efficient preparation of the biexciton via ARP is no longer possible.

The temperature dependence of the efficiency of the two-photon ARP scheme is illustrated in Fig. 4(d), where the final biexciton occupation is shown as a function of A for a chirped pulse with $\alpha = 20$ ps^2, a biexciton binding energy of $\Delta = 2$ meV, and three different temperatures, $T = 1$, 4, and 20 K. While occupations of about 90% are reached for 4 K and pulse areas above the ARP threshold, the situation drastically deteriorates at elevated temperatures, where phonon absorption processes gain in importance due to a higher number of thermal phonons. Already at 20 K, the biexciton generation turns out to be very inefficient, with typical biexciton occupations staying below 0.5. On the contrary, it is interesting to note that for temperatures well below 4 K, an almost ideal biexciton preparation can be realized, as exemplarily shown for $T = 1$ K, where in the adiabatic regime a high-fidelity preparation of the biexciton with occupations higher than 0.98 is achieved. This remarkably strong difference between 1 and 4 K contrasts wide-spread expectations that for low temperatures the impact of phonons is not very sensitive to a variation of a few degrees Kelvin and emphasizes the importance of realizing low temperatures.

A closer look on the curves plotted in Fig. 4(d) reveals further that, for pulse intensities above the threshold, the biexciton occupation depends nonmonotonically on the pulse area: an initial decrease is followed by a slight increase. This nonmonotonic behavior in the ARP regime corresponds to the reappearance of Rabi rotations in the usual Rabi regime[32,33] and can be traced back to the resonance character of the carrier-phonon coupling.[34] The slow increase of the signal at high pulse areas, as shown in Fig. 4(d), is mainly due to the Gaussian pulse envelope, which in the Rabi regime is known to lead to a rather weak reappearance because of an incomplete dynamical decoupling between lattice vibrations and electronic dynamics.[33]

B. Two-color pulse ARP scheme

Let us next turn to an alternative ARP scheme. The QD is now driven by two simultaneously applied frequency-swept pulses of equal chirp, where the first pulse is circularly σ_+ polarized and at the pulse maximum resonant to the ground-state exciton transition, i.e., $\omega_1 = \omega_0$, while the second pulse is circularly σ_- polarized and at its maximum in resonance to the exciton biexciton transition, i.e., $\omega_2 = \omega_0 - \Delta/\hbar$. A schematic sketch of this two-color protocol is drawn as an inset in Fig. 5(a). Neglecting the exciton-phonon coupling, also the two-color scheme allows for an ideal and stable preparation of the biexciton. As an example, Fig. 5(a) shows the final biexciton occupation as a function of A and α for $\Delta = 2$ meV, where A now denotes the original pulse area of each circularly polarized pulse. We checked that even considerable deviations

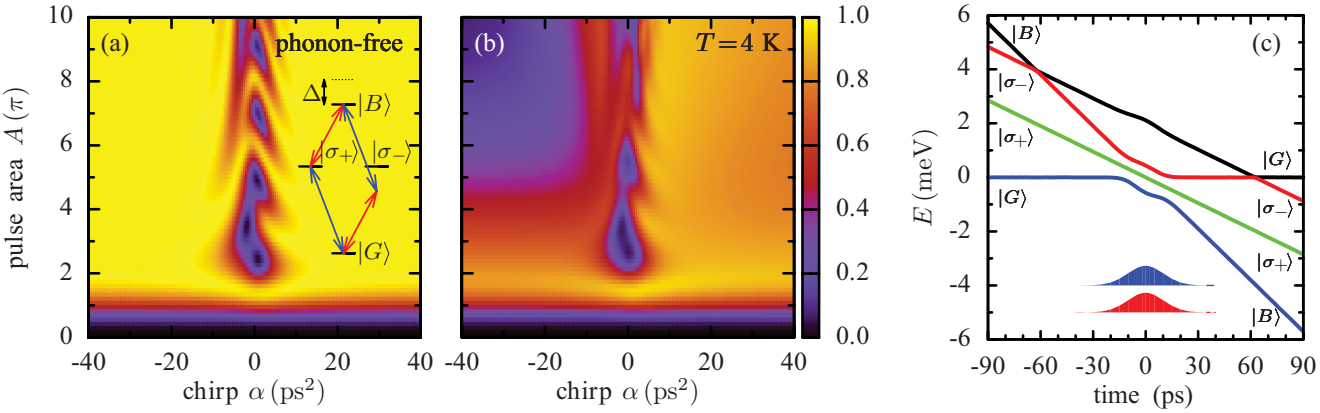

FIG. 5. (Color online) Results for the two-color pulse ARP scheme that is schematically sketched in the inset in (a). The final biexciton occupation is shown as a function of the original pulse area A of each circularly polarized pulse and the chirp α for $\tau_0 = 2$ ps and a biexciton binding energy of $\Delta = 2$ meV (a) in the phonon-free case and (b) in the full model at $T = 4$ K. (c) The evolution of the adiabatic spectral branches for $\tau_0 = 2$ ps, $A = 4\pi$, $\alpha = 20$ ps^2 and $\Delta = 2$ meV. The evolution for $\alpha = -20$ ps^2 can be read off the plot by following the branches from the right to the left. The shaded areas represent the envelope functions of both pulses, which have been shifted downwards for clarity.

between both pulses with regard to the pulse intensity or the frequency sweep do not reduce the efficiency of the scheme provided that both components fulfill the condition for ARP. Also a finite delay between both pulses has no significant effect on the efficiency as long as the pulse that drives the ground-state exciton transition precedes the pulse driving the exciton-biexciton transition or at least has a sufficiently large temporal overlap and provided that the systems evolves adiabatically. Thus, the protocol is robust with respect to these changes, and therefore, it is justified to concentrate on the case of equal pulse parameters and zero delay for reasons of simplicity.

An analysis of the adiabatic spectral branches for the two-color protocol shares many similarities with that given in Sec. III A for the two-photon resonance scheme and shall therefore not be presented at length. For positive chirps, the ground state transforms into the biexciton state via the lowest branch, whereas for negative chirps, the same transformation can be achieved by following the uppermost branch

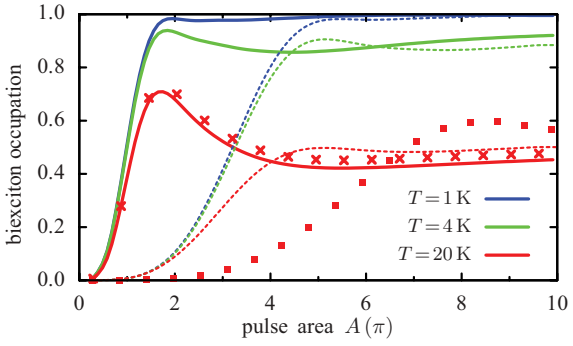

FIG. 6. (Color online) Final biexciton occupation after the two-color pulse ARP scheme (solid lines) and the two-photon resonance ARP scheme (dashed lines) as a function of the original pulse area A for $\Delta = 2$ meV and $\alpha = 20$ ps^2 at different temperatures. Crosses and squares represent results for $\Delta = 5$ meV, $\alpha = 20$ ps^2, and $T = 20$ K for the two-color pulse ARP protocol and the two-photon resonance ARP protocol, respectively.

[cf. Fig. 5(c)]. Therefore, in the presence of the carrier-phonon coupling, a stable preparation is again only possible for positive chirps, as illustrated in Fig. 5(b) for $T = 4$ K. A further similarity to the first protocol is that the two-color scheme is sensitive to the sign of the chirp even in the phonon-free case and that for negative chirps and small biexciton binding energies a Rabi-like behavior is realized due to a neither purely adiabatic nor purely nonadiabatic evolution, this time in the subspace spanned by $|\sigma_-\rangle$ and $|B\rangle$. The resulting patterns seen in the occupations of $|\sigma_-\rangle$ and $|B\rangle$ when recorded as a function of A and α (not shown) resemble those discussed in Figs. 1(b) and 3(a). Here, these patterns are most pronounced for $\Delta \sim 0.5$ meV, which is half of the value of $\Delta \sim 1$ meV, where the Rabi-like behavior is strongest in the two-photon resonance scheme. Recall that for these values of Δ the detuning of the respective off-resonant levels is identical for both protocols.

Despite these similarities, one can also note significant and interesting differences between both considered protocols. Unlike for the two-photon resonance scheme, for the two-color protocol the pulse area threshold that must be exceeded in order to ensure an adiabatic dynamics is independent of the biexciton binding energy, as the transition to the biexciton never involves excitation paths via strongly detuned intermediate levels. Independent of the chirp, the threshold is roughly given by $A = 2\pi$. Therefore, the two-color protocol is particularly advantageous for QDs with large biexciton binding energies. For example, for a high but still realistic value of $\Delta = 5$ meV and a chirp of $\alpha = 20$ ps^2, the two-photon resonance scheme would require pulse areas above 8π to reach the adiabatic limit and thus 16 times as intense pulses as within the two-color protocol. This is exemplarily shown in Fig. 6 for $T = 20$ K.

Besides the threshold characteristics, the detailed temperature and pulse area dependencies in the respective ARP regimes differ. This is illustrated in Fig. 6, where the biexciton occupation is plotted for both protocols as a function of the pulse area for a chirp of $\alpha = 20$ ps^2 and at temperatures of 1, 4, and 20 K. Solid lines represent the results within the two-color scheme, and dashed lines show the results of the two-photon resonance protocol that have already been

displayed in Fig. 4(d). While for $T = 20$ K the two-color scheme is, for pulse areas around 2π, much more efficient than the two-photon resonance protocol, the situation is reversed at high pulse areas, where the efficiency is worse for the two-color scheme. For low temperatures, the two-color protocol performs slightly better, in particular at high pulse areas, where for $T = 1$ K an almost perfect inversion to the biexciton state is achieved. Common to the two-photon resonance scheme is the pronounced difference in the protocol efficiency between $T = 1$ and 4 K as well as the nonmonotonic pulse area dependence. However, for the two-color scheme, the latter is slightly stronger and shows minima at smaller pulse areas. This finding is in line with recent calculations for transform-limited pulses that have revealed that the reappearance of Rabi rotations sets in at smaller pulse areas when the polarization of the excitation is changed from linear to circular.[35]

IV. CONCLUSIONS

We have analyzed the impact of acoustic phonons on two protocols aiming at a robust preparation of the biexciton state in a semiconductor QD. In the absence of the carrier-phonon interaction, either driving the system with a single linearly polarized chirped pulse tuned at its maximum to the two-photon resonance of the ground-state biexciton transition or using a two-color scheme where two circularly polarized chirped pulses are, at their maxima, in resonance with the ground-state exciton and the exciton biexciton transition, respectively, enables a perfect preparation of the biexciton state provided that the conditions for adiabatic rapid passage are fulfilled. The most remarkable difference between both schemes, which is seen already without phonons, is the finding that the threshold for ARP rises drastically for the first protocol with rising biexciton binding energies, while in the second protocol there is essentially no such dependence on the threshold. In contrast to related investigations of the preparation of the exciton state we here find a strong asymmetry with respect to the sign of the frequency sweep already in the idealized phonon-free case. In particular, we observe for finite negative chirps and intermediate biexciton binding energies a Rabi-like behavior, indicating a regime where the system neither evolves fully adiabatically along the adiabatic spectral branches nor switches between different branches without interference as would be the case in the extreme nonadiabatic limit.

Accounting for phonons in general reduces the fidelity of both protocols and introduces an additional asymmetry with respect to the sign of the chirp that, as also known from earlier studies of the exciton preparation, results from the fact that for positive chirp the phonon emission is suppressed. A robust biexciton preparation is thus restricted to positive chirps and low temperatures. It is interesting to note that already at 4 K the efficiency is reduced to about 90%, while at 1 K an almost perfect biexciton preparation is possible in spite of the phonons.

Taking the efficiency of the biexciton preparation as the only criterion, it turns out that the two-color scheme performs slightly better for low temperatures. Moreover, for all temperatures the threshold is lower. Nevertheless, evaluating both schemes for practical usability, these advantages should be weighed against some obvious drawbacks: the need for two pulses with different colors and (when thinking of using the biexciton decay cascade) the problem of stray laser light at the detection wavelength. The latter problem can be overcome by using up-conversion techniques[36] or nonresonant emitter-cavity coupling.[37] Thus, by paying the price of increased effort one can indeed benefit from the better performance of the two-color scheme. We expect that our analysis shall provide helpful guidance for making an adequate decision between performance and effort in upcoming experiments.

ACKNOWLEDGMENTS

M.G. is grateful for financial support from the Studienstiftung des Deutschen Volkes. M.D.C. is supported by the Alexander von Humboldt Foundation. P.M. and T.K. gratefully acknowledge financial support in the framework of a Research Group Linkage Project of the Alexander von Humboldt Foundation.

*martin.glaessl@uni-bayreuth.de

[1] D. Bouwmeester, A. K. Ekert, and A. Zeilinger, *The Physics of Quantum Information* (Springer, Berlin, 2000).
[2] S. Haroche and J. Raimond, *Exploring the Quantum* (Oxford University Press, Oxford, 2006).
[3] M. A. Nielsen and I. Chuang, *Quantum Computation and Quantum Information* (Cambridge University Press, Cambridge, 2000).
[4] D. Bouwmeester, J. Pan, K. Mattle, M. Eibl, H. Weinfurter, and A. Zeilinger, Nature (London) **390**, 575 (1997).
[5] N. Gisin, G. Ribordy, W. Tittel, and H. Zbinden, Rev. Mod. Phys. **74**, 145 (2002).
[6] E. Moreau, I. Robert, L. Manin, V. Thierry-Mieg, J. M. Gérard, and I. Abram, Phys. Rev. Lett. **87**, 183601 (2001).
[7] R. Stevenson, R. J. Young, P. Atkinson, K. Cooper, D. A. Ritchie, and A. J. Shields, Nature (London) **439**, 179 (2006).
[8] N. Akopian, N. H. Lindner, E. Poem, Y. Berlatzky, J. Avron, D. Gershoni, B. D. Gerardot, and P. M. Petroff, Phys. Rev. Lett. **96**, 130501 (2006).
[9] R. Trotta, E. Zallo, C. Ortix, P. Atkinson, J. D. Plumhof, J. van den Brink, A. Rastelli, and O. G. Schmidt, Phys. Rev. Lett. **109**, 147401 (2012).
[10] A. Dousse, J. Suffczyński, A. Beveratos, O. Krebs, A. Lemaître, I. Sagnes, J. Bloch, P. Voisin, and P. Senellart, Nature (London) **466**, 217 (2010).
[11] P. Machnikowski, Phys. Rev. B **78**, 195320 (2008).
[12] S. Stufler, P. Machnikowski, P. Ester, M. Bichler, V. M. Axt, T. Kuhn, and A. Zrenner, Phys. Rev. B **73**, 125304 (2006).
[13] Y. Wu, I. M. Piper, M. Ediger, P. Brereton, E. R. Schmidgall, P. R. Eastham, M. Hugues, M. Hopkinson, and R. T. Phillips, Phys. Rev. Lett. **106**, 067401 (2011).

[14]C. M. Simon, T. Belhadj, B. Chatel, T. Amand, P. Renucci, A. Lemaitre, O. Krebs, P. A. Dalgarno, R. J. Warburton, X. Marie *et al.*, Phys. Rev. Lett. **106**, 166801 (2011).
[15]E. R. Schmidgall, P. R. Eastham, and R. T. Phillips, Phys. Rev. B **81**, 195306 (2010).
[16]S. Lüker, K. Gawarecki, D. E. Reiter, A. Grodecka-Grad, V. M. Axt, P. Machnikowski, and T. Kuhn, Phys. Rev. B **85**, 121302 (2012).
[17]A. Debnath, C. Meier, B. Chatel, and T. Amand, Phys. Rev. B **86**, 161304 (2012).
[18]P. R. Eastham, A. O. Spracklen, and J. Keeling, arXiv:1208.5001.
[19]K. Gawarecki, S. Lüker, D. E. Reiter, T. Kuhn, M. Glässl, V. M. Axt, A. Grodecka-Grad, and P. Machnikowski, Phys. Rev. B **86**, 235301 (2012).
[20]H. Y. Hui and R. B. Liu, Phys. Rev. B **78**, 155315 (2008).
[21]M. Glässl, M. D. Croitoru, A. Vagov, V. M. Axt, and T. Kuhn, Phys. Rev. B **85**, 195306 (2012).
[22]B. Saleh and M. Teich, *Fundamentals of Photonics*, Wiley Series in Pure and Applied Optics (Wiley Interscience, New York, 2007).
[23]G. D. Mahan, *Many-Particle Physics*, 2nd ed. (Plenum, New York, 1990).
[24]A. Vagov, V. M. Axt, T. Kuhn, W. Langbein, P. Borri, and U. Woggon, Phys. Rev. B **70**, 201305(R) (2004).
[25]A. J. Ramsay, A. V. Gopal, E. M. Gauger, A. Nazir, B. W. Lovett, A. M. Fox, and M. S. Skolnick, Phys. Rev. Lett. **104**, 017402 (2010).
[26]B. Krummheuer, V. M. Axt, and T. Kuhn, Phys. Rev. B **65**, 195313 (2002).
[27]P. Borri, W. Langbein, S. Schneider, U. Woggon, R. L. Sellin, D. Ouyang, and D. Bimberg, Phys. Rev. Lett. **87**, 157401 (2001).
[28]M. Glässl, A. Vagov, S. Lüker, D. E. Reiter, M. D. Croitoru, P. Machnikowski, V. M. Axt, and T. Kuhn, Phys. Rev. B **84**, 195311 (2011).
[29]A. Vagov, M. D. Croitoru, M. Glässl, V. M. Axt, and T. Kuhn, Phys. Rev. B **83**, 094303 (2011).
[30]V. S. Malinovsky and J. L. Krause, Eur. Phys. J. D **14**, 147 (2001).
[31]L. Allen and J. H. Eberly, *Optical Resonance and Two-Level Atoms* (Wiley, New York, 1975).
[32]A. Vagov, M. D. Croitoru, V. M. Axt, T. Kuhn, and F. M. Peeters, Phys. Rev. Lett. **98**, 227403 (2007).
[33]M. Glässl, M. D. Croitoru, A. Vagov, V. M. Axt, and T. Kuhn, Phys. Rev. B **84**, 125304 (2011).
[34]P. Machnikowski and L. Jacak, Phys. Rev. B **69**, 193302 (2004).
[35]M. Glässl and V. M. Axt, Phys. Rev. B **86**, 245306 (2012).
[36]M. Paillard, X. Marie, P. Renucci, T. Amand, A. Jbeli, and J. M. Gérard, Phys. Rev. Lett. **86**, 1634 (2001).
[37]S. Ates, S. M. Ulrich, A. Ulhaq, S. Reitzenstein, A. Löffler, S. Höfling, A. Forchel, and P. Michler, Nat. Photonics **3**, 724 (2009).

Publication 3

Proposed Robust and High-Fidelity Preparation of Excitons and Biexcitons in Semiconductor Quantum Dots Making Active Use of Phonons

M. Glässl, A. M. Barth and V. M. Axt,

Physical Review Letters **110**, 147401 (2013)

DOI: 10.1103/PhysRevLett.110.147401

Proposed Robust and High-Fidelity Preparation of Excitons and Biexcitons in Semiconductor Quantum Dots Making Active Use of Phonons

M. Glässl,[1,*] A. M. Barth,[1] and V. M. Axt[1]

[1]*Institut für Theoretische Physik III, Universität Bayreuth, 95440 Bayreuth, Germany*

(Received 25 January 2013; published 2 April 2013)

It is demonstrated how the exciton and the biexciton state of a quantum dot can be prepared with high fidelity on a picosecond time scale by driving the dot with a strong laser pulse that is tuned above the exciton resonance for exciton preparation and in resonance with the exciton transition for biexciton preparation. The proposed protocols make use of the phonon-induced relaxation towards photon dressed states in optically driven quantum dots and combine the simplicity of traditional Rabi oscillation schemes with the robustness of adiabatic rapid passage schemes. Our protocols allow for an on-demand, fast, and almost perfect state preparation even at strong carrier-phonon interaction where other schemes fail. In fact, the performance of the presented protocols is shown to be better the stronger the carrier-phonon interaction is.

DOI: 10.1103/PhysRevLett.110.147401 PACS numbers: 78.67.Hc, 03.65.Yz, 63.20.kk, 78.47.−p

Realizing a high-quality, robust, on-demand, and fast exciton or biexciton preparation in semiconductor quantum dots (QDs) is of great importance for many promising QD-based devices such as single [1,2] or entangled [3–6] photon sources that are crucial for various applications in the field of quantum information processing [7,8] as well as for tests of fundamental aspects of quantum mechanics [9]. While a perfect initiation of the QD in both states can in principle be realized via Rabi oscillations [10,11], these simple schemes suffer from a high sensitivity on the dipole moments and the pulse intensity. A preparation that is robust against fluctuations in the coupling strengths can be achieved using protocols with frequency swept pulses that rely on adiabatic rapid passage (ARP) [12–14]. However, the degree of exciton inversion realized in ARP-based experiments [13,14] stayed considerably below the ideal case and most recent theoretical works gave compelling evidence that this reduction can be attributed to acoustic phonon coupling [15,16] that is also known to strongly limit the fidelity of traditional Rabi oscillation schemes [17–19].

In this Letter, we shall present protocols that combine the simplicity of Rabi oscillation schemes with the robustness of ARP schemes and give the discussion of phonon influences a completely different perspective by demonstrating how one can highly benefit from the otherwise undesired carrier-phonon coupling. To be specific, we propose protocols allowing for a high-fidelity and robust phonon-assisted preparation of the exciton as well as the biexciton state in strongly confined QDs that rely on exciting the system with an off-resonant intense pulse. Our schemes make active use of the acoustic phonon coupling by exploiting the characteristics of the stationary nonequilibrium state towards which the QD is driven due to the system-environment interaction and are shown to perform better the stronger the carrier phonon coupling is.

Let us first concentrate on preparing the single exciton state. To this end, we assume a circularly polarized excitation, which allows us to model the laser-driven QD as an electronic two-level system that consists of the ground state $|G\rangle$ without electron-hole pairs and the single exciton state $|X\rangle$ described by the Hamiltonian

$$H_{\mathrm{QD},L} = \hbar\omega_X |X\rangle\langle X| - \left[\frac{\hbar f(t)}{2} e^{-i\omega_L t}|X\rangle\langle G| + \mathrm{H.c.}\right], \quad (1)$$

where ω_L is the laser frequency and $f(t)$ denotes the instantaneous Rabi frequency that for a Gaussian pulse is given by $f(t) = \alpha/(\sqrt{2\pi}\tau_0)\exp(-t^2/2\tau_0^2)$, where α is the pulse area and τ_0 defines the pulse length. The pure dephasing carrier-phonon coupling is modeled by the Hamiltonian

$$H_{\mathrm{QD,ph}} = \sum_{\mathbf{q}} \hbar\omega_{\mathbf{q}} b_{\mathbf{q}}^\dagger b_{\mathbf{q}} + \sum_{\mathbf{q},\nu} \hbar n_\nu (g_{\mathbf{q}} b_{\mathbf{q}} + g_{\mathbf{q}}^* b_{\mathbf{q}}^\dagger)|\nu\rangle\langle\nu|, \quad (2)$$

where ν labels the electronic states, n_ν counts the excitons present in the state $|\nu\rangle$, $b_{\mathbf{q}}^\dagger$ creates a longitudinal acoustic (LA) bulk phonon with wave vector $\mathbf{q}$ and energy $\hbar\omega_{\mathbf{q}}$, and $g_{\mathbf{q}}$ denote the exciton-phonon coupling constants. We concentrate on the deformation potential coupling to LA phonons that is dominant for GaAs QDs [19,20], we choose a radial electron confinement length of 3 nm and use the same coupling parameters as in Ref. [21] that have been shown to nicely reproduce experimental results [21]. To calculate the coupled carrier-phonon dynamics, we shall apply a numerically exact real-time path-integral approach that allows us to study the system evolution without invoking any approximations to the model given above. Details of this method can be found in Ref. [22].

The phonon coupling strongly affects the QD dynamics. Most important for our present discussion, it pushes the laser driven electronic system towards a stationary

nonequilibrium state. We demonstrated in Ref. [23] that, for a two-level system with weak carrier-phonon coupling as realized in GaAs QDs and a constant optical driving with $f(t) = \text{const}$, this stationary state can be well approximated by a thermal distribution over the eigenstates of $H_{\text{QD},L}$, often referred to as photon dressed states, leading to a stationary exciton occupation of

$$C_X(t=\infty) = \frac{1}{2}\left[1 + \frac{\Delta}{\hbar\Omega}\tanh\left(\frac{\hbar\Omega}{2k_BT}\right)\right], \qquad (3)$$

where $\Omega = \sqrt{f^2 + (\Delta/\hbar)^2}$ and $\Delta = \hbar(\omega_L - \omega_X)$ is the detuning between the laser and the QD transition. Obviously, Eq. (3) predicts a stationary inversion for $\Delta/(\hbar\Omega) \approx 1$ and $\hbar\Omega/2kT \gg 1$. Indeed, the exact stationary exciton occupation as calculated by using the path-integral approach and shown in Fig. 1(a) as a function of Δ and T is almost perfectly described by Eq. (3): while for redshifted excitation with $\Delta < 0$ the stationary occupation is below 1/2, an almost perfect stationary inversion is found at low T for a blueshifted laser, similar to what was previously predicted for a two-level system consisting of two tunneling-coupled QDs within a Born-Markov approximation [24]. However, for the system considered here, several comments are in order. First, the time needed to reach the stationary state strongly depends on the excitation conditions and can be up to several hundreds of picoseconds at small f, low T, and large Δ. On these time scales other relaxation processes like radiative decay, that are not included in our model, gain in importance and reduce the accessible degree of inversion [25]. Further, cw excitations as assumed in Fig. 1 and Eq. (3) are of no use when an on-demand inversion is the target. Instead, pulsed excitations are needed to complete a preparation at a given time. Therefore, to evaluate whether the stationary inversion as shown in Fig. 1(a) has relevance for state preparation, several questions have to be answered. For example, which degree of inversion can be reached for off-resonant pulses of finite length? What determines the optimal detuning and how sensitive is the achieved inversion against variations in the pulse intensity? In this Letter, we will demonstrate that by applying an off-resonant intense pulse at low temperatures it is not only possible to achieve some inversion (as achieved in recent experiments with moderate pulse intensities [26]) but an almost perfect state preparation on a time scale of several picoseconds.

Shown in Fig. 2 is the exciton occupation C_X after a Gaussian pulse of $\tau = 2\sqrt{2\ln 2}\tau_0 = 15$ ps FWHM as a function of the pulse area α for different detunings Δ at $T = 4$ K. While for $\Delta = 0$ the occupation performs damped Rabi oscillations around a mean value of 1/2, the results do already considerably change for a slightly blueshifted excitation with $\Delta = 0.2$ meV: not only does the oscillation amplitude decrease (as it is well known for off-resonant driving [27]), but at high pulse areas, where the phonon damping is stronger [17,18] and the system is efficiently pushed towards its stationary state, significantly higher occupations are reached with C_X taking values of roughly 0.9. Even higher occupations are realized for larger Δ. For $\Delta = 1.0$ meV, which turns out to be the optimal choice for the detuning, an almost ideal and robust exciton preparation is realized at high pulse areas. We would like to stress that an almost equally high inversion is found for a rather wide range of detunings, as shown in Fig. 3(a), where C_X is plotted as a function of Δ for a fixed pulse area of $\alpha = 20\pi$. Thus, the phonon-assisted state preparation as realized by exciting the system off-resonantly by a single intense pulse is not only of high fidelity but is also robust against variations in the pulse intensity or the detuning provided that the pulse is strong enough.

It should be noted that, although the stationary occupation rises monotonically with rising detuning, cf. Fig. 1, for

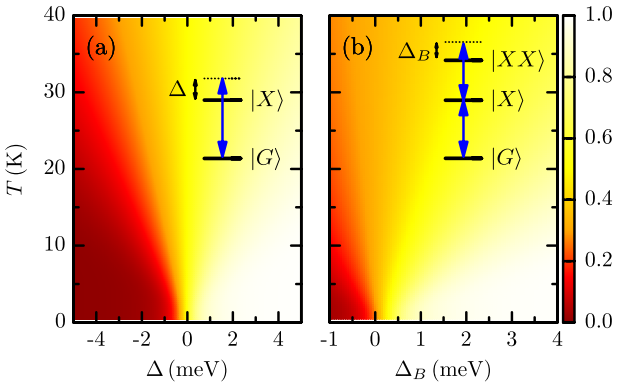

FIG. 1 (color online). Stationary (a) exciton and (b) biexciton occupation that is reached under constant optical driving with $f = 1.0$ ps^{-1} as a function of (a) the temperature and the detuning Δ between the laser frequency and the QD transition frequency and (b) the temperature and the biexciton binding energy Δ_B. Inset: Sketch of the excitation schemes (see text).

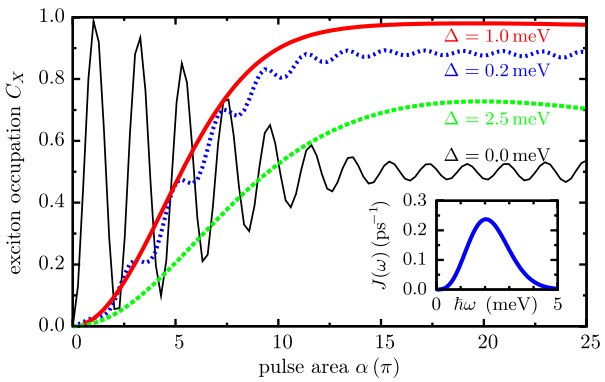

FIG. 2 (color online). Final exciton occupation C_X after a Gaussian pulse of 15 ps FWHM at $T = 4$ K as a function of the applied pulse area α for different detunings Δ as indicated. Inset: Phonon spectral density for a spherical GaAS QD with a radial electron confinement length of 3 nm.

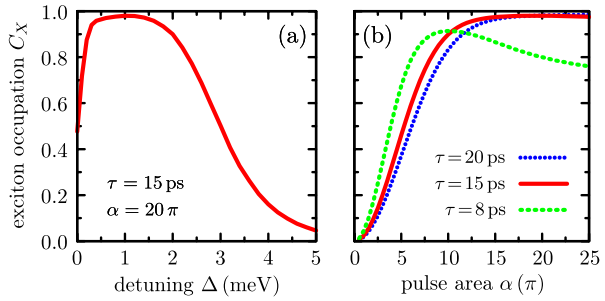

FIG. 3 (color online). Final exciton occupation C_X after a Gaussian pulse with pulse length τ (FWHM) at $T = 4$ K. (a) C_X as a function of Δ for $\tau = 15$ ps and $\alpha = 20\pi$. (b) C_X as a function of α for $\Delta = 1$ meV and different τ as indicated.

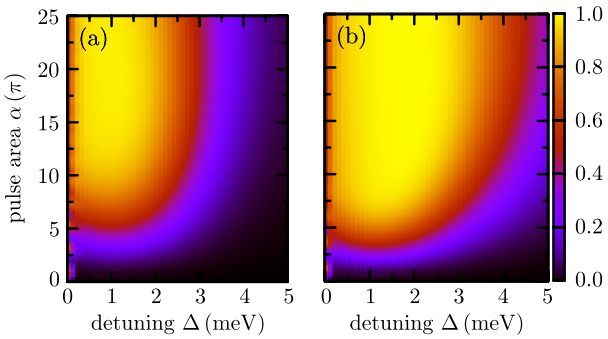

FIG. 4 (color online). Final exciton occupation C_X after a Gaussian pulse of 15 ps FWHM at $T = 4$ K as a function of the detuning Δ and the pulse area α for (a) GaAs parameters and (b) a phonon coupling where $|g_{\mathbf{q}}|^2$ has been increased by a factor of 3.

large Δ, the degree of inversion achieved for a finite pulse no longer increases with Δ, but eventually decreases again as illustrated in Figs. 2 and 3(a). To understand this nonmonotonic dependence of the protocol efficiency on Δ, two things must be borne in mind: first, the phonon coupling, that drives the system towards the stationary state, exhibits a spectral cutoff, i.e., the phonon spectral density $J(\omega) = \sum_{\mathbf{q}} |g_{\mathbf{q}}|^2 \delta(\omega - \omega_{\mathbf{q}})$, that is shown in the inset of Fig. 2, vanishes for large ω, and second, the strength of the phonon-induced relaxation can be approximately described by $J(\Omega)$ [19,28]. As soon as the Rabi frequency Ω exceeds the frequency $\omega_{\max}$, where $J(\omega)$ is maximal, the phonon coupling becomes less efficient and the inversion that is reached for finite pulses is reduced. Further, as $\Omega = \sqrt{f^2 + (\Delta/\hbar)^2}$, the optimal detuning is less than $\hbar\omega_{\max}$, as is clearly seen from Figs. 2 and 3(a).

Obviously, the proposed scheme becomes less efficient when the pulse is too short and the system is not driven close enough to its stationary state. This is illustrated in Fig. 3(b). While pulses longer than those considered so far do not affect the efficiency, for a pulse length below 10 ps, the achieved inversion drops and the protocol is less robust with respect to variations in the pulse intensity. However, we would like to stress that the pulse length of 10–15 ps that is needed to guarantee a stable phonon-assisted preparation via off-resonant driving is very much the same as the one that was needed in recent ARP-based experiments to ensure an adiabatic evolution [13,14].

Unique to the present protocol is that its performance becomes better when the strength of the carrier-phonon coupling is increased, thus allowing for an almost ideal state preparation in the regime of strong system-environment interaction, where traditional Rabi oscillation or ARP schemes are known to fail [15,17–19]. Shown in Fig. 4 is the exciton occupation after a 15 ps lasting pulse (FWHM) as a function of Δ and α for the carrier-phonon coupling of GaAs as studied so far [Fig. 4(a)] and for a situation, where we have increased $|g_{\mathbf{q}}|^2$ by a factor of 3 by hand [Fig. 4(b)] in order to roughly simulate the coupling strength of materials like GaN [29]. Clearly, the efficiency increases with rising coupling: the maximal inversion is even closer to 1 and the range of pulse intensities and detunings for which high occupations are reached extends considerably. We stress that carrying out calculations for strong phonon couplings is a challenge and that even highly elaborate approximate methods such as a fourth-order correlation expansion are known to break down in this regime [23]. Here, the performance of reliable simulations is possible by using a numerically exact path-integral approach [22] that accounts fully for all non-Markovian effects and arbitrary multiphonon processes.

In light of recent progress in realizing QD-based entangled photon sources [6,30], the task of preparing the biexciton state $|XX\rangle$ has also become of topical interest. Whether or not the ideas so far developed for the preparation of the single exciton state can be transferred to this task is not obvious, because now we have to deal with more electronic levels, and thus a perfect preparation of the biexciton requires that not only the ground state but also the single exciton state is completely depopulated. Furthermore, there is not only a single resonance. In particular, the biexciton state can be optically excited either by a two-photon process [11] that is resonant when $2\hbar\omega = 2\hbar\omega_X - \Delta_B$, where Δ_B is the biexciton binding energy, or by a sequential process where first the single exciton is excited and then a transition from the exciton to the biexciton is induced. The resonance for the latter process at $\hbar\omega = \hbar\omega_X - \Delta_B$ is known to be a dephasing-induced resonance, which in $\chi^{(3)}$ signals shows up only due to the coupling of the electronic system to a bath [31].

To couple the biexciton we switch the polarization of the exciting pulse from circular to linear. Then, the light-matter Hamiltonian reads as [32]

$$H_{\mathrm{QD},L} = \hbar\omega_X |X\rangle\langle X| + (2\hbar\omega_X - \Delta_B)|XX\rangle\langle XX| - \left[\frac{\hbar f(t)}{2} e^{-i\omega_L t}(|X\rangle\langle G| + |XX\rangle\langle X|) + \mathrm{H.c.}\right]. \quad (4)$$

In general, Δ_B can be positive as well as negative, but for self-assembled GaAs QDs it typically takes values ranging from 1 to 3 meV [19,33,34]. The carrier-phonon coupling is the same as in Eq. (2), with the only difference that now the sum over $|\nu\rangle$ runs over three electronic states, $|G\rangle$, $|X\rangle$, and $|XX\rangle$.

In the remainder of this Letter we shall demonstrate that an almost perfect phonon-assisted biexciton preparation is possible by choosing an excitation that is resonant to the ground state to exciton transition provided that the exciton to biexciton transition is redshifted, which typically is the case. This situation is schematically sketched in the inset of Fig. 1(b).

Again, it turns out to be instructive to look first at the stationary state, that for this excitation is reached due to the acoustic phonon coupling. Figure 1(b) shows the stationary biexciton occupation as calculated within the path-integral approach for constant driving as a function of temperature and biexciton binding energy: very high values of C_{XX} are found for low T and positive Δ_B, indicating that a phonon-mediated preparation of the biexciton should be possible for the typical case where the biexciton binding energy shifts the biexciton down in energy. This supposition is indeed confirmed by the results shown in Fig. 5, where the biexciton occupation that is reached after a Gaussian pulse with 15 ps FWHM is plotted as a function of the pulse area and Δ_B at $T = 4$ K: an almost perfect biexciton preparation is realized for a wide range of biexciton binding energies which is robust against variations in the pulse intensity provided that the pulse is strong enough. It should be noted that an occupation probability for $|XX\rangle$ near 1 implies that, due to the action of the phonons, the exciton state as well as the ground state are practically unoccupied although the ground state to exciton transition is resonantly driven. As discussed before in detail for the case of the single exciton preparation, the performance of the scheme becomes worse when the pulse is chosen too short, but improves with rising strength of the carrier-phonon coupling (not shown).

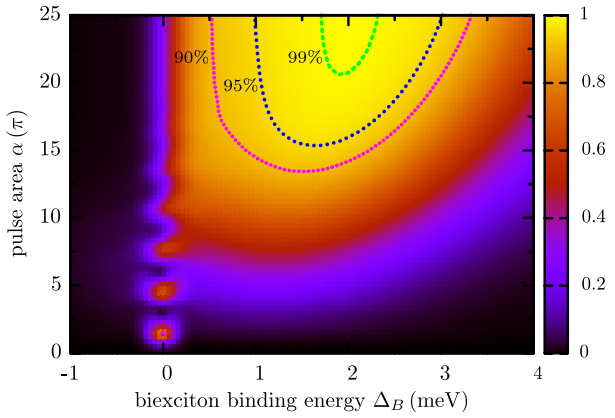

FIG. 5 (color online). Final biexciton occupation C_{XX} after a Gaussian pulse with a FWHM of 15 ps at $T = 4$ K as a function of the biexciton binding energy Δ_B and the pulse area α. The laser frequency is chosen in resonance with the ground state to exciton transition. The contour lines display where certain values of C_{XX} are reached.

In summary, we have presented schemes allowing for an on-demand, high-fidelity, and robust preparation of the single exciton as well as the biexciton state in semiconductor QDs that are based on off-resonant excitations with strong optical pulses and make active use of the carrier-phonon coupling. In particular, we predict that the biexciton can be prepared by resonantly driving the ground state to exciton transition, implying that the exciton state will be unoccupied despite its resonant excitation. The proposed protocols allow for fast state preparations on the time scale of 10 ps. We expect our findings to inspire future experimental research as the regime of off-resonant driving at high intensities is so far almost unexplored and we believe that the proposed phonon-assisted state preparation schemes can pave the way to more efficient sources for single or entangled photons. Importantly, the presented protocols not only combine the simplicity of traditional Rabi oscillation schemes (without the need of realizing chirped laser pulses) with the robustness of ARP-based schemes, but they perform better the stronger the carrier phonon coupling is, thus allowing for an ideal state preparation even in situations with strong system-environment interaction that are usually thought of as making control protocols impossible.

M. G. gratefully acknowledges financial support by the Studienstiftung des Deutschen Volkes.

*martin.glaessl@uni-bayreuth.de

[1] P. Michler, A. Kiraz, C. Becher, W. V. Schoenfeld, P. Petroff, L. D. Zhang, E. Hu, and A. Imamoğlu, Science **290**, 2282 (2000).
[2] D. Press, S. Götzinger, S. Reitzenstein, C. Hofmann, A. Löffler, M. Kamp, A. Forchel, and Y. Yamamoto, Phys. Rev. Lett. **98**, 117402 (2007).
[3] E. Moreau, I. Robert, L. Manin, V. Thierry-Mieg, J. M. Gérard, and I. Abram, Phys. Rev. Lett. **87**, 183601 (2001).
[4] R. Stevenson, R. J. Young, P. Atkinson, K. Cooper, D. A. Ritchie, and A. J. Shields, Nature (London) **439**, 179 (2006).
[5] N. Akopian, N. H. Lindner, E. Poem, Y. Berlatzky, J. Avron, D. Gershoni, B. D. Gerardot, and P. M. Petroff, Phys. Rev. Lett. **96**, 130501 (2006).
[6] A. Dousse, J. Suffczyński, A. Beveratos, O. Krebs, A. Lemaître, I. Sagnes, J. Bloch, P. Voisin, and P. Senellart, Nature (London) **466**, 217 (2010).
[7] D. Bouwmeester, A. K. Ekert, and A. Zeilinger, *The Physics of Quantum Information* (Springer, Berlin, 2000).
[8] M. A. Nielsen and I. Chuang, *Quantum Computation and Quantum Information* (Cambridge University Press, Cambridge, England, 2000).
[9] S. Haroche and J. Raimond, *Exploring the Quantum* (Oxford University Press, Oxford, England, 2006).

[10] A. Zrenner, E. Beham, S. Stufler, F. Findeis, M. Bichler, and G. Abstreiter, Nature (London) **418**, 612 (2002).
[11] S. Stufler, P. Machnikowski, P. Ester, M. Bichler, V. M. Axt, T. Kuhn, and A. Zrenner, Phys. Rev. B **73**, 125304 (2006).
[12] E. R. Schmidgall, P. R. Eastham, and R. T. Phillips, Phys. Rev. B **81**, 195306 (2010).
[13] C. M. Simon, T. Belhadj, B. Chatel, T. Amand, P. Renucci, A. Lemaitre, O. Krebs, P. A. Dalgarno, R. J. Warburton, X. Marie *et al.*, Phys. Rev. Lett. **106**, 166801 (2011).
[14] Y. Wu, I. M. Piper, M. Ediger, P. Brereton, E. R. Schmidgall, P. R. Eastham, M. Hugues, M. Hopkinson, and R. T. Phillips, Phys. Rev. Lett. **106**, 067401 (2011).
[15] S. Lüker, K. Gawarecki, D. E. Reiter, A. Grodecka-Grad, V. M. Axt, P. Machnikowski, and T. Kuhn, Phys. Rev. B **85**, 121302 (2012).
[16] A. Debnath, C. Meier, B. Chatel, and T. Amand, Phys. Rev. B **86**, 161304 (2012).
[17] J. Förstner, C. Weber, J. Danckwerts, and A. Knorr, Phys. Rev. Lett. **91**, 127401 (2003).
[18] A. Vagov, M. D. Croitoru, V. M. Axt, T. Kuhn, and F. M. Peeters, Phys. Rev. Lett. **98**, 227403 (2007).
[19] A. J. Ramsay, A. V. Gopal, E. M. Gauger, A. Nazir, B. W. Lovett, A. M. Fox, and M. S. Skolnick, Phys. Rev. Lett. **104**, 017402 (2010).
[20] B. Krummheuer, V. M. Axt, and T. Kuhn, Phys. Rev. B **65**, 195313 (2002).
[21] A. Vagov, V. M. Axt, T. Kuhn, W. Langbein, P. Borri, and U. Woggon, Phys. Rev. B **70**, 201305 (2004).
[22] A. Vagov, M. D. Croitoru, M. Glässl, V. M. Axt, and T. Kuhn, Phys. Rev. B **83**, 094303 (2011).
[23] M. Glässl, A. Vagov, S. Lüker, D. E. Reiter, M. D. Croitoru, P. Machnikowski, V. M. Axt, and T. Kuhn, Phys. Rev. B **84**, 195311 (2011).
[24] T. M. Stace, A. C. Doherty, and S. D. Barrett, Phys. Rev. Lett. **95**, 106801 (2005).
[25] P. Borri, W. Langbein, S. Schneider, U. Woggon, R. L. Sellin, D. Ouyang, and D. Bimberg, Phys. Rev. Lett. **87**, 157401 (2001).
[26] A. J. Ramsay, T. M. Godden, S. J. Boyle, E. M. Gauger, A. Nazir, B. W. Lovett, A. V. Gopal, A. M. Fox, and M. S. Skolnick, J. Appl. Phys. **109**, 102415 (2011).
[27] L. Allen and J. H. Eberly, *Optical Resonance and Two-Level Atoms* (John Wiley and Sons, New York, 1975).
[28] P. Machnikowski and L. Jacak, Phys. Rev. B **69**, 193302 (2004).
[29] B. Krummheuer, V. M. Axt, T. Kuhn, I. D'Amico, and F. Rossi, Phys. Rev. B **71**, 235329 (2005).
[30] R. Trotta, E. Zallo, C. Ortix, P. Atkinson, J. D. Plumhof, J. van den Brink, A. Rastelli, and O. G. Schmidt, Phys. Rev. Lett. **109**, 147401 (2012).
[31] V. M. Axt, K. Victor, and A. Stahl, Phys. Rev. B **53**, 7244 (1996).
[32] Note that here $|X\rangle$ denotes the single exciton state coupled to linearly polarized light which is different from the exciton state used in Eq. (1) that couples to circularly polarized light.
[33] S. J. Boyle, A. J. Ramsay, F. Bello, H. Y. Liu, M. Hopkinson, A. M. Fox, and M. S. Skolnick, Phys. Rev. B **78**, 075301 (2008).
[34] M. Zecherle, C. Ruppert, E. C. Clark, G. Abstreiter, J. J. Finley, and M. Betz, Phys. Rev. B **82**, 125314 (2010).

Publication 4

Phonon-Assisted Population Inversion of a Single InGaAs/GaAs Quantum Dot by Pulsed Laser Excitation

J. H. Quilter, A. J. Brash, F. Liu, M. Glässl, A. M. Barth, V. M. Axt, A. J. Ramsay, M. S. Skolnick and A. M. Fox

Physical Review Letters **114**, 137401 (2015)

DOI: 10.1103/PhysRevLett.114.137401

Phonon-Assisted Population Inversion of a Single InGaAs/GaAs Quantum Dot by Pulsed Laser Excitation

J. H. Quilter,[1] A. J. Brash,[1] F. Liu,[1,*] M. Glässl,[2] A. M. Barth,[2] V. M. Axt,[2] A. J. Ramsay,[3] M. S. Skolnick,[1] and A. M. Fox[1]
[1]Department of Physics and Astronomy, University of Sheffield, Sheffield S3 7RH, United Kingdom
[2]Institut für Theoretische Physik III, Universität Bayreuth, 95440 Bayreuth, Germany
[3]Hitachi Cambridge Laboratory, Hitachi Europe Ltd., Cambridge CB3 0HE, United Kingdom
(Received 2 September 2014; published 30 March 2015)

We demonstrate a new method to realize the population inversion of a single InGaAs/GaAs quantum dot excited by a laser pulse tuned within the neutral exciton phonon sideband. In contrast to the conventional method of inverting a two-level system by performing coherent Rabi oscillation, the inversion is achieved by rapid thermalization of the optically dressed states via incoherent phonon-assisted relaxation. A maximum exciton population of 0.67 ± 0.06 is measured for a laser tuned 0.83 meV to higher energy. Furthermore, the phonon sideband is mapped using a two-color pump-probe technique, with its spectral form and magnitude in very good agreement with the result of path-integral calculations.

DOI: 10.1103/PhysRevLett.114.137401 PACS numbers: 78.67.Hc, 03.67.Lx, 42.50.Hz, 78.45.+h

It is a basic tenet of laser physics that a population inversion cannot be achieved through incoherent excitation of a two-level atom. At best, a laser pulse with duration much longer than the coherence time of the two-level system T_2 can only drive the system to the transparency point where the populations of the upper and lower levels are equal [1]. However, if the two-level atom is coupled to a vibrational continuum, it has been predicted that inversion can be possible even in the incoherent regime through the interaction of the dressed states with the Boson bath [2]. Excitons in semiconductor quantum dots (QDs) form a near ideal system for investigating these effects, since their behavior approximates well to that of a two-level atom [3], while their coupling to the acoustic phonons in the crystal provides a mechanism to thermalize the dressed states.

The possibility of creating population inversion in QDs through phonon coupling was first investigated for microwave-driven electrostatic quantum dots [4]. Recently, it has been demonstrated that the conditions for population inversion can be met via a microwave Raman effect [5,6]. Theoretical work has indicated that similar effects should be possible for optically driven excitons [7–11]. The underlying mechanism is the coupling of the excitons to longitudinal acoustic (LA) phonons through the deformation potential [12], which generates sidebands in the excitonic spectra [13] that can also be observed in four-wave mixing [14] and resonance fluorescence experiments [15], as well as through off-resonant coupling of excitons to nanocavities [16,17]. In a strong driving field regime, evidence for phonon-induced relaxation between optically dressed states is observed in the intensity damping of Rabi rotations [18–20], and more recently in adiabatic rapid passage experiments [21,22].

In this Letter we report a population inversion of the excitonic two-level system of a single InGaAs/GaAs QD excited by a strong laser pulse tuned into the phonon sideband of the neutral exciton transition following the theoretical proposal of Ref. [9]. The population inversion is achieved in an incoherent regime where the dephasing time is shorter than the laser pulse duration. Pump-probe measurements are presented, where the phonon-assisted population inversion is observed clearly as a gainlike dip in the photocurrent absorption spectrum. Furthermore, the dependence of the exciton population on the pump detuning is measured. The experiments are supplemented by simulations based on the path-integral approach described in Ref. [23] and good agreement is obtained with the theory. This work may form the basis of quasiresonantly pumped single QD lasers. It also shows that the phonon-assisted quasiresonant excitation scheme can be used to create spin-polarized excitons whilst allowing the QD emission to be spectrally filtered from the pump laser, with potential applications for QD-based high-brightness single photon sources [17] and on-chip quantum optical circuits [24].

The physical mechanism for generating the population inversion can be understood as follows. A circularly polarized laser pulse with a large pulse area excites the neutral exciton transition of an InGaAs/GaAs quantum dot at a positive detuning within the phonon sideband, which typically peaks around 1 meV above the exciton [see Fig. 4(a) inset]. Since the laser bandwidth of 0.2 meV is large compared with the fine-structure splitting of 13 μeV, the dynamics of the exciton spin can be neglected [25]. Also, since the laser is far detuned from the two-photon

biexciton transition, the QD can be treated as a two-level system composed of two bare states: a crystal ground state $|0\rangle$ and neutral exciton $|X\rangle$ [see Fig. 1(a)(i)], with respective populations C_0 and C_X. With the presence of a laser pulse, the two bare states are optically dressed [see Figs. 1(a)(ii) and 1(a)(iii)]. In the rotating frame, $|0_R\rangle$ comprises the crystal ground state and the incoming laser photons. $|X_R\rangle$ comprises the exciton state and laser field with one photon less. The Hamiltonian in a rotating frame reads

$$H_{\mathrm{QD}} = -\hbar\Delta|X_R\rangle\langle X_R| + \frac{\hbar\Omega(t)}{2}|0_R\rangle\langle X_R| + \mathrm{H.c.}, \quad (1)$$

where the detuning $\Delta = \omega_L - \omega_X$, and $\Omega(t)$ is the Rabi frequency, which varies in time following the envelope of the laser pulse. The energy eigenstates of H_{QD}, $|\alpha\rangle$, $|\beta\rangle$ are described by an admixing angle $2\theta(t) = \arctan(\Omega(t)/\Delta)$, and are split by the effective Rabi energy $\hbar\Lambda(t) = \hbar\sqrt{\Delta^2 + \Omega(t)^2}$. We define the bare pulse area $\Theta = \int_{-\infty}^{+\infty}\Omega(t)dt$.

The QD resides in a crystal lattice, and the exciton interacts with the LA phonons due to the deformation potential [12]. In the absence of a laser field, the exciton-phonon interaction leads to nonexponential pure dephasing of the excitonic dipole, as observed in time-resolved four-wave mixing experiments [14]. In the presence of a strong laser, both dressed states have an excitonic component, thereby enabling relaxation between them by the emission of a phonon with energy equal to the effective Rabi splitting $\hbar\Lambda$, as shown in Fig. 1(a)(iii) for the case of positive detuning. This process gives rise to intensity damping of Rabi rotations when resonantly pumping [18,19], and also explains the difference in the population inversions created by adiabatic rapid passage when using laser pulses of positive and negative chirp [21,22].

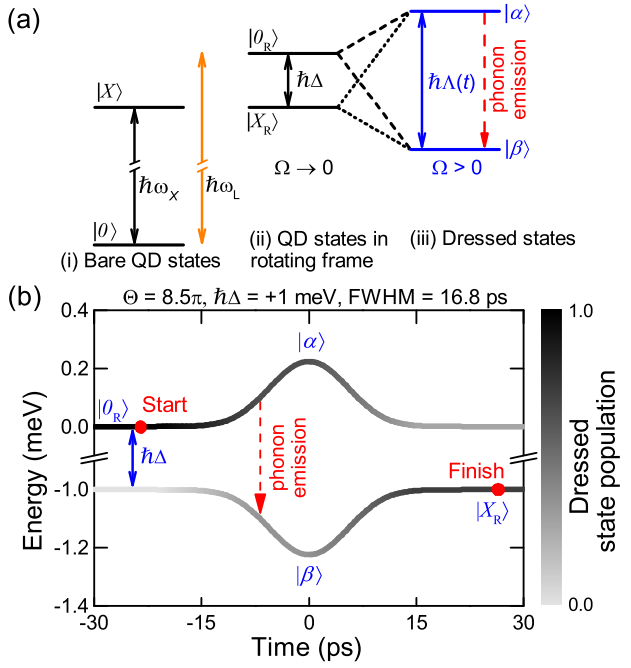

FIG. 1 (color online). (a) Bare QD states viewed in the (i) lab frame and (ii) rotating frame. $|0\rangle$, $|X\rangle$ and $|0_R\rangle$, $|X_R\rangle$ denote the ground state and exciton state in the lab frame and rotating frame, respectively. $\hbar\omega_X$ is the exciton transition energy. ω_L is the angular frequency of the laser. $\hbar\Delta$ is the positive detuning from the exciton transition. (iii) Optically dressed states $|\alpha\rangle$ and $|\beta\rangle$. (b) Evolution of the dressed QD energy levels with time during the absorption of an 8.5π pulse with $\hbar\Delta = +1$ meV. The gray scale of the curves corresponds to the instantaneous population of each state.

Figure 1(b) depicts the dynamics in the rotating frame of the phonon-assisted population inversion of the quantum dot exciton. For a positively detuned laser ($\Delta > 0$), the state $|0_R\rangle$ initially coincides with the higher-energy dressed state $|\alpha\rangle$. When the laser is applied, excitonic admixture to the state $|\alpha\rangle$ occurs, activating relaxation to the lower-energy dressed state $|\beta\rangle$ by phonon emission. In the lab frame [see Fig. 1(a)(i)], this process corresponds to the absorption of a photon together with the creation of an exciton and the emission of a phonon. The gray scale indicates the time-dependent populations of each dressed state, as calculated by our path-integral method, and shows the continuous transfer of population from $|\alpha\rangle$ to $|\beta\rangle$. As the laser intensity drops off at the end of the pulse, the admixing of the dressed states is reduced and the phonon relaxation is deactivated. If the time-integrated phonon relaxation is strong, the final occupation of the lower-energy, excitonlike, dressed state can dominate and a population inversion in the excitonic basis occurs. According to our theoretical model, near-unity exciton population that is robust against variations in both the pulse area and the detuning can be achieved at high pulse areas [9]. The amount of inversion is ultimately limited by the thermal occupation of the two states to $C_X - C_0 = \tanh(\hbar\Delta/2k_BT)$ [9]. In our experiments with $\hbar\Delta = 0.83$ meV and $T = 4.2$ K, this implies a maximum exciton population of 0.91.

The experiments were performed on a device consisting of a layer of InGaAs/GaAs quantum dots embedded in the intrinsic region of an n-i-Schottky diode structure. The sample is held at 4.2 K in a helium bath cryostat and is excited at normal incidence with circularly polarized Gaussian pulses, derived by pulse shaping of the output from a 100 fs Ti:sapphire laser with a repetition rate of 76.2 MHz. The FWHM of the electric field amplitude is 16.8 ps. Single QD peaks are observed in our sample at energies close to 1.3 eV. Photocurrent detection is used, where photogenerated electron-hole pairs tunnel from the quantum dot under an applied electric field. The amplitude of the photocurrent signal reflects the final occupation of the exciton or biexciton states. Full details of the wafer structure can be found in Ref. [26].

To demonstrate the phonon-assisted population inversion, two-pulse pump probe experiments were performed. First, the zero-phonon neutral exciton transition was found by measuring the absorption spectrum of a single π pulse (blue line in Fig. 2). Then, the pump pulse was detuned by +0.83 meV, where the exciton population is predicted to be

most efficiently created [see blue line in Fig. 4(a)], and the probe energy was scanned through the transition. The probe pulse area is π and the pump pulse area is 8.46π, the maximum available in our setup. The delay time between the pump and probe pulses τ_{delay} ranges from 10 to 34 ps [27].

As illustrated in the energy-level diagram shown in Fig. 2, the photon energy of the probe pulse and its polarization relative to the pump selects the transition that is probed. We consider first the case for a copolarized probe pulse, where both the pump and probe pulses have the same σ^+ polarization. In this case, the pump pulse (orange arrow) excites a dephased, mixed exciton population C_X (see the inset in Fig. 2). Since the probe has a pulse area of π, it exchanges the $|0\rangle$ population with the $|X\rangle$ population when it is resonant with the neutral exciton transition (see black arrow in the inset to Fig. 2), resulting in a change in photocurrent proportional to the populations after the pump but before the probe: $\Delta\text{PC}_{0-X} \propto C_0 - C_X$ [27]. ΔPC is the change in the photocurrent signal resulting from the dot that is induced by the probe pulse. ΔPC is measured relative to the photocurrent measured for a detuned probe. A key signature of population inversion is that ΔPC_{0-X} should be negative, independent of the photocurrent to exciton population calibration. Figure 2 shows the experimental results (black). The dip at zero detuning clearly demonstrates that a population inversion has been achieved between the $|0\rangle$ and $|X\rangle$ states.

The red line in Fig. 2 shows the results obtained for crosspolarized excitation (σ^+ pump, σ^- probe). At zero detuning, the probe addresses the orthogonally polarized exciton transition $|0\rangle \rightarrow |\bar{X}\rangle$ as shown by the lower red arrow in the inset to Fig. 2, providing a measure of the occupation of the crystal ground state C_0. The amplitude of the peak at zero detuning falls to less than half the amplitude measured by the single pulse, again confirming that a population inversion between $|0\rangle$ and $|X\rangle$ has been achieved since $\Delta\text{PC}_{0-\bar{X}} \propto C_0 - C_{\bar{X}}$. The second peak at a detuning of -1.96 meV corresponds to the $|X\rangle \rightarrow |2X\rangle$ transition, and provides a third measure of C_X (see Ref. [27]). The absence of the biexciton peak in the copolarized spectra proves that the phonon-assisted channel is spin preserving because the phonon-assisted relaxation (few picoseconds) [30] is much faster than exciton spin relaxation (few nanoseconds) [31].

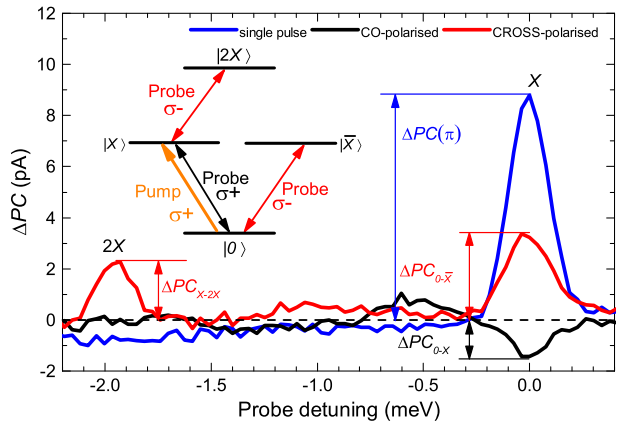

FIG. 2 (color online). Photocurrent signal ΔPC as a function of the probe detuning. Blue: a single probe-pulse only spectrum is presented for reference. Two pulse spectra where the probe is copolarized (black) and crosspolarized (red) with the pump. Pump detuning $= +0.83$ meV and $\tau_{\text{delay}} = 10$ ps. The peak at a detuning of -1.96 meV corresponds to the $|X\rangle \rightarrow |2X\rangle$ transition. Inset: energy level diagram for the exciton-biexciton system. Arrows represent transitions induced by the σ^+ polarized pump pulse tuned to the phonon sideband and the σ^+ (σ^-) polarized probe pulse tuned either to the exciton or biexciton transition. X and $\bar{X}$ label the orthogonally circularly polarized exciton states. $2X$ denotes the biexciton state.

Figure 3 plots the occupation of the neutral exciton versus the area of the pump pulse. The three data points for each pulse area are obtained from an analysis of the co- and crosspolarized signals at zero detuning, and from the biexciton peak. The exciton population is deduced by comparison with the neutral exciton photocurrent peak for resonant excitation with a single π pulse (for details see Ref. [27]). Since the electron can tunnel out from the QD before the arrival of the probe, which reduces the measured exciton population created by the pump, a correction is made to account for an electron tunneling time of $\sim$50 ps [27]. The three measurements of the exciton population are in close agreement, and pass the transparency point, $C_X = 0.5$, at a pulse area of 6.5π–7π. The largest exciton population observed is 0.67 ± 0.06 for a pump pulse detuned by $+0.83$ meV, limited by the power available in our setup. The blue line in Fig. 3 shows the results of our path-integral simulations, which quantitatively reproduce the experiments.

To investigate the dependence of the phonon-assisted population inversion on the pump frequency, a series of two-color photocurrent spectra, similar to Fig. 2, were measured for a crosspolarized 7.24π pump pulse as a function of pump detuning with a π probe. Figure 4(a) presents the exciton population generated by the pump pulse.

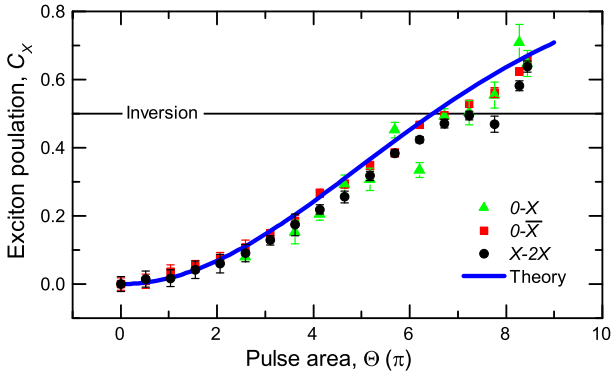

FIG. 3 (color online). The exciton population C_X generated by the pump pulse with $\hbar\Delta = +0.83$ meV, as extracted from the exciton and biexciton peak in two-pulse spectra versus the pump pulse area. For a full derivation, see Ref. [27]. Blue: calculated C_X.

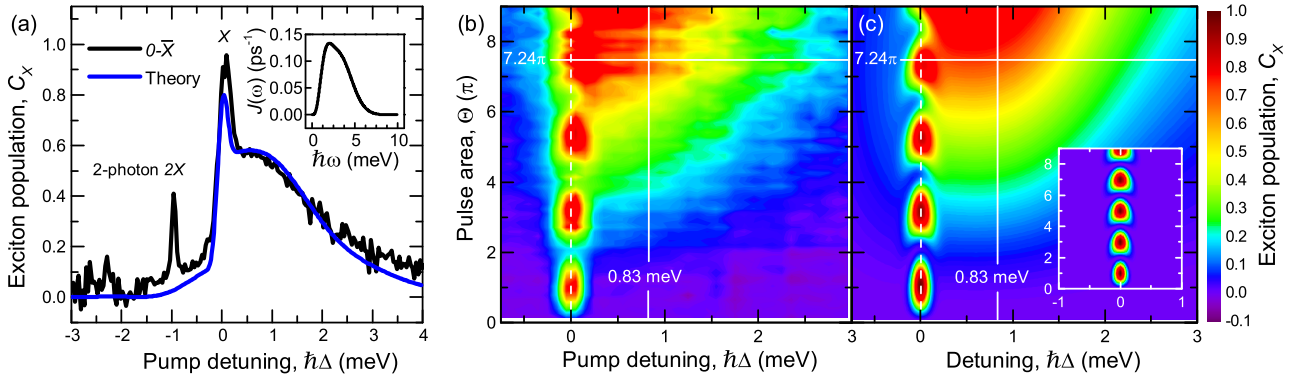

FIG. 4 (color online). (a) Exciton population created by a 7.24π pump as a function of the pump detuning. $\tau_{\text{delay}} = 15$ ps. Blue: calculated C_X. Inset: theoretical spectral density of the exciton-phonon interaction $J(\omega)$. (b) Experimentally obtained C_X versus Θ and $\hbar\Delta$ with $\tau_{\text{delay}} = 33.6$ ps. (c) Path-integral results for the same pulse area and detuning range as in (b). The vertical line is where $\hbar\Delta = +0.83$ meV and the horizontal line is for $\Theta = 7.24\pi$ as shown in Figs. 3 and 4(a), respectively. Inset: calculated values with no phonon interaction. All plots in (b) and (c) use the same color scale.

The spectrum has three features. At zero detuning there is a pulse width–limited peak corresponding to the zero-phonon $|0\rangle \rightarrow |X\rangle$ transition. At positive detuning there is a broad feature due to phonon emission. The absence of discrete features in the phonon sideband indicates that phonon confinement effects are weak, as expected given the similar lattice properties of the QD and barrier materials. In principle, there can also be a phonon feature at negative detuning due to phonon absorption. However, the phonon absorption is negligible at low temperature. The third feature is a narrow peak at a pump detuning of -1 meV, corresponding to the two-photon $|0\rangle \rightarrow |2X\rangle$ biexciton transition [32], indicating that the pump pulse is slightly elliptically polarized.

In the theory, the phonon influence on the dot dynamics is mediated mainly by the phonon spectral density: $J(\omega) = \sum_{\mathbf{q}} |\gamma_{\mathbf{q}}|^2 \delta(\omega - \omega_{\mathbf{q}})$, where $\gamma_{\mathbf{q}}$ is the exciton-phonon coupling. In the absence of detailed information on the shape of the QD we consider spherically symmetric, parabolic potentials. For bulk LA phonons coupled via the deformation potential we then obtain [23]

$$J(\omega) = \frac{\omega^3}{4\pi^2 \rho \hbar v_c^5} \left[D_e e^{(-\omega^2 a_e^2/4v_c^2)} - D_h e^{(-\omega^2 a_h^2/4v_c^2)} \right]^2, \quad (2)$$

where ρ is the mass density, v_c is the sound velocity, and $D_{e(h)}$ denote the deformation potential constants for electrons(holes). These material parameters are taken from the literature and are given explicitly in the Supplemental Material [27], while the electron(hole) confinement lengths $a_{e(h)}$ are used as fitting parameters. Good agreement with our experiments is obtained for $a_e = 4.5$ nm and $a_h = 1.8$ nm, resulting in the spectral density shown in the inset of Fig. 4(a). We note that the low frequency asymptote $\sim\omega^3$ is characteristic for bulk acoustic phonons and occurs independent of the material or the dot shape. On the other hand, the Gaussians in Eq. (2) result from the Fourier transforms of the electron and hole probability densities, reflecting the assumption of parabolic confinement potentials.

The blue line in Fig. 4(a) shows the theoretical values of the exciton population generated by the pump pulse, which excellently replicates the broadband feature observed at positive detuning. The line shape of this feature is implicitly determined by $J(\omega)$; more detailed information on $J(\omega)$ can be obtained here than from fitting the intensity damping of Rabi rotations [19]. Equation (2) shows that the high frequency behavior of $J(\omega)$ follows the Fourier transform of the electron and hole probability densities, and so a line shape analysis in principle provides a way to obtain insight on the spatial distributions of the electrons and holes. However, accessing this information would require more detailed studies, which are beyond the scope of the present Letter. The asymmetry of the spectrum with respect to the sign of $\hbar\Delta$ unambiguously proves that the population created by the off-resonant pump pulse is the result of phonon-assisted relaxation into the lower energy dressed state [33]. This is further demonstrated by a calculation without exciton-phonon coupling, where no broad sideband is observed [see inset in Fig. 4(c)]. We also note that the measured low-energy phonon sideband is stronger than expected. This may be due to an elevated temperature of about 6–7 K caused by heating of the sample by the laser.

Figures 4(b) and 4(c) compare the exciton population generated by the pump pulse measured as in Fig. 4(a) at different pulse areas with corresponding path-integral calculations. On resonance, the zero-phonon line exhibits intensity-damped Rabi rotations. To positive detuning, there is the phonon-emission sideband that broadens for higher pulse areas. The calculations are in good agreement with the experimental data, further confirming the model. Even the slight shift of the resonant peaks towards higher energies with increasing pulse area is reproduced by the theory.

In conclusion, we have experimentally demonstrated the population inversion of a neutral exciton in a single QD excited by a quasiresonant laser pulse tuned within the

exciton phonon sideband. The population inversion arises due to the incoherent phonon-induced relaxation between optically dressed states that arises at high driving intensities. Phonon interactions, which are usually a hindrance in quantum dot physics, in this case enable the population inversion and lead to qualitatively distinct behavior. The phonon-mediated population inversion we report may have potential as the basis of quasiresonantly pumped single QD lasers with dots embedded in cavities, and as high repetition rate single photon sources [17], with easy spectral filtering of excitation lasers, especially relevant to on-chip geometries [24].

This work was funded by the EPSRC (UK) EP/J007544/1. M. G., A. M. B., and V. M. A. gratefully acknowledge the financial support from Deutsche Forschungsgemeinschaft via the Project No. AX 17/7-1. The authors thank H. Y. Liu and M. Hopkinson for sample growth.

Note added in proof.—Following submission of our paper, we became aware of related results by two other groups [35,36].

*fengliu@sheffield.ac.uk

[1] A. E. Siegman, *Lasers* (University Science Books, Oxford, 1986).
[2] A. J. Leggett, S. Chakravarty, A. T. Dorsey, M. P. A. Fisher, A. Garg, and W. Zwerger, Rev. Mod. Phys. **59**, 1 (1987).
[3] T. H. Stievater, X. Li, D. G. Steel, D. Gammon, D. S. Katzer, D. Park, C. Piermarocchi, and L. J. Sham, Phys. Rev. Lett. **87**, 133603 (2001).
[4] J. R. Petta, A. C. Johnson, C. M. Marcus, M. P. Hanson, and A. C. Gossard, Phys. Rev. Lett. **93**, 186802 (2004).
[5] T. M. Stace, A. C. Doherty, and S. D. Barrett, Phys. Rev. Lett. **95**, 106801 (2005).
[6] J. I. Colless, X. G. Croot, T. M. Stace, A. C. Doherty, S. D. Barrett, H. Lu, A. C. Gossard, and D. J. Reilly, Nat. Commun. **5**, 3716 (2014).
[7] M. Glässl, A. Vagov, S. Lüker, D. E. Reiter, M. D. Croitoru, P. Machnikowski, V. M. Axt, and T. Kuhn, Phys. Rev. B **84**, 195311 (2011).
[8] D. E. Reiter, S. Lüker, K. Gawarecki, A. Grodecka-Grad, P. Machnikowski, V. M. Axt, and T. Kuhn, Acta Phys. Pol. A **122**, 1065 (2012).
[9] M. Glässl, A. M. Barth, and V. M. Axt, Phys. Rev. Lett. **110**, 147401 (2013).
[10] S. Hughes and H. J. Carmichael, New J. Phys. **15**, 053039 (2013).
[11] D. E. Reiter, T. Kuhn, M. Glässl, and V. M. Axt, J. Phys. Condens. Matter **26**, 423203 (2014).
[12] B. Krummheuer, V. M. Axt, and T. Kuhn, Phys. Rev. B **65**, 195313 (2002).
[13] L. Besombes, K. Kheng, L. Marsal, and H. Mariette, Phys. Rev. B **63**, 155307 (2001).
[14] P. Borri, W. Langbein, U. Woggon, V. Stavarache, D. Reuter, and A. D. Wieck, Phys. Rev. B **71**, 115328 (2005).
[15] S. Weiler, A. Ulhaq, S. M. Ulrich, D. Richter, M. Jetter, P. Michler, C. Roy, and S. Hughes, Phys. Rev. B **86**, 241304 (2012).
[16] U. Hohenester, A. Laucht, M. Kaniber, N. Hauke, A. Neumann, A. Mohtashami, M. Seliger, M. Bichler, and J. J. Finley, Phys. Rev. B **80**, 201311 (2009).
[17] K. H. Madsen, S. Ates, J. Liu, A. Javadi, S. M. Albrecht, I. Yeo, S. Stobbe, and P. Lodahl, Phys. Rev. B **90**, 155303 (2014).
[18] A. J. Ramsay, A. V. Gopal, E. M. Gauger, A. Nazir, B. W. Lovett, A. M. Fox, and M. S. Skolnick, Phys. Rev. Lett. **104**, 017402 (2010).
[19] A. J. Ramsay, T. M. Godden, S. J. Boyle, E. M. Gauger, A. Nazir, B. W. Lovett, A. M. Fox, and M. S. Skolnick, Phys. Rev. Lett. **105**, 177402 (2010).
[20] L. Monniello, C. Tonin, R. Hostein, A. Lemaitre, A. Martinez, V. Voliotis, and R. Grousson, Phys. Rev. Lett. **111**, 026403 (2013).
[21] Y.-J. Wei, Y.-M. He, M.-C. Chen, Y.-N. Hu, Y. He, D. Wu, C. Schneider, M. Kamp, S. Höfling, C.-Y. Lu *et al.*, Nano Lett. **14**, 6515 (2014).
[22] R. Mathew, E. Dilcher, A. Gamouras, A. Ramachandran, H. Y. Shi Yang, S. Freisem, D. Deppe, and K. C. Hall, Phys. Rev. B **90**, 035316 (2014).
[23] A. Vagov, M. D. Croitoru, M. Glässl, V. M. Axt, and T. Kuhn, Phys. Rev. B **83**, 094303 (2011).
[24] M. Makhonin, J. Dixon, R. Coles, B. Royall, I. J. Luxmoore, E. Clarke, M. Hugues, M. Skolnick, and A. M. Fox, Nano Lett. **14**, 6997 (2014).
[25] Q. Q. Wang, A. Muller, M. T. Cheng, H. J. Zhou, P. Bianucci, and C. K. Shih, Phys. Rev. Lett. **95**, 187404 (2005).
[26] R. S. Kolodka, A. J. Ramsay, J. Skiba-Szymanska, P. W. Fry, H. Y. Liu, A. M. Fox, and M. S. Skolnick, Phys. Rev. B **75**, 193306 (2007).
[27] See Supplemental Material at http://link.aps.org/supplemental/10.1103/PhysRevLett.114.137401 for detailed derivation of the exciton population and description of the model, which includes Refs. [9,23,26,28,29].
[28] S. J. Boyle, A. J. Ramsay, F. Bello, H. Y. Liu, M. Hopkinson, A. M. Fox, and M. S. Skolnick, Phys. Rev. B **78**, 075301 (2008).
[29] B. Krummheuer, V. M. Axt, T. Kuhn, I. D'Amico, and F. Rossi, Phys. Rev. B **71**, 235329 (2005).
[30] D. P. S. McCutcheon and A. Nazir, New J. Phys. **12**, 113042 (2010).
[31] K. Roszak, V. M. Axt, T. Kuhn, and P. Machnikowski, Phys. Rev. B **76**, 195324 (2007).
[32] S. Stufler, P. Machnikowski, P. Ester, M. Bichler, V. M. Axt, T. Kuhn, and A. Zrenner, Phys. Rev. B **73**, 125304 (2006).
[33] We note that in single pulse experiments at 15 K, more symmetric phonon sidebands can be observed [34].
[34] A. J. Ramsay, T. M. Godden, S. J. Boyle, E. M. Gauger, A. Nazir, B. W. Lovett, A. V. Gopal, A. M. Fox, and M. S. Skolnick, J. Appl. Phys. **109**, 102415 (2011).
[35] P.-L. Ardelt, L. Hanschke, K. A. Fischer, K. Müller, A. Kleinkauf, M. Koller, A. Bechtold, T. Simmet, J. Wierzbowski, H. Riedl, G. Abstreiter, and J. J. Finley, Phys. Rev. B **90**, 241404 (2014).
[36] S. Bounouar, M. Müller, A. M. Barth, M. Glässl, V. M. Axt, and P. Michler, arXiv:1408.7027.

Phonon-assisted population inversion of a single quantum dot - supplemental material

J. H. Quilter,[1] A. J. Brash,[1] F. Liu,[1] M. Glässl,[2] A. M. Barth,[2]
V. M. Axt,[2] A. J. Ramsay,[3] M. S. Skolnick,[1] and A. M. Fox[1]

[1]*Department of Physics and Astronomy, University of Sheffield, Sheffield, S3 7RH, United Kingdom*
[2]*Institut für Theoretische Physik III, 'Universität Bayreuth, 95440 Bayreuth, Germany*
[3]*Hitachi Cambridge Laboratory, Cavendish Laboratory,*
University of Cambridge, Cambridge CB3 0HE, United Kingdom
(Dated: February 5, 2015)

I. EXTRACTION OF THE EXCITON POPULATION FROM MEASURED DATA

The exciton population created by a pump pulse tuned into the phonon sideband can be extracted from our two-pulse spectra in three different ways by analyzing the peak heights of the three transitions: $|0\rangle \rightarrow |X\rangle$, $|0\rangle \rightarrow |\bar{X}\rangle$ and $|X\rangle \rightarrow |2X\rangle$ (see Fig. 1(b) based on Fig. (2) in the main text). The photocurrent (PC) measured in our experiment is determined by the number of electron-hole pairs created by the laser pulses. For our pump-probe measurement, PC can be subdivided into three parts: a reference level PC_{R} induced by the pump pulse, a background level PC_{bg} and the change of the photocurrent signal ΔPC induced by the probe pulse according to:

$$PC = PC_{\mathrm{R}} + PC_{bg} + \Delta PC. \tag{1}$$

$PC_{\mathrm{R}} + PC_{bg}$ is determined by measuring the photocurrent signal from an off-resonant measurement where the pump pulse is tuned into the phonon sideband and the probe frequency is far from any of the resonances of the dot or the surrounding material such that ΔPC becomes negligible and the photocurrent signal coincides with $PC_{\mathrm{R}} + PC_{bg}$ in this case.

The information on the exciton population created by the pump pulse only lies in ΔPC. At $t = 0$, the σ^+ polarized pump pulse creates an exciton population C_X (see the orange arrow in Fig. 1(a)). Consequently, the occupations of the $(0, X, \bar{X}, 2X)$ states following the pump pulse are

$$\mathbf{C}(0) = (C_0(0), C_X(0), C_{\bar{X}}(0), C_{2X}(0)) = (1 - C_X, C_X, 0, 0). \tag{2}$$

At a time $t < \tau_{\mathrm{delay}}$, before the arrival of the probe pulse, the exciton population decays exponentially because the electron tunnels away from the QD. The radiative decay of the exciton is neglected here because the radiative decay time ($\sim$ 600 ps) is much longer than our delay time. The delay time is chosen to maximize the pump-probe signal. Typically this occurs between 10 and 15 ps, depending on the pulse width and the electron tunnelling time. To

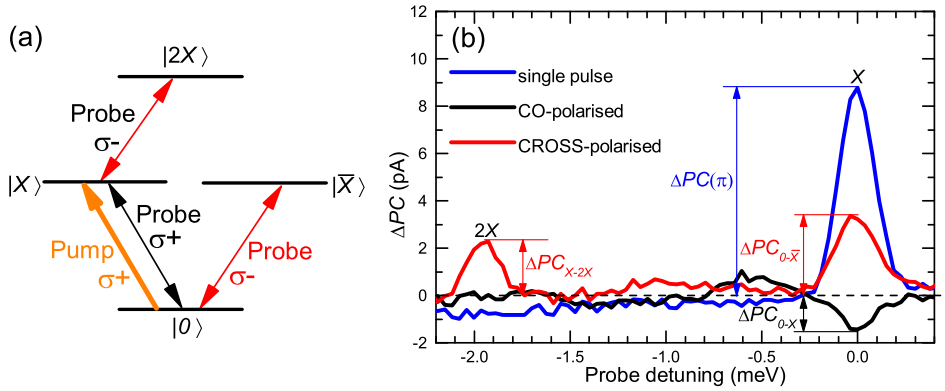

FIG. 1: Color online. (a) Energy level diagram for the exciton-biexciton system. $|0\rangle$ denotes the crystal ground state. $|X\rangle$ and $|\bar{X}\rangle$ denote the orthogonally circularly polarized exciton states. $|2X\rangle$ denotes the biexciton state. Arrows represent transitions induced by the σ^+ polarized pump pulse tuned to the phonon sideband and the σ^+/σ^- polarized probe pulse tuned either to the exciton or biexciton transition. (b) Photocurrent signal ΔPC as a function of the probe detuning. (Blue) A single probe-pulse only spectrum is presented for reference. Two pulse spectra where the probe is co- (black) and cross- (red) polarized with the pump. Pump detuning = +0.83 meV and τ_{delay} = 10 ps. The peak at a detuning of -1.96 meV corresponds to the $|X\rangle \rightarrow |2X\rangle$ transition.

exclude the possibility that a small temporal overlap between the pump and probe may affect the evaluated exciton population, the data in Fig. 4(b) in the main text were measured with a longer delay time (33.6 ps) where the pump and probe are completely separated. The result agrees well with that measured with shorter delay time after correction for the population loss due to electron tunneling. The ground-state occupancy however is not affected by the electron tunneling due to a long hole tunneling time (few ns). The electron tunneling time ($T_1 = 50$ ps) is measured using an inversion recovery technique as described in ref. [26]. This leads to occupations of:

$$\mathbf{C}(t) = (1 - C_X, C_X e^{-t/T_1}, 0, 0). \tag{3}$$

At time $t = \tau_{\text{delay}}$, the probe pulse of pulse-area π resonantly excites an optical transition $\alpha \rightarrow \beta$ and swaps the populations of the states α and β. Here α, β represent $0, X, \bar{X}$ or $2X$ states. This results in a change in photocurrent due to the probe of:

$$\Delta PC_{0-X} = a(C_0(\tau_{\text{delay}}) - C_X(\tau_{\text{delay}})) = a(1 - C_X - C_X e^{-\tau_{\text{delay}}/T_1}), \tag{4}$$

$$\Delta PC_{0-\bar{X}} = a(C_0(\tau_{\text{delay}}) - C_{\bar{X}}(\tau_{\text{delay}})) = a(1 - C_X), \tag{5}$$

$$\Delta PC_{X-2X} = (b-a)(C_X(\tau_{\text{delay}}) - C_{2X}(\tau_{\text{delay}})) = (b-a)C_X e^{-\tau_{\text{delay}}/T_1}, \tag{6}$$

where a is the photocurrent corresponding to one exciton, and b is the photocurrent due to one biexciton. $a = \Delta PC(\pi)$ is the amplitude of the photocurrent peak at zero detuning measured with a single π pulse (see blue line Fig. 1(b)). $b - a = \Delta PC_{\text{X-2X}}(\pi)e^{\tau_{\text{delay}}/T_1}$ is deduced from a separate experiment where an exciton is prepared with a pump pulse of pulse-area π resonant with the $0 - X$ transition and then the biexciton is created by a π probe resonant with the $X - 2X$ transition [28]. The exciton population C_X generated by the pump pulse is then calculated from the amplitude of the change in photocurrent peaks using Eqs.(4-6), and the experimentally determined parameters a, b, T_1.

By inspection of Fig. 1(b) it is clear that an exciton population inversion has been achieved. Firstly, the dip in the co-polarized photocurrent spectra indicates that $\Delta PC_{0-X} < 0$ and hence $C_X > C_0$ independent of the calibration of a or T_1. Secondly, the ratio of the cross-polarized change in photocurrent peak $\Delta PC_{0-\bar{X}}$ to the single pulse photocurrent peak of the $0 - X$ transition $\Delta PC(\pi)$ indicates that $C_0 < 1/2$ and hence provides a second proof of population inversion. We note that the data presented in Fig. 4 of the main text is measured using cross-polarized excitation, and is therefore independent of the tunneling rates.

II. MODEL

For our calculations we used the same model for an optically driven strongly confined quantum dot as in Ref. [9], which is based on the Hamiltonian

$$H = H_{\text{QD-light}} + H_{\text{QD-phonon}}, \tag{7}$$

where

$$H_{\text{QD-light}} = \hbar\omega_X^0 |X\rangle\langle X| + \frac{\hbar\Omega(t)}{2}[|0\rangle\langle X|e^{i\omega_L t} + |X\rangle\langle 0|e^{-i\omega_L t}], \tag{8}$$

and

$$H_{\text{QD-phonon}} = \sum_{\mathbf{q}} \hbar\omega_{\mathbf{q}}\, b_{\mathbf{q}}^\dagger b_{\mathbf{q}} + \sum_{\mathbf{q}} \hbar\big(\gamma_{\mathbf{q}} b_{\mathbf{q}} + \gamma_{\mathbf{q}}^* b_{\mathbf{q}}^\dagger\big)|X\rangle\langle X|. \tag{9}$$

The ground-state $|0\rangle$ is chosen as the zero of the energy and the phonon-free energy of the transition to the single exciton state $|X\rangle$ is denoted by $\hbar\omega_X^0$. The Rabi frequency $\Omega(t)$ is proportional to the electric field envelope of a circularly polarized Gaussian laser pulse with frequency ω_L, which is detuned from the ground-state to exciton transition by $\Delta = \omega_L - \omega_X$, where ω_X is the frequency of the single exciton resonance which deviates from ω_X^0 by the polaron shift that results from the dot-phonon coupling in Eq. (9). The coupling to the laser field is treated in the common rotating wave and dipole approximations. The operator $b_{\mathbf{q}}^\dagger$ creates a longitudinal acoustic (LA) bulk phonon with wave vector $\mathbf{q}$ and energy $\hbar\omega_{\mathbf{q}}$. We assume a linear dispersion relation $\omega_{\mathbf{q}} = c_s|\mathbf{q}|$, where c_s denotes the speed of sound. The phonons are coupled via the deformation potential only to the exciton state. This coupling is expressed by the exciton-phonon coupling $\gamma_{\mathbf{q}} = \frac{|\mathbf{q}|}{\sqrt{2V\rho\hbar\omega_{\mathbf{q}}}}\big(D_{\text{e}}\Psi^{\text{e}}(\mathbf{q}) - D_{\text{h}}\Psi^{\text{h}}(\mathbf{q})\big)$, where ρ denotes the mass density of the crystal, V the mode volume, $D_{\text{e/h}}$ the deformation potential constants, and $\Psi^{\text{e/h}}(\mathbf{q})$ the form factors of electron and hole,

respectively. As explained in the main article, we calculate the form factors from the ground-state wavefunctions of a spherically symmetric, parabolic confinement potential. It should be noted that, in the pure dephasing model for the dot-phonon coupling, no transitions between the bare electronic states can be induced by the continuum of LA phonons, which can change the electronic occupations only in the presence of the laser field. We assume the system to be initially in a product state of a thermal phonon-distribution at the temperature of the cryostat and a pure ground-state of the electronic subsystem. We use the material parameters given in Ref. [29] for GaAs, which are: $\rho = 5370\ \mathrm{kg/m^3}$, $c_s = 5110\ \mathrm{m/s}$, $D_\mathrm{e} = 7.0\ \mathrm{eV}$, and $D_\mathrm{h} = -3.5\ \mathrm{eV}$.

To obtain the time evolution of the electronic density matrix elements predicted by this model, we make use of a numerically exact real-time path-integral approach, described in detail in Ref. [23]. This gives us the opportunity to calculate the dynamics of the quantum dot with a high and controllable numerical precision and without further approximations to the given Hamiltonian. This includes taking into account all multi-phonon processes and non-Markovian effects.

Publication 5

Phonon-assisted robust and deterministic two-photon biexciton preparation in a quantum dot

S. Bounouar, M. Müller, A. M. Barth, M. Glässl, V. M. Axt and P. Michler

Physical Review B **91**, 161302(R) (2015)

DOI: 10.1103/PhysRevB.91.161302

PHYSICAL REVIEW B **91**, 161302(R) (2015)

Phonon-assisted robust and deterministic two-photon biexciton preparation in a quantum dot

S. Bounouar,[1] M. Müller,[1,*] A. M. Barth,[2,†] M. Glässl,[2] V. M. Axt,[2] and P. Michler[1]
[1]*Institut für Halbleiteroptik und Funktionelle Grenzflächen, Universität Stuttgart, 70569 Stuttgart, Germany*
[2]*Institut für Theoretische Physik III, Universität Bayreuth, 95440 Bayreuth, Germany*
(Received 27 August 2014; revised manuscript received 10 March 2015; published 9 April 2015)

We investigate both experimentally and theoretically a simple yet more robust and flexible alternative to Rabi oscillation-type biexciton preparation protocols traditionally used for semiconductor quantum dots. The quantum dot is excited by a strong laser pulse positively detuned from the two-photon resonance yielding an on demand initialization of the biexciton state by making use of the phonon-induced thermalization of the photon dressed states. It is shown that for excitation pulses in the picosecond range, a stable and high occupation of up to $C_{XX} = 0.95 \pm 0.02$ is reached. Notably, the generated photons show similar coherence properties as measured in the resonant two-photon scheme. This protocol is a powerful tool for the control of complex solid state systems combining radiative cascades, entanglement, and resonant cavity modes.

DOI: 10.1103/PhysRevB.91.161302 PACS number(s): 78.67.Hc, 03.65.Yz, 63.20.kk, 78.47.−p

One strong advantage of atomiclike systems, especially semiconductor quantum dots (QD), in the development of quantum computing or communication devices is their ability to deliver on-demand single [1,2] or entangled photon pairs [3,4]. This first step towards the possibility of deterministic quantum operations is a crucial complement to the achievements obtained in the field of quantum information processing [5,6] as well as for tests of fundamental aspects of quantum mechanics [7]. The initial state is usually prepared through a population inversion thanks to a strong coherent pulsed laser field brought to resonance with the two-level system [8–10]. This Rabi oscillation protocol can be very efficient, but is strongly sensitive to fluctuations of the excitation parameters like the pulse area. Other more complex protocols, using chirped laser pulses to populate adiabatically the upper state, are in principle more robust [11], but the degree of population inversion realized in experiments devoted to the single exciton preparation [12,13] stayed below the ideal case. In contrast to real atomic systems, solid state systems experience a coupling to their environment, in particular with the surrounding crystal vibrational modes [14–18]. This has always been considered as a strong limitation to their efficient use because of the occurring decoherence. In particular, phonons have been identified as the cause for the nonideal state preparation using chirped pulse protocols [19–21]. However, it has been recently proposed for semiconductor quantum dots that, when addressed with a controlled off-resonant pulse, this weakness can become an advantage and make the state preparation more efficient, robust, and flexible [22]. The phonons cannot only be used to achieve an inversion in simple two-level systems consisting of the ground $|0\rangle$ and an exciton state $|X\rangle$ [23–25], but also for the initialization of the biexciton state $|XX\rangle$ that forms the upper level of a radiative cascade, which can potentially result in emission of entangled photon pairs [26,27].

In this paper, we investigate the biexciton preparation in a quantum dot through a controlled two-photon excitation scheme taking benefit of the normally undesired carrier-phonon coupling. By tuning the laser energy and pulse length, such that the relaxation processes due to this coupling are most efficient, it is shown that one can transit from a resonant Rabi oscillation regime to an adiabatic, efficient, and robust biexciton state initialization. The results for a sufficiently long pulse are compared to a situation where the pulse length is too short to complete the relaxation and the consequences on the state preparation are studied. The coherence of the resulting emitted photons is evaluated and reveals to be comparable in the Rabi π-pulse case and for the phonon-assisted protocol, adding to efficiency and robustness, a long coherence time. Accompanying our experiment, we have studied theoretically the dynamics of a quantum dot driven by a laser with frequency close to the two-photon resonance, and we find a good overall agreement to the predictions of our simulations. From this, we can conclude that the underlying mechanism of the state preparation is indeed the pure dephasing induced by longitudinal acoustic phonons [28], which we included in our model to account for the solid state environment of the quantum dot. We used an epitaxially grown (In,Ga)As/GaAs QD kept at a temperature of 4.2 K to investigate the photoluminescence under pulsed two-photon excitation. In order to address the biexciton in a resonant or a quasiresonant way, by setting the pulse length at a constant value and by controlling its wavelength, the laser is tailored through a pulse shaping setup. The quantum dot is excited from the side with linearly polarized light and the detection is done after a perpendicularly oriented polarizer in order to reject the scattered laser (for more information concerning sample structure and experimental setup see Ref. [3]). The pulse length as well as the pulse shape was controlled via intensity autocorrelation measurements. More details about the pulse shaping setup are given in Ref. [29].

Figure 1(a) shows a photoluminescence spectrum under above band-gap excitation. The exciton (1.4212 eV) and biexciton lines (1.4189 eV) are separated by the biexciton binding energy (2.3 meV). Direct excitation of the biexciton is obtained by setting a shaped laser in resonance between the exciton and the biexciton [see Fig. 1(b)]. Although the biexciton and the ground state are not directly dipole coupled, the dynamics induced by a resonant laser field results in Rabi-type oscillations where similar to a directly coupled two-level

*m.mueller@ihfg.uni-stuttgart.de
†andreas.barth@uni-bayreuth.de

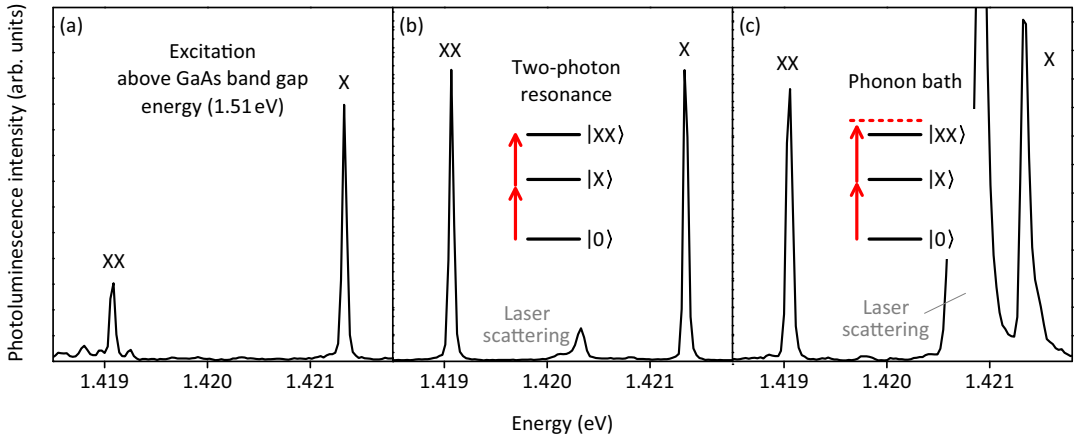

FIG. 1. (Color online) Single QD emission spectrum (a) under nonresonant above band gap excitation, (b) under resonant two-photon biexciton state excitation, and (c) with phonon-assisted 13-ps pulsed, 0.65-meV positively detuned excitation.

system the oscillation frequency scales with the square-root of the laser intensity [10]. Therefore the final inversion obtained after a pulse of finite length also oscillates between ± 1 as a function of the excitation power. These Rabi oscillations were probed with power dependent PL intensity measurements where the results for 13-ps pulses are shown as blue dots in Fig. 2(a). The solid lines are the result of a numerically exact real-time path-integral simulation [30], which allows us to calibrate the scaling of the measured intensity by fitting the theoretically predicted Rabi oscillations for resonant excitation to the corresponding experimental data. Because the size of the quantum dot and the strength of the chirp of the laser pulse where not directly measured, we treated these quantities as fitting parameters. We would like to note that the path-integral approach gives us the ability to solve our model of an optically driven quantum dot without further approximations taking into account arbitrary multiphonon processes as well as all non-Markovian effects. Further information about our model and other system parameters [31] used in the calculations are given in Ref. [32].

The first maximum of the blue curve for resonant excitation in Fig. 2(a) indicates the inversion of the biexciton population and the corresponding pulse will be referred to as a π pulse. At the π-pulse power, the $|XX\rangle$ occupation is estimated to be $C_{XX}^{\mathrm{res}} = 0.94 \pm 0.01$, whereby the error is calculated by means of a least square analysis using the experimental data and the theoretically calculated curves. Two other noticeable features of these oscillations are the decrease of the Rabi period with increasing pulse area and a damping of the amplitude. The first characteristic is a signature of the two-photon excitation process [10] and the damping is due to a coupling to phonons [33,34]. The average value of the oscillation is above 0.5 due to an imperfection of the excitation pulse, which is weakly chirped in the pulse shaping setup. For a positive sign of the chirp and low temperatures, such an increase of the biexciton population has already been predicted [35]. However, here it should be noted that according to our simulations the frequency sweep mostly affects the dynamics for resonant excitation, while for detuned laser pulses targeted in this paper the chirp only has a very small effect.

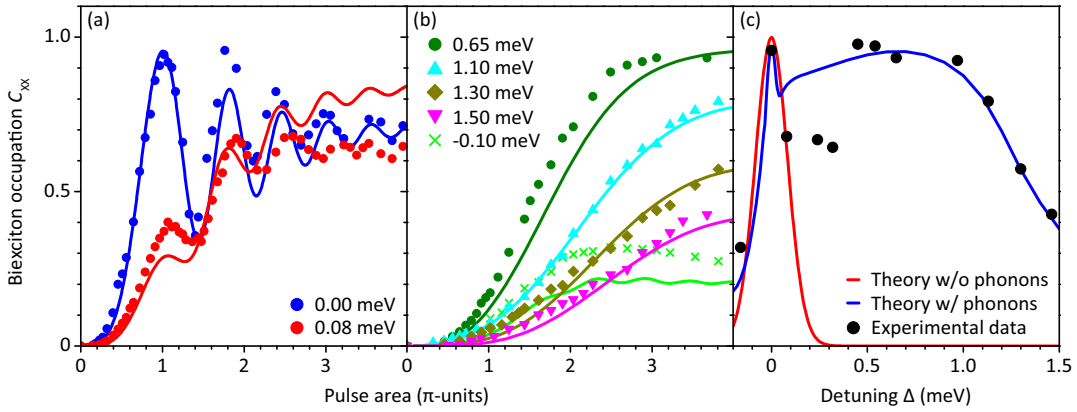

FIG. 2. (Color online) (a) Biexciton occupation C_{XX} as obtained from comparison with simulations (see text) vs renormalized pulse area with excitation pulse length of 13 ps superposed to path-integral simulation results for different laser detunings from the TPBR: in resonance represented in blue, 0.08-meV detuning in red, (b) 0.65-meV detuning in green, 1.1-meV detuning in light blue, 1.3-meV detuning in dark yellow, 1.5-meV detuning in magenta, -0.1-meV detuning in light green. (c) Maximum biexciton occupation (see text) reached for different laser detunings from the TPBR. The points represent occupations measured in the experiment and the full lines are results of the simulations (in blue with phonon coupling included in the calculations, in red without any phonon coupling).

Let us now focus on the case of off-resonant excitation of the QD exemplarily shown in the spectrum in Fig. 1(c) for 0.65-meV detuning. The laser detuning Δ is referred to the two-photon biexciton resonance (TPBR) and in our measurements ranges from -0.1 up to 1.5 meV. For such detuned excitation in a system with few isolated, discrete levels it is a well known result that the amplitude as well as the mean value of the Rabi oscillations rapidly decrease as the laser frequency is increased. In fact, for a small positive detuning of $\Delta = +0.08$ meV, shown in Fig. 2(a) in red color, reduced Rabi oscillations are still visible and when the detuning is increased, they disappear completely. However, as both our calculations and our experimental data show, there is also an overall increase of the biexciton population for positive detunings. This can be seen even more clearly in Fig. 2(b), which shows the power dependence of the biexciton population, for a few more selected detunings. The state initialization is most efficient between 0.45- and 1.00-meV detuning (only the 0.65-meV detuning data are shown in dark green), where the measured $|XX\rangle$ occupation at high-pulse area ($C_{XX}^{\mathrm{det}} = 0.95 \pm 0.02$) is similar to the one reached with the resonant π pulse ($C_{XX}^{\mathrm{res}} = 0.94 \pm 0.01$). In this range, the occupation is not only stable against small changes of the excitation frequency, but also shows a pronounced region where the biexciton population stays unaffected by fluctuations of the laser power, which is a clear advantage compared to the traditional resonant π-pulse scheme. For larger detunings (light blue for 1.1 meV, dark yellow for 1.3 meV, violet for 1.5 meV), the preparation becomes less efficient consistent with our calculations.

The detuning dependence of the biexciton occupation can be seen in more detail in Fig. 2(c), where we have plotted the maximum biexciton population measured in the laser power range between 0 π and 4 π (black dots) for the whole series together with the corresponding results of the simulations (blue line). Also shown are results of calculations where the exciton-phonon coupling was disregarded (red line). The strong influence of the environment visible from the discrepancy between the blue and the red line on the one hand, and the close overall agreement between the experimental data and the calculations including the phonon interaction on the other hand, provide clear evidence that the state preparation can be attributed to the carrier-phonon coupling. To understand the physics behind this feature, it is important to note that a phonon-induced relaxation is possible as the bare electronic states become dressed by the laser field. This relaxation can lead to a thermal occupation of the photon dressed states, which for positive detunings yields a high biexciton population [22,36]. For negative detunings [also shown in Fig. 2(b) in light green], the energetic order of the dressed states changes, and thus the biexciton state is no longer the final state of the relaxation at low temperatures, which explains the steep decrease of the biexciton population seen in Fig. 2(c) for $\Delta < 0$. Around the two-photon resonance, we can see a sharp peak in Fig. 2(c) as the maximum occupation in the observed pulse area interval is determined by the height of the π-pulse peak. When further increasing the laser frequency the $|XX\rangle$ population decreases until the transition from the resonant Rabi oscillation scheme to the off-resonant phonon-assisted state preparation occurs. In the

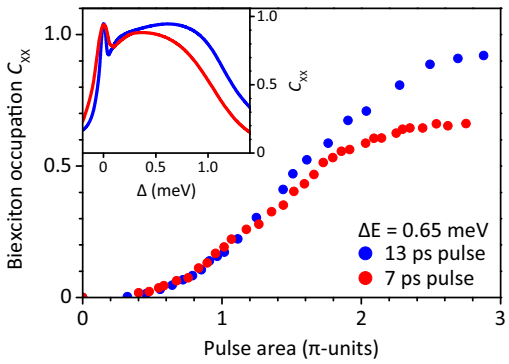

FIG. 3. (Color online) Measured biexciton population vs renormalized excitation power for excitation pulse length of 13 ps (blue dots) and 7 ps (red dots) at laser detuning of 0.65 meV. (Inset) Maximal biexciton occupation as a function of the detuning for excitation with an unchirped pulse of length 13 ps (blue) and 7 ps (red).

experiments, the population stays below the calculated values for detunings between 0.08 and 0.32 meV. While it is, so far, not clear why the quantitative agreement between theory and experiment is not as perfect as for detunings below and above this range, the qualitative behavior is still as expected. In particular, C_{XX} steeply decreases from the maximum at zero detuning, but always stays at a finite value well above what is predicted without phonons (cf. the red curve). Moreover, for higher detunings, a wide plateau is reached where the phonon-assisted relaxation is most efficient and therefore ideal for deterministic state initialization. The maximal efficiency of the phonon coupling in this region is due to the resonance of the most pronounced phonon energies to the transitions between the relevant dressed states. For even higher detunings, the splitting between the dressed states becomes too large and hence the phonon relaxation does not take place efficiently yielding lower and lower values for the maximal biexciton population as is nicely seen in both experiment and theory. It should be noted that the resonance structure described above has the same origin as the nonmonotonic dependence of the phonon induced damping of Rabi oscillations on the pulse area [34,37,38].

In order to test the influence of the excitation pulse length, the same experiment was carried out for shorter excitation pulses of 7-ps width. Figure 3 shows the power dependencies at $\Delta = 0.65$ meV detuning for excitation pulse widths of 13 ps (blue dots) and 7 ps (red triangles), respectively. The biexciton occupation at high pulse areas becomes much less efficient for the shorter excitation pulse (7 ps) and whatever the detuning used, the occupation of the biexciton obtained with short pulses stays below 0.62 and is therefore insufficient for schemes requiring photons on-demand (data are shown in Ref. [39]). The same tendencies are also found in the theory as seen from the inset of Fig. 3, where as in Fig. 2(c), but for an unchirped excitation, the detuning dependence of the maximal biexciton occupation is plotted for pulse durations of 13 ps (blue) and 7 ps (red), respectively. While the maximal attainable biexciton occupation is practically independent of the pulse length for resonant excitation, it is significantly

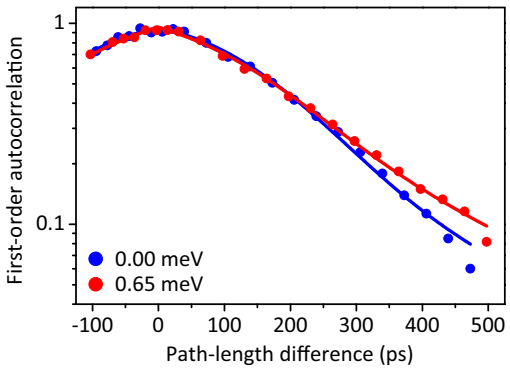

FIG. 4. (Color online) Biexcitonic photon first-order interference visibility vs time delay, under resonant π-pulse excitation (blue dots), under phonon-assisted, 0.65-meV detuned, 3π-pulse excitation (red dots). Full curves are fits of the Fourier transform of a Voigt profile to the experimental data from which the coherence times (277 ± 8 ps in resonance, 271 ± 7 ps for the 0.65-meV detuned excitation) are extracted.

reduced at larger positive detunings for the 7-ps pulse. The calculations support the conclusion that robust and efficient preparation can be obtained provided that the pulse is long enough to relax the system to the energetically lowest dressed state during the pulse, whereas under too short excitation no robust biexciton preparation can be achieved.

In order to check the usefulness of the protocol in quantum optics applications, we investigated the coherence of the generated photons and compared them to coherence times observed in resonance. Figure 4 displays the measured coherence time curves under 13-ps resonant π pulses (blue) and 0.65-meV detuned excitation (at large pulse area, i.e., around 3π, in red). For both excitation schemes, the first-order autocorrelation functions are nearly identical. The full curves are Fourier transforms of a Voigt profile from which we extracted a coherence time of 277 ± 8 and 271 ± 7 ps, respectively. This is in contrast with measurements made with above band-gap excitation pulses which resulted in significantly lower coherence times ($\tau = 114 \pm 4$ ps [3]), because of the electronic fluctuations generated in the surrounding of the quantum dots [40]. This conservation of the coherence obtained in resonance is of crucial importance since the coherence of the emitted photons is a decisive parameter determining their degree of indistinguishability [41,42].

In summary, it is demonstrated experimentally in this paper that one can obtain a robust biexciton preparation with near unity occupation probability and a long coherence time by using a simple protocol involving excitations detuned from the two-photon resonance. Comparing with theoretical results, we find a good agreement revealing that the preparation is due to phonon-induced relaxation processes. Applied to the optical preparation of biexcitons in quantum dots, this is a particularly flexible and efficient scheme for the initialization of entangled photon states. Since this protocol leaves the TPBR free from laser scattering, it is particularly suitable for a recently proposed two-photon emission ($|X\rangle$ and $|XX\rangle$) in a large Q-factor cavity mode set between $|X\rangle$ and $|XX\rangle$, which was demonstrated as highly entangled whatever the $|X\rangle$ fine structure splitting is [43]. The approach presented in this paper for the biexciton preparation would solve practical problems encountered in such two-photon emission observations in QD-photonic crystals systems [44] enabling clean photon statistic measurements.

Note added in proof. Recently, we became aware of related results by two other groups [45,46].

ACKNOWLEDGMENTS

The authors acknowledge L. Wang, A. Rastelli and O. G. Schmidt for providing the high-quality sample, K. D. Jöns for technical advice and discussion, and Deutsche Forschungsgemeinschaft for financial support via the projects MI 500/23-1 and AX 17/7-1.

[1] P. Michler, A. Kiraz, C. Becher, W. V. Schoenfeld, P. M. Petroff, L. Zhang, E. Hu, and A. Imamoglu, Science **290**, 2282 (2000).

[2] Y.-M. He, Y. He, Y.-J. Wei, D. Wu, M. Atatüre, C. Schneider, S. Höfling, M. Kamp, C.-Y. Lu, and J.-W. Pan, Nat. Nanotechnol. **8**, 213 (2013).

[3] M. Müller, S. Bounouar, K. D. Jöns, M. Glässl, and P. Michler, Nat. Photon. **8**, 224 (2014).

[4] N. Akopian, N. H. Lindner, E. Poem, Y. Berlatzky, J. Avron, D. Gershoni, B. D. Gerardot, and P. M. Petroff, Phys. Rev. Lett. **96**, 130501 (2006).

[5] D. Bouwmeester, A. K. Ekert, and A. Zeilinger, *The Physics of Quantum Information* (Springer, Berlin, 2000).

[6] M. A. Nielsen and I. Chuang, *Quantum Computation and Quantum Information* (Cambridge University Press, Cambridge, 2000).

[7] S. Haroche and J. Raimond, *Exploring the Quantum* (Oxford University Press, Oxford, 2006).

[8] H. Jayakumar, A. Predojević, T. Huber, T. Kauten, G. S. Solomon, and G. Weihs, Phys. Rev. Lett. **110**, 135505 (2013).

[9] K. Brunner, G. Abstreiter, G. Böhm, G. Tränkle, and G. Weimann, Phys. Rev. Lett. **73**, 1138 (1994).

[10] S. Stufler, P. Machnikowski, P. Ester, M. Bichler, V. M. Axt, T. Kuhn, and A. Zrenner, Phys. Rev. B **73**, 125304 (2006).

[11] Y.-J. Wei, Y.-M. He, M.-C. Chen, Y.-N. Hu, Y. He, D. Wu, C. Schneider, M. Kamp, S. Höfling, C.-Y. Lu, and J.-W. Pan, Nano Lett. **14**, 6515 (2014).

[12] C.-M. Simon, T. Belhadj, B. Chatel, T. Amand, P. Renucci, A. Lemaitre, O. Krebs, P. A. Dalgarno, R. J. Warburton, X. Marie, and B. Urbaszek, Phys. Rev. Lett. **106**, 166801 (2011).

[13] Y. Wu, I. M. Piper, M. Ediger, P. Brereton, E. R. Schmidgall, P. R. Eastham, M. Hugues, M. Hopkinson, and R. T. Phillips, Phys. Rev. Lett. **106**, 067401 (2011).

[14] A. V. Fedorov, A. V. Baranov, and K. Inoue, Phys. Rev. B **56**, 7491 (1997).

[15] P. Borri, W. Langbein, S. Schneider, U. Woggon, R. L. Sellin, D. Ouyang, and D. Bimberg, Phys. Rev. Lett. **87**, 157401 (2001).

[16] L. Besombes, K. Kheng, L. Marsal, and H. Mariette, Phys. Rev. B **63**, 155307 (2001).

[17] A. Nysteen, P. Kaer, and J. Mork, Phys. Rev. Lett. **110**, 087401 (2013).

[18] D. P. S. McCutcheon and A. Nazir, Phys. Rev. Lett. **110**, 217401 (2013).

[19] S. Lüker, K. Gawarecki, D. E. Reiter, A. Grodecka-Grad, V. M. Axt, P. Machnikowski, and T. Kuhn, Phys. Rev. B **85**, 121302 (2012).
[20] A. Debnath, C. Meier, B. Chatel, and T. Amand, Phys. Rev. B **86**, 161304 (2012).
[21] P. R. Eastham, A. O. Spracklen, and J. Keeling, Phys. Rev. B **87**, 195306 (2013).
[22] M. Glässl, A. M. Barth, and V. M. Axt, Phys. Rev. Lett. **110**, 147401 (2013).
[23] M. Glässl, A. Vagov, S. Lüker, D. E. Reiter, M. D. Croitoru, P. Machnikowski, V. M. Axt, and T. Kuhn, Phys. Rev. B **84**, 195311 (2011).
[24] D. E. Reiter, S. Lüker, K. Gawarecki, A. Grodecka-Grad, P. Machnikowski, V. M. Axt, and T. Kuhn, Acta Phys. Pol. A **122**, 1065 (2012).
[25] S. Hughes and H. J. Carmichael, New J. Phys. **15**, 053039 (2013).
[26] R. M. Stevenson, R. J. Young, P. Atkinson, K. Cooper, D. A. Ritchie, and A. J. Shields, Nature (London) **439**, 179 (2006).
[27] R. Hafenbrak, S. M. Ulrich, P. Michler, L. Wang, A. Rastelli, and O. G. Schmidt, New J. Phys. **9**, 315 (2007).
[28] A. Vagov, V. M. Axt, T. Kuhn, W. Langbein, P. Borri, and U. Woggon, Phys. Rev. B **70**, 201305 (2004).
[29] See Supplemental Material at http://link.aps.org/supplemental/10.1103/PhysRevB.91.161302 for the experimental setup of the pulse shaper.
[30] A. Vagov, M. D. Croitoru, M. Glässl, V. M. Axt, and T. Kuhn, Phys. Rev. B **83**, 094303 (2011).
[31] B. Krummheuer, V. M. Axt, and T. Kuhn, Phys. Rev. B **65**, 195313 (2002).
[32] See Supplemental Material at http://link.aps.org/supplemental/10.1103/PhysRevB.91.161302 for further information about the theoretical model and system parameters used in the calculations.
[33] J. Förstner, C. Weber, J. Danckwerts, and A. Knorr, Phys. Rev. Lett. **91**, 127401 (2003).
[34] P. Machnikowski and L. Jacak, Phys. Rev. B **69**, 193302 (2004).
[35] M. Glässl, A. M. Barth, K. Gawarecki, P. Machnikowski, M. D. Croitoru, S. Lüker, D. E. Reiter, T. Kuhn, and V. M. Axt, Phys. Rev. B **87**, 085303 (2013).
[36] D. E. Reiter, T. Kuhn, M. Glässl, and V. M. Axt, J. Phys.: Condens. Matter **26**, 423203 (2014).
[37] A. Vagov, M. D. Croitoru, V. M. Axt, T. Kuhn, and F. M. Peeters, Phys. Rev. Lett. **98**, 227403 (2007).
[38] A. J. Ramsay, A. V. Gopal, E. M. Gauger, A. Nazir, B. W. Lovett, A. M. Fox, and M. S. Skolnick, Phys. Rev. Lett. **104**, 017402 (2010).
[39] See Supplemental Material at http://link.aps.org/supplemental/10.1103/PhysRevB.91.161302 for the detuning dependency of the biexciton occupation using short excitation pulses (7 ps).
[40] A. Berthelot, I. Favero, G. Cassabois, C. Voisin, C. Delalande, P. Roussignol, R. Ferreira, and J. M. Gerard, Nat. Phys. **2**, 759 (2006).
[41] C. Santori, D. Fattal, J. Vuckovic, G. S. Solomon, and Y. Yamamoto, New J. Phys. **6**, 89 (2004).
[42] F. Troiani, J. I. Perea, and C. Tejedor, Phys. Rev. B **73**, 035316 (2006).
[43] S. Schumacher, J. Förstner, A. Zrenner, M. Florian, C. Gies, P. Gartner, and F. Jahnke, Opt. Express **20**, 5335 (2012).
[44] Y. Ota, S. Iwamoto, N. Kumagai, and Y. Arakawa, Phys. Rev. Lett. **107**, 233602 (2011).
[45] P.-L. Ardelt, L. Hanschke, K. A. Fischer, K. Müller, A. Kleinkauf, M. Koller, A. Bechtold, T. Simmet, J. Wierzbowski, H. Riedl, G. Abstreiter, and J. J. Finley, Phys. Rev. B **90**, 241404 (2014).
[46] J. H. Quilter, A. J. Brash, F. Liu, M. Glässl, A. M. Barth, V. M. Axt, A. J. Ramsay, M. S. Skolnick, and A. M. Fox, Phys. Rev. Lett. **114**, 137401 (2015).

Supplementary information to "Phonon-assisted robust and deterministic two-photon biexciton preparation in a quantum dot"

S. Bounouar,[1] M. Müller,[1,*] A. M. Barth,[2,†] M. Glässl,[2] V. M. Axt,[2] and P. Michler[1]

[1] *Institut für Halbleiteroptik und Funktionelle Grenzflächen, Universität Stuttgart, 70569 Stuttgart, Germany*
[2] *Institut für Theoretische Physik III, Universität Bayreuth, 95440 Bayreuth, Germany*

(Dated: March 9, 2015)

PULSE SHAPING

Fig.1 shows the pulse shaping setup used for the control of the excitation pulse length. After traveling through a beam expander in order to illuminate a 1800 l/mm grating with an enlarged spot size, the beam goes through a lens placed at the focal distance (1709 mm) from the grating, which allows to have a spatial access to the Fourier domain. The imaging of this Fourier transformation is done on a mirror placed on the focal plane of the lens, and the spectral selection of the pulse is done with a slit positioned just in front of the mirror. The beam then travels back in order to be Fourier transformed again to the time domain and is driven to the sample through a short single mode fiber. The tuning of the pulse length is done by opening or closing the slit in front of the mirror.

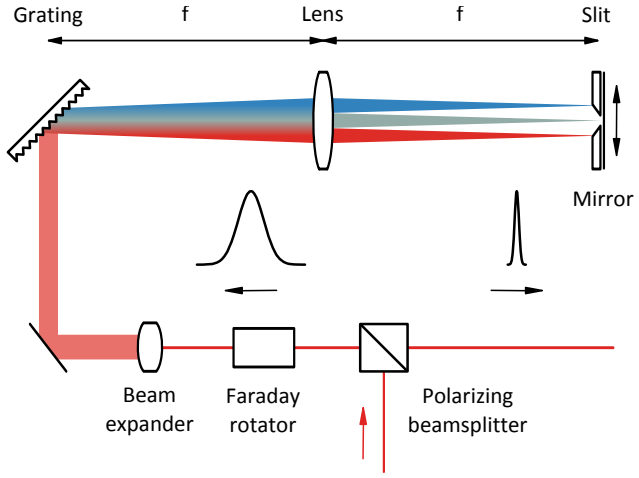

FIG. 1: Scheme of the pulse shaping setup.

In Fig. 2, we give an example of such a pulse shaping by showing the measured autocorrelation of the pulse in the time domain and the spectrum for a completely open (only a reflection takes place on the mirror) and a 1 mm opened slit. After fitting and deconvolution we found that the unshaped pulse (blue dots, open slit) is 2.5 ps FWHM long (spectral width of 580μeV) and that the shaped pulse (red dots, 1 mm slit) is 13 ps FWHM long (spectral width of 180μeV). The Gaussian functions fit

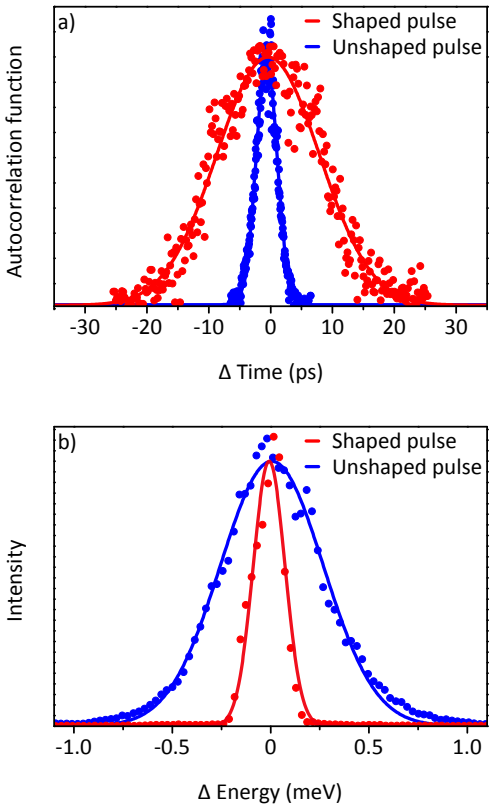

FIG. 2: a) Autocorrelation signals and b) spectral distribution recorded at the output of the pulse shaping setup for a totally opened slit in blue, and a 1 mm slit in red. Plotted in black, the fits are Gaussian for temporal and spectral domain as well as for signals from both slit apertures.

very nicely the data and are also used for the simulations. Anyway, applying other bell-shaped pulse envelopes in the theoretical calculations (such as squared hyperbolic secant) yield very similar results to those obtained from Gaussians.

ADDITIONAL DATA

Additional measurement and theoretical data for 13 ps and 7 ps excitation pulses are shown in Fig. 3 a), b) and c), d), respectively.

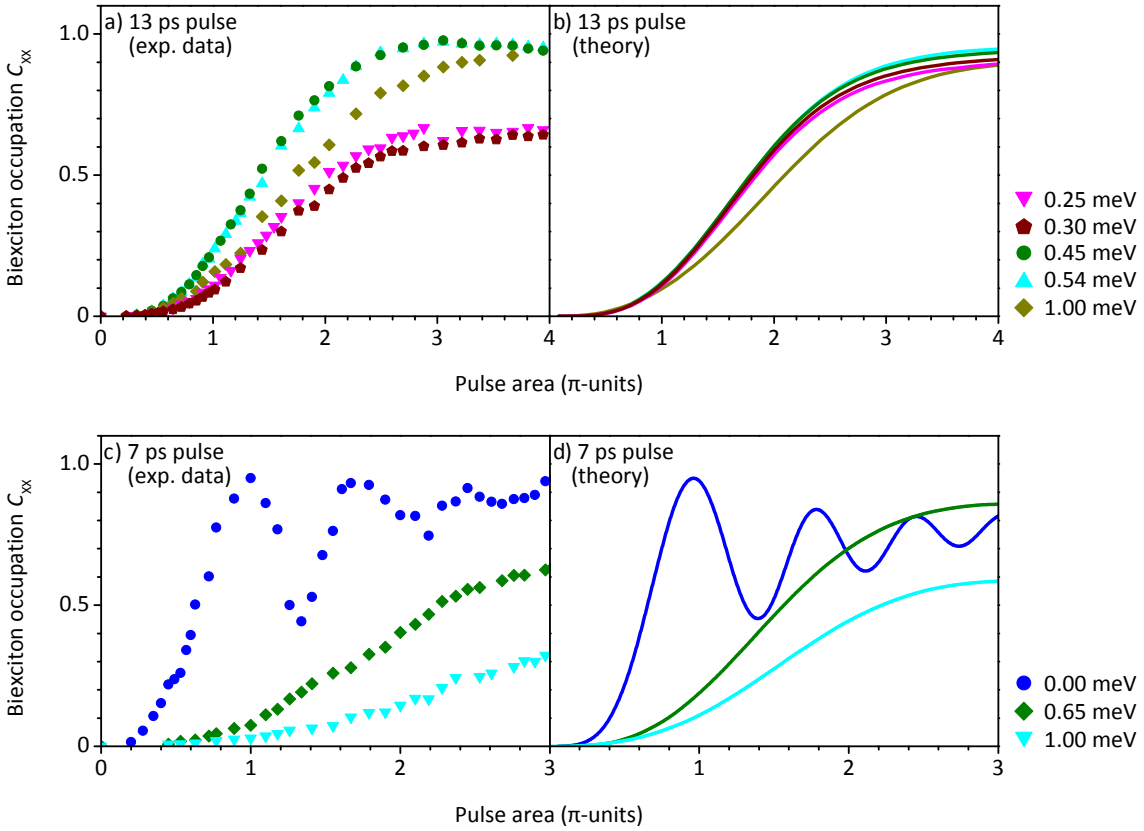

FIG. 3: Biexciton occupation probability versus renormalized pulse area with excitation pulse length of 13 ps [a) exp. data, b) theory], corresponding to the remaining data points in Fig 2 c) in the main text and 7 ps excitation pulse length [c) exp. data, d) theory].

THEORY

To study the biexciton state preparation process theoretically, we applied the commonly used model for an optically driven strongly confined quantum dot defined by the system Hamiltonian $H = H_{\mathrm{dot-light}} + H_{\mathrm{dot-phonon}}$. The first part describes the coupling of the three relevant electronic quantum dot states to a linearly polarized classical light field, using the dipole and rotating wave approximation, and reads

$$H_{\mathrm{dot-light}} = \hbar\omega_X |X\rangle\langle X| + (2\hbar\omega_X - \Delta_B)|B\rangle\langle B| + [\frac{\hbar f(t)}{2}(|X\rangle\langle G| + |B\rangle\langle X|) + \mathrm{h.c.}]\,. \quad (1)$$

The energy of the ground-state $|G\rangle$ was set to zero, $\hbar\omega_X$ denotes the transition energy to the single exciton state $|X\rangle$ and the biexciton state $|XX\rangle$ is lowered in energy by the biexciton binding energy $\Delta_B = 2.3$ meV. The quantity $f(t) = 2\mathbf{d}\cdot\mathbf{E}^{(+)}(t)/\hbar$, with $\mathbf{d}$ being the dipole moment of both transitions and $\mathbf{E}^{(+)}$ denoting the positive frequency component of the monochromatic laser field, captures the strength of the light-matter coupling. The laser excitation was assumed to be a linearly chirped Gaussian pulse with

$$f(t) \propto \frac{1}{\sqrt{2\pi\tau_0\tau}} \exp(-\frac{t^2}{2\tau^2}) \exp(-i\omega t - i\frac{at^2}{2})\,. \quad (2)$$

The length of the laser pulse τ and the rate of the frequency chirp a are governed by both the length of the corresponding unchirped pulse τ_0 and the chirp coefficient α and are given by the two formulas $\tau = \sqrt{\alpha^2/\tau_0^2 + \tau_0^2}$ and $a = \alpha/(\alpha^2 + \tau_0^4)$. The central laser frequency in the limit of vanishing chirp is denoted by ω and differs from the ground-state to exciton transition frequency by $\Delta/\hbar$. We extracted the chirp parameters, that have not been determined by independent experiments, by comparing the simulated pulse area dependence of the biexciton population for excitation resonant to the two-photon transition to the corresponding experimental data as shown for the 13 ps data in Fig.2 a) in the main article. Taking into account the pulse length obtained from the autocorrelation measurements we found $\tau_0 = 7.2$ ps and $\alpha = 23.6$ ps^2 for the 13 ps data and $\tau_0 = 3.6$ ps and $\alpha = 7.8$ ps^2 for the 7 ps data.

The second part of the Hamiltonian accounts for the pure dephasing deformation potential coupling to a con-

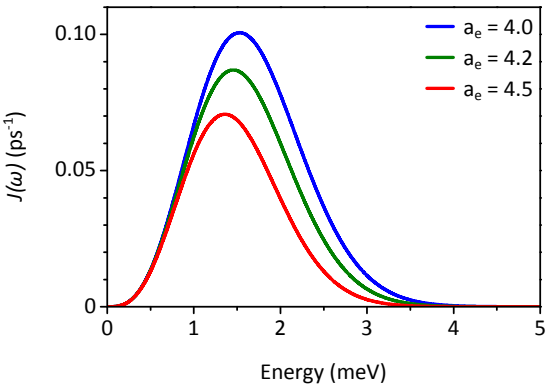

FIG. 4: Spectral density of the phonon coupling for different radial electron confinement lengths a_e.

tinuum of longitudinal acoustic (LA) phonons which is known to be responsible for the dominant dephasing mechanism in GaAs quantum dots [1, 2], and can be written as:

$$H_\mathrm{dot,ph} = \sum_{\mathbf{q}} \hbar\omega_{\mathbf{q}}\, b^\dagger_{\mathbf{q}} b_{\mathbf{q}} + \sum_{\mathbf{q},\nu} \hbar n_\nu \left(g_{\mathbf{q}} b_{\mathbf{q}} + g^*_{\mathbf{q}} b^\dagger_{\mathbf{q}}\right) |\nu\rangle\langle\nu|. \quad (3)$$

The phonons are assumed to be initially in thermal equilibrium at 4.2 K before the pulse. As the lattice properties of (In,Ga)As/GaAs are similar in the dot and its surrounding, a bulk model for the phonons is suitable. The LA bulk phonons with wave vector $\mathbf{q}$ and energy $\hbar\omega_{\mathbf{q}}$ are created by the operator $b^\dagger_{\mathbf{q}}$, and n_ν represents the number of electron-hole pairs in the state $|\nu\rangle$.

$g_{\mathbf{q}}$ denotes the coupling constant of the carrier-phonon interaction, as for example given in Ref. [3]: $g_{\mathbf{q}} = \frac{|\mathbf{q}|}{\sqrt{2V\rho\hbar\omega_{\mathbf{q}}}}(D_\mathrm{e}\exp(-\mathbf{q}^2 a_\mathrm{e}^2/4) - D_\mathrm{h}\exp(-\mathbf{q}^2 a_\mathrm{h}^2/4))$, where ρ is the mass density of the crystal, V the mode volume, $D_{\mathrm{e/h}}$ the deformation potential constants, and $2\sqrt{2\ln 2}\, a_{\mathrm{e/h}}$ the FWHM of the Gaussian wavefunction of the electron and hole, respectively. The Gaussian formfactors result from the assumption of a parabolic confinement and the ratio $a_\mathrm{e}/a_\mathrm{h}$ is assumed to be 1.15 due to the different masses of electron and hole. The radial electron confinement length was set to 4.2 nm and for all other material parameters we used the same values as in Ref. [4], which are also given in Ref. [5]: $\rho = 5370\,\mathrm{kg/m^3}$, $D_\mathrm{e} = 7.0\,\mathrm{eV}$, and $D_\mathrm{h} = -3.5\,\mathrm{eV}$. The resulting spectral density $J(\omega)$ of the phonon coupling is shown in Fig. 4 for a few different values of a_e.

To obtain the biexciton state population after a pulse and plot it as a function of the applied pulse area, we simulated the time-dependent behavior of the reduced density matrix using the real-time path-integral approach described in Ref. [3], specialized to the case of chirped pulsed excitation close to the two-photon transition. This allows us to calculate the combined carrier-phonon dynamics without further approximations to our model and with a high, reliable, and controllable numerical precision.

* m.mueller@ihfg.uni-stuttgart.de
† andreas.barth@uni-bayreuth.de

[1] A. J. Ramsay, A.V. Gopal, E. M. Gauger, A. Nazir, B.W. Lovett, A. M. Fox, and M. S. Skolnick, Phys. Rev. Lett. **104**, 017402 (2010).
[2] A. Vagov, V. M. Axt, T. Kuhn, W. Langbein, P. Borri, and U. Woggon, Phys. Rev. B **70**, 201305 (2004).
[3] A. Vagov, M. D. Croitoru, M. Glässl, V. M. Axt, and T. Kuhn, Phys. Rev. B **83**, 094303 (2011).
[4] M. Glässl, A. M. Barth, and V. M. Axt, Phys. Rev. Lett. **110**, 147401 (2013).
[5] B. Krummheuer, V. M. Axt, and T. Kuhn, Phys. Rev. B. **65**, 195313 (2002).

Publication 6

Fast and selective phonon-assisted state preparation of a quantum dot by adiabatic undressing

A. M. Barth, S. Lüker, A. Vagov, D. E. Reiter, T. Kuhn and V. M. Axt

Physical Review B **94**, 045306 (2016)

DOI: 10.1103/PhysRevB.94.045306

Fast and selective phonon-assisted state preparation of a quantum dot by adiabatic undressing

A. M. Barth,[1,*] S. Lüker,[2] A. Vagov,[1] D. E. Reiter,[2,3] T. Kuhn,[2] and V. M. Axt[1]
[1]*Institut für Theoretische Physik III, Universität Bayreuth, 95440 Bayreuth, Germany*
[2]*Institut für Festkörpertheorie, Universität Münster, 48149 Münster, Germany*
[3]*Imperial College London, South Kensington Campus, London SW7 2AZ, UK*
(Received 18 December 2015; revised manuscript received 1 July 2016; published 18 July 2016)

We investigate theoretically the temporal behavior of a quantum dot under off-resonant optical excitation targeted at fast acoustic phonon-assisted state preparation. We demonstrate that in a preparation process driven by short laser pulses, three processes can be identified: a dressing of the states during the switch-on of the laser pulse, a subsequent phonon-induced relaxation, and an undressing at the end of the pulse. By analyzing excitation scenarios with different pulse shapes we highlight the decisive impact of an adiabatic undressing on the final state in short-pulse protocols. Furthermore, we show that in exciton-biexciton systems the laser characteristics such as the pulse detuning and the pulse length as well as the biexciton binding energy can be used to select the targeted quantum dot state.

DOI: 10.1103/PhysRevB.94.045306

I. INTRODUCTION

Many of today's proposals for quantum information applications [1] rely on the controlled and fast manipulation of the discrete states of the corresponding devices' underlying structures. Semiconductor quantum dots (QDs) are frequently discussed as building blocks for such materials because they hold out the prospect of tailor-made energy spectra and a high integrability in a solid-state environment. The excitonic QD states are promising candidates to be used as qubits for quantum computing [2–7], while the radiative decay from the biexciton cascade offers the possibility of an on-demand creation of indistinguishable entangled photon pairs [8–11].

It has been shown that both exciton and biexciton states of a QD can be prepared by using ultrafast laser pulses under a variety of excitation conditions [12,13]. The most commonly known schemes for this purpose are resonant excitation leading to Rabi rotations [14–17], different protocols using chirped laser pulses exploiting the adiabatic rapid passage effect [18–26], and phonon-assisted off-resonant driving [27–30]. Recently, the latter method has also been experimentally demonstrated [31–33]. Indeed, there is an increased interest in this approach because it is not only stable against fluctuations of the applied field intensity, but also leaves the quantum dot transition laser free, which can be important when the emitted photons need to be spectrally separated from the laser pulse. Furthermore, in contrast to the other two protocols, the phonon-assisted scheme makes active use of the phonon coupling and even works the better the stronger this coupling is.

In this paper, we examine the influence of the pulse shape on the phonon-assisted state preparation. We identify three distinct processes that take place during the laser-driven evolution of the QD states. When the pulse starts, the coupling to the laser field leads to a *dressing* of the bare QD states. This enables a *phonon-induced relaxation* between the dressed states [27,34,35] and finally when the pulse is switched off an *undressing* takes place. While previous studies mostly concentrated on the resulting exciton and biexciton occupation obtained when applying an off-resonant driving pulse [30] and were focused on the phonon-induced relaxation, here we will explain the impact of all three different processes and examine in detail the role of the switch-on and switch-off phases of the excitation. We will show that within the relaxation process there is a tradeoff situation between a sufficiently fast preparation and an optimal preparation fidelity and that for a high-fidelity preparation of the bare QD states an adiabatic undressing, that can be realized by a long enough switch-off time, is indispensable in short-pulse protocols. Our analysis also shows that even though Gaussian pulses, as used in very recent experiments [31–33], are not the ideal choice for the phonon-assisted protocol they fulfill the requirements for fast state preparation surprisingly well for a wide intensity range provided that the regime of nonadiabatic dynamics is not yet reached. The latter condition sets a lower bound to the pulse duration.

The pulse characteristics not only allow to control the fidelity of the achieved inversion, but in addition can be used to select the QD state that is targeted by the phonon-assisted process. For the two-level case, the sign of the pulse detuning determines whether the QD is driven towards the ground state or the exciton state. For the exciton-biexciton system also the biexciton binding energy and the pulse length play a critical role in determining the targeted QD state. Understanding that the preparation is a three-step process gives us an intuitive answer to the important question which state is selected by the phonon-assisted preparation scheme and we present a comprehensive study including different detunings for the case of both positive and negative biexciton binding energy showing the populations of all relevant QD states.

II. MODEL

We consider a strongly confined GaAs QD driven by an external laser field and coupled to a continuum of acoustic bulk phonons. Our model is defined by the Hamiltonian $H = H_{\text{dot, light}} + H_{\text{dot-ph}}$, i.e., the electronic system coupled to the laser field and an additional phonon part. Let us first

*andreas.barth@uni-bayreuth.de

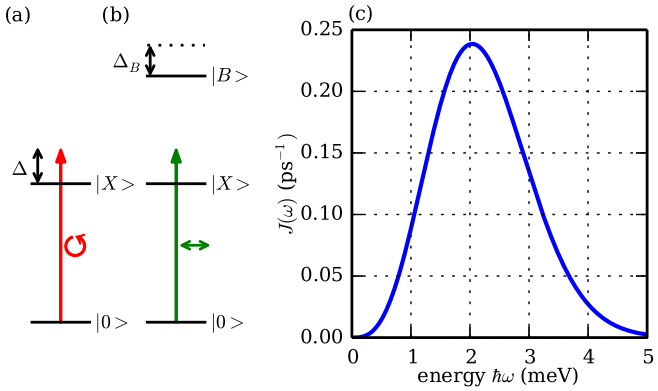

FIG. 1. Energetic level diagram of (a) the exciton system with circular polarized excitation and (b) the exciton-biexciton system with linear polarized excitation. (c) Spectral density of the phonon coupling as a function of energy for the parameters used in our simulations (see text).

concentrate on

$$H_{\text{dot, light}} = \sum_{\nu} \hbar\omega_{\nu} |\nu\rangle\langle\nu| + \sum_{\nu\nu'} \hbar M_{\nu\nu'} |\nu\rangle\langle\nu'|, \qquad (1)$$

where $|\nu\rangle$ are the electronic basis states with corresponding energies $\hbar\omega_{\nu}$. The matrix element $M_{\nu\nu'}$ describes the coupling between the QD and the classical laser field using the common dipole and rotating wave approximations. In the first part of the paper we will restrict ourselves to a two-level system consisting of the ground state $|0\rangle$, for which we set $\hbar\omega_0 = 0$, and a single exciton state $|X\rangle$ with energy $\hbar\omega_X$ as illustrated in Fig. 1(a). The two-level approximation is valid when considering circularly polarized light with a single polarization orientation and the exchange interaction is negligibly small. The exchange interaction strongly depends on the QD geometry [36] and can be close to zero, as it is favorable for, e.g., entangled photon creation [10]. In this case, the nonzero matrix elements of the light-matter coupling are given by

$$M_{0X} = \tfrac{1}{2} f(t) e^{i\omega_L t}, \qquad M_{X0} = M_{0X}^{*}, \qquad (2)$$

where $f(t)$ is a real pulse envelope function, which in the following is referred to as field strength. The field strength $f(t)$ is related to the electric field $\mathbf{E}(t)$ with frequency ω_L and the QD dipole matrix element $\mathbf{d}$ by $-\mathbf{d}\cdot\mathbf{E}(t) = \frac{\hbar}{2} f(t) e^{-i\omega_L t}$.

A very useful picture for strongly driven few-level systems, which we will employ to analyze our results, is the dressed-state picture. The dressed states are the eigenstates of the coupled light-matter Hamiltonian in a frame rotating with the laser frequency [37]. For the two-level system driven by a laser field with a fixed field strength f and a detuning Δ they are given by the expressions

$$|\psi_{\text{up}}\rangle = +\cos(\Theta)|0\rangle + \sin(\Theta)|X\rangle, \qquad (3a)$$

$$|\psi_{\text{low}}\rangle = -\sin(\Theta)|0\rangle + \cos(\Theta)|X\rangle, \qquad (3b)$$

where Θ is the mixing angle defined by $\tan(\Theta) = \frac{\hbar f}{\Delta + \hbar\Omega}$ and Ω is the Rabi frequency given by

$$\hbar\Omega = \sqrt{(\hbar f)^2 + \Delta^2}. \qquad (4)$$

The corresponding dressed-state energies read as

$$E_{\text{up/low}} = \tfrac{1}{2}(-\Delta \pm \hbar\Omega). \qquad (5)$$

It is worth noting that the contributions of the ground and exciton states to the dressed states vary depending on the detuning and the field strength.

The final part of this paper will be devoted to excitations with linearly polarized light. In this case, one also has to take into account the biexciton state, and the system described so far needs to be extended to a three-level model consisting of the ground state $|0\rangle$, the single exciton state $|X\rangle$, and the biexciton state $|B\rangle$. Note that the single exciton state $|X\rangle$ in the three-level system has different polarization than in the two-level system described further above. As is illustrated in Fig. 1(b), the biexciton state has the energy $\hbar\omega_B = 2\hbar\omega_X - \Delta_B$, where Δ_B is the biexciton binding energy. The dipole matrix elements are nonvanishing only for the ground-state-to-exciton transition and the exciton-to-biexciton transition and are given by

$$M_{0X} = M_{XB} = \tfrac{1}{2} f(t) e^{i\omega_L t}, \quad M_{X0} = M_{BX} = M_{0X}^{*}. \qquad (6)$$

Here, we have assumed both dipole elements to be equal as it is approximately justified in the limit of small quantum dots with a strong confinement [38,39].

Let us now focus on the coupling of the QD to the phonon environment. We model the electron-phonon interaction by a pure-dephasing Hamiltonian as it is commonly done for strongly confined quantum dots [40]. Together with the free phonon Hamiltonian it has the form

$$H_{\text{dot-ph}} = \sum_{\mathbf{q}} \hbar\omega_{\mathbf{q}} b_{\mathbf{q}}^{\dagger} b_{\mathbf{q}} + \sum_{\mathbf{q}\nu} \hbar n_{\nu} (\gamma_{\mathbf{q}} b_{\mathbf{q}} + \gamma_{\mathbf{q}}^{*} b_{\mathbf{q}}^{\dagger}) |\nu\rangle\langle\nu|. \qquad (7)$$

The operators $b_{\mathbf{q}}^{\dagger}$ ($b_{\mathbf{q}}$) create (annihilate) a phonon with wave vector $\mathbf{q}$ and linear dispersion $\hbar\omega_{\mathbf{q}} = \hbar c_s |\mathbf{q}|$, where c_s denotes the longitudinal sound velocity. n_{ν} counts the number of excitons present in the state $|\nu\rangle$. The coupling constants $\gamma_{\mathbf{q}}$ are chosen specific for the deformation potential coupling to longitudinal acoustic phonons, which has been shown to be dominant for typical self-assembled GaAs QDs [17,41]. As described in more detail in Ref. [41], the coupling constants $\gamma_{\mathbf{q}}$ depend on the electronic wave functions $\Psi_{e(h)}$ as well as on the deformation potential constants $D_{e(h)}$ for electrons (e) and holes (h), respectively. For simplicity, we assume the wave functions to be the ground-state solutions of a spherically symmetric harmonic potential, i.e., $\Psi_{e(h)}(\mathbf{r}) \propto \exp[-r^2/(2a_{e(h)}^2)]$, and refer to a_e as the QD radius. The characteristics of the exciton-phonon coupling can be expressed by the spectral density $J(\omega) = \sum_{\mathbf{q}} |\gamma_{\mathbf{q}}|^2 \delta(\omega - \omega_{\mathbf{q}})$, which under the above assumptions reads as [41]

$$J(\omega) = \frac{\omega^3}{4\pi^2 \rho \hbar c_s^5} [D_e e^{-\omega^2 a_e^2/(4c_s^2)} - D_h e^{-\omega^2 a_h^2/(4c_s^2)}]^2 \qquad (8)$$

with ρ being the mass density. For our present calculations, we use material parameters specific for GaAs taken from the literature [42] $\rho = 5370$ kg/m^3, $c_s = 5110$ m/s, $D_e = 7.0$ eV, and $D_h = -3.5$ eV. The QD radius is assumed to be $a_e = 3$ nm roughly corresponding to a diameter of the QD that is on the order of the typical layer thickness of GaAs-based quantum dots. The effective phonon coupling

strength is mostly determined by the QD extension in the direction of the strongest confinement. We set $a_e/a_h = 1.15$ assuming equal potentials but taking into account the different effective masses of electrons and holes for GaAs. The spectral density for these parameters is shown in Fig. 1(c) where it can be seen that $J(\omega)$ exposes a clear maximum at $\hbar\omega = E_J^{\max} \approx 2$ meV. Despite the fact that self-assembled quantum dots often have a shape that is closer to a disk than a sphere, a very good agreement with spherical models was found in recent experiments [32,43]. This is due to the fact that the important characteristics of the spectral density do not strongly depend on the dot geometry [44].

The electron-phonon interaction leads to a polaron shift δ_{ph} of the exciton and biexciton energy, such that when driving the exciton-to-ground-state transition the resonant excitation is on the shifted exciton energy $\hbar\tilde{\omega}_X = \hbar\omega_X - \delta_{ph}$. In this paper, we are mostly interested in detuned excitations and define the detuning as the difference between the laser energy and the polaron-shifted exciton energy, i.e.,

$$\Delta = \hbar\omega_L - \hbar\tilde{\omega}_X.$$

To study the time evolution of the electronic QD occupations under excitation with the laser field, we employ an implementation of a real-time path-integral approach [45]. This method allows a numerically exact treatment of the above model despite the infinite number of LA phonon modes and yields the dynamics of the reduced electronic density matrix of the QD including arbitrary multiphonon processes and taking into account all non-Markovian effects. We assume the QD to be initially in a product state of the electronic ground state and a thermal equilibrium of the phonon modes at temperature $T = 1$ K.

III. RESULTS

We start by analyzing the phonon-induced relaxation using continuous excitation that is switched on instantaneously. Then, we will apply short pulses with different pulse shapes to analyze the influence of the adiabaticity of the dressing and undressing process in view of high-fidelity state preparation. For this analysis we will also visualize the system trajectory on the Bloch sphere. Finally, we will demonstrate the selective addressing of all three states in the exciton-biexciton system using the phonon-assisted state preparation protocol.

A. Phonon-induced relaxation

The phonon-induced relaxation can be best analyzed by considering a continuous excitation of the QD with a constant field strength. Further, the laser field shall be circularly polarized such that our model can be restricted to two electronic levels, as we explained in the previous section. Generally, for a weak coupling between the electronic states and the phonon environment the standard expectation for the driven QD dynamics is that the Markovian approximation is well justified and that in the long-time limit the relaxation leads to a thermal occupation of the dot-photon dressed states [34,46] [cf. Eq. (3)]. In a very good approximation, this has been shown to hold also true for the two-level model of the QD with standard GaAs-type parameters considered here [27].

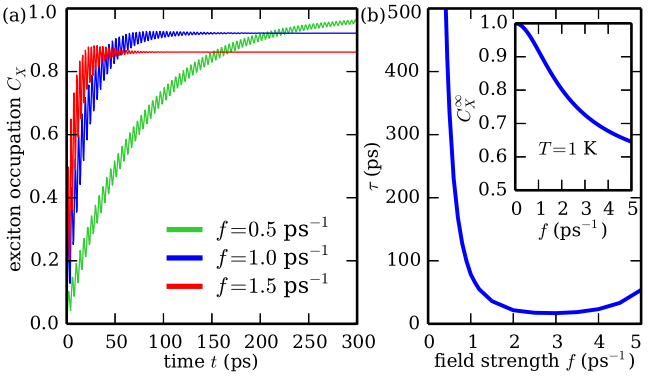

FIG. 2. (a) Exciton occupation C_X as a function of time for different field strengths $f = 0.5$ ps^{-1}, 1.0 ps^{-1}, and 1.5 ps^{-1}. (b) Time τ after which the time average of the oscillations of C_X has reached 99% of C_X^∞ (see text) as a function of the field strength f. Inset of (b): C_X^∞ as a function of the field strength f. The detuning is $\Delta = 1.0$ meV.

For very low temperatures, the system ends up mainly in the lower dressed state $|\psi_{\text{low}}\rangle$, which corresponds to an exciton occupation of

$$C_X^\infty \approx \cos^2(\Theta) = \frac{1}{2}\left(1 + \frac{\Delta}{\sqrt{\hbar^2 f^2 + \Delta^2}}\right). \tag{9}$$

Figure 2(a) shows the simulated temporal evolution of the exciton state under constant excitation for a detuning of $\Delta = 1.0$ meV and three different field strengths f. Here, the laser field is switched on instantaneously at $t = 0$ ps. The occupations perform damped Rabi oscillations around a mean value that approaches a constant value. For a decreasing field strength, the stationary exciton occupation rises as can also be seen in the inset of Fig. 2(b) where C_X^∞ given by Eq. (9) is shown as a function of f for $\Delta = 1.0$ meV. Most importantly for phonon-assisted exciton preparation, the stationary exciton occupation is very close to one and only limited by the finite temperature for sufficiently small field strengths. Larger values of f, however, strongly reduce C_X^∞.

On the other hand, when we look at the time required to reach the final state, we find that for small field strengths f, the time to reach the final state becomes longer. This is quantified in Fig. 2(b), where we have plotted the time τ it takes for the mean value of the oscillations to reach 99% of the exciton occupation expected for a thermal distribution of the dot-photon dressed states C_X^∞ as a function of the field strength. For example, at $f = 0.5$ ps^{-1} a relaxation time of several hundred ps is required, which might exceed the time until other relaxation processes occurring on longer time scales than the phonon-induced relaxation, such as the radiative decay, which is not considered here, come into play. Therefore, such a low driving strength does not yield a sufficiently fast relaxation for phonon-assisted state preparation. Indeed, we find that for $f \to 0$ the time needed for the state preparation diverges.

To understand the varying relaxation times for different driving strengths, one has to keep in mind that the pure dephasing type phonon coupling does not induce direct transitions between the electronic states, but the phonon-induced relaxation is only enabled by the laser field. Transitions

between the QD states only take place due to a nonvanishing overlap of both of the photon dressed states with the exciton state, which in turn is coupled to the phonon environment. For an efficient relaxation also the Rabi splitting Ω, i.e., the difference between the two dressed-state energies, needs to be close to typical phonon energies and ideally matches the maximum of the spectral density of the phonon coupling $J(\omega)$ [cf. Eq. (8)]. Both of these properties of the relaxation rate are also captured by a simple application of Fermi's golden rule, which yields a relaxation time between the upper dressed state without phonons and the lower dressed state with one phonon of

$$\tau_{\text{relax}} = \left(\frac{\pi}{2} \sin^2(2\Theta)\, J(\Omega) \right)^{-1}. \tag{10}$$

Here, it can be seen that the mixing angle Θ as well as the spectral density evaluated at the Rabi splitting $J(\Omega)$ enter the relaxation rate. According to the simulations, the maximal relaxation for the detuning $\Delta = 1.0$ meV used here occurs for a field strength around 2.7 ps^{-1}, which is reflected by the position of the minimum of the time needed for an almost complete relaxation plotted in Fig. 2(b). In a good approximation, this is expected from the rough estimation in Eq. (10). Despite the short relaxation time at the optimal field strength, which is below 20 ps, such a strong driving field is not applicable for high-fidelity state preparation either because the achieved final occupation of below 0.8 is too far from the desired fidelity of one.

Looking at our results, it becomes clear that the maximum exciton occupation for a given detuning can only be realized for almost vanishing field strengths where, on the other hand, it takes arbitrarily long times to complete the relaxation process. Therefore, we conclude that when only the phonon relaxation process of the preparation takes place, there is a tradeoff between reaching the targeted state with high fidelity and realizing fast preparation times, which implies that the phonon-assisted state preparation on a short time scale can not be explained solely by the phonon-induced relaxation.

B. Dressing and undressing

In the previous section, the switch-on of the laser field has been taken to be instantaneous. This implies that a sudden transformation of the photon-dressed states occurs at the beginning of the pulse. Similarly, when switching off the laser field the photon dressed states are transformed back to the pure ground and exciton states. To understand the importance of these *dressing* and *undressing* processes in terms of fast and high-fidelity phonon-assisted state preparation, we now look at excitations with different pulse shapes. First, we compare an excitation of the two-level system with rectangular and Gaussian pulses. Later, we approximate the Gaussian pulse using a rectangular pulse with softened edges. Choosing these different pulse shapes allows us to systematically make a distinction between the effects of the pure relaxation process and the influence of the dressing and undressing processes on the QD occupations.

Figure 3 shows the temporal evolution under excitation for the rectangular (left) and Gaussian (right) pulses including (a), (b) the exciton occupation; (c), (d) the lower dressed-state occupation; (e), (f) the instantaneous dressed-state energies; and (g), (h) the pulse envelopes of the electric field. The length of the rectangular pulses is chosen as 40 ps, which is twice the full width of half-maximum (FWHM) of the Gaussian pulses, which is set to 20 ps. The pulse length has been chosen similar to what is realized in state-of-the-art experiments exploiting coherent QD excitation to produce indistinguishable single photons and photon pairs [11,20].

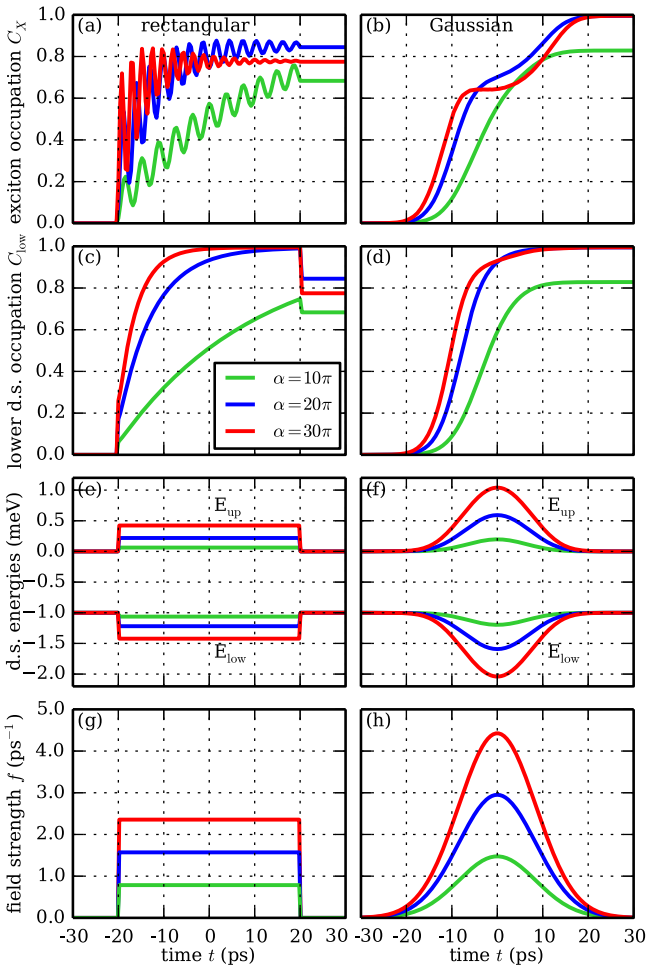

FIG. 3. Dynamics for an off-resonant excitation of the QD with rectangular pulses (left) having a length of 40 ps and Gaussian pulses (right) with a FWHM of 20 ps. The pulse areas are $\alpha = 10\pi$ (green), 20π (blue), and 30π (red). (a), (b) Exciton occupation C_X; (c), (d) occupation of the energetically lower dressed state C_{low}; (e), (f) instantaneous energy of the upper and lower dressed state $E_{\text{up/low}}$; (g), (h) pulse envelopes. The detuning is $\Delta = 1$ meV.

All calculations are performed for a detuning of $\Delta = 1.0$ meV and for three different pulse areas $\alpha = \int_{-\infty}^{\infty} f(t)dt$ with $\alpha = 10\pi$ (green curves), 20π (blue curves), and 30π (red curves).

Let us start with the rectangular pulse (left panels in Fig. 3). The laser pulse sets in instantaneously at $t = -20$ ps and aside from damped Rabi oscillations, there is an overall increase of the exciton occupation that depends on the strength of the pulse [Fig. 3(a) and see also Fig. 2(a)]. In the dressed-state picture, this behavior can be understood as follows: When there is no laser pulse, the dressed states are equal to the

bare states where for a positive detuning the ground state corresponds to the upper dressed state E_{up} and the exciton state corresponds to the lower dressed state E_{low}. Note that in this picture the energies of the photons needed for the excitation are counted as part of the dressed-state energies. As soon as the laser pulse sets in, the dressed states become a mixture of ground and exciton states [cf. Eq. (3)] with shifted energies shown in Fig. 3(e), i.e., the bare QD states become dressed by the laser field. Due to their overlap with the ground state, both dressed states instantly become occupied, which is reflected by Rabi oscillations in the bare states [29]. Phonons induce transitions between the dressed states [12,21] and at low temperatures, transitions to the lower dressed state, that correspond to phonon emission, outweigh. Therefore, during the pulse the lower dressed state becomes more and more occupied as it can be seen in Fig. 3(c). This also means that the exciton occupation successively approaches its stationary value C_X^{∞}, which depends on the exciton contribution to the lower dressed state but is above 0.5 for all field strengths and positive detunings [cf. Eq. (9)]. When the laser pulse is switched off at $t = 40$ ps, the exciton occupation [Fig. 3(a)] keeps the value it has right before the switch-off. At the same time, the dressed states are abruptly transformed back to the bare QD states due to the sudden stop of the rectangular pulse, which means that the undressing takes place instantaneously. This is reflected by a steplike drop of the occupation of the lower dressed state that can be seen in Fig. 3(c). For the weakest pulse ($\alpha = 10\pi$), the final state is not reached within the time window of 40 ps, while for the higher pulse areas, the relaxation process is mostly completed. Either way, the final exciton occupation stays below 0.9 for all of the three rectangular pulses and, in fact, no matter which rectangular shape is assumed for pulse lengths of a few tens of ps, one never achieves a final value close to one due to the tradeoff situation described in the previous section.

The situation is quite different for the Gaussian pulses shown in the right column of Fig. 3. In this case, no oscillations of the exciton occupation are visible and instead C_X smoothly rises to its final value that for pulse areas $\alpha = 20\pi$ and 30π is considerably higher than for the rectangular pulses and practically reaches 1.0 as it can be seen in Fig. 3(b). Like for the rectangular pulses, a phonon relaxation process takes place from the upper to the lower dressed state yielding a steady increase of the occupation of the lower dressed state in Fig. 3(d). However, because the field strength for Gaussian pulses is time dependent, the bare QD state contributions of the dressed states change during the pulse. This is also reflected by the time dependence of the dressed-state energies shown in Fig. 3(f), which can be used to extract the Rabi splitting at a given time. For the weakest Gaussian pulse shown here ($\alpha = 10\pi$), and similar to the case of the weakest rectangular pulse, the phonon-induced relaxation is too weak to complete the relaxation process within the duration of the pulse. This is because the Rabi splitting is well below the maximum of the phonon density at energy $E_J^{\max} \approx 2$ meV [cf. Fig. 1(c)] even at the maximum of the pulse where the Rabi splitting reaches its maximum value of approximately 1.4 meV [cf. Fig. 3(f)]. In contrast, for the higher pulse areas $\alpha = 20\pi$ and 30π, the relaxation is more effective and leads to a full occupation of the lower dressed state. At the pulse maximum, the Rabi splitting for the 30π pulse already becomes larger (3.0 meV) than $E_J^{\max}$ temporarily leading to a weakening of the relaxation which is visible by a reduced gain of the lower dressed-state occupation [red curve in Fig. 3(d)] around $t = 0$ ps. Most interestingly, the phonon-induced relaxation is practically complete around $t = 10$ ps while the exciton occupation obtained by the stronger pulses is still far from its final value and therefore the remaining increase of C_X cannot be attributed to the relaxation. The final value of C_X is only reached within a second phase of increase that takes place while the pulse is switched off. This is only possible because during the switch-off the dressed states are *adiabatically undressed*, i.e., adiabatically transformed back to the bare QD states. In this process, the ground-state component of the then almost fully occupied lower dressed state is reduced to zero which yields a drastic increase of the exciton occupation. Importantly, a necessary precondition for this increase is that the undressing takes place slow enough such that the system can follow the transformation of the dressed states adiabatically and the occupation stays in the lower dressed state. This is the case if the field strength changes slowly on the time scale of the effective Rabi frequency. A similar precondition [47] is necessary when using adiabatic rapid passage protocols that also rely on an adiabatic transformation between dressed states. On the other hand, the precondition is not fulfilled for the instantaneous undressing in case of the rectangular pulses discussed earlier where the lower dressed-state occupation experiences a steplike drop at the end of the pulse [Fig. 3(c)] that does not occur for Gaussian pulses [Fig. 3(d)].

As it turns out, the adiabatic undressing towards the end of the pulse is in fact essential for a successful *fast* exciton preparation. The absence of the adiabatic ending prevents the phonon-assisted state preparation protocol from working with high fidelity for short rectangular pulses and any other pulse shapes with too fast switch-off times.

Having seen that aside from the phonon-induced relaxation the temporal evolution of the dressing and undressing also plays a crucial role, we investigate in more detail the role of the switch-on and switch-off phases. To this end, we choose a special pulse shape that is designed to highlight the important role of these two processes on the preparation process. The thermalization of the dressed states is obviously achieved best by a constant part of the pulse that is chosen such that the coupling to the phonon environment is maximal ($f = 2.7\,\mathrm{ps}^{-1}$ for the parameters chosen here) and that is sufficiently long to complete the thermalization. In our case, the duration of this part of constant driving is chosen to be 40 ps. In order to systematically study the influences of the switch-on (switch-off) characteristics we add the left (right) half of a Gaussian pulse with FWHM τ_{on} (τ_{off}) before (after) the constant part of the pulse envelope as illustrated in Fig. 4(e) [(f)]. Here, we compare a strictly rectangular pulse with $\tau_{\mathrm{on/off}} = 0$ ps (green) with pulses of different switch-on/-off times $\tau_{\mathrm{on/off}} = 1$ ps (black), 3 ps (blue), and 5 ps (red). The first row [Figs. 4(a) and 4(b)] shows the corresponding evolution of C_X, while the lower dressed-state occupation is plotted in the second row [Figs. 4(c) and 4(d)] and the pulse envelopes are shown in the third row [Figs. 4(e) and 4(f)].

Looking at the left panels of Fig. 4, we find that a longer switch-on time does not alter the resulting exciton occupation

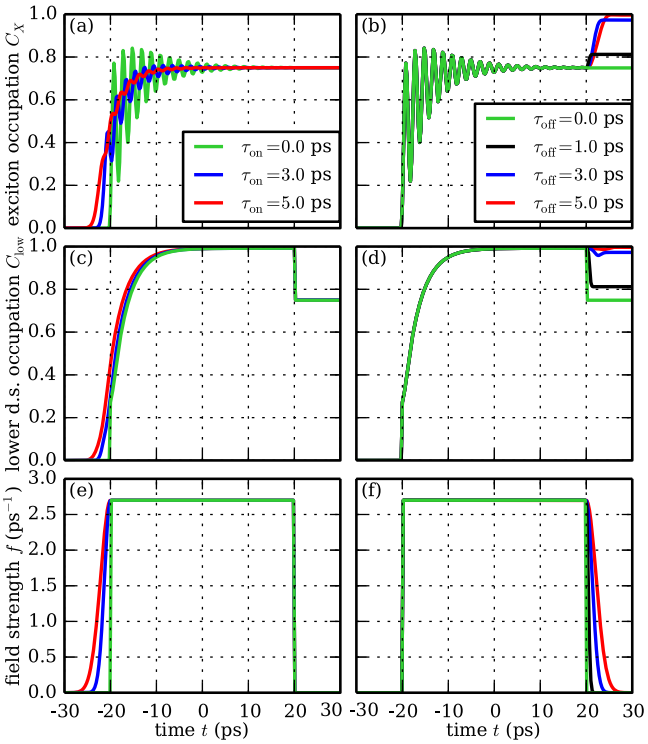

FIG. 4. Time-dependent exciton occupation C_X under pulsed excitation detuned by $\Delta = 1.0$ meV for different (a) switch-on (b) and switch-off times (see key). (c), (d) Corresponding occupations of the energetically lower dressed state C_{low} and (e), (f) corresponding pulse envelopes.

after the pulse, which is about 0.75 for all three cases. However, we find a significant reduction of the Rabi oscillations, which almost disappear for $\tau_{on} = 5$ ps. The insensitivity of the final occupation with respect to the switch-on dynamics is related to the irreversible nature of the relaxation process which, in case of a complete relaxation, leads to a complete loss of memory of the initial state. We thus find that the first phase, i.e., the dressing, is necessary to start the relaxation process, but for a sufficiently long relaxation phase the details of the switch-on are irrelevant for the final fidelity.

In contrast, as demonstrated in the right panels of Fig. 4, a slower switch-off gives rise to a further gain of exciton occupation when the field strength is reduced to zero. This effect is considerably less pronounced if the switch-off time becomes too short and does not occur at all if the pulse stops instantaneously. For example, for $\tau_{off} = 5$ ps (red curve) C_X increases by more than 0.2 during the switch-off, while for $\tau_{off} = 1$ ps (black) the increase is below 0.05. Thus, to yield a high-fidelity state preparation the transformation of the dressed states into the bare QD states needs to happen slow enough such that an adiabatic evolution takes place, i.e., the undressing needs to be adiabatic.

To sum up, for an efficient and fast phonon-assisted state preparation there are basically two features of the pulse envelope that are significant: First, there has to be a phase of the pulse where the QD thermalizes in the dressed-state basis, which must be long enough to complete the relaxation. This phase can be chosen the shorter the stronger the phonon-induced relaxation is and therefore can be minimized when the field strength is such that the strength of the phonon coupling is maximal. Therefore, in this phase a constant field strength corresponding to the maximal relaxation rate is optimal to achieve a complete thermalization with a minimal pulse length. Second, the pulse must be switched off slowly enough to allow for an adiabatic undressing of the QD states.

Although a Gaussian pulse shape does not meet these requirements in an optimal fashion it still works surprisingly well, mostly because the optimum for the ideal field strength at which the dressed-state relaxation is maximal is not a sharp maximum, but rather a broad peak as it can be seen from Fig. 1. Therefore, even though a Gaussian pulse does not have a constant plateau, a sufficient relaxation takes place during most of the time of the pulse provided a reasonable value of the pulse area is chosen. Most importantly, deviations from the Gaussian pulse shape that go towards faster switch-off times, as they might be induced by a pulse-shaping setup, can be harmful to the efficiency of the phonon-assisted preparation protocol.

C. Interpretation on the Bloch sphere

Another interesting aspect not highlighted so far is that the incoherent phonon scattering can result in a pure state, which even can be transformed to a bare QD state. This is best illustrated using the Bloch vector picture [48]. In this picture, the projection of the Bloch vector on the z axis represents the inversion, i.e., the difference between the occupations of the upper and the lower levels of the two-level system, while the in-plane component reflects the polarization. Resonant lossless driving of a two-level system is reflected by the Bloch vector moving at the surface of the Bloch sphere taking the shortest path from one pole to the other corresponding to the well-known coherent Rabi oscillations. Preparing the exciton state using a π pulse then means going from the lower pole corresponding to the ground level to the upper pole corresponding to the excited level. A detuned excitation leads to a tilted oscillation, which starting from the lower pole does not reach the upper pole. If the system is fully coherent, the Bloch vector stays on the surface, i.e., its length is constantly one. If decoherence takes place, the length of the Bloch vector is decreased. Clearly, the phonon-assisted preparation involves an incoherent phonon-induced relaxation, but as we have seen it can still eventually lead to an almost perfect exciton state.

To analyze this in more detail, we have calculated the trajectory of the Bloch vector of the driven QD system, which is shown in Figs. 5(a) and 5(b) alongside the time evolution of the length of the Bloch vector presented in Figs. 5(c) and 5(d) for an excitation with Gaussian pulses (left panel) and for rectangular pulses with softened switch-on or switch-off (right panel). The corresponding pulse shapes can be seen in Figs. 3(h) and 4(e) and 4(f).

Let us first look at the Gaussian pulses in the left column. When the pulse is switched on, the Bloch vector leaves the surface of the sphere for all pulse areas in Fig. 5(a) [$\alpha = 10\pi$ (green), $\alpha = 20\pi$ (blue), and $\alpha = 30\pi$ (red)]. The corresponding vector length shown in Fig. 5(c) decreases as it is expected as the result of the pure-dephasing phonon coupling. Indeed, the loss of coherence turns out to be as

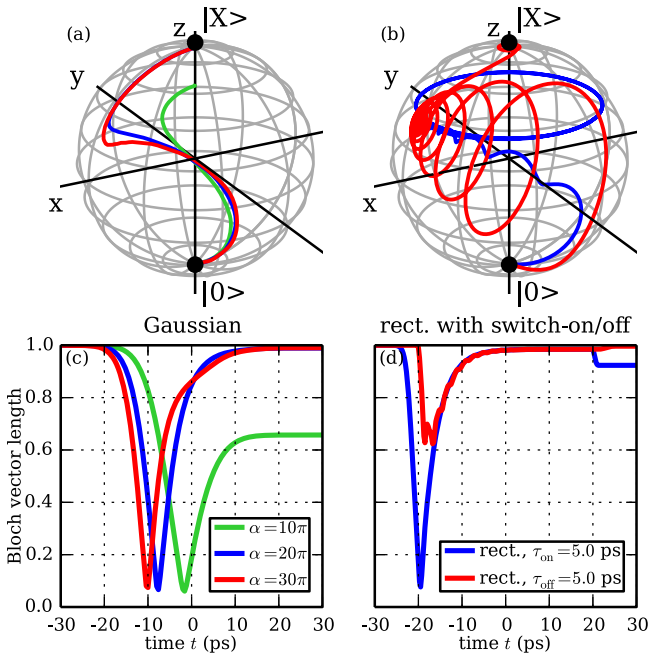

FIG. 5. (a), (b) Illustration of the system trajectory on the Bloch sphere and (c), (d) length of the Bloch vector as a function of time for (a), (c) a Gaussian excitation with pulse areas $\alpha = 10\pi$ (green), 20π (blue), and 30π (red) and (b), (d) a rectangular excitation with different switch-on/-off times $\tau_{on} = 5$ ps; $\tau_{off} = 0$ ps (blue) and $\tau_{on} = 0$ ps; $\tau_{off} = 5$ ps (red). The detuning is $\Delta = 1$ meV.

high as 95%. The time to reach the minimal Bloch vector length depends on the pulse area and is shorter for the stronger pulses where the relaxation is more efficient. The vector length would vanish at the minimum in the ideal case of a completely adiabatic dressing process and provided that the phonons realize a fully incoherent occupation transfer between the dressed states. In that case, the electronic density matrix would stay diagonal in the dressed-state basis all the time and coherences between the dressed states would neither build up due to the laser driving nor due to the phonons. The continuous occupation transfer from the upper to the lower dressed state would then necessarily lead to a zero of the Bloch vector length at some point in time. In our case, however, the minimal Bloch vector length has a small but finite value because the Gaussian pulses used in the simulations already induce some small coherences between the dressed states (not shown). Subsequently, the coherence between $|0\rangle$ and $|X\rangle$ is restored to a large degree and the Bloch vector length approaches 1 for the two stronger pulses as the phonon-assisted transitions result in an almost complete occupation of the lower dressed state which is again a pure state lying on the surface of the Bloch sphere. For the weaker pulse $\alpha = 10\pi$ (green), the trajectory ends inside the Bloch sphere and the vector length stays well below 0.5 because due to the insufficient pulse strength, the relaxation does not complete. For the stronger pulses, the dressed states transform from a superposition of ground and exciton states into the pure exciton state during the adiabatic undressing, which corresponds to a motion of the Bloch vector on the surface towards the upper pole. It thus becomes obvious that the laser-driven QD evolution describes a way *through* the Bloch sphere to the upper pole, which is very different to the motion along the surface in the case of an inversion yielded by applying a resonant π pulse.

A similar analysis can be done for the Bloch vector trajectory for rectangular pulses where the switch-on or the switch-off edge is softened. The red curve in Figs. 5(b) and 5(d) has a sharp switch-on and a smooth switch-off with $\tau_{off} = 5$ ps, while the blue curve corresponds to a smooth switch-on with $\tau_{on} = 5$ ps and a sharp switch-off. When the switch-on is instantaneous (red curve), we see that the Bloch vector trajectory exhibits a spiral movement within the Bloch sphere reflecting the damped Rabi oscillations. In agreement with the essentially complete relaxation, the spiral ends up on a point close to the surface of the Bloch sphere. For $\tau_{on} = 5$ ps (blue curve), the oscillations are less pronounced and the motion goes roughly along the axis of the spiral movement. The spiraling will eventually vanish for even larger values of τ_{on}, but the end point after the relaxation will be the same. If the laser pulse is switched off rapidly (blue curve), the z component of the Bloch vector stays constant after the end of the pulse and performs a circular motion. In contrast, for $\tau_{off} = 5$ ps, an adiabatic undressing takes place during the switch-off and the Bloch vector approaches the upper pole.

D. Selective state preparation in the exciton-biexciton system

The clear understanding of the different phases of the phonon-assisted relaxation mechanism worked out so far turns out to be highly valuable to predict in an easy way the QD state that can be obtained by pulsed off-resonant excitation for arbitrary initial states and also for the exciton-biexciton system illustrated in Fig. 1(b). To this end, it is required as before that during the switch-off phase of the pulse the system evolves adiabatically. When the pulse duration is sufficiently long such that the relaxation all the way to the lowest dressed state is fully completed, the prepared state at the end of the pulse is determined exclusively by the energetic order of the dressed states in the limit of vanishing pulse strength. Recalling that the dressed states are defined with respect to the rotating frame, the prepared state can technically be determined by subtracting from the energies of the QD states without light coupling the energy of the corresponding number of photons needed for reaching that state and looking at the resulting order of the states. More specifically, zero photons have to be subtracted for the ground state, one photon for an exciton state and two photons for the biexciton state. The resulting state lowest in energy will be occupied predominantly at the end of the preparation process.

For example, in the two-level system, subtracting the laser energy from the laser-free QD state energies yields dressed-state energies that are in the limit of vanishing field strength separated by the detuning between the laser and the polaron-shifted QD transition. For a positive detuning, the energy of the excitonlike dressed state will be below the corresponding ground-state-like dressed-state energy in the rotating frame and, consequently, the phonon-assisted preparation protocol with adiabatic undressing prepares the exciton state. On the other hand, a negative detuning reverses the order of the dressed-state energies and at low temperatures where

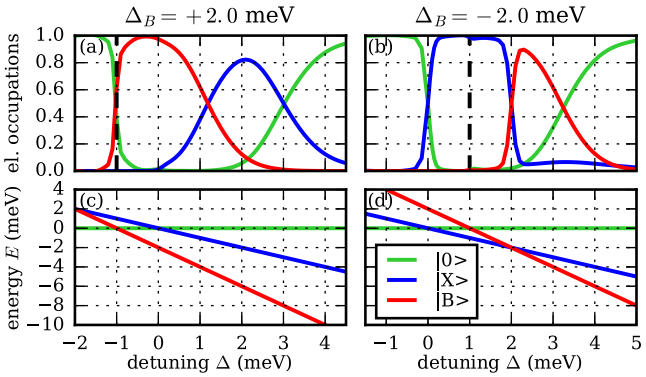

FIG. 6. Occupations of the electronic levels $|0\rangle$ (green), $|X\rangle$ (blue), and $|B\rangle$ (red) after optically exciting the exciton-biexciton system with a Gaussian pulse of pulse area $\alpha = 20\pi$ and FWHM = 20 ps as a function of the detuning Δ for a (a) positive biexciton binding energy $\Delta_B = 2.0$ meV and (b) negative biexciton binding energy $\Delta_B = -2.0$ meV. The black dashed lines indicate the two-photon resonance between $|0\rangle$ and $|B\rangle$. (c), (d) Corresponding energies of the QD states in the rotating frame.

there is mostly phonon emission the protocol prepares the QD ground state independent of the initial state [30].

In the case of an exciton-biexciton system subtracting the energy of the corresponding photons gives the energies of the QD states in the frame rotating with the laser frequency as $E'_0 = 0$, $E'_X = -\Delta$, $E'_B = -\Delta_B - 2\Delta$. Thus, the energetic ordering depends also on the biexciton binding energy and we will consider both cases with positive and negative biexciton binding energies, which can both be realized depending on the QD geometry [49]. In the following, we will refer to the dressed state that in the limit of vanishing field strength transforms into the $|0\rangle$ [$|X\rangle$, $|B\rangle$] state as $|0'\rangle$ [$|X'\rangle$, $|B'\rangle$].

Let us first discuss the most commonly encountered situation of a QD with a positive biexciton binding energy $\Delta_B = 2$ meV. Figure 6(a) shows the final occupation after excitation with a detuned Gaussian pulse with a FWHM of 20 ps and a pulse area of $\alpha = 20\pi$ as a function of the detuning, while Fig. 6(c) shows the corresponding energies in the rotating frame. It can be seen that for detunings below the two-photon resonance (indicated by the black dashed line), i.e., $\Delta < -\Delta_B/2 = -1$ meV, the occupation remains in the ground state (green curve). This is consistent with the energetic order of the states since E'_0 is the lowest energy in this parameter region. At $\Delta = -1$ meV the energetic order of the dressed states changes because for detunings above the two-photon resonance, E'_B is the lowest energy. This leads to a significant drop of the final ground-state occupation in favor of the biexciton occupation (red curve), which approaches its maximum close to one at $\Delta \approx -0.5$ meV. At the one-photon resonance at $\Delta = 0$, the energetic order changes once again and for all positive detunings $|0'\rangle$ is the highest-energy dressed state, while E'_B remains being the lowest energy. For sufficiently long pulses, all the occupation would, of course, end up in the lowest branch resulting in the preparation of the biexciton. However, for $\Delta > 1$ meV, the energetic splitting $E'_X - E'_B > 3$ meV exceeds the maximum of the phonon spectral density $E_J^{\max}$ lying around 2 meV by far, which results in a very inefficient relaxation to the $|B'\rangle$ state, which is not completed in the time window set by the pulse length. Therefore, instead, we observe a gain of the exciton occupation (blue curve) as soon as E'_X crosses E'_0. The maximal exciton occupation of about 0.8 is reached around $\Delta = 2$ meV, where the energy splitting $E'_0 - E'_X = 2$ meV agrees with $E_J^{\max}$. Therefore, it turns out that for a system with more than two states like the one considered here, an incomplete relaxation can also be advantageous for preparation purposes if a preparation of a QD state that in the rotating frame is not the lowest-lying state, like in our case the exciton, is intended. An even higher exciton occupation is possible for a larger biexciton binding energy which favors transitions to $|X'\rangle$ because the coupling to the lowest dressed state $|B'\rangle$ in this case gets even more out of resonance. It also follows that whether the prepared state is the exciton or the biexciton can in principle be selected by suitably adjusting the pulse length for all positive detunings because the final state depends on whether the relaxation completes during the pulse or whether the intermediate level corresponding to the exciton is still predominantly occupied when the pulse is switched off. Detunings higher than 2.0 meV lead to a decrease of both the final exciton and the biexciton occupations because the phonon-induced relaxation becomes weaker and weaker as the phonon environment becomes more and more out of resonance. Finally, for very large detunings above $\Delta = 4.0$ meV the energetic splittings between the dressed states are so large that for the given pulse length practically no relaxation takes place and the QD remains in the ground state.

The case of a negative biexciton binding energy of $\Delta_B = -2$ meV is shown in the right column. Figure 6(b) shows the final occupations and the corresponding energies are plotted in Fig. 6(d). Similar to the case of positive biexciton binding energies, the system remains in the ground state up to a detuning of 0 since E'_0 is the lowest energy. Between $\Delta = 0$ and 2 meV, $|X'\rangle$ is the dressed state with the lowest energy. This energetic order appears exclusively for negative biexciton binding energies, resulting in a broad region where a complete preparation of the exciton occurs. This finding is somewhat surprising because the two-photon biexciton resonance at $\Delta = 1$ meV also lies within this interval and driving the QD in the vicinity of the resonance one might expect the preparation of the biexciton, instead of an efficient preparation of the exciton state, but the results can easily be understood in the context described here. At $\Delta = 2$ meV, the energetically lowest state changes a second time and notably a sharp transition of the prepared state from the exciton to the biexciton occurs within a small detuning interval. However, for $\Delta > 2.5$ meV, the energy splittings between the dressed states that are connected to the excitonic states and $|0'\rangle$ already become too large for a complete thermalization to take place during the length of the pulse. This leads to a significant reduction of the biexciton occupation for higher detunings, and above $\Delta = 5$ meV the QD does not get affected by the pulse anymore staying in the ground state. Importantly, also in the case of a negative biexciton binding energy the targeted state can be derived from the energetic order shown in Fig. 6(d), demonstrating the correctness of the description found for the dynamics of the phonon-induced preparation process also in the case of the exciton-biexciton system.

As we have seen, to selectively address a state in an exciton-biexciton system by phonon-assisted state preparation, the biexciton binding energy needs to be considered carefully, while the detuning Δ and the pulse length can act as control parameters to choose the targeted state. Interestingly, the QD state that gets selected when driving close to the two-photon resonance strongly depends on the sign of the biexciton binding energy.

IV. CONCLUSIONS

We have analyzed the dynamics of an optically driven semiconductor QD coupled to longitudinal acoustic phonons for different off-resonant excitation conditions focusing on two main questions: (a) What are the requirements for a fast state preparation using off-resonant driving, and (b) how is the prepared state selected? We demonstrated that a fast high-fidelity preparation process not only relies on the previously discussed efficient phonon-induced relaxation between the dot-photon dressed states, but also on a successful adiabatic undressing of the states, which also turned out to be important to answer both questions. To separate the influence of the adiabatic undressing from that of the relaxation we compared the exciton occupations produced by Gaussian and rectangular pulse shapes and systematically studied the influence of the switch-on and switch-off times. This analysis revealed that while the switch-on time plays a subordinate role, it is crucial that the pulse is switched off slowly enough. Furthermore, we analyzed the coherence properties during the state preparation process and revealed that the incoherent phonon scattering can also restore coherence and the system trajectory takes a way through the Bloch sphere to the opposite pole. Finally, we showed that the concept of phonon-assisted state preparation by adiabatic undressing also applies to the exciton-biexciton system, where an easy prediction of the prepared state is possible. When the pulse is long enough to support a full relaxation, the prepared state is the one that is lowest in energy in the rotating frame in the limit of vanishing field strength. We demonstrated that even pulses too short for a full relaxation can be used for preparing intermediate states that are not the lowest in energy in the rotating frame. Altogether, it is demonstrated that in an exciton-biexciton system the decisive parameters for selecting the prepared state are the detuning, the biexciton binding energy, and the pulse length.

ACKNOWLEDGMENTS

A.M.B. and V.M.A. gratefully acknowledge the financial support from Deutsche Forschungsgemeinschaft via the Project No. AX 17/7-1. D.E.R. is thankful for financial support from the German Academic Exchange Service (DAAD) within the P.R.I.M.E. programme.

[1] D. Bouwmeester, A. K. Ekert, and A. Zeilinger, *The Physics of Quantum Information* (Springer, Berlin, 2000).
[2] E. Biolatti, R. C. Iotti, P. Zanardi, and F. Rossi, Phys. Rev. Lett. **85**, 5647 (2000).
[3] P. Chen, C. Piermarocchi, and L. J. Sham, Phys. Rev. Lett. **87**, 067401 (2001).
[4] X. Q. Li, Y. W. Wu, D. Steel, D. Gammon, T. H. Stievater, D. S. Katzer, D. Park, C. Piermarocchi, and L. J. Sham, Science **301**, 809 (2003).
[5] C. Piermarocchi, P. Chen, Y. S. Dale, and L. J. Sham, Phys. Rev. B **65**, 075307 (2002).
[6] S. J. Boyle, A. J. Ramsay, F. Bello, H. Y. Liu, M. Hopkinson, A. M. Fox, and M. S. Skolnick, Phys. Rev. B **78**, 075301 (2008).
[7] M. A. Nielsen and I. Chuang, *Quantum Computation and Quantum Information* (Cambridge University Press, England, 2000).
[8] E. Moreau, I. Robert, L. Manin, V. Thierry-Mieg, J. M. Gérard, and I. Abram, Phys. Rev. Lett. **87**, 183601 (2001).
[9] N. Akopian, N. H. Lindner, E. Poem, Y. Berlatzky, J. Avron, D. Gershoni, B. D. Gerardot, and P. M. Petroff, Phys. Rev. Lett. **96**, 130501 (2006).
[10] R. Stevenson, R. J. Young, P. Atkinson, K. Cooper, D. A. Ritchie, and A. J. Shields, Nature (London) **439**, 179 (2006).
[11] M. Müller, S. Bounouar, K. D. Jöns, M. Glässl, and P. Michler, Nat. Photonics **8**, 224 (2014).
[12] D. E. Reiter, T. Kuhn, M. Glässl, and V. M. Axt, J. Phys.: Condens. Matter **26**, 423203 (2014).
[13] A. J. Ramsay, Semicond. Sci. Technol. **25**, 103001 (2010).
[14] A. Zrenner, E. Beham, S. Stufler, F. Findeis, M. Bichler, and G. Abstreiter, Nature (London) **418**, 612 (2002).
[15] P. Machnikowski and L. Jacak, Phys. Rev. B **69**, 193302 (2004).
[16] A. Vagov, M. D. Croitoru, V. M. Axt, T. Kuhn, and F. M. Peeters, Phys. Rev. Lett. **98**, 227403 (2007).
[17] A. J. Ramsay, A. V. Gopal, E. M. Gauger, A. Nazir, B. W. Lovett, A. M. Fox, and M. S. Skolnick, Phys. Rev. Lett. **104**, 017402 (2010).
[18] E. R. Schmidgall, P. R. Eastham, and R. T. Phillips, Phys. Rev. B **81**, 195306 (2010).
[19] C. M. Simon, T. Belhadj, B. Chatel, T. Amand, P. Renucci, A. Lemaitre, O. Krebs, P. A. Dalgarno, R. J. Warburton, X. Marie, and B. Urbaszek, Phys. Rev. Lett. **106**, 166801 (2011).
[20] Y.-J. Wei, Y.-M. He, M.-C. Chen, Y.-N. Hu, Y. He, D. Wu, C. Schneider, M. Kamp, S. Höfling, C.-Y. Lu, and J.-W. Pan, Nano Lett. **14**, 6515 (2014).
[21] S. Lüker, K. Gawarecki, D. E. Reiter, A. Grodecka-Grad, V. M. Axt, P. Machnikowski, and T. Kuhn, Phys. Rev. B **85**, 121302 (2012).
[22] M. Glässl, A. M. Barth, K. Gawarecki, P. Machnikowski, M. D. Croitoru, S. Lüker, D. E. Reiter, T. Kuhn, and V. M. Axt, Phys. Rev. B **87**, 085303 (2013).
[23] K. Gawarecki, S. Lüker, D. E. Reiter, T. Kuhn, M. Glässl, V. M. Axt, A. Grodecka-Grad, and P. Machnikowski, Phys. Rev. B **86**, 235301 (2012).
[24] A. Debnath, C. Meier, B. Chatel, and T. Amand, Phys. Rev. B **86**, 161304 (2012).
[25] A. Debnath, C. Meier, B. Chatel, and T. Amand, Phys. Rev. B **88**, 201305 (2013).

[26] R. Mathew, E. Dilcher, A. Gamouras, A. Ramachandran, H. Y. S. Yang, S. Freisem, D. Deppe, and K. C. Hall, Phys. Rev. B **90**, 035316 (2014).
[27] M. Glässl, A. Vagov, S. Lüker, D. E. Reiter, M. D. Croitoru, P. Machnikowski, V. M. Axt, and T. Kuhn, Phys. Rev. B **84**, 195311 (2011).
[28] D. E. Reiter, S. Lüker, K. Gawarecki, A. Grodecka-Grad, P. Machnikowski, V. M. Axt, and T. Kuhn, Acta Phys. Pol. A **122**, 1065 (2012).
[29] S. Hughes and H. J. Carmichael, New J. Phys. **15**, 053039 (2013).
[30] M. Glässl, A. M. Barth, and V. M. Axt, Phys. Rev. Lett. **110**, 147401 (2013).
[31] P.-L. Ardelt, L. Hanschke, K. A. Fischer, K. Müller, A. Kleinkauf, M. Koller, A. Bechtold, T. Simmet, J. Wierzbowski, H. Riedl, G. Abstreiter, and J. J. Finley, Phys. Rev. B **90**, 241404 (2014).
[32] J. H. Quilter, A. J. Brash, F. Liu, M. Glässl, A. M. Barth, V. M. Axt, A. J. Ramsay, M. S. Skolnick, and A. M. Fox, Phys. Rev. Lett. **114**, 137401 (2015).
[33] S. Bounouar, M. Müller, A. M. Barth, M. Glässl, V. M. Axt, and P. Michler, Phys. Rev. B **91**, 161302 (2015).
[34] A. J. Leggett, S. Chakravarty, A. T. Dorsey, M. P. A. Fisher, A. Garg, and W. Zwerger, Rev. Mod. Phys. **59**, 1 (1987).
[35] H. Dekker, J. Phys. C: Solid State Phys. **20**, 3643 (1987).
[36] W. Langbein, P. Borri, U. Woggon, V. Stavarache, D. Reuter, and A. D. Wieck, Phys. Rev. B **69**, 161301 (2004).
[37] D. J. Tannor, *Introduction to Quantum Mechanics* (University Science Books, Sausalito, California, 2007).
[38] T. Takagahara, Phys. Rev. B **39**, 10206 (1989).
[39] G. Bacher, R. Weigand, J. Seufert, V. D. Kulakovskii, N. A. Gippius, A. Forchel, K. Leonardi, and D. Hommel, Phys. Rev. Lett. **83**, 4417 (1999).
[40] L. Besombes, K. Kheng, L. Marsal, and H. Mariette, Phys. Rev. B **63**, 155307 (2001).
[41] B. Krummheuer, V. M. Axt, and T. Kuhn, Phys. Rev. B **65**, 195313 (2002).
[42] B. Krummheuer, V. M. Axt, T. Kuhn, I. D'Amico, and F. Rossi, Phys. Rev. B **71**, 235329 (2005).
[43] A. J. Ramsay, T. M. Godden, S. J. Boyle, E. M. Gauger, A. Nazir, B. W. Lovett, A. M. Fox, and M. S. Skolnick, Phys. Rev. Lett. **105**, 177402 (2010).
[44] T. E. Hodgson, L. Viola, and I. D'Amico, Phys. Rev. B **78**, 165311 (2008).
[45] A. Vagov, M. D. Croitoru, M. Glässl, V. M. Axt, and T. Kuhn, Phys. Rev. B **83**, 094303 (2011).
[46] U. Weiss, *Quantum Dissipative Systems*, 2nd ed. (World Scientific, Singapore, 1999).
[47] J. S. Melinger, S. R. Gandhi, A. Hariharan, D. Goswami, and W. S. Warren, J. Chem. Phys. **101**, 6439 (1994).
[48] L. Allen and J. H. Eberly, *Optical Resonance and Two-Level Atoms* (Wiley, New York, 1975).
[49] P. Michler, *Single Semiconductor Quantum Dots* (Springer, Berlin, 2009).

Publication 7

Ultrafast depopulation of a quantum dot by LA-phonon-assisted stimulated emission

F. Liu, L. M. P. Martins, A. J. Brash, A. M. Barth, J. H. Quilter, V. M. Axt, M. S. Skolnick and A. M. Fox

Physical Review B **93**, 161407(R) (2016)

DOI: 10.1103/PhysRevB.93.161407

PHYSICAL REVIEW B **93**, 161407(R) (2016)

Ultrafast depopulation of a quantum dot by LA-phonon-assisted stimulated emission

F. Liu,[1,*] L. M. P. Martins,[1] A. J. Brash,[1] A. M. Barth,[2] J. H. Quilter,[1,3] V. M. Axt,[2] M. S. Skolnick,[1] and A. M. Fox[1]

[1]*Department of Physics and Astronomy, University of Sheffield, Sheffield, S3 7RH, United Kingdom*

[2]*Institut für Theoretische Physik III, Universität Bayreuth, 95440 Bayreuth, Germany*

[3]*Department of Physics, Royal Holloway, University of London, Egham, TW20 0EX, United Kingdom*

(Received 1 February 2016; revised manuscript received 24 March 2016; published 18 April 2016)

We demonstrate ultrafast *incoherent* depopulation of a quantum dot from above to below the transparency point using LA-phonon-assisted emission stimulated by a redshifted laser pulse. The QD is turned from a weakly vibronic system into a strongly vibronic one by laser driving which enables the phonon-assisted relaxation between the excitonic components of two dressed states. The depopulation is achieved within a laser pulse-width-limited time of 20 ps and exhibits a broad tuning range of a few meV. Our experimental results are well reproduced by path-integral calculations.

DOI: 10.1103/PhysRevB.93.161407

The exciton-phonon coupling in semiconductor quantum dots (QDs) has attracted much interest due to its importance both in fundamental physics and in semiconductor-based quantum technologies [1–4]. It has been known for some time that QDs can be excited by phonon-assisted transitions when the laser is detuned within the phonon sideband [5]. Very recently, it has been shown that population inversion can be achieved under these incoherent pumping conditions in the strong driving regime [6–13]. However, the opposite process in which an exciton in an inverted QD is de-excited with the assistance of longitudinal acoustic (LA) phonons has yet to be investigated. This process could be important for the development of tunable single QD lasers [14,15] or of QD single-photon sources in cavities with improved timing jitter [1,16,17].

The significance of the LA phonon-assisted de-excitation process can be appreciated by comparing it to the conventional understanding of inverted two-level systems. Consider a quantum dot in which population inversion has been created as shown in Fig. 1(a). A resonant laser pulse that is short compared to the spontaneous emission time, but long compared to the coherence time will only drive the system towards the transparency point, never crossing it due to the equal cross sections of stimulated emission (SE) and absorption [see Fig. 1(b)]. However, if the dot is coupled to the lattice, stimulated emission can be induced by a redshifted pulse via phonon emission, provided that the temperature is low enough that phonon absorption is weak [see Fig. 1(c)]. The decoupling of stimulated emission and absorption enables depopulation of the inverted two-level system to below the transparency point before spontaneous emission occurs, which is impossible for exactly resonant excitation in the incoherent limit. This process is fundamentally different to conventional vibronic systems—e.g., Ti:sapphire [18]—in that the phonon coupling is weak at low light intensities and only becomes effective at high optical powers during a strong laser pulse. In this sense, the new mechanism can be regarded as de-excitation by *dynamic* vibronic coupling.

In this Rapid Communication, we demonstrate the LA-phonon-assisted stimulated emission (LAPSE) process by using a redshifted laser pulse to *incoherently* de-excite an inverted quantum dot to below the transparency point. The time dynamics indicate that the depopulation occurs in 20 ps, limited by the laser pulse width. We show that the process occurs over a broad tuning range of ∼4 meV (in contrast to the fixed frequency of resonant excitation) and that the results are in good agreement with path-integral calculations [19]. The new mechanism provides a route to ultrafast reset of an excited quantum dot, which should be important for quantum photonic systems incorporating dots as the nonlinear element.

Our experiments are performed on a device consisting of InGaAs QDs embedded in the intrinsic region of an *n*-*i*-Schottky diode. The sample is held at $T = 4.2$ K in a helium bath cryostat. The excitation laser pulse is derived by spectral shaping of the output from a mode-locked Ti:sapphire laser with repetition rate 76.2 MHz. The spectral FWHM is 0.2 meV for the π pulse in all measurements and 0.2 or 0.42 meV for the redshifted laser pulse, corresponding to a Fourier transform limited pulse duration τ_L of 16.8 or 8 ps. τ_L is defined as the FWHM of the electric field envelope. The exciton population created by the circularly polarized laser pulse is determined by measuring the photocurrent (PC) generated when a reverse bias voltage is applied to the diode [20]. More details of the sample and experimental setup can be found in Refs. [21–23].

A phenomenological description of the LAPSE process is as follows. Assume a QD is initially in the exciton state. A strong laser pulse redshifted relative to the exciton state by $\hbar\Delta$ leads to the recombination of the exciton and the emission of a phonon and photon illustrated by thick down arrows in Fig. 1(c). To fully understand the underlying mechanism, we use the dressed state picture [see Fig. 1(d)]. In the rotating frame, the crystal ground state $|0\rangle$ and the incident laser field are treated as one state: $|0_R\rangle$. The exciton state $|X\rangle$ and the laser field with one photon less are treated as $|X_R\rangle$. The relative energies of the two states are shown by the dashed/dotted lines in Fig. 1(d) as a function of the laser detuning $\hbar\Delta = \hbar(\omega_X - \omega_L)$, where ω_X and ω_L are the angular frequencies of the exciton transition and laser, respectively. Since $|0_R\rangle$ and $|X_R\rangle$ are admixed by the laser field, the eigenstates of the system become two new optically dressed states: $|\alpha\rangle$ and $|\beta\rangle$, split by the effective

*To whom correspondence should be addressed: fengliu@sheffield.ac.uk.

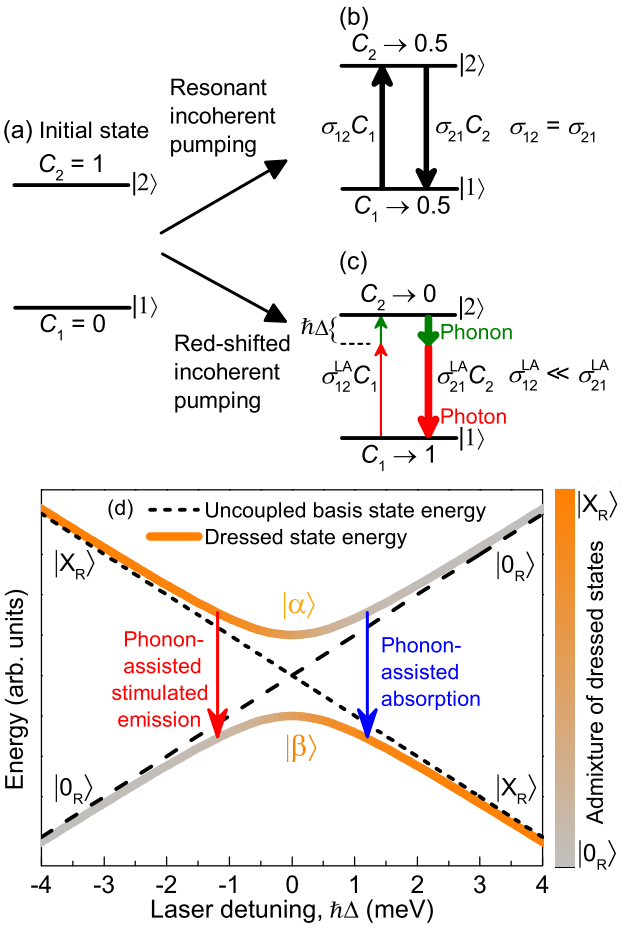

FIG. 1. (a)–(c): Difference between resonant incoherent pumping and redshifted incoherent pumping. (a) A two-level system is initially inverted ($C_2 > C_1$). C_i denotes the population of the ith state. (b) Resonant incoherent pumping induces absorption and SE with equal cross sections ($\sigma_{12} = \sigma_{21}$), moving the system towards transparency ($C_1 = C_2$). σ denotes the absorption/stimulated emission cross section. (c) If pumped by redshifted incoherent excitation, C_2 can be almost completely depleted as the redshifted laser mainly induces SE ($\sigma_{12}^{\mathrm{LA}} \ll \sigma_{21}^{\mathrm{LA}}$). Absorption hardly occurs due to the lack of additional phonons at low temperature. (d) The mechanism of the LA-phonon-assisted SE and absorption explained in the dressed-state picture. $|0_{\mathrm{R}}\rangle$, $|X_{\mathrm{R}}\rangle$: uncoupled ground state and exciton state viewed in the rotating frame. $|\alpha\rangle$, $|\beta\rangle$: optically dressed states split by the effective Rabi energy $\hbar\Lambda$.

Rabi energy $\hbar\Lambda(t) = \hbar\sqrt{\Delta^2 + \Omega(t)^2}$, where Ω is the Rabi frequency for resonant excitation proportional to the electric field amplitude E. The dressed state energies are shown by the thick solid lines in Fig. 1(d) and the color gradient illustrates the excitonic contribution to the corresponding states. Owing to their excitonic components, $|\alpha\rangle$ and $|\beta\rangle$ are coupled by LA-phonons via the deformation potential [24].

In the LAPSE process, the QD is initially in the $|X_{\mathrm{R}}\rangle$ state. By applying a redshifted laser pulse ($\Delta < 0$), the phonon-assisted relaxation channel is activated and the system relaxes from the higher-energy more excitonlike state $|\alpha\rangle$ to the lower-energy more ground-state-like state $|\beta\rangle$ by emitting phonons with an energy of $\hbar\Lambda$ [see red arrow in Fig. 1(d)]. If the phonon relaxation is fast enough, the system will reach thermal equilibrium between the two dressed states during the laser pulse. At low temperatures ($k_{\mathrm{B}}T \ll \hbar\Lambda$) the lower dressed state $|\beta\rangle$ will be occupied predominantly and approaches $|0_{\mathrm{R}}\rangle$ when the laser field is switched off [26]. Inverting the sign of the laser detuning $\hbar\Delta$ leads to the opposite process: the creation of an exciton by absorbing a photon and emitting a phonon [7,10–13] [see blue arrow in Fig. 1(d)]. Here we note that LAPSE is fundamentally different from existing depopulation schemes, such as coherent control schemes [20,27] and adiabatic rapid passage protocols [28–30] in which exciton-phonon coupling is usually a hindrance, whereas LAPSE is enabled by the exciton-phonon interaction.

To demonstrate the depopulation of a QD from above to below the transparency point, we first resonantly pump the QD to the exciton state at $t = 0$ using a laser pulse with pulse area $\Theta = \pi$ [see Fig. 2(a)]. Θ is defined as $(\mu_X/\hbar)\int_{-\infty}^{+\infty} E(t)\mathrm{d}t$ and was determined from a Rabi oscillation measurement at $\hbar\Delta = 0$ meV [24,31–33]. μ_X is the optical dipole matrix element for the $|0\rangle \to |X\rangle$ transition. The black line in Fig. 2(b) shows a PC spectrum measured as a function of the detuning of the π pulse. The peak at zero detuning corresponds to the $|0\rangle \to |X\rangle$ transition. Its amplitude PC_{π}^{X} corresponds to an exciton population of 1. Next, we apply a strong redshifted pulse ($\hbar\Delta = -0.7$ meV, $\Theta = 5.25\pi$) to depopulate the inverted QD. In the text below, we call this redshifted laser pulse the "LAPSE pulse." To maximize the efficiency of LAPSE, the width of the LAPSE pulse should be spectrally broad to cover as many phonon modes as possible, whereas the pulse duration $\tau_{\mathbf{L}}$ needs to be long enough for the dressed states to complete the phonon-assisted relaxation. To fulfill both conditions, consistent with theory, we set the FWHM and $\tau_{\mathbf{L}}$ of the LAPSE pulse to 0.42 meV and 8 ps. The red line in Fig. 2(b) shows the PC spectrum measured in the presence of the LAPSE pulse. The peak at $\hbar\Delta = -0.7$ meV is due to the interference between the π pulse and the LAPSE pulse. The reduction of the amplitude of the exciton peak $PC_{2\mathrm{pulse}}^{X}$ relative to PC_{π}^{X} directly demonstrates the depopulation of the exciton state. In the PC measurement, the total population of the ground state and exciton state C_{Total} drops to 0.88 at the arrival of the LAPSE pulse due to the electron tunneling out from the QD during the delay time $\tau_{\mathrm{delay}} = 7$ ps; therefore the transparency point defined as $C_{\mathrm{Total}}/2$ is shifted to 0.44 [see details in Ref. [24]]. The fact that $PC_{2\mathrm{pulse}}^{X} < 0.44\,PC_{\pi}^{X}$ proves that the inverted QD is depopulated below the transparency point.

Figure 2(c) shows the remaining exciton population obtained after the LAPSE pulse versus the pulse area Θ. In order to improve the spectral resolution and the signal to noise ratio, in the following measurements we reduce the FWHM of the LAPSE pulse to 0.2 meV. It can be seen that C_X decreases with the increase of Θ as predicted by the simulation in Fig. 4(b) and crosses the transparency point at $\Theta > 6.25\pi$. The minimum C_X measured here is limited by the laser power available in our setup. The efficiency of the LAPSE process strongly depends on the pulse area because the laser detuning and power determine the effective Rabi splitting $\hbar\Lambda$ that needs to be in resonance with the phonon environment for an efficient phonon-assisted relaxation to occur [34]. Figure 2(c)

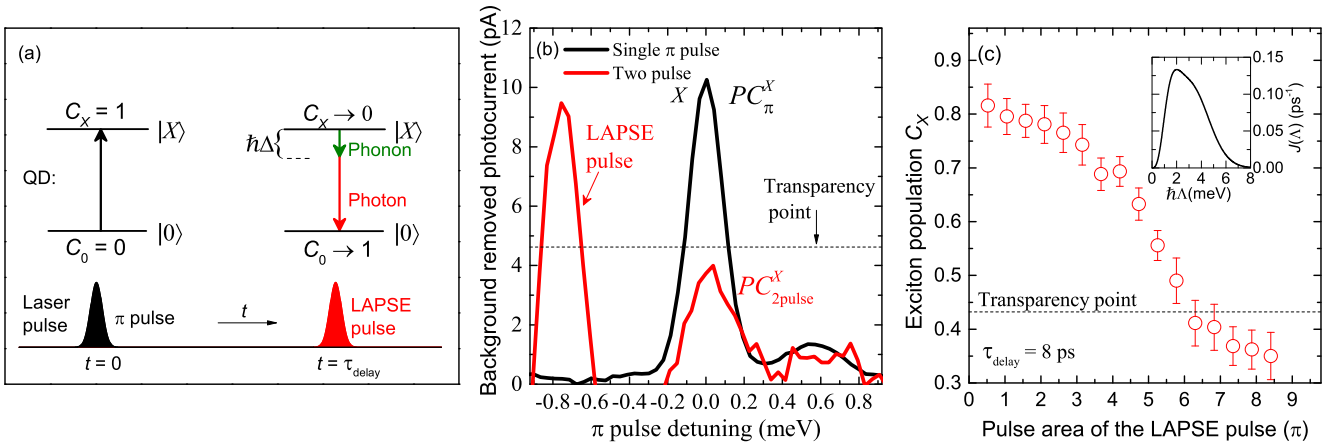

FIG. 2. (a) Scheme of the two-pulse measurement. The QD is excited to the $|X\rangle$ state by a π pulse at $t = 0$ and then depopulated by a redshifted laser pulse (LAPSE pulse) after τ_{delay}. (b) Black: PC spectrum measured only with a π pulse (FWHM $= 0.2$ meV, $\tau_L = 16.8$ ps). Red: Two-pulse spectrum measured in the presence of a -0.7 meV detuned LAPSE pulse (FWHM $= 0.42$ meV, $\tau_L = 8$ ps, $\Theta = 5.25\pi$, $\tau_{delay} = 7$ps). PC_π^X and PC_{2pulse}^X denote the amplitude of the exciton peak in the single-pulse and two-pulse spectra, respectively. The background of the PC spectra have been removed. (c) Remaining exciton population C_X after the LAPSE pulse versus the pulse area Θ. LAPSE pulse: $\hbar\Delta = -0.7$ meV, FWHM $= 0.2$ meV, $\tau_L = 16.8$ ps, $\tau_{delay} = 8$ ps. C_X is deduced according to: $C_X = e^{-\tau_{delay}/\tau_e} - (1 - PC_{2pulse}^X/PC_\pi^X)$, where τ_e is the electron tunneling time [see details in Ref. [24]]. Inset: Calculated exciton-phonon coupling spectral density $J(\Lambda)$.

inset shows the calculated exciton-phonon coupling spectral density J as a function of the effective Rabi splitting: $J(\Lambda) = \sum_{\mathbf{q}} |\gamma_{\mathbf{q}}|^2 \delta(\Lambda - \omega_{\mathbf{q}})$, where $\gamma_{\mathbf{q}}$ is the exciton-phonon coupling and $\mathbf{q}$ is the wave vector of bulk LA phonons [see details in Ref. [24]]. Here it becomes clear that the QD can be dynamically turned from a weakly vibronic system into a strongly vibronic one by laser driving when $\hbar\Lambda$ approaches 2 meV.

We next investigate the time dynamics of LAPSE by measuring PC_{2pulse}^X/PC_π^X versus the delay time between the π pulse and the LAPSE pulse [see red circles in Fig. 3]. At negative delay time, the LAPSE pulse arrives before the exciton is created by the π pulse and therefore cannot depopulate the exciton. The signal ($\sim$0.9) is not exactly 1 as

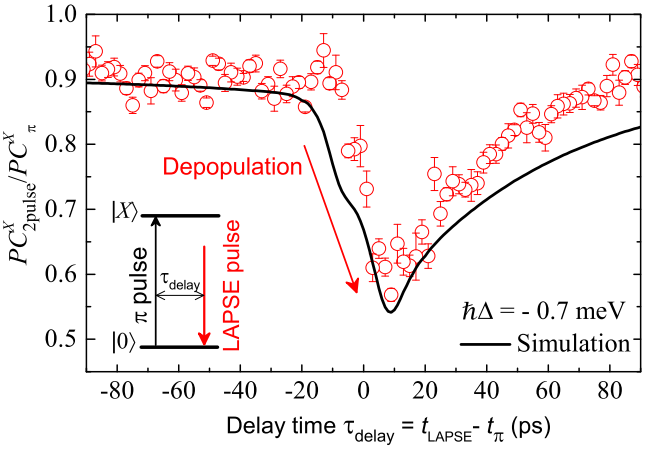

FIG. 3. Time dynamics of the LAPSE process. Red circles: PC_{2pulse}^X/PC_π^X measured as a function of τ_{delay} under the same condition as Fig. 2(c). $\tau_{delay} = t_{LAPSE} - t_\pi$, where t_{LAPSE} and t_π are the arrival times of the LAPSE pulse and the π pulse. The pulse area of the LAPSE pulse is 5.25π. Black line: Numerical simulation. Inset: Excitation scheme.

the redshifted LAPSE pulse can also create excitons with very small probability by absorbing phonons at $T > 0$. When the π pulse overlaps with the LAPSE pulse, PC_{2pulse}^X decreases to a minimum from $\tau_{delay} = -10$ to $+10$ ps, indicating that the LAPSE process can be as fast as 20 ps. The signal then slowly recovers due to the electron tunneling before the arrival of the LAPSE pulse. The electron tunneling time (55 ps) is measured using inversion recovery techniques [23]. The depopulation time is determined by the laser pulse width and in principle can be further reduced by using shorter laser pulses which however can diminish the efficiency of the LAPSE process when there is not enough time for the phonon-assisted relaxation to complete [10,13]. In Ref. [10] it is found that a pulse duration of about 10 ps is sufficient for the QD to reach thermal equilibrium between the two dressed states [see Fig. 1(d)].

To further verify our understanding of the time dynamics of LAPSE, we have performed path-integral calculations based on a model of a laser-driven QD coupled to LA phonons [see details in Ref. [24]]. The electron tunneling occurring during the PC measurement is integrated as a Lindblad-type relaxation term into the path-integral approach without taking away the numerically complete treatment that includes all multiphonon processes and non-Markovian effects. The calculation (black line) well reproduces all the features observed in the experiment, proving that the decrease of the PC signal is indeed caused by LAPSE.

By contrast to the fixed frequency of stimulated emission under resonant excitation, LAPSE can occur within a broad tuning range. To demonstrate this tunability, we measure the decrease of exciton population caused by a LAPSE pulse as a function of the laser detuning $\hbar\Delta$ [see Fig. 4(a)]. In this measurement, a π pulse creates a reference PC level [dashed line in Fig. 4(a)] by resonantly pumping the QD. The reference level corresponds to an exciton population of 1. Then we apply a LAPSE pulse to depopulate the exciton state and measure the PC signal as a function of the laser detuning. To isolate the

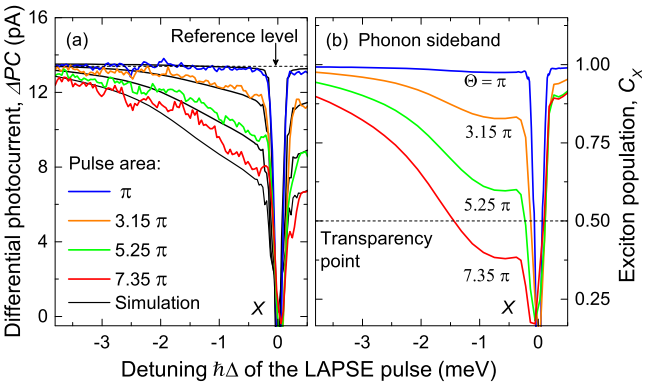

FIG. 4. Tunability of the LAPSE process. (a) Differential photocurrent spectra measured by pumping the QD resonantly with a π pulse and then depopulating the exciton by applying a LAPSE pulse at different detunings and pulse areas. To isolate the signal of the target QD from other QDs in the same sample, a reference spectrum where only the LAPSE pulse is applied is subtracted. $\tau_{\text{delay}} = 17$ ps. Solid black lines: simulation. (b) Calculated phonon sideband without taking into account the electron tunneling and the subtraction of the reference spectra.

signal of the QD under study from other QDs in the sample, a reference spectrum is measured with only the LAPSE pulse and subtracted [24]. The colored lines in Fig. 4(a) are the differential spectra ΔPC measured at different pulse areas. The dip at zero detuning corresponds to the resonant transition between $|X\rangle$ and $|0\rangle$. The reduction of the PC signal at negative detuning originates from the LAPSE process. The broad tuning range ($\sim$4 meV) is clearly demonstrated by the negative sidebands. The good agreement between the experimental result and the path-integral calculations (black lines) supports our interpretation.

Although the shape and amplitude of the sidebands shown in Fig. 4(a) are primarily determined by the spectral dependence of the exciton-phonon coupling shown in the inset in Fig. 2(c), the differential spectra ΔPC are also slightly influenced by the exciton depopulation due to electron tunneling and the shape of the subtracted reference spectra [24]. To obtain more insight into the spectral dependence of LAPSE, we calculate the remaining exciton population obtained after the LAPSE pulse without taking into account the electron tunneling and subtraction of the reference spectra. This simulation directly shows how the probability of LAPSE depends on the laser detuning [see Fig. 4(b)]. Furthermore the simulation for $\Theta = 7.35\pi$ clearly shows that the inverted QD is depopulated to below the transparency point at $\hbar\Delta \sim -0.7$ meV.

In conclusion, we have demonstrated the ultrafast depopulation of a QD from above to below the transparency point using redshifted incoherent excitation via LA-phonon-assisted stimulated emission. The depopulation time ($\sim$20 ps) is determined by the laser pulse width, making it possible to reset a QD exciton much faster than the speed limitation imposed by the exciton lifetime. Due to the broadness of the phonon sideband, this scheme can occur in a tuning range of a few meV and may form the basis of tunable single QD lasers. Additionally, it can be potentially used for ultrafast optical switching [27,35–39], semiconductor optical amplifiers [40], and precisely controlling the emission time of a single photon source in cavities [1,16,17].

This work was funded by the EPSRC (UK) programme Grant No. EP/J007544/1. A.M.B. and V.M.A. gratefully acknowledge the financial support from Deutsche Forschungsgemeinschaft via the Project No. AX 17/7-1. The authors thank A. J. Ramsay for very helpful discussions and H. Y. Liu and M. Hopkinson for sample growth.

[1] K. Müller, K. A. Fischer, A. Rundquist, C. Dory, K. G. Lagoudakis, T. Sarmiento, Y. A. Kelaita, V. Borish, and J. Vučković, Phys. Rev. X **5**, 031006 (2015).

[2] K. Müller, A. Rundquist, K. A. Fischer, T. Sarmiento, K. G. Lagoudakis, Y. A. Kelaita, C. Sánchez Muñoz, E. del Valle, F. P. Laussy, and J. Vučković, Phys. Rev. Lett. **114**, 233601 (2015).

[3] A. Majumdar, A. Papageorge, E. D. Kim, M. Bajcsy, H. Kim, P. Petroff, and J. Vučković, Phys. Rev. B **84**, 085310 (2011).

[4] A. Majumdar, M. Bajcsy, A. Rundquist, E. Kim, and J. Vučković, Phys. Rev. B **85**, 195301 (2012).

[5] S. Weiler, A. Ulhaq, S. M. Ulrich, D. Richter, M. Jetter, P. Michler, C. Roy, and S. Hughes, Phys. Rev. B **86**, 241304 (2012).

[6] J. R. Petta, A. C. Johnson, C. M. Marcus, M. P. Hanson, and A. C. Gossard, Phys. Rev. Lett. **93**, 186802 (2004).

[7] J. H. Quilter, A. J. Brash, F. Liu, M. Glässl, A. M. Barth, V. M. Axt, A. J. Ramsay, M. S. Skolnick, and A. M. Fox, Phys. Rev. Lett. **114**, 137401 (2015).

[8] T. M. Stace, A. C. Doherty, and S. D. Barrett, Phys. Rev. Lett. **95**, 106801 (2005).

[9] J. I. Colless, X. G. Croot, T. M. Stace, A. C. Doherty, S. D. Barrett, H. Lu, A. C. Gossard, and D. J. Reilly, Nat. Commun. **5**, 3716 (2014).

[10] M. Glässl, A. M. Barth, and V. M. Axt, Phys. Rev. Lett. **110**, 147401 (2013).

[11] S. Hughes and H. J. Carmichael, New J. Phys. **15**, 053039 (2013).

[12] P.-L. Ardelt, L. Hanschke, K. A. Fischer, K. Müller, A. Kleinkauf, M. Koller, A. Bechtold, T. Simmet, J. Wierzbowski, H. Riedl, G. Abstreiter, and J. J. Finley, Phys. Rev. B **90**, 241404 (2014).

[13] S. Bounouar, M. Müller, A. M. Barth, M. Glässl, V. M. Axt, and P. Michler, Phys. Rev. B **91**, 161302 (2015).

[14] M. Nomura, N. Kumagai, S. Iwamoto, Y. Ota, and Y. Arakawa, Nat. Phys. **6**, 279 (2010).

[15] E. U. Rafailov, M. A. Cataluna, and W. Sibbett, Nat. Photon. **1**, 395 (2007).

[16] D. Heinze, D. Breddermann, A. Zrenner, and S. Schumacher, Nat. Commun. **6**, 8473 (2015).

[17] S. L. Portalupi, G. Hornecker, V. Giesz, T. Grange, A. Lemaître, J. Demory, I. Sagnes, N. D. Lanzillotti-Kimura, L. Lanco, A. Auffèves, and P. Senellart, Nano Lett. **15**, 6290 (2015).

[18] J. Klein and J. D. Kafka, Nat. Photon. **4**, 289 (2010).

[19] A. Vagov, M. D. Croitoru, M. Glässl, V. M. Axt, and T. Kuhn, Phys. Rev. B **83**, 094303 (2011).

[20] A. Zrenner, E. Beham, S. Stufler, F. Findeis, M. Bichler, and G. Abstreiter, Nature (London) **418**, 612 (2002).

[21] A. J. Brash, L. M. P. P. Martins, F. Liu, J. H. Quilter, A. J. Ramsay, M. S. Skolnick, and A. M. Fox, Phys. Rev. B **92**, 121301 (2015).

[22] T. M. Godden, J. H. Quilter, A. J. Ramsay, Y. Wu, P. Brereton, I. J. Luxmoore, J. Puebla, A. M. Fox, and M. S. Skolnick, Phys. Rev. B **85**, 155310 (2012).

[23] R. S. Kolodka, A. J. Ramsay, J. Skiba-Szymanska, P. W. Fry, H. Y. Liu, A. M. Fox, and M. S. Skolnick, Phys. Rev. B **75**, 193306 (2007).

[24] See Supplemental Material at http://link.aps.org/supplemental/10.1103/PhysRevB.93.161407 for the description of the model and the derivation of the exciton population, which includes Refs. [7,19,25].

[25] H.-P. Breuer and F. Petruccione, *The Theory of Open Quantum Systems* (Oxford University Press, New York, 2002).

[26] A. M. Barth, S. Lüker, A. Vagov, D. E. Reiter, T. Kuhn, and V. M. Axt, arXiv:1601.07886.

[27] A. P. Heberle, J. J. Baumberg, and K. Köhler, Phys. Rev. Lett. **75**, 2598 (1995).

[28] Y.-J. Wei, Y.-M. He, M.-C. Chen, Y.-N. Hu, Y. He, D. Wu, C. Schneider, M. Kamp, S. Höfling, C.-Y. Lu, and J.-W. Pan, Nano Lett. **14**, 6515 (2014).

[29] R. Mathew, E. Dilcher, A. Gamouras, A. Ramachandran, Hong Yi Shi Yang, S. Freisem, D. Deppe, and K. C. Hall, Phys. Rev. B **90**, 035316 (2014).

[30] S. Lüker, K. Gawarecki, D. E. Reiter, A. Grodecka-Grad, V. M. Axt, P. Machnikowski, and T. Kuhn, Phys. Rev. B **85**, 121302 (2012).

[31] A. J. Ramsay, T. M. Godden, S. J. Boyle, E. M. Gauger, A. Nazir, B. W. Lovett, A. M. Fox, and M. S. Skolnick, Phys. Rev. Lett. **105**, 177402 (2010).

[32] A. J. Ramsay, A. V. Gopal, E. M. Gauger, A. Nazir, B. W. Lovett, A. M. Fox, and M. S. Skolnick, Phys. Rev. Lett. **104**, 017402 (2010).

[33] L. Monniello, C. Tonin, R. Hostein, A. Lemaitre, A. Martinez, V. Voliotis, and R. Grousson, Phys. Rev. Lett. **111**, 026403 (2013).

[34] A. Nazir, Phys. Rev. B **78**, 153309 (2008).

[35] N. H. Bonadeo, Science **282**, 1473 (1998).

[36] R. Bose, D. Sridharan, H. Kim, G. S. Solomon, and E. Waks, Phys. Rev. Lett. **108**, 227402 (2012).

[37] T. Volz, A. Reinhard, M. Winger, A. Badolato, K. J. Hennessy, E. L. Hu, and A. Imamolu, Nat. Photon. **6**, 607 (2012).

[38] D. Englund, A. Majumdar, M. Bajcsy, A. Faraon, P. Petroff, and J. Vučković, Phys. Rev. Lett. **108**, 093604 (2012).

[39] E. Cancellieri, A. Hayat, A. M. Steinberg, E. Giacobino, and A. Bramati, Phys. Rev. Lett. **112**, 053601 (2014).

[40] A. Capua, O. Karni, G. Eisenstein, V. Sichkovskyi, V. Ivanov, and J. P. Reithmaier, Nat. Commun. **5**, 5025 (2014).

Ultrafast Depopulation of a Quantum Dot by LA-phonon-assisted Stimulated Emission - Supplemental Material

F. Liu,[1] L. M. P. Martins,[1] A. J. Brash,[1] A. M. Barth,[2] J. H. Quilter,[1,3] V. M. Axt,[2] M. S. Skolnick,[1] and A. M. Fox[1]

[1]*Department of Physics and Astronomy, University of Sheffield, Sheffield, S3 7RH, United Kingdom*
[2]*Institut für Theoretische Physik III, Universität Bayreuth, 95440 Bayreuth, Germany*
[3]*Department of Physics, Royal Holloway, University of London, Egham, TW20 0EX, United Kingdom*

I. THEORETICAL DESCRIPTION OF A DRIVEN QD

To model the optically driven quantum dot (QD) coupled to longitudinal accoustic (LA) phonons we use the Hamiltonian [1]:

$$H = H_{\mathrm{QD-light}} + H_{\mathrm{QD-phonon}}, \tag{S1}$$

where

$$H_{\mathrm{QD-light}} = \hbar\omega_X^0 |X\rangle\langle X| + \tag{S2}$$

$$\frac{\hbar\Omega(t)}{2}[|0\rangle\langle X|e^{i\omega_L t} + |X\rangle\langle 0|e^{-i\omega_L t}], \tag{S3}$$

and

$$H_{\mathrm{QD-phonon}} = \sum_{\mathbf{q}} \hbar\omega_{\mathbf{q}}\, b_{\mathbf{q}}^\dagger b_{\mathbf{q}} + \sum_{\mathbf{q}} \hbar\left(\gamma_{\mathbf{q}} b_{\mathbf{q}} + \gamma_{\mathbf{q}}^* b_{\mathbf{q}}^\dagger\right)|X\rangle\langle X|. \tag{S4}$$

$\hbar\omega_X^0$ denotes the transition energy between $|0\rangle$ and $|X\rangle$ states. $\Omega(t)$ denotes the Rabi frequency proportional to the electric field envelope of a circularly polarized laser pulse. We refer to the difference between the laser frequency ω_L and the exciton energy by $\Delta = \omega_L - \omega_X$, where ω_X is the frequency of the single exciton resonance deviating from ω_X^0 by the polaron shift resulting from the dot-phonon coupling in Eq. (S4). $b_{\mathbf{q}}^\dagger$ and $b_{\mathbf{q}}$ are the creation and annihilation operators for a LA phonon with wave vector $\mathbf{q}$ and energy $\hbar\omega_{\mathbf{q}}$. A linear dispersion relation $\omega_{\mathbf{q}} = c_s|\mathbf{q}|$ is assumed, where c_s denotes the speed of sound. The phonons are coupled to the QD via the deformation potential and the exciton-phonon coupling is expressed by $\gamma_{\mathbf{q}} = \frac{|\mathbf{q}|}{\sqrt{2V\rho\hbar\omega_{\mathbf{q}}}}\left(D_{\mathrm{e}}\Psi^{\mathrm{e}}(\mathbf{q}) - D_{\mathrm{h}}\Psi^{\mathrm{h}}(\mathbf{q})\right)$, where ρ denotes the mass density of the crystal, V the mode volume, $D_{\mathrm{e/h}}$ the deformation potential constants, and $\Psi^{\mathrm{e/h}}(\mathbf{q})$ the form factors of electron and hole, respectively. We assume the system to be initially in a product state of a thermal phonon-distribution at 4.2 K and a pure ground-state of the electronic subsystem. For bulk LA phonons coupled via the deformation potential we obtain for a parabolic confinement [2]:

$$J(\omega) = \frac{\omega^3}{4\pi^2\rho\hbar v_c^5}\left[D_{\mathrm{e}}\, e^{\left(-\omega^2 a_{\mathrm{e}}^2/4v_c^2\right)} - D_{\mathrm{h}}\, e^{\left(-\omega^2 a_{\mathrm{h}}^2/4v_c^2\right)}\right]^2. \tag{S5}$$

We use the same material parameters given in ref. 1 for GaAs, which are: $\rho = 5370$ kg/m^3, $c_s = 5110$ m/s, $D_{\mathrm{e}} = 7.0$ eV, and $D_{\mathrm{h}} = -3.5$ eV. The electron and hole confinement lengths $a_{\mathrm{e/h}}$ are used as fitting parameters obtained from ref. 1: $a_{\mathrm{e}} = 4.5$ nm, $a_{\mathrm{h}} = 1.8$ nm.

To also take into account the electron tunneling during the photocurrent (PC) measurements in the time-dependent path-integral simulation, we add to the two QD levels $|0\rangle$ and $|X\rangle$ a third electronic level $|h\rangle$ accounting for the hole state remaining after an electron tunnels out from the QD. The hole tunneling time is significantly longer than the measurement time and therefore does not need to be included. This third level is hence only coupled to the exciton state $|X\rangle$ and the relaxation from $|X\rangle$ to $|h\rangle$ is modelled as it is done in the Lindblad master equation approach [3]. The relaxation rate is given by the measured electron tunneling time of 55 ps. Details of the incorporation of the Lindblad relaxation within the path integral approach will be given elsewhere. When the simulation time is sufficiently long to complete all relaxation processes the measured PC signal $PC_{2\mathrm{pulse}}^X$ and PC_π^X [see Fig. 3 in the main text] can be directly compared with the occupation of the $|h\rangle$ state, because it is a direct measure for the electrons tunneling out of the QD and hence must be proportional to the induced PC.

II. DETERMINING THE PULSE AREA BY RABI OSCILLATION MEASUREMENT

The pulse area Θ of the laser pulse can be determined from the Rabi oscillation measurement. Fig. S1(a) shows the PC spectra of a QD measured as a function of the laser detuning. The peak at 0 detuning corresponds to the neutral exciton transition. Then we measured the PC as a function of the laser power at detuning = 0 meV. The data in Fig. S1(b) shows the Rabi oscillation of the exciton population after subtracting a PC background increasing linearly with the laser power. The laser power at the first maximum of the Rabi oscillation corresponds to a π pulse. The peak amplitude of the PC spectrum of the QD measured with a π pulse corresponds to an exciton population of 1.

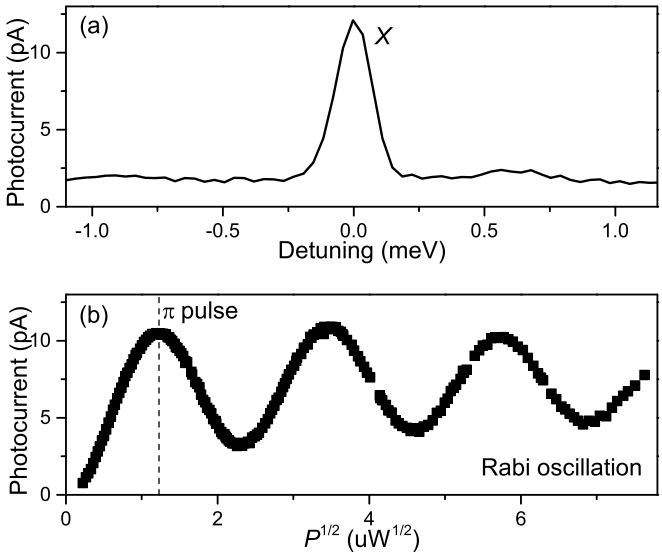

FIG. S1: (a) PC spectrum of a QD measured as a function of the π pulse detuning. (b) Rabi oscillation measured as a function of the square root of the laser power at detuning = 0 meV.

III. EFFECT OF ELECTRON TUNNELLING ON MEASURED VALUES OF C_X

In the two-pulse measurement shown in Fig. 2 in the main text, the remaining exciton population C_X obtained after the red-shifted laser pulse (LAPSE pulse) is deduced in the following way. At $t = 0$, the π pulse creates an exciton population of 1. Then the exciton population decays exponentially since the electron tunnels out from the QD with a tunneling time $\tau_{\rm e}$. The hole tunnelling and exciton radiative recombination are neglected because the hole tunnelling time $\tau_{\rm h}$ (few ns) and the exciton radiative lifetime ($\sim$ 600 ps) [1] is significantly longer than $\tau_{\rm e}$ (55 ps) and the delay time $\tau_{\rm delay}$ (7-17 ps) between the π pulse and the LAPSE pulses. At $t = \tau_{\rm delay}$ when the LAPSE pulse arrives, the exciton population is reduced from $e^{-\tau_{\rm delay}/\tau_{\rm e}}$ to C_X by the LAPSE pulse via phonon-assisted stimulated emission. Since the amplitude of the measured PC signal is proportional to the time-integrated exciton population created by the two pulses, the change of the exciton population ΔC induced by the LAPSE pulse is proportional to the reduction of the PC signal $PC^X_{\rm 2pulse}$ measured in the presence of the LAPSE pulse relative to PC^X_π measured with only a π pulse [see Fig. 2(b) in the main text]:

$$\Delta C = e^{-\tau_{\rm delay}/\tau_{\rm e}} - C_X = 1 - PC^X_{\rm 2pulse}/PC^X_\pi. \tag{S6}$$

Hence we obtain:

$$C_X = e^{-\tau_{\rm delay}/\tau_{\rm e}} - (1 - PC^X_{\rm 2pulse}/PC^X_\pi). \tag{S7}$$

The transparency point $C_{\rm TP}(t)$ of the QD at $t = \tau_{\rm delay}$ is defined as half of the total population of the ground state and exciton state, thus we have $C_{\rm TP}(t = \tau_{\rm delay}) = e^{-\tau_{\rm delay}/\tau_{\rm e}}/2$.

IV. DIFFERENTIAL PHOTOCURRENT MEASUREMENT

The differential PC spectra ΔPC shown in Fig. 4 in the main text were measured in two steps. In the first step, a two-pulse spectrum is obtained by pumping the QD to the $|X\rangle$ state using a circularly polarized resonant π pulse and then measuring the PC as a function of the detuning of a strong laser pulse (LAPSE pulse) applied after a delay time τ_{delay}. The exciton prepared by the π pulse is expected to be deexcited via LAPSE when the depopulation pulse is negatively detuned ($\Delta < 0$). This can be seen in Fig. S2(a) which shows the simulated exciton occupation of a single QD obtained after the two pulses. However, in practice the phonon sideband in the negative detuning region is overlaid by the PC signal from nearby QDs in the same sample (not shown). In order to isolate the PC signal of the dot under study from that of the other QDs, in the second step a reference spectrum was measured by scanning the detuning of only a LAPSE pulse. The calculated exciton occupation is shown in Fig. S2(b). Since the signals from the other QDs are present in both the two-pulse spectrum and the reference spectrum, they can be removed by subtracting the two spectra from each other. Fig. S2(c) shows the measured differential PC spectrum (red line) and the simulated spectrum (black line) obtained by subtracting the reference spectrum from the two-pulse spectrum. The calculated exciton population can be directly compared with the measured differential PC spectra by multiplying the exciton population with the amplitude of the exciton peak PC_{π}^{X} measured with a π pulse as shown in Fig. 4(a) in the main text. The sideband feature in the negative detuning region corresponds to the deexcitation of the exciton by the LAPSE process.

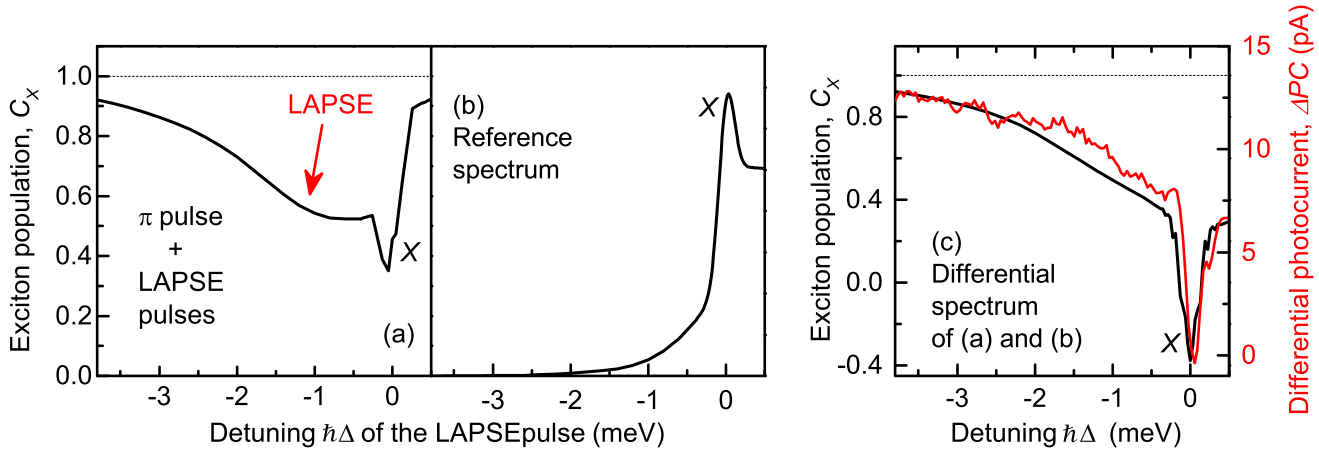

FIG. S2: (a) - (c): Simulated single-QD spectra illustrating the steps of the differential PC measurement. (a) Exciton occupation as a function of the detuning of the LAPSE pulse which is applied after a resonant π pulse and a delay time τ_{delay}; (b) Exciton occupation obtained by scanning the detuning of only a LAPSE pulse; (c) Differential spectrum obtained by subtracting the spectrum in (b) from that in (a). Red line: measured differential PC spectra. $\Theta = 7.35\ \pi$. $\tau_{\mathrm{delay}} = 17$ ps.

[1] J. H. Quilter, A. J. Brash, F. Liu, M. Glässl, A. M. Barth, V. M. Axt, A. J. Ramsay, M. S. Skolnick, and A. M. Fox, Physical Review Letters **114**, 137401 (2015)

[2] A. Vagov, M. D. Croitoru, M. Glässl, V. M. Axt, and T. Kuhn, Physical Review B **83**, 094303 (2011)

[3] H.-P. Breuer and F. Petruccione, The Theory of Open Quantum Systems (Oxford University Press, USA, 2002).

Publication 8

Dynamic vibronic coupling in InGaAs quantum dots [Invited]

A. J. Brash, L. M. P. P. Martins, A. M. Barth, F. Liu, J. H. Quilter, M. Glässl, V. M. Axt, A. J. Ramsay, M. S. Skolnick and A. M. Fox

Journal of the Optical Society of America B **33**, C115-C122 (2016)

DOI: 10.1364/JOSAB.33.00C115

Journal of the Optical Society of America B
OPTICAL PHYSICS

Dynamic vibronic coupling in InGaAs quantum dots [Invited]

A. J. Brash,[1] L. M. P. P. Martins,[1] A. M. Barth,[2] F. Liu,[1] J. H. Quilter,[1,3] M. Glässl,[2] V. M. Axt,[2] A. J. Ramsay,[4] M. S. Skolnick,[1] and A. M. Fox[1,*]

[1]Department of Physics & Astronomy, University of Sheffield, Sheffield S3 7RH, UK
[2]Institut für Theoretische Physik III, Universität Bayreuth, 95440 Bayreuth, Germany
[3]Department of Physics, Royal Holloway, University of London, Egham TW20 0EX, UK
[4]Hitachi Cambridge Laboratory, Hitachi Europe Ltd., Cambridge CB3 0HE, UK
*Corresponding author: mark.fox@sheffield.ac.uk

Received 16 February 2016; revised 12 April 2016; accepted 26 April 2016; posted 28 April 2016 (Doc. ID 259423); published 24 May 2016

The electron–phonon coupling in self-assembled InGaAs quantum dots is relatively weak at low light intensities, which means that the zero-phonon line in emission is strong compared to the phonon sideband. However, the coupling to acoustic phonons can be dynamically enhanced in the presence of an intense optical pulse tuned within the phonon sideband. Recent experiments have shown that this dynamic vibronic coupling can enable population inversion to be achieved when pumping with a blueshifted laser and for rapid de-excitation of an inverted state with red detuning. In this paper we confirm the incoherent nature of the phonon-assisted pumping process and explore the temperature dependence of the mechanism. We also show that a combination of blueshifted and redshifted pulses can create and destroy an exciton within a timescale of ∼20 ps as determined by the pulse duration and ultimately limited by the phonon thermalization time.

OCIS codes: (320.7130) Ultrafast processes in condensed matter, including semiconductors; (300.6470) Spectroscopy, semiconductors.

http://dx.doi.org/10.1364/JOSAB.33.00C115

1. INTRODUCTION

Vibronic sidebands are observed in the optical spectra of many solid-state materials [1], with Ti:sapphire [2] and nitrogen-vacancy (NV) centers in diamond [3–5] being good examples. The key point about a vibronic transition is that it involves the simultaneous absorption or emission of a photon and a phonon (or phonons) as the electron jumps between two electronic states. The sideband spectra are continuous bands, although substructure can frequently be identified due to the involvement of specific phonon modes, especially at low temperatures. For example, in the case of NV centers in diamond, clear structure can be identified that corresponds to the coupling of the electronic state to the A_1 mode ($\hbar\omega = 65$ meV), giving rise to resolved side peaks in both absorption and emission at integer multiples of the phonon energy [3,4]. The coupling to the vibrational modes is so strong that only a few percent of the emission occurs in the zero-phonon line, with most of the photons emitted from the sidebands [5]. The relatively weak intensity of the zero-phonon line has serious consequences for practical applications of NV centers in optical quantum information processing.

The reason that the phonon sidebands in materials like diamond NV centers and Ti:sapphire are so strong is that both the electronic and vibrational modes are strongly localized on length scales similar to the unit cell size. This means that the overlap between the electronic wave functions and the phonon modes is large, and, hence, the vibronic coupling is strong. By contrast, InGaAs quantum dots (QDs) have envelope wave functions localized on much larger length scales that are determined by the size of the dot, i.e., ∼10 nm. This means that the coupling to phonons is relatively weak, with the dominant interaction being to longitudinal-acoustic (LA) phonons via deformational potential scattering. The weak vibronic coupling in these dots gives rise to very strong emission in the zero-phonon line, with only ∼8% in the sideband at cryogenic temperature [6,7]. This makes InGaAs QDs excellent single-photon sources [8]. It also ensures that the light–matter coupling is strong, with optical dipole moments typically in the range of ∼30 Debye ($\sim 1 \times 10^{-28}$ cm) [9]. Moreover, the relatively weak electron–phonon coupling leads to long coherence times that are ultimately limited only by the radiative lifetime [10], which facilitates their application in coherent control experiments [11–14]. This contrasts with bulk and quantum well samples, where the coherence time is only a few picoseconds at best [15–17].

The vibronic sideband in InGaAs QDs manifests itself in a number of important experimental situations. One example is

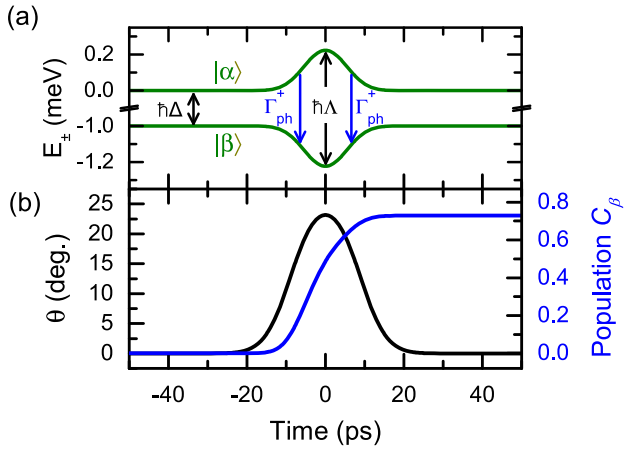

Fig. 1. Calculation of the dynamics of the dressed states when excited with a 16.8 ps laser pulse centered at $t = 0$ with $\hbar\Delta = +1$ meV and $\Theta = 8.5\pi$. (a) Energies of the dressed states (green lines) $|\alpha\rangle$ and $|\beta\rangle$ plotted against time. At $t \to -\infty$, the states are split by the laser detuning $\hbar\Delta$. During the passage of the pulse, the states are admixed and the splitting becomes $\hbar\Lambda$ as shown by the shift centered at $t = 0$. This enables relaxation from $|\alpha\rangle$ to $|\beta\rangle$ (blue arrows) by emission of an LA phonon with energy $\hbar\Lambda$. (b) Plot of the admixing angle θ (black line) and the population of the dressed state $|\beta\rangle$ (blue line) against time. θ also follows the envelope of the laser pulse and, as expected, relaxation into $|\beta\rangle$ occurs only when the states are admixed.

the emission of photons from a nanocavity when the dot and cavity are out of resonance, with the emission involving either the absorption or emission of a phonon depending on the sign of the detuning [8,18]. Another case is the observation of QD emission when pumping in the phonon sideband in a resonance fluorescence geometry [19]. The difference in the frequency of the pump laser and the QD exciton line facilitates spectral selection of the QD photons [20] and can be exploited for stabilizing the frequency of the zero-phonon line [21]. The sideband also appears in four-wave mixing experiments [22].

A key point about the experiments described above is that the optical pumping is relatively weak, so that the QD–laser system is in the weak-coupling limit. In this paper we explore the other limit where the QD–laser coupling is strong, such that a dressed-state picture is appropriate. This limit was addressed in a theoretical paper in 2013 by Glässl *et al.*, where it was predicted that strong driving in the phonon sideband could lead to exciton populations approaching full inversion [23]. The predictions of the theory were confirmed independently by three experimental groups in 2014–2015, both for pumping of the neutral exciton and the biexciton [14,24,25]. Most recently, it has also been demonstrated that the process works in reverse, so that an inverted system can be rapidly depopulated by pumping with a laser with red detuning relative to the exciton [26]. In these experiments the phonon coupling becomes strong when an intense laser field is present. The pulse durations in the experiments are short, and so the vibronic coupling is turned from weak to strong and back to weak again on picosecond timescales. We therefore call this process *dynamic vibronic coupling* (DVC). The DVC is fundamentally different from conventional excitation schemes, such as coherent Rabi oscillation [27–29] and adiabatic rapid passage protocols [30,31] where exciton–phonon coupling is usually an obstacle.

In this paper we first review the process underlying the DVC and summarize the results from our previous experiments [24,26]. After discussing the experimental methods in Section 3, we then present Ramsey interference data to demonstrate that the mechanism of DVC is incoherent, i.e., that the exciton created by phonon-sideband pumping is incoherent with the pumping laser (Section 4). We next consider the temperature dependence of the DVC in Section 5, comparing the population generated at ~15 K to that at base temperature (4.2 K). Finally we show in Section 6 how we can combine pumping with a blue-detuned and a red-detuned pulse to create and destroy an exciton within ~20 ps. Section 7 gives the conclusions and outlook.

2. MECHANISM OF DYNAMIC VIBRONIC COUPLING

The starting point for DVC is the coupling of excitons to the acoustic phonon bath by the deformation potential [32,33]. In the absence of a laser field this leads to nonexponential pure dephasing of the excitonic dipole [22]. The behavior of the coupled system becomes more interesting, however, when a strong laser field is applied. We consider a laser pulse with energy detuning $\hbar\Delta$ and area Θ:

$$\Theta = \int_{-\infty}^{+\infty} \Omega_R(t)\mathrm{d}t, \tag{1}$$

where $\Omega_R(t)$ is the time-dependent Rabi frequency determined by the optical dipole moment and the time-varying electric field amplitude of the pulse. Using the rotating wave approximation, the Hamiltonian in the rotating frame becomes time independent and one can thus define the dressed states of the laser–QD states as the corresponding eigenstates. These are given by

$$|\alpha\rangle = \sin(\theta)|0\rangle + \cos(\theta)|X\rangle \tag{2}$$

$$|\beta\rangle = \cos(\theta)|0\rangle - \sin(\theta)|X\rangle, \tag{3}$$

where θ is an admixing angle defined by

$$\tan(2\theta) = -\Omega_R/\Delta, \qquad 0 \le 2\theta \le 180°. \tag{4}$$

The energies of the dressed states are given by

$$E_\pm = \frac{\hbar}{2}(-\Delta \pm \Lambda(t)), \tag{5}$$

where $\Lambda(t)$ is an effective Rabi frequency defined as

$$\Lambda(t) = \sqrt{\Omega_R(t)^2 + \Delta^2}. \tag{6}$$

The significance of these dressed states is that, in the presence of a driving laser such that $\theta > 0$, both eigenstates of the system contain an excitonic component and may couple to the acoustic phonon bath. This enables phonon-mediated relaxation from $|\alpha\rangle$ to $|\beta\rangle$. However, this relaxation is possible only when the states are admixed by the laser, giving rise to the dynamic nature of the vibronic coupling.

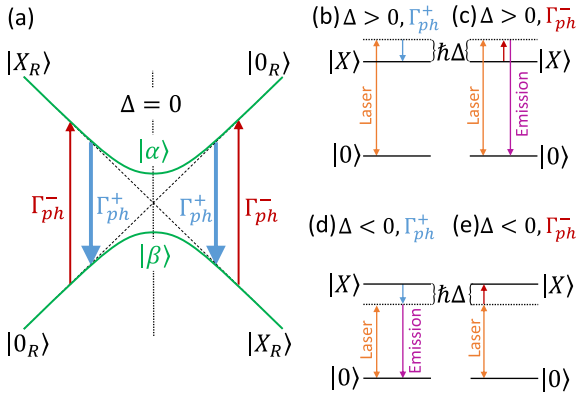

Fig. 2. (a) Illustration of the energies of the dressed states $|\alpha\rangle$ and $|\beta\rangle$ plotted against detuning Δ at a fixed time. The bare QD states in the frame of the laser are plotted for reference as dotted black lines. At $\Delta = 0$, the states anti-cross with a splitting of $\hbar\Omega_R$. It can be seen that $|\alpha\rangle$ is dominated by the ground state at $\Delta > 0$, leading to phonon-assisted excitation of the exciton. Conversely, $|\alpha\rangle$ is primarily excitonic in character at $\Delta < 0$, and thus phonon-assisted de-excitation of the exciton occurs. The blue arrows illustrate the relaxation process corresponding to the emission of an LA phonon, while the red arrows show the competing phonon absorption process. (b)–(e) Phenomenological energy level diagrams of the phonon emission and absorption processes for both positive and negative detunings. For simplicity, the phonon relaxation is incorporated as a virtual state (dashed lines).

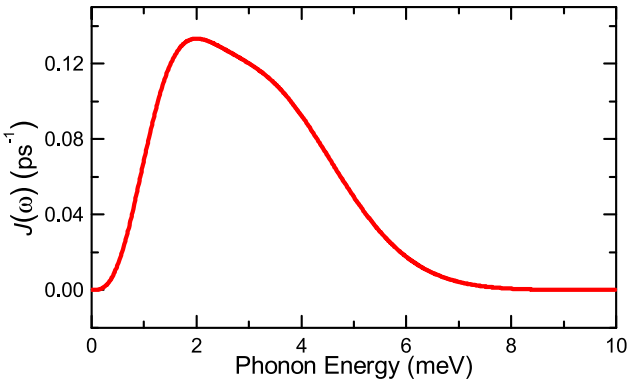

Fig. 3. Plot of the exciton–phonon interaction strength $J(\omega)$ as determined by fitting data measured in Ref. [24]. The interaction strength peaks at a cutoff of around 2 meV and rolls off rapidly beyond this.

Figure 1 illustrates the dressed state energies (green lines), admixture angle θ (black line), and occupancy of $|\beta\rangle$ (blue line) against time during the passage of a $\Theta = 8.5\pi$ pulse with $\hbar\Delta = 1$ meV. The pulse has a temporal FWHM of 16.8 ps and is centered on $t = 0$. The figure illustrates that the dressed state splitting rises and falls in line with the envelope of the laser pulse [34], and that the admixing angle follows it. The transfer of population into $|\beta\rangle$ occurs only while the states are admixed, tuning the system from weakly to strongly vibronic and back again in approximately 20 ps.

The transfer between the dressed states shown in Fig. 1 can be exploited to achieve ultrafast incoherent excitation and de-excitation of the exciton by detuned laser pulses. Beginning with excitation, in the case of $\Delta > 0$ the higher energy dressed state $|\alpha\rangle$ is dominated by the crystal ground state, while the lower energy state $|\beta\rangle$ is primarily excitonic in character, as illustrated to the right in Fig. 2(a). During the passage of the laser pulse, admixing of the states allows relaxation to occur from $|\alpha\rangle$ to $|\beta\rangle$ by emission of an LA phonon (Γ^+_{ph}—blue arrows).

For a sufficiently strong pulse, most of the population relaxes into $|\beta\rangle$ and the exciton-dominated nature of $|\beta\rangle$ means that the population of the exciton state after the passage of the pulse is high. Figure 2(b) shows a phenomenological level diagram of the phonon-assisted excitation process, while Fig. 2(c) illustrates the competing process whereby a phonon is absorbed (Γ^-_{ph}—red arrows) and a photon emitted (purple arrow). The latter process is weak at low temperatures.

In the case of $\Delta < 0$, the main difference is that the characteristics of the dressed states are now exchanged. During the passage of the laser pulse, relaxation by phonon emission again occurs into the $|\beta\rangle$ state. However, as this state is now dominated by the crystal ground state, the effect of the relaxation is instead to de-excite the exciton with most of the population left in the ground state after the passage of the laser pulse. Figure 2(d) shows an illustrative schematic of this process with the emission of a photon (purple arrow) accounting for the rest of the energy difference. This emission is stimulated by the laser and, hence, the process is termed LA-phonon stimulated emission (LAPSE). Figure 2(e) illustrates the competing phonon absorption process.

The physical factors that determine the efficiency of phonon-assisted excitation and de-excitation may be considered by analyzing the parameters that enter Eq. (4). The degree of admixing increases by increasing the driving strength (Ω_R) or decreasing the detuning (Δ) (noting that Δ should exceed the laser linewidth to exclude resonant coherent driving), leading to more efficient relaxation. However, both of these dependencies are modified by the properties of the phonon bath. The exciton–phonon interaction strength is characterized by the function $J(\omega)$, which increases with ω at first due to the rising phonon density of states, and then rolls off rapidly beyond a cutoff frequency, which is typically around 1–2 meV [12]. The physical origin of this cutoff is the point at which the phonon wavelength is comparable to the spatial FWHM of the carrier wavefunction. As a result, the cutoff frequency depends strongly on the height of the QD, and phonon sideband measurements may be used to probe the confinement potential. A plot of $J(\omega)$ derived from fitting data measured in Ref. [24] is shown in Fig. 3. The form of $J(\omega)$ modifies the detuning dependence of the DVC and also weakens the exciton–phonon interaction for very strong driving where the effective Rabi frequency Λ exceeds the cutoff frequency (although this regime has not been reached in the present experiments).

The processes of interest for DVC both rely on phonon emission rather than phonon absorption and are, therefore, highly sensitive to temperature. Increasing the bath temperature increases the phonon occupation, leading to a higher probability of phonon emission and thus faster relaxation. However, the probability of phonon absorption generally increases more than that of emission. As illustrated by the red arrows

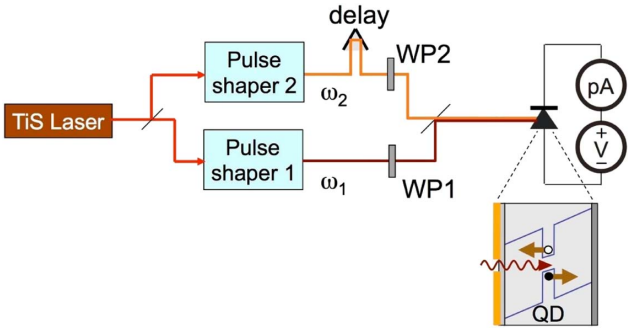

Fig. 4. Experimental arrangement. A femtosecond pulsed laser beam is split into two paths. The wavelength, FWHM, arrival time, and polarization of the two pulses are controlled independently by the pulse shapers, delay stage, and wave plates (WP). Finally the two beams are combined and sent to the sample, which is kept in a variable temperature liquid-He cryostat. The exciton created by the laser pulse is measured by detecting the PC generated from the QD.

in Fig. 2(a), phonon absorption (Γ_{ph}^{-}) causes the opposite population transfer between the dressed states to phonon emission (Γ_{ph}^{+}—blue arrows) and results in a lower final occupation of $|\beta\rangle$. As such, DVC processes are generally optimized by low bath temperatures to maximize the difference between phonon emission and absorption rates. The influence of temperature on phonon-assisted excitation is studied both experimentally and theoretically in Section 5.

It is only by combining all of these influences that the full spectral and power dependence of the DVC emerges. Analytical approximations do not accurately predict these dependencies; hence, numerical methods such as path integral calculations [23,24] or the master equation formalism [14] are employed. The result of such calculations is a broad (few meV) spectral sideband feature that appears at high driving strengths and persists until the Rabi splitting exceeds the cutoff energy for phonon coupling.

3. EXPERIMENTAL METHODS

Figure 4 gives a schematic diagram of the apparatus used in the experiments. A mode-locked Ti:sapphire laser with 76 MHz pulse repetition rate is passed through two pulse shapers to obtain independently tunable pulses from within the ~10 meV bandwidth of the ~100 fs pulses [35]. The spectral FWHM is selected to be either 0.2 or 0.42 meV corresponding to a Fourier-transform-limited pulse duration of 16.8 or 8 ps. Both pulses pass through wave plates to permit independent control of their polarizations, and one of them follows a variable path length controlled by a delay stage to enable pump–probe experiments with precise relative time control.

The pulses are incident on the sample in a variable temperature liquid He cryostat with piezo actuators for precise positioning of the sample relative to the focused beams. The sample consists of a layer of InGaAs QDs embedded in a Schottky diode. The exciton created by the laser pulses can be measured by detecting the photocurrent (PC) from the QD when a reverse bias is applied to the diode [11]. Further details of the experimental methods may be found in Ref. [36].

4. COHERENCE AND SPIN PERSISTENCE OF DYNAMIC VIBRONIC COUPLING

In Ref. [24], Quilter *et al.* demonstrated the DVC by creating a QD exciton using a slightly blueshifted laser pulse via emitting an LA phonon. Since it involves emission of a phonon, in theory the DVC should be incoherent, namely, the phase of the exciton is random relative to that of the blueshifted laser pulse. The exciton coherence time in this case is limited by the phonon relaxation time (a few picoseconds [37]). To demonstrate the incoherent nature of the DVC, we performed Ramsey-like interference measurements [38–40] using an unstabilized interferometer.

The QD is pumped with a blue-detuned pulse with $\hbar\Delta = 1$ meV at $t = 0$. The pulse area (8.4π) is chosen to give an exciton population of $C_X = 0.5$. (Note that this is slightly higher than in Ref. [24] due to different laser detunings.) Once the QD has been excited, the state is then probed by a $\pi/2$ pulse resonant with the exciton at $t = \tau_{\text{delay}}$. The relative phase between the pump and probe is proportional to τ_{delay}. If the system is coherent, the probe pulse drives the QD to either $C_X = 0$ or 1 depending on the phase of the exciton with respect to the probe. The degree of coherence can then be determined by measuring the visibility of the Ramsey fringes as a function of τ_{delay}. In our experiment, the relative phase between the pump and probe is unstabilized, and so the final state fluctuates randomly within the visibility envelope.

Figure 5 shows the time-integrated PC signal versus τ_{delay}. The red squares show the results for phonon-sideband pumping with $\hbar\Delta = 1$ meV. A flat line is observed, with no Ramsey-like fringes, indicating that the phase of the exciton is random relative to the probe pulse. The slow increase of the PC signal in time is most probably related to the decay of the exciton population created by the pump via electron/hole tunneling before the arrival of the probe. By contrast, the black dots show the results measured when the pump pulse is tuned to resonance ($\Delta = 0$) and the pulse area is set to $\pi/2$. In this fully resonant situation, Ramsey-like fringes are

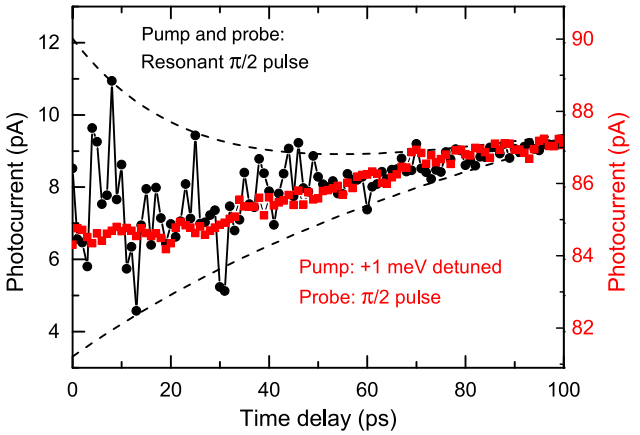

Fig. 5. Comparison of Ramsey-like fringe data on the exciton for pumping in the phonon sideband (red) and at the exciton (black) at $T = 4.2$ K. In both cases, the second $\pi/2$-pulse is resonant with the exciton. The pulse area Θ of the +1 meV detuned pump pulse is set to be 8.4π to generate $C_X = 0.5$. The dashed line is a guide to the eye.

observed provided τ_{delay} is shorter than or comparable to the exciton coherence time. The exciton coherence time of ~40 ps can be estimated from the dashed line envelope and is limited by the electron tunneling rate [40]. The incoherent nature of the DVC is clearly demonstrated by the absence of the fluctuations in the PC signal in the red data compared with that in the black data. Our result is consistent with that reported by Weiler *et al.* [19], showing that the coherence properties of the emitted photon created via DVC is much worse than resonant CW excitation. However, Bounouar *et al.* [25] demonstrate that the photons generated by quasi-resonantly pumping the biexciton state using pulsed excitation show similar coherence properties as measured in the resonant two-photon scheme. The relation of the coherence properties of the emitted photon and exciton prepared via DVC is still unclear and require further investigation.

It should be noted that the fact that the DVC process is incoherent does not imply that the exciton spin is random. The results published in Ref. [24] clearly show in the phonon-assisted excitation process that the spin of the exciton is the same as that of the photon in the blueshifted laser pulse. In theory, the spin of the emitted photon in the LAPSE process should also be the same as that of the laser photon, since the phonon-assisted excitation and de-excitation are two opposite processes in the dressed state picture [see Fig. 2(a)].

Directly demonstrating the spin-preserving nature of the LAPSE process is beyond the scope of this paper, but it has been observed that the LAPSE process occurs only when the spin of the exciton and the redshifted laser pulse are the same. This spin selectivity of the LAPSE process can be demonstrated by preparing a spin-up exciton using a σ^+ circularly polarized π pulse and then comparing the effects of co- or cross-polarized redshifted pulses. In the text below, we call this redshifted pulse the "LAPSE pulse." Figure 6 shows the results of such a comparison as a function of the detuning of the LAPSE pulse. The first π pulse creates a reference PC level corresponding to an exciton population of 1. This reference level is calibrated by ΔPC at $\hbar\Delta < 0$ measured with a weak ($\Theta = \pi$) LAPSE pulse [see the black line in Fig. 6(a)]. In this spectrum, no phonon-assisted de-excitation occurs since the exciton–phonon coupling in the weak driving regime is negligible. However, in the case that a strong ($\Theta = 7.35\pi$) co-polarized LAPSE pulse is applied, efficient de-excitation occurs, as shown by the negative sideband relative to the reference level at $\hbar\Delta < 0$ [see the red line in Fig. 6(a)]. By contrast, no negative sideband occurs in the cross-polarized case [see the red line in Fig. 6(b)]. (The peak and weak positive sideband in Fig. 6(b) at around $\hbar\Delta = -1.96$ meV can be attributed to the resonant and phonon-assisted excitation of the biexciton.) The absence of the negative phonon sideband in the cross-polarized differential spectrum unambiguously proves the spin selectivity of the LAPSE process. Based on this observation and the fact that the spin is preserved during the emission of the LA phonon as demonstrated in Ref. [24], we conclude that DVC is incoherent, but spin-preserving.

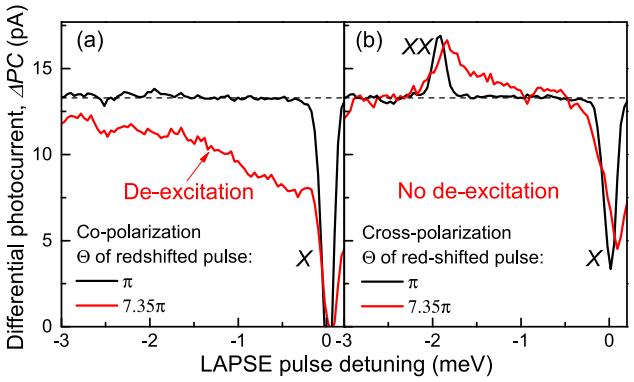

Fig. 6. Demonstration of the spin selectivity of the LAPSE process. (a), (b) Differential PC spectra ΔPC were obtained by preparing an exciton in the QD using a circularly polarized π pulse and then measuring the PC as a function of a co-/cross-polarized LAPSE pulse. To isolate the PC signal of the QD under study from other QDs in the same sample, a reference spectrum measured with only a redshifted laser pulse is subtracted. The pulse area Θ of the redshifted laser pulse is (black) π or (red) 7.35π. The delay time between the π pulse and the redshifted pulse is 17 ps. *XX*: biexciton.

5. TEMPERATURE DEPENDENCE OF DYNAMIC VIBRONIC COUPLING

In previous studies, DVC processes have mainly been studied at $T = 4.2$ K [14,24,25], the temperature of liquid He. It is interesting, however, to consider the influence of temperature on the mechanism. Increasing the temperature increases the strength of the exciton–phonon interaction, observed, for instance, by stronger damping and frequency renormalization of excitonic Rabi rotations [12]. As discussed in Section 2, this increases the rate of phonon relaxation between the dressed states, and, for relatively weak excitation, increases the resulting exciton population as more population relaxes during the pump pulse. This is shown by the higher population observed at positive detuning for $T = 15$ K (red triangles) compared to $T = 4.2$ K (black circles) in Fig. 7(a) and also by the steeper initial gradient for higher temperatures observed in the calculations of Fig. 7(b).

However, this does not illustrate the complete picture. At higher bath temperatures, the increased number of phonons increases the probability of the competing process at positive detuning, namely, the annihilation of an exciton by absorption of a phonon [see Fig. 2(c)]. This is shown in our measurements by the reduced detuning asymmetry of the phonon sidebands at $T = 15$ K in Fig. 7(a). The origin of the negative detuning signal is the creation of exciton population by phonon absorption, illustrating the increased probability of the competing absorption processes discussed in Section 2. As such, the reduced asymmetry in the phonon sidebands can be considered equivalent to the reduced difference between the probability of phonon emission and absorption.

The consequence of this competition is that, for driving that is sufficiently strong to allow complete relaxation [i.e., in the plateau region of Fig. 7(b)], the final occupancy of the exciton state is in fact lower at higher temperatures owing to the thermalization of the dressed states. This is illustrated by the reduced maximum exciton population attained at higher bath temperatures in Fig. 7(b). In summary, a higher bath temperature will lead to a faster rise with pulse area, but a lower maximum population transfer by DVC. As such, increasing the bath

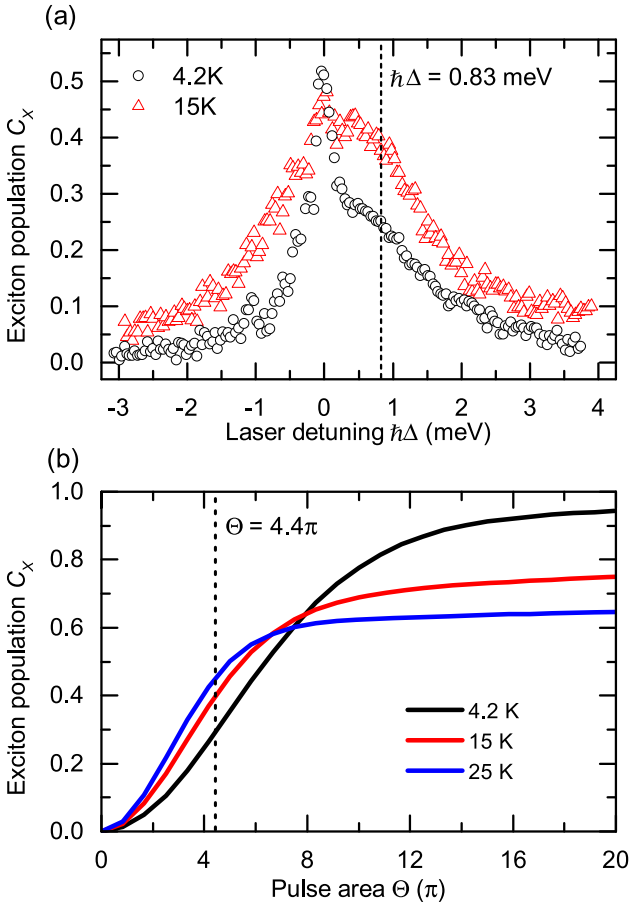

Fig. 7. (a) Exciton population versus laser detuning (Δ) at 15 K (red triangles) compared to 4.2 K (black circles) for excitation with pulse area $\Theta = 4.4\pi$. The dashed line indicates a detuning of $\hbar\Delta = +0.83$ meV. (b) Calculated variation of the exciton population versus pulse area (Θ) for $T = 4.2$ K (black), $T = 15$ K (red), and $T = 25$ K (blue) for positive detuning of $\hbar\Delta = +0.83$ meV. The dashed line shows $\Theta = 4.4\pi$.

temperature may provide a means to enhance DVC processes when the driving is relatively weak, as in Fig. 7(a).

6. PICOSECOND TIMESCALE EXCITATION AND DE-EXCITATION

The three first experimental observations of DVC in QDs [14,24,25] focused on the LA-phonon-assisted excitation process [see Figs. 2(a) and 2(b)]. Recently Liu *et al.* have demonstrated the reverse process—LA-phonon-assisted de-excitation [see Fig. 2]—by observing the reduction of the exciton population of an excited QD by a redshifted laser pulse [26]. A combination of the LA-phonon-assisted excitation and de-excitation processes allows us to create and destroy an exciton within picosecond time scales, enabling ultrafast incoherent optical switching with a single QD much faster than the exciton radiative lifetime (a few nanoseconds [24,41]).

To demonstrate this, a two-color pump–probe experiment is performed with a blueshifted (excitation) and redshifted (de-excitation) pulse with the same pulse area. The pulses are equally detuned ($\hbar\Delta = \pm 0.7$ meV) from the exciton. At negative delay times, the excitation pulse creates a certain exciton population corresponding to the background PC level. The de-excitation pulse arrives before excitons are created, and therefore does nothing. When the two pulses overlap, the PC signal decreases to a minimum within 20 ps, as shown in Fig. 8. This occurs due to erasure of the exciton created by the excitation pulse by the de-excitation pulse. The PC signal then slowly recovers due to the electron tunneling out from the QD before the de-excitation pulse arrives [26]. The increase of the PC signal at ~ – 10 ps is most probably related to the phonon-assisted excitation of the biexciton by a very small portion of imperfectly circularly polarized light in the excitation/de-excitation pulses. Figure 8(b) shows the calculated exciton population with parameters similar to those of Fig. 8(a). The phase relation between the two pulses has been assumed to be random, and we show the average of multiple repetitions of the simulation. The numerically complete path-integral method takes into account the electron tunneling in the PC experiment by incorporating it as a Lindblad-type relaxation term [26]. Before the arrival of the pulses, the QD is assumed to be in the ground state and the phonon modes follow a thermal distribution. This model well reproduces the de-excitation of the QD and the subsequent recovery of the PC signal. The oscillation of the exciton population at ~5 ps is not clearly visible in the measured data in Fig. 8(a) due to the limited time resolution of the experiment.

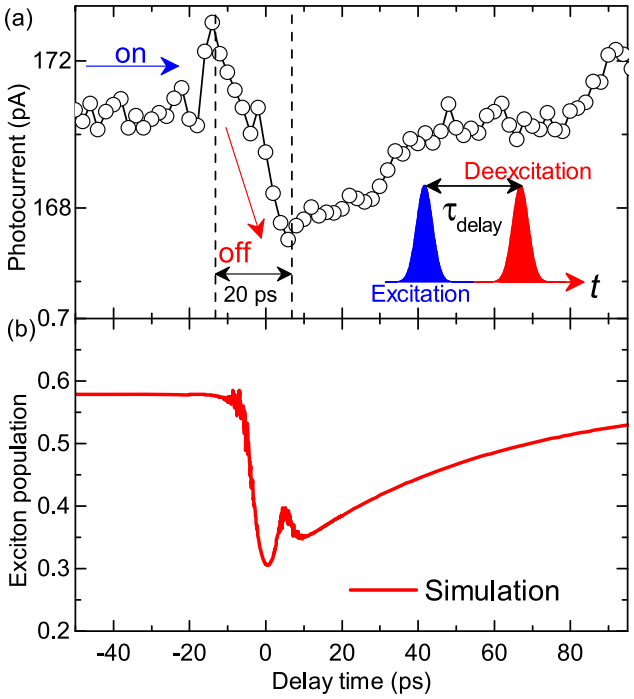

Fig. 8. (a) PC signal measured with positively and negatively detuned control pulses as a function of the delay time $\tau_{delay} = t_{OFF} - t_{ON}$, where t_{OFF} and t_{ON} are the arrival time of the de-excitation and excitation pulses, respectively. $\hbar\Delta = \pm 0.7$ meV; $\Theta = 5.25\pi$; FWHM = 0.42 meV; Pulse duration = 8 ps. Inset: pulse sequence. (b) Exciton population calculated in the two-color pump–probe measurement using parameters similar to those of Fig. 8(a). $\hbar\Delta = \pm 0.7$ meV; $\Theta = 5.25\pi$; pulse duration = 10 ps.

The ~20 ps excitation/de-excitation time in our experiment is determined by the laser pulse duration. The ultimate limit is set by the phonon thermalization time (a few picoseconds [37]). We note that, in contrast to the optical switching scheme employing resonant coherent excitation [15], our scheme is robust against the fluctuation of laser power and detuning [23]. Furthermore, the incoherent nature of the phonon-assisted relaxation process determines that no phase locking is needed, in contrast to fully coherent excitation schemes.

7. CONCLUSIONS AND OUTLOOK

In summary, we have investigated the dynamic vibronic coupling in a single InGaAs QD. The DVC enables the population inversion and ultrafast depopulation of a QD by incoherent quasi-resonant excitation with the assistance of phonons [24,26]. We prove that the DVC is an incoherent process by performing Ramsey-like interference measurements. The temperature dependence study shows that, at high temperature, the phonon-assisted absorption induced by both the blue-shifted and redshifted laser pulses are enhanced, and the strong asymmetry of the phonon sidebands observed at low temperatures disappears. Furthermore, we demonstrate that it is possible to create and destroy an exciton within a pulse-width limited picosecond time scale by combining a blue-detuned and a red-detuned pulse, opening the door to ultrafast incoherent optical switching with a single QD [15,42,43]. The DVC may also be used to reduce the timing jitter of single/entangled photon sources [8,44] or make tunable single QD lasers [45].

Compared with resonant coherent excitation, one factor that limits the potential applications of DVC is the high laser power required to achieve an efficient phonon-assisted excitation/de-excitation. This problem may be solved by incorporating the QD into a nanocavity with a small mode volume where the light–matter interaction is strongly enhanced [8,46]. When cavities are involved, the knowledge of phonon interactions in the strong QD–phonon coupling regime becomes an essential requirement for a full understanding of the behavior of optically driven QDs. Various recent studies have shown new physical phenomena that arise from this coupling [47–51].

Funding. Engineering and Physical Sciences Research Council (EPSRC) (EP/J007544/1); Deutsche Forschungsgemeinschaft (DFG) (AX 17/7-1).

Acknowledgment. The authors thank H.Y. Liu and M. Hopkinson for sample growth.

REFERENCES

1. M. Fox, *Optical Properties of Solids*, 2nd ed. (Oxford University, 2010).
2. J. Klein and J. D. Kafka, "The Ti:sapphire laser: the flexible research tool," Nat. Photonics **4**, 289 (2010).
3. G. Davies, "The Jahn-Teller effect and vibronic coupling at deep levels in diamond," Rep. Prog. Phys. **44**, 787–830 (1981).
4. G. Davies and M. F. Hamer, "Optical studies of the 1.945 eV vibronic band in diamond," Proc. R. Soc. Lond. A **348**, 285–298 (1976).
5. R. Schirhagl, K. Chang, M. Loretz, and C. L. Degen, "Nitrogen-vacancy centers in diamond: nanoscale sensors for physics and biology," Ann. Rev. Phys. Chem. **65**, 83–105 (2014).
6. I. Favero, G. Cassabois, R. Ferreira, D. Darson, C. Voisin, J. Tignon, C. Delalande, G. Bastard, and Ph. Roussignol, "Acoustic phonon sidebands in the emission line of single InAs/GaAs quantum dots," Phys. Rev. B **68**, 233301 (2003).
7. S. L. Portalupi, G. Hornecker, V. Giesz, T. Grange, A. Lemaître, J. Demory, I. Sagnes, N. D. Lanzillotti-Kimura, L. Lanco, A. Auffèves, and P. Senellart, "Bright phonon-tuned single-photon source," Nano Lett. **15**, 6290–6294 (2015).
8. P. Lodahl, S. Mahmoodian, and S. Stobbe, "Interfacing single photons and single quantum dots with photonic nanostructures," Rev. Mod. Phys. **87**, 347–400 (2015).
9. P. G. Eliseev, H. Li, A. Stintz, G. T. Liu, T. C. Newell, K. J. Malloy, and L. F. Lester, "Transition dipole moment of InAs/InGaAs quantum dots from experiments on ultralow-threshold laser diodes," Appl. Phys. Lett. **77**, 262–264 (2000).
10. P. Borri, W. Langbein, S. Schneider, U. Woggon, R. L. Sellin, D. Ouyang, and D. Bimberg, "Ultralong dephasing time in InGaAs quantum dots," Phys. Rev. Lett. **87**, 157401 (2001).
11. A. Zrenner, E. Beham, S. Stuer, F. Findeis, M. Bichler, and G. Abstreiter, "Coherent properties of a two-level system based on a quantum-dot photodiode," Nature **418**, 612–614 (2002).
12. A. J. Ramsay, T. M. Godden, S. J. Boyle, E. M. Gauger, A. Nazir, B. W. Lovett, A. M. Fox, and M. S. Skolnick, "Phonon-induced Rabi-frequency renormalization of optically driven single InGaAs/GaAs quantum dots," Phys. Rev. Lett. **105**, 177402 (2010).
13. T. M. Godden, J. H. Quilter, A. J. Ramsay, Y. Wu, P. Brereton, S. J. Boyle, I. J. Luxmoore, J. Puebla-Nunez, A. M. Fox, and M. S. Skolnick, "Coherent optical control of the spin of a single hole in an InAs/GaAs quantum dot," Phys. Rev. Lett. **108**, 017402 (2012).
14. P.-L. Ardelt, L. Hanschke, K. A. Fischer, K. Müller, A. Kleinkauf, M. Koller, A. Bechtold, T. Simmet, J. Wierzbowski, H. Riedl, G. Abstreiter, and J. J. Finley, "Dissipative preparation of the exciton and biexciton in self-assembled quantum dots on picosecond time scales," Phys. Rev. B **90**, 241404(R) (2014).
15. A. P. Heberle and J. J. Baumberg, "Ultrafast coherent control and destruction of excitons in quantum wells," Phys. Rev. Lett. **75**, 2598–2601 (1995).
16. O. Svelto, S. De Silvestri, and G. Denardo, *Ultrafast Processes in Spectroscopy* (Springer, 1996).
17. J. Shah, *Ultrafast Spectroscopy of Semiconductors and Semiconductor Nanostructures*, 2nd ed. (Springer, 1999).
18. S. Ates, S. M. Ulrich, A. Ulhaq, S. Reitzenstein, A. Löffler, S. Höfling, A. Forchel, and P. Michler, "Non-resonant dot-cavity coupling and its potential for resonant single-quantum-dot-spectroscopy," Nat. Photonics **3**, 724–728 (2009).
19. S. Weiler, A. Ulhaq, S. M. Ulrich, D. Richter, M. Jetter, P. Michler, C. Roy, and S. Hughes, "Phonon-assisted incoherent excitation of a quantum dot and its emission properties," Phys. Rev. B **86**, 241304(R) (2012).
20. K. H. Madsen, S. Ates, J. Liu, A. Javadi, S. M. Albrecht, I. Yeo, S. Stobbe, and P. Lodahl, "Efficient out-coupling of high-purity single photons from a coherent quantum dot in a photonic-crystal cavity," Phys. Rev. B **90**, 155303 (2014).
21. J. Hansom, C. H. H. Schulte, C. Matthiesen, M. J. Stanley, and M. Atatüre, "Frequency stabilization of the zero-phonon line of a quantum dot via phonon-assisted active feedback," Appl. Phys. Lett. **105**, 172107 (2014).
22. P. Borri, W. Langbein, U. Woggon, V. Stavarache, D. Reuter, and A. Wieck, "Exciton dephasing via phonon interactions in InAs quantum dots: dependence on quantum confinement," Phys. Rev. B **71**, 115328 (2005).
23. M. Glässl, A. M. Barth, and V. M. Axt, "Proposed robust and high-fidelity preparation of excitons and biexcitons in semiconductor quantum dots making active use of phonons," Phys. Rev. Lett. **110**, 147401 (2013).
24. J. H. Quilter, A. J. Brash, F. Liu, M. Glässl, A. M. Barth, V. M. Axt, A. J. Ramsay, M. S. Skolnick, and A. M. Fox, "Phonon-assisted population inversion of a single InGaAs/GaAs quantum dot by pulsed laser excitation," Phys. Rev. Lett. **114**, 137401 (2015).
25. S. Bounouar, M. Müller, A. M. Barth, M. Glässl, V. M. Axt, and P. Michler, "Phonon-assisted robust and deterministic two-photon

biexciton preparation in a quantum dot," Phys. Rev. B **91**, 161302 (2015).
26. F. Liu, L. M. P. Martins, A. J. Brash, A. M. Barth, J. H. Quilter, V. M. Axt, M. S. Skolnick, and A. M. Fox, "Ultrafast depopulation of a quantum dot by LA-phonon-assisted stimulated emission," Phys. Rev. B **93**, 161407(R) (2016).
27. A. J. Ramsay, A. V. Gopal, E. M. Gauger, A. Nazir, B. W. Lovett, A. M. Fox, and M. S. Skolnick, "Damping of exciton Rabi rotations by acoustic phonons in optically excited InGaAs/GaAs quantum dots," Phys. Rev. Lett. **104**, 017402 (2010).
28. L. Monniello, C. Tonin, R. Hostein, A. Lemaitre, A. Martinez, V. Voliotis, and R. Grousson, "Excitation-induced dephasing in a resonantly driven InAs/GaAs quantum dot," Phys. Rev. Lett. **111**, 026403 (2013).
29. A. J. Ramsay, T. M. Godden, S. J. Boyle, E. M. Gauger, A. Nazir, B. W. Lovett, A. V. Gopal, A. M. Fox, and M. S. Skolnick, "Effect of detuning on the phonon induced dephasing of optically driven InGaAs/GaAs quantum dots," J. Appl. Phys. **109**, 102415 (2011).
30. Y. J. Wei, Y. M. He, M. C. Chen, Y. N. Hu, Y. He, D. Wu, C. Schneider, M. Kamp, S. Höfling, C. Y. Lu, and J.-W. Pan, "Deterministic and robust generation of single photons from a single quantum dot with 99.5% indistinguishably using adiabatic rapid passage," Nano Lett. **14**, 6515–6519 (2014).
31. R. Mathew, E. Dilcher, A. Gamouras, A. Ramachandran, H. Y. Shi Yang, S. Freisem, D. Deppe, and K. C. Hall, "Subpicosecond adiabatic rapid passage on a single semiconductor quantum dot: phonon-mediated dephasing in the strong-driving regime," Phys. Rev. B **90**, 035316 (2014).
32. B. Krummheuer, V. M. Axt, and T. Kuhn, "Theory of pure dephasing and the resulting absorption line shape in semiconductor quantum dots," Phys. Rev. B **65**, 195313 (2002).
33. A. M. Barth, S. Lüker, A. Vagov, D. E. Reiter, T. Kuhn, and V. M. Axt, "Fast and selective phonon-assisted state preparation of a quantum dot by adiabatic undressing," Phys. Rev. B, arXiv:1601.07886 (to be published).
34. S. J. Boyle, A. J. Ramsay, A. M. Fox, M. S. Skolnick, A. P. Heberle, and M. Hopkinson, "Beating of exciton dressed states in a single semiconductor InGaAs/GaAs quantum dot," Phys. Rev. Lett. **102**, 207401 (2009).
35. S. J. Boyle, A. J. Ramsay, F. Bello, H. Y. Liu, M. Hopkinson, A. M. Fox, and M. S. Skolnick, "Two-qubit conditional quantum-logic operation in a single self-assembled quantum dot," Phys. Rev. B **78**, 075301 (2008).
36. A. J. Brash, L. M. P. P. Martins, F. Liu, J. H. Quilter, A. J. Ramsay, M. S. Skolnick, and A. M. Fox, "High-fidelity initialization of long-lived quantum dot hole spin qubits by reduced fine-structure splitting," Phys. Rev. B **92**, 121301 (2015).
37. D. P. S. McCutcheon and A. Nazir, "Quantum dot Rabi rotations beyond the weak exciton-phonon coupling regime," New J. Phys. **12**, 113042 (2010).
38. H. Kamada, H. Gotoh, J. Temmyo, T. Takagahara, and H. Ando, "Exciton Rabi oscillation in a single quantum dot," Phys. Rev. Lett. **87**, 246401 (2001).
39. S. Stufler, P. Ester, A. Zrenner, and M. Bichler, "Exciton Rabi oscillation in a single quantum dot," Phys. Rev. B **72**, 121301(R) (2005).
40. R. S. Kolodka, A. J. Ramsay, J. Skiba-Szymanska, P. W. Fry, H. Y. Liu, A. M. Fox, and M. S. Skolnick, "Inversion recovery of single quantum-dot exciton based qubit," Phys. Rev. B **75**, 193306(R) (2007).
41. P. A. Dalgarno, J. M. Smith, J. McFarlane, B. D. Gerardot, K. Karrai, A. Badolato, P. M. Petroff, and R. J. Warburton, "Coulomb interactions in single charged self-assembled quantum dots: radiative lifetime and recombination energy," Phys. Rev. B **77**, 245311 (2008).
42. T. Volz, A. Reinhard, M. Winger, A. Badolato, K. J. Hennessy, E. L. Hu, and A. Imamoglu, "Ultrafast all-optical switching by single photons," Nat. Photonics **6**, 607–611 (2012).
43. E. Cancellieri, A. Hayat, A. M. Steinberg, E. Giacobino, and A. Bramati, "Ultrafast Stark-induced polaritonic switches," Phys. Rev. Lett. **112**, 053601 (2014).
44. D. Heinze, D. Breddermann, A. Zrenner, and S. Schumacher, "A quantum dot single-photon source with on-the-fly all-optical polarization control and timed emission," Nat. Commun. **6**, 8473 (2015).
45. M. Nomura, N. Kumagai, S. Iwamoto, Y. Ota, and Y. Arakawa, "Laser oscillation in a strongly coupled single-quantum-dot-nanocavity system," Nat. Phys. **6**, 279–283 (2010).
46. S. Hughes and H. J. Carmichael, "Phonon-mediated population inversion in a semiconductor quantum-dot cavity system," New J. Phys. **15**, 053039 (2013).
47. D. P. S. McCutcheon and A. Nazir, "Model of the optical emission of a driven semiconductor quantum dot: phonon-enhanced coherent scattering and off-resonant sideband narrowing," Phys. Rev. Lett. **110**, 217401 (2013).
48. Y.-J. Wei, Y. He, Y.-M. He, C.-Y. Lu, J.-W. Pan, C. Schneider, M. Kamp, S. Höfling, D. P. S. McCutcheon, and A. Nazir, "Temperature-dependent Mollow triplet spectra from a single quantum dot: Rabi frequency renormalization and sideband linewidth insensitivity," Phys. Rev. Lett. **113**, 097401 (2014).
49. K. Müller, K. A. Fischer, A. Rundquist, C. Dory, K. G. Lagoudakis, T. Sarmiento, Y. A. Kelaita, V. Borish, and J. Vučković, "Ultrafast polariton-phonon dynamics of strongly coupled quantum dot-nanocavity systems," Phys. Rev. X **5**, 031006 (2015).
50. J. Iles-Smith and A. Nazir, "Quantum correlations of light and matter through environmental transitions," Optica **3**, 207 (2016).
51. F. Hargart, M. Müller, K. Roy-Choudhury, S. L. Portalupi, C. Schneider, S. Höfling, M. Kamp, S. Hughes, and P. Michler, "Cavity-enhanced simultaneous dressing of quantum dot exciton and biexciton states," Phys. Rev. B **93**, 115308 (2016).

Publication 9

Compensation of phonon-induced renormalization of vacuum Rabi splitting in large quantum dots: Towards temperature-stable strong coupling in the solid state with quantum dot-micropillars

C. Hopfmann, A. Musial, M. Strauß, A. M. Barth, M. Glässl, A. Vagov, M. Strauß, C. Schneider, S. Höfling, M. Kamp, V. M. Axt and S. Reitzenstein

Physical Review B **92**, 245403 (2015)

DOI: 10.1103/PhysRevB.92.245403

Compensation of phonon-induced renormalization of vacuum Rabi splitting in large quantum dots: Towards temperature-stable strong coupling in the solid state with quantum dot-micropillars

C. Hopfmann,[1] A. Musiał,[1,2,*] M. Strauß,[1] A. M. Barth,[3] M. Glässl,[3] A. Vagov,[3] M. Strauß,[4] C. Schneider,[4] S. Höfling,[4,5] M. Kamp,[4] V. M. Axt,[3] and S. Reitzenstein[1]

[1]*Institut für Festkörperphysik, Technische Universität Berlin, Hardenbergstraße 36, 10623 Berlin, Germany*

[2]*Laboratory for Optical Spectroscopy of Nanostructures, Department of Experimental Physics, Faculty of Fundamental Problems of Technology, Wrocław University of Technology, Wybrzeże Wyspiańskiego 27, 50-370 Wrocław, Poland*

[3]*Institut für Theoretische Physik III, Universität Bayreuth, 95440 Bayreuth, Germany*

[4]*Technische Physik, Physikalisches Institut and Wilhelm-Conrad-Röntgen-Research Center for Complex Material Systems, Universität Würzburg, Am Hubland, D-97074 Würzburg, Germany*

[5]*SUPA, School of Physics and Astronomy, University of St. Andrews, St. Andrews, KY16 9SS, United Kingdom*

(Received 1 September 2015; published 3 December 2015)

We study experimentally the influence of temperature on the emission characteristics of quantum dot-micropillars in the strong coupling regime of cavity quantum electrodynamics (cQED). In particular, we investigate its impact on the vacuum Rabi splitting (VRS) and we address the important question of the temperature stability of the coherent coupling regime in a semiconductor system, which is relevant in view of both fundamental study and future applications. To study the temperature dependence we investigate an unprecedentedly large number of strong coupling cases (89) in a wide temperature range from 10 up to 50 K, which constitutes a good basis for statistical analysis. The experiment indicates a statistically significant increase of the VRS with temperature in contrast to an expected decrease of the VRS due to the dephasing induced by acoustic phonons. From the theoretical point of view, the phonon-induced renormalization of the VRS is calculated using a real-time path-integral approach for strongly confined quantum dots (QDs), which allows for a numerical exact treatment of the coupling between the QD and a continuum of longitudinal acoustic phonons. The absence of the expected decrease of the VRS with temperature in our experimental data can be attributed to a unique optical property of laterally extended $In_{0.4}Ga_{0.6}As$ QDs used in this study. Their electronic structure facilitates an effective temperature-driven increase of the oscillator strength of the excitonic state by up to 40% in the given temperature range. This leads to enhanced light-matter interaction and overcompensates the phonon-related decrease of the VRS. The observed persistence of strong coupling in the presence of phonon-induced decoherence demonstrates the appealing possibility to counteract detrimental phonon effects in the cQED regime via engineering the electronic structure of QDs.

DOI: 10.1103/PhysRevB.92.245403 PACS number(s): 78.67.Hc, 63.20.kk, 78.55.Cr, 42.50.Pq

I. INTRODUCTION

The first experimental observations of strong coupling between a single exciton (X) and a single photon realized in semiconductor microcavities [1,2] have triggered enormous research activities in the important field of cavity quantum electrodynamics (cQED). The huge interest in quantum dot (QD)-microcavity systems is motivated by their relevance in both the study on fundamental aspects of quantum optics [3] as well as possible applications in quantum technology. The strong coupling regime is of particular interest because it could pave the way for the implementation of quantum networks [4] or quantum computation schemes [5,6], and to couple its building blocks via flying qubits. In order to implement such complex systems relying on the strong coupling regime, it is crucial that the light-matter interaction rate exceeds dissipative loss rates, which puts stringent requirements on the device technology. At low temperatures cavity photon losses are still the main source of dissipation, despite the significant optimization of fabrication techniques which has led to a strong increase of the quality (Q) factors of micro- and nanocavities [7,8]. The situation can change significantly at elevated temperatures when phonon-related dissipation sets in, which is of particular importance for possible applications. In fact, a strong influence of phonons on cQED phenomena has been predicted theoretically [9–16], but the few existing experimental observations are rather limited [17–19].

In this work we focus on investigating the influence of temperature on the vacuum Rabi splitting (VRS) in a strongly coupled QD-microcavity system. The experimental studies have been performed on high-Q low-mode volume micropillar cavities with a single layer of self-assembled $In_{0.4}Ga_{0.6}As$ QDs as the active medium. Within a statistical approach, 89 strong coupling cases with different resonance temperatures have been studied to establish the temperature dependence of the VRS. It should be noted that the temperature range from 10 to 50 K covered by our investigation of coupled QD-micropillars is by a factor of 4 larger than in a previous study on a single QD-nanocavity system by Ota *et al.* [17].

The obtained experimental results were compared and contrasted with a model of the QD-micropillar accounting for the influence of acoustic phonons and photon losses on the VRS in the case of strongly confined QDs. To this end we used a hybrid approach combining a numerically exact microscopic calculation of phonon-related pure dephasing [20] with a phenomenological treatment of the cavity photon losses [21]. We thus present a comprehensive theoretical study

*anna.musial@physik.tu-berlin.de

on the influence of the properties of both the emitter as well as of the cavity (QD size, cavity Q-factor, and light-matter coupling constant—g) on the vacuum Rabi splitting renormalization.

The paper is organized as follows: Sec. II introduces the investigated structures and the experimental setup. Section III describes and justifies the applied statistical approach. In Sec. IV the experimental results are presented. Section V addresses theoretically the VRS behavior under influence of acoustic phonons and comprises a comparison with the experimental results. Section VI concludes the paper.

II. EXPERIMENT

The systems under study are QD-micropillar cavities. The planar microcavity consists of a GaAs λ cavity with high reflectivity AlAs/GaAs distributed Bragg reflectors (DBRs)—26 (30) $\lambda/4$ pairs on the top (bottom) side, respectively. The micropillars are defined by high-resolution electron beam lithography and patterned by plasma etching of the planar microcavity [7]. In this way high Q-factor (13 000 on average) microcavities with a nominal diameter of 1.8 μm (mode volume: 0.43 μm^3 or $10(\frac{\lambda}{n})^3$, where λ is a cavity resonance wavelength in vacuum and n is the effective refractive index of the cavity material), are fabricated. The active medium consists of a single layer of large $In_{0.4}Ga_{0.6}As$ QDs featuring a more than a factor of 2 higher oscillator strength (OS) if compared to smaller strongly confined QDs in the same material system [1,22–25]. To differentiate the QDs investigated here from typical strongly confined QDs we refer to them as "large" QDs. The typical dimensions of these nanostructures are: (20–30) nm in width, (20–50) nm in length, and (5–7) nm in the vertical direction (including wetting layer). The increase in the lateral size in the strain-based Stranski-Krastanow growth mode was possible due to lowering the strain via decreasing the amount of indium in the InGaAs alloy compound [26]. This has been proven to be a very effective method of enhancing the oscillator strength of QD transitions, leading to the observation of the strong coupling in the single X–single photon regime in QD-micropillar cavities [1]. It turns out that the structures described above are a perfect choice for our statistical study on the temperature influence on VRS in a wide temperature range since up to 50% of the investigated QD-micropillars allow for the observation of strong coupling.

The spectroscopic studies were performed by means of high-resolution microphotoluminescence (μPL) spectroscopy. The QD-micropillars were excited nonresonantly with a frequency doubled Nd:YAG laser at 532 nm operating in continuous wave mode. The measurements were performed in the low excitation regime (typical excitation power: 10 μW), i.e., well below saturation of the QD X, to prevent excitation power-induced dephasing of the excitonic system. The excitation was focused on the chosen micropillar via a long working-distance (20 mm) microscope objective (0.4 numerical aperture) which is simultaneously used for the detection. The spatial resolution of the optical setup is about 3 μm, which enables addressing individual micropillars—the distance between adjacent micropillars is 10 μm. The sample was mounted in a continuous-flow helium cryostat enabling temperature variation in the range of 5–340 K. The emission was spectrally resolved using a 0.75-m-focal-length spectrometer equipped with a liquid nitrogen-cooled Si-CCD detector providing an overall spectral resolution of about 25 μeV.

III. EXPERIMENTAL METHODOLOGY: STATISTICAL APPROACH

Previous experimental reports on the temperature dependence of the Rabi splitting were restricted to low temperatures below 15 K, very narrow temperature ranges (12 K at most) [17,19] and standard strongly confined InAs QDs. In the low temperature regime (below 10 K) the dominating effect is the influence of the imbalance between phonon absorption- and emission-assisted processes on off-resonant QD-cavity coupling. Additionally, a monotonic decrease of VRS up to 14.8 K attributed to the phonon-induced reduction of the light-matter coupling strength was observed. Up till now the latter has not been investigated experimentally at higher temperatures. In Ref. [19] the Rabi splitting of a coherently driven QD has been investigated and the decrease of the Mollow-triplet sidebands splitting with increasing temperature was observed and attributed to phonon-induced renormalization of the Rabi splitting. This study was also limited to temperatures below 15 K and without involving cavity effects. Theoretical reports in the high temperature regime predict a decreasing tendency in renormalized VRS as a function of temperature (for 10, 50, and 100 K) in the case of g values typical for coupled QD-microcavity systems and a reversed trend for much larger coupling strength—typical for laser-driven QDs [21].

Hereby we present an alternative, statistical approach to investigate the influence of the temperature on the emission characteristics of a strongly coupled QD-microcavity system. The comparatively high surface QD density of $10^{10}/cm^2$ leads to a spectral density of approximately five single QD emission lines per meV near the fundamental cavity mode (CM) of a micropillar with $d_c = 1.8\,\mu$m diameter. For this reason and because of high sample quality, we find on average two Xs per micropillar coupling strongly to the fundamental CM which constitutes a good basis for our statistical approach. We used temperature as a tuning parameter to shift the single QD X emission line into resonance with the fundamental CM [Fig. 1(a)]. Therefore, we are limited to QDs with a spectral separation below 1 meV from the CM and are thus probing only a very small subset of the whole QD ensemble which shows an inhomogeneous broadening of 62 meV [26]. As a consequence the investigated QDs are similar in both their vertical size and their In content, which are the crucial factors determining the emission energy. Due to spectral differences in the initial (low-temperature 10 K) separation between the CM and the X transition energy, the resonance conditions are reached for various temperatures. For each QD-micropillar, the vacuum Rabi splitting and the resonance temperature can be determined (we restricted our study to perfect spectral matching, i.e., zero detuning between the energy of the X transition and the CM). Therefore, a comprehensive examination of many strong coupling cases should allow for an observation of the temperature dependence of the VRS. The essential condition for this approach to be successful is that the scattering of the experimental data related

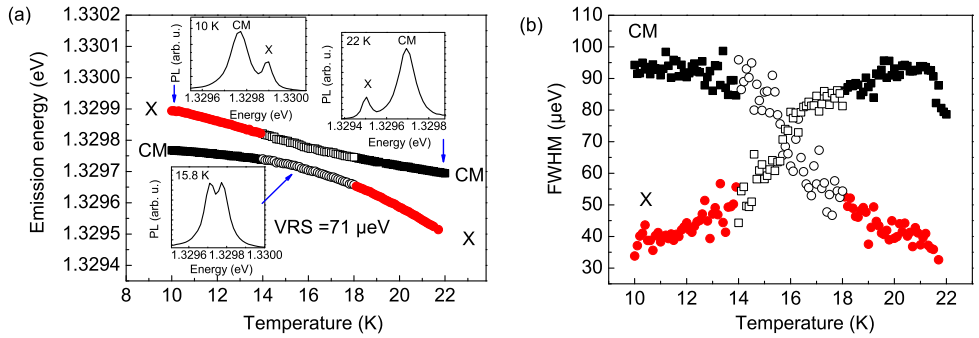

FIG. 1. (Color online) Experimental data for a strongly coupled single $In_{0.4}Ga_{0.6}As$ QD X and a CM of a 1.8 μm diameter micropillar exhibiting a VRS of 71 μeV. (a) Emission energy dependence of the QD X (red dots) and the CM (black squares) on the temperature with characteristic anticrossing on resonance (coupling regime indicated by open symbols) with insets showing exemplary spectra for different detunings between the CM and the QD X (10, 15.8, and 22 K). (b) Temperature dependence of the QD X (red dots) and the CM (black squares) linewidth with characteristic crossing on resonance with the coupling regime indicated by open symbols.

to individual differences between the investigated systems is smaller than the temperature influence. We have good evidence that this is the case for the chosen QD-micropillar system, which will be explained further in this section.

Before we discuss our experimental findings, we first introduce all the factors that can lead to the differences in VRS between various QD-micropillar systems at a given temperature (equal resonance temperatures). If the strongly coupled QD microcavity is simply described as a system of two coupled oscillators and the presence of phonon-induced dephasing is not taken into account, the on-resonance splitting between the two modes depends on the light-matter coupling constant g and the cavity- and exciton-related losses described by the respective linewidths γ_C and γ_X, and is given by [1]

$$\Delta E = 2\sqrt{g^2 - \frac{(\gamma_C - \gamma_X)^2}{16}}. \quad (1)$$

However, for our present systems the homogeneous (lifetime-limited) broadening of the excitonic line γ_X, which at low temperatures is in the range of a few μeV reflecting the relatively short X lifetime of about 350 ps [22,27], is negligible in comparison to the cavity linewidth γ_C, which is up to two orders of magnitude larger for an average Q factor of 13 000 (Fig. 3). In the data post-processing we can restrict ourselves to the pillars exhibiting Q-factors within a specified range to post-select only strong coupling cases in which CM featuring similar γ_C are involved, which allows our ensemble to be homogeneous in terms of this loss mechanism. Additionally, the light-matter coupling constant g itself may vary between the different strong coupling cases due to various properties of the QD-micropillar system, which we shall discuss now. The coupling constant depends on both QD and cavity properties:

$$g_{\max} \propto \sqrt{\frac{f_{\text{osc}}}{V_m}}, \quad (2)$$

where f_{osc} is the oscillator strength of the X transition and V_m is the CM volume. A possible variation of V_m can be neglected as the study is restricted to only one pillar size. A nominal diameter of $dc = 1.8\ \mu$m has been chosen as optimal for the realization of strong coupling because pillars with this diameter exhibit a maximum Q/d_c ratio which is the technological figure of merit for the observation of strong coupling [1]. Due to negligible variations of the mode volume, the light-matter coupling strength is therefore determined by the oscillator strength. In the case of large QDs the oscillator strength is governed mainly by the in-plane size of the QD [28] which, according to structural data, varies in the range of (20–30) nm in width and (20–50) nm in length. This variation results from a local strain at the position where the QD is formed, which is in our case determined by the In concentration. Our previous magneto-optical study [22] on a series of $In_xGa_{1-x}As$ QD structures showed that increasing the In content from 0.3 to 0.6 leads to a reduction of the mean lateral extension of the wave function from 15 to 7 nm and consequently the OS is also reduced from 50 to 10. This indicates that a significant variation of the In content is needed to affect the OS. Therefore, the question arises how strongly the In concentration varies within the ensemble of QDs under study. For the structures used here the emission energy can be used as an indicator for the In concentration, because it has been shown that a variation of the In content leads to a significant change of the QD transition energy [29], which can even overcome the influence of the variation in QD height. Most importantly, this means that the OS and light-matter coupling strength is expected to be similar for all studied QDs.

Beyond the simple approximation of Eq. (1), different QD-micropillar systems can be subjected to different phonon-induced dephasing leading to different renormalization of the VRS at a given temperature. The strength of the X-phonon coupling is typically determined by the size of the smallest extension of the electronic wave function, because this corresponds to the largest contribution of phonon modes in k space [30,31]. As we discussed above, the relevant QD height distribution is expected to be very narrow and therefore also the phonon effects are expected to be similar for all QDs in the probed ensemble.

So far our analysis was restricted to the case of the QD being perfectly matched to the CM. Deviations from this ideal situation will cause a lowering of the coupling constant

which can lead to further differences between the investigated systems. The spectral mismatch (detuning) is not relevant for our discussion, because we limit ourselves to QDs in resonance with the CM. The light-matter coupling is also affected by the dipole direction relative to the electric field as well as by the position of the QD with respect to the center of the cavity, i.e., the distance of the QD to the antinode of the electromagnetic field distribution of the fundamental CM. This is reflected by the formula $g \propto \boldsymbol{dE}$, i.e., the light-matter coupling constant is proportional to the dot product between the dipole moment of the QD transition $\boldsymbol{d}$ as well as the electric field $\boldsymbol{E}$ at the emitter location. As far as the linear polarization directions are concerned, we can, within a first approximation, assume that the QD polarization axes are elongated in crystallographic [1-10] and [110] directions due to the preferential elongation of the nanostructures in [1-10] direction, as proved by structural studies [26]. On the other hand, the polarization of the cavity modes is related to a slight unintentional deviation from the circular cross section which lifts the degeneracy of the two fundamental modes. The nondegenerate modes are linearly polarized perpendicular to each other and tilted on average by 45 deg with respect to the QD elongation direction [7,32]. Even though distinguished optical axes are present in our system, local strain and piezoelectric field distributions can still lead to deviations from the crystallographic directions described above. The largest deviations observed in the case of self-assembled QDs without rotational symmetry are up to 20° [33], which still translates into only 6% variation in the coupling constant. On the other hand, the spatial mismatch between the QD and the CM can vary in a broad range from the QD being located in the very center of the micropillar and at its edge. The maximal coupling constant expected in the investigated micropillars for a QD perfectly matched to the CM equals 56 μeV [1]. The minimal coupling constant relevant in our case is related to the transition to the weak coupling regime. A simple estimation based on Eq. (1) for a typical cavity linewidth of 100 μeV gives $g_{\min} \approx \frac{\gamma_C}{4} \approx 25\ \mu$eV, which translates into a difference of almost 50% in the coupling constant. This brings us to the conclusion that the random spatial mismatch between the QD position and the antinode of the electromagnetic field distribution at the center of the cavity will most probably be the main source for scattering of the measured VRS in our set of experimental data points for a given temperature. Assuming that the QD distribution within the cavity is spatially homogeneous on the scale of the micropillar cross-section area, the distribution of the light-matter coupling constants g for a given temperature is therefore expected to be alike the electric field E radial distribution of the fundamental HE_{11} CM described by the Bessel function $J[0,r]$ [34] weighted with the probability of the QD being located at a certain distance from the micropillar center. In the ideal case of an isolated system without any kind of losses, this would also be reflected in a similar distribution of the VRS according to Eq. (1). However, as argued above, imperfect matching of the QD to the CM is not expected to lead to a systematic temperature dependence.

Besides temperature-independent changes of the VRS due to the different properties of the strong coupling cases with the same resonance temperature, the temperature itself influences the physics of a single QD-micropillar system in a way that affects the VRS. For example an increased temperature leads to stronger phonon effects, and it is well known that this implies a distinct decrease of the VRS with rising temperature, which is in sharp contrast to the previously described unsystematic temperature-independent scattering when looking at different strong coupling cases. On the other hand, the maximal VRS for a given temperature should certainly correspond to QDs that are spatially matched to the CM. As a result, looking at the envelope function of the experimental results, i.e., extracting the maximum VRS observed for each temperature, should allow us to extract the temperature-dependent behavior independently of the possible differences between the investigated QD-micropillar systems.

IV. EXPERIMENTAL RESULTS AND DISCUSSION

The proposed statistical approach has been utilized to experimentally study the influence of phonons on the vacuum Rabi splitting. A large and statistically significant number (89) of strong coupling cases from a single sample was experimentally studied by temperature tuning and the respective resonance temperatures were determined based on the energy vs temperature dependence [cf. Fig. 1(a)]. Each of the strong coupling cases was verified by the observation of the characteristic mode anticrossing in the energy dispersion as well as by crossing in the linewidth dependence on temperature [Fig. 1(b)], indicating an exchange in character between the CM and the X and the formation of polaritonic states on resonance. The results of the measurements are summed up in Fig. 2 where the extracted VRS is presented as a function of the resonance temperature. At first glance no clear tendency can be observed due to the scattering of the experimental data, which can be attributed predominantly to the varying QD positions

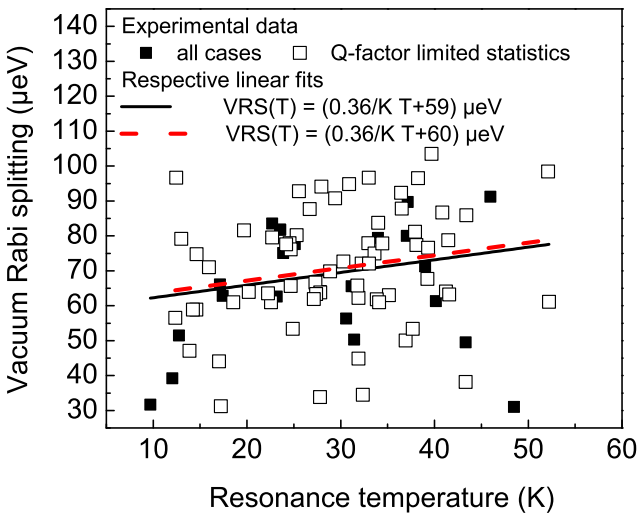

FIG. 2. (Color online) VRS as a function of the resonance temperature for all (89) measured strong QD-micropillar CM coupling cases (black squares) and for cases with Q-factors in the range of 11 000–15 000 (empty symbols) with respective linear fits—black solid line for full statistics and red dashed line for the Q-factor limited statistics. Each experimental data point represents a strong coupling case for a different QD-micropillar system.

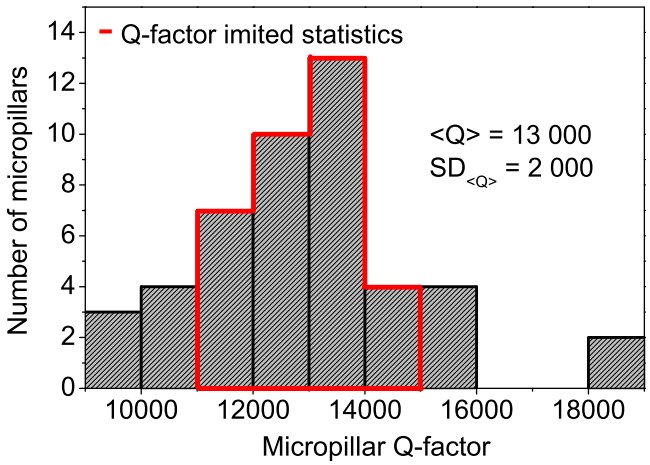

FIG. 3. (Color online) The histogram of Q-factors for investigated micropillar cavities with the range of Q-factors used in the post-selection process for Q-factor limited statistics marked in red.

with respect to the maximum of the mode field distribution in the systems under study. For the same reason, the envelope of the measured dependence is not well defined. The simplest least-squares linear fit to the experimental data (solid black line) exhibits a slope of $0.36\,\mu$eV/K, but a quantitative statistical analysis is needed to evaluate the significance of this tendency. We performed a standard analysis of variance using a statistical F-test to evaluate the *goodness* of the fit with the null hypothesis being that there is no tendency in the experimental data (which would be the case if the VRS is constant as a function of the temperature). This would mean that the slope of the linear fit is a result of random scattering of the experimental data. The *p value* calculated for the experimental data equals 0.049, which means that the probability that the null hypothesis is true is as low as 4.9%. While for strongly confined QDs one would expect a temperature-dependent decrease of the VRS due to the increasing phonon induced dephasing of the system, we find that for the large QDs studied here there is a 95.1% probability that the experimental data shows an increasing trend. To exclude possible variations of the VRS due to different cavity Q factors we employed a post-selection scheme and restricted the data to micropillars with Q factors within one standard deviation of 2 000 from the mean value of 13 000 (Fig. 3). Such a limited statistics is presented in Fig. 2 (empty symbols). The slope of the linear fit to the experimental data ($0.36\,\mu$eV/K) does not change in comparison to the full statistics (Fig. 2 red dashed line) and the probability that the trend is increasing is equal to 90.1%. This supports the hypothesis that there is an additional effect that counteracts the temperature-dependent phonon-induced decrease of the VRS, which was not observed in the case of strongly confined QDs.

Naturally the question arises what physical reason can lead to such an increase of the VRS as a function of temperature, counteracting the phonon influence. The differences between the QD-micropillars can only lead to a substantial scattering of the experimental data for a given temperature as was described in the previous section, but not to an experimentally observed distinct dependence. In particular, one cannot explain the increase of the VRS if all the relevant parameters influencing the splitting are scattering randomly for the different QD micropillars. Thus, to explain the experimentally observed positive trend, we either have to conclude that the commonly expected phonon-induced decrease of the VRS with temperature does not apply to our systems or one of the parameters exhibits a temperature dependence that we did not consider so far. The strength of the phonon coupling depends on the deformation potential constants and the extension of the wave function in the direction of the strongest confinement (the growth direction in our case)—for neither of these parameters has a temperature dependence been reported so far, nor is it expected. Moreover, Eq. (1) indicates that the VRS depends on the losses in the system and the light-matter coupling constant. The properties of the cavity are only slightly affected by the temperature. The length of the cavity changes due to thermal expansion and the refractive index of the cavity material is modified which slightly changes the resonance frequency of the cavity as can be seen in Fig. 1, but the cavity losses are not temperature dependent. On the other hand, the excitonic losses increase with temperature due to the activation of nonradiative recombination channels as well as increased pure dephasing due to acoustic phonons [35–39]. The increase of the X homogeneous linewidth translates into a decrease of the second term in Eq. (1) which can indeed result in the increase of the Rabi frequency with temperature. The strength of this effect can be estimated based on the measurements of the temperature-induced changes in the homogeneous linewidth performed for QDs in the same material system [35]. One has to keep in mind that the QDs in this reference paper are smaller than the investigated ones and stronger dephasing is expected for smaller QDs, which means that the estimated effect would be the absolute upper limit for our case. Bayer *et al.* reported an increase of the homogeneous linewidth from 2 up to $30\,\mu$eV at 60 K. Assuming a constant cavity linewidth of $100\,\mu$eV typical for our experiments, this would only lead to a change in the VRS below 2%, which is much weaker than the predicted phonon-induced renormalization. As far as the light-matter coupling constant is taken into account, we have to consider the oscillator strength of the X transition and the mode volume [Eq. (2)]. As discussed above, the mode volume is not altered significantly with temperature, but the oscillator strength which is determined by the overlap of the electron and hole wave functions as well as the wave function extension [40] might in principle be temperature dependent. In fact, a previous study on larger QDs in the same material system $In_{0.3}Ga_{0.7}As/GaAs$ proved that the wave function extension of the state from which the emission takes place can actually undergo changes [29] that can be attributed to a temperature-induced carrier redistribution within the closely spaced electronic sublevels related to possible confining potential fluctuations within large QDs. Similar effects have been observed in the case of quantum dashes [41] featuring an even larger nanostructure volume in the range of $4.5 \times 20{-}30 \times 100{-}150\,\mathrm{nm}^3$. The strength of this effect can be estimated based on available magneto-optical experimental data [29]. As the QDs in the above reference are larger than the ones investigated in this work, this estimation will constitute an upper limit of the expected changes. The lateral mean wave function extension $2\sqrt{\langle \rho_X^2 \rangle}$ can be experimentally

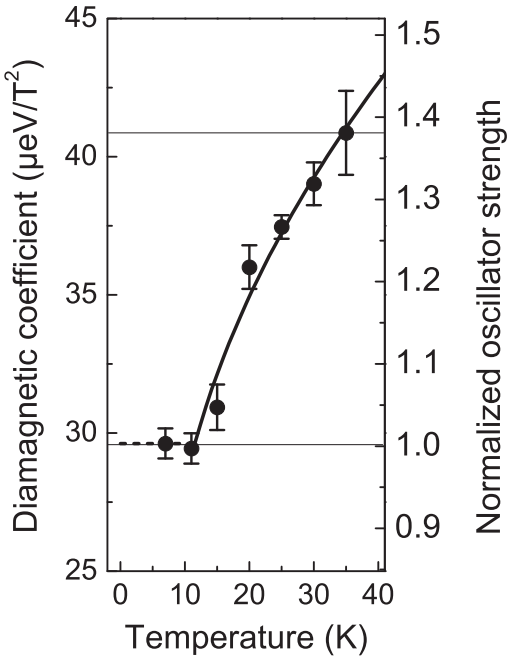

FIG. 4. Experimentally obtained temperature dependence of the diamagnetic coefficient (left axis) for a single $In_{0.3}Ga_{0.7}As$ QD (from Ref. [29]) and oscillator strength normalized to its low-temperature value (right axis) determined based on this measurements. The black line represents a square root fit to experimental data for $T > 11$ K and constant value for $T < 11$ K.

probed via the diamagnetic coefficient κ according to the relation

$$2\sqrt{\langle \rho_X^2 \rangle} = \frac{2\sqrt{8\mu\kappa}}{e}, \tag{3}$$

where μ is the reduced effective mass of the exciton and e is the elementary charge. This means that the temperature-induced change of the diamagnetic coefficient from (29.6 ± 0.6) to $(40.9 \pm 1.5)\,\mu\text{eV/T}^2$ (as shown in Fig. 4 for an exemplary single QD–QD1 from Ref. [29]) corresponds to a change of the lateral wave function extension from (15.7 ± 0.8) to (18.4 ± 2.2) nm. This increase of the wave function extension by a factor of 1.17 in the temperature range from 7 to 35 K (Fig. 4), translates into a similar increase of the light-matter coupling constant through its square root dependence on the oscillator strength [Eq. (2)]. In the case of an isolated system without losses ($\gamma_C = \gamma_X = 0$) also the VRS should increase by a factor of 1.17. This effect provides a possible qualitative explanation of the experimentally observed tendency of an increasing VRS as a function of temperature.

V. THEORETICAL RESULTS AND COMPARISON WITH THE EXPERIMENT

In this section the modeling of a strongly coupled QD-microcavity system is presented and the phonon influence on the coherent dynamics in terms of the VRS is discussed. The QD is modeled as an electronic two-level system consisting of the ground state and an X state, which are resonantly coupled to a single quantized CM making the details of the cavity design and absolute emission energy irrelevant. The Jaynes-Cummings type light-matter interaction preserves the excitation number of the system, which therefore can be restricted to the X state without cavity photons and the QD ground state with a single photon. However, because the Jaynes-Cummings model does not account for cavity losses it has to be extended accordingly, as will be explained further below. Furthermore, we include the coupling of the excitonic system to a continuum of longitudinal (bulk) acoustic phonons via the deformation potential, which is the dominant coupling mechanism in nonpolar materials without permanent dipole moments. We assume the QD confinement potential to be spherically symmetric and adjusted to the expected vertical dimension of the QDs in the sample, which is justified because this is the direction of the strongest confinement of the QD and is therefore responsible for the restriction of the phonon wavelengths, which can effectively couple to the electronic system. Furthermore, we assume electrons and holes being in the harmonic ground state implying Gaussian wave functions. Material specific effective mass differences are included and translate into a fixed ratio between the localization lengths of the electron and hole. Therefore, in this model the spatial extension of the electron wave function, which we refer to as the QD size, is the only parameter determining the strength of the X-phonon coupling besides material parameters, which are the same for all QDs in the sample such as the deformation potential constants, mass density, etc. More details of the described model are given in Ref. [12]. It should be noted that this kind of modeling has been proven to quite accurately describe the dynamics of self-assembled InGaAs/GaAs QDs observed experimentally [42–44]. To calculate the dynamics of this coupled system we use a previously developed real-time path-integral approach [12,20], which is especially suitable, because it allows for treating the carrier-phonon coupling in a numerically exact way. As we pointed out earlier, besides the coupling to phonons, also cavity losses have to be included in the model due to the different Q-factors of the micropillars. However, within the path-integral approach this is very challenging and might not be practical, because of the increased number of paths required when taking into account more states with different photon numbers. Instead, the cavity losses can be described within a hybrid approach proposed in [21] which uses the exact results of the microscopic model of phonon-induced pure dephasing described so far as input parameters for a phenomenological rate model describing the remaining loss channels (cavity losses and radiative decay) within the Lindblad formalism.

The results of our calculations for the phonon-induced renormalization of the VRS are presented in Fig. 5. It shows the temperature dependence of the VRS for two different values of the light-matter coupling constant of 56 μeV (the maximum value expected in the investigated QD-micropillar ensemble) and 25 μeV (the minimal coupling constant for which the strong coupling regime is maintained) and various QD sizes, respectively. These calculations have been performed without taking photon losses into account. The presented results show that the phonon coupling leads to a strong decrease (down to 50%) of the VRS in the experimentally accessible temperature range of 5–60 K. The decrease is linear for low temperatures (up to 20 K) and followed by sublinear behavior resulting

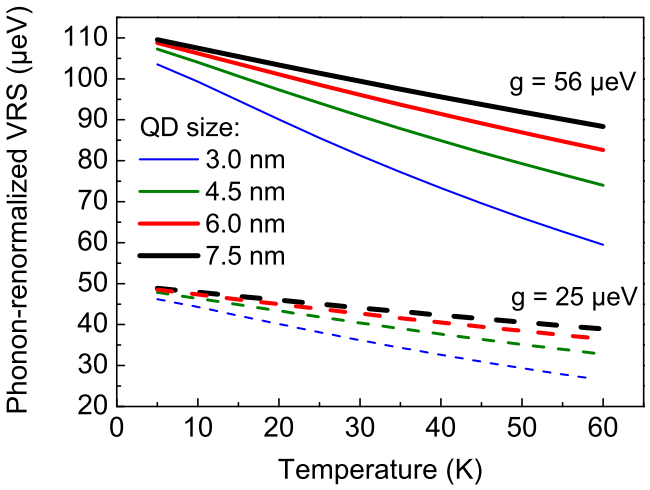

FIG. 5. (Color online) Calculated acoustic phonon-induced temperature dependence of the VRS for two light-matter coupling constants of 25 μeV (dashed lines) and 56 μeV (solid lines) as well as for various QD sizes: 3.0 nm (blue, the thinnest line), 4.5 nm (green), 6.0 nm (red), and 7.5 nm (black, the thickest line).

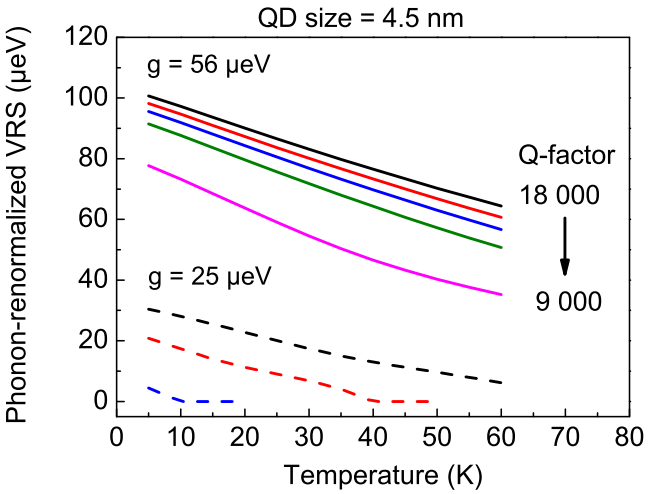

FIG. 6. (Color online) Calculated acoustic phonon-induced temperature dependence of the VRS of a 4.5 nm QD for two light-matter coupling constants of 25 μeV (dashed lines) and 56 μeV (solid lines) as well as for various cavity Q-factors in the experimentally relevant range from 9 000 to 18 000.

from the subsequent occupation of all phonon states that can effectively couple to the electronic system and an equalization of the probability for phonon emission- and absorption-assisted processes at elevated temperatures. The decrease is stronger for smaller QDs. The light-matter coupling constant slightly changes the slope of the observed dependences, but most importantly it changes the initial (low-temperature) value of the VRS by even more than a factor of 2. This is very important for the comparison with the experiment, because the phonon-free case is not accessible experimentally and the value of the light-matter coupling constant would have a striking effect on the observed dependence and as a result would be the most important source of scattering in the experimental data.

In the next step, another possible difference between individual QD-micropillars, namely the photonic losses described by means of the Q-factor, are included. In Fig. 6 the Q-factor is varied in the experimentally relevant range from 9 000 to 18 000 (Fig. 3) for two extreme values of the light-matter coupling constant (25 and 56 μeV). For large g, the Q-factor variation introduces a very slight change of the slope of the VRS dependence on temperature, which is more pronounced for larger Q factors. The Q factor also influences the initial value of the VRS and, in the extreme case, i.e., for Q $=$ 9 000, can change it by 25%, which is on a similar scale as the impact of a variation of the coupling constant g. Looking at the low g case, the decrease of the Q-factor can lead to a transition from the strong to the weak coupling regime when the losses overcome the coupling strength and the cavity is not able to store the photon for long enough (indicated by a VRS equal to 0 in Fig. 6).

All previous considerations predict a decreasing trend in the VRS dependence on temperature which cannot be clearly seen in the experimental results. However, modeling a possible temperature-induced redistribution of the carriers over several electronic sublevels related to confining potential fluctuations that might lead to higher OS, microscopically is clearly beyond the scope of this work. It cannot simply be included in the path-integral calculations as extending the involved electronic states beyond the two-level system is already very challenging and models with more than four levels have not been addressed so far. However, the effect can be addressed in the calculations in a phenomenological way by considering a temperature dependence of the light-matter coupling constant based on a fit to the experimental data shown in Fig. 4 taken from Ref. [29]. The OS and its dependence on temperature have a complex microscopic origin and cannot be described analytically. In the present case, the $f_{\mathrm{osc}}(T)$ dependence can be described phenomenologically to a good approximation by a square root dependence reproducing well the data in Fig. 4 above 10 K. The associated light-matter coupling constant is calculated according to Eq. (2) assuming that the light-matter coupling constant at low temperature $g(T = 7\,\mathrm{K}) = g_{\mathrm{max}} = 56\,\mu$eV, where g_{max} is the maximal achievable value estimated for investigated QD-micropillars. For temperatures exceeding 35 K (i.e., beyond the available experimental data) we estimated a lower and upper bound of the $f_{\mathrm{osc}}(T)$ dependence and extracted the relevant $g(T)$ to use it as an input for the calculations of the VRS vs temperature for the two extreme cases. As a lower limit, g is assumed to be constant and equal to the g value for 35 K. This estimation is based on the assumption that the light-matter coupling constant does not increase substantially for $T > 35\,\mathrm{K}$, which is supported by the expected saturation of $g(T)$ due to abovementioned QD size limit. An upper limit is obtained by extrapolating the square root fit to the $f_{\mathrm{osc}}(T)$ dependence in Fig. 4 (black solid line) beyond 35 K. In this way the increase of the OS with temperature is likely to be overestimated as the expected saturation is not accounted for because only experimental data points below saturation are extrapolated. The associated VRS calculated for a low temperature coupling constant equal to 56 μeV, a Q-factor of 13 000 and QD sizes of 4.5, 6.0, and 7.5 nm is presented

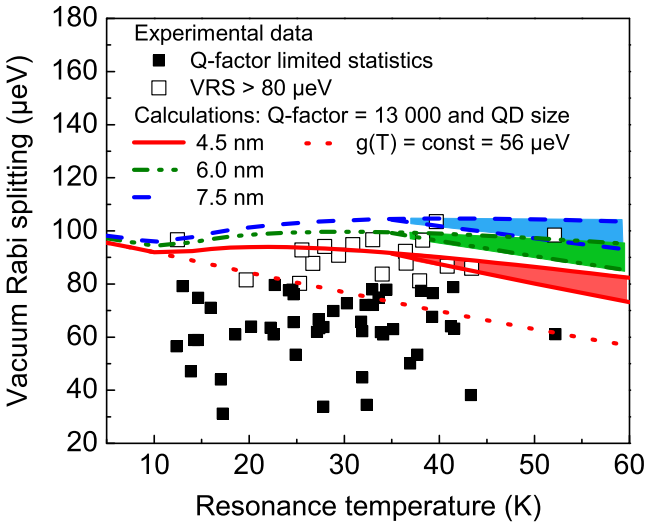

FIG. 7. (Color online) Comparison of the experimental dependence of the VRS on the resonance temperature (black squares, cases with VRS exceeding 80 μeV marked with empty symbols) with theoretical calculations of acoustic phonon-induced changes of the VRS for a cavity with Q-factor equal to 13 000 and QD size of 4.5 nm with (red solid line) and without (red dotted line) temperature dependence of the light-matter coupling constant included. For the case of a temperature-dependent coupling constant calculations for QD sizes of 6.0 nm (green dash-dotted line) and 7.0 nm (dashed blue line) are also presented. For each QD size a lower [assuming $g = g(T = 35\,\mathrm{K}) = \mathrm{const}$] and upper bound [$g(T)$ obtained by extrapolating the square root fit to the experimental $f_{\mathrm{osc}}(T)$ dependence in Fig. 4] of the temperature dependence of the VRS above 35 K is presented.

in Fig. 7. For comparison the red dotted line also shows the simulated temperature dependence of the VRS for a constant value of g for the 4.5-nm-sized QD as it is expected for typical strongly confined QDs. Indeed, in agreement with our experimental observations, the increase of the OS strength overcompensates the temperature-induced decrease of the VRS due to the phonon coupling, yielding a roughly constant value of the VRS. Although for higher temperatures the experimental temperature-dependent light-matter coupling strength is not available in the present experiment (Fig. 4), it is clear that at some point g will saturate and therefore for very high temperatures the VRS is expected to decrease due to the dominating phonon-induced dephasing. As shown in Fig. 7 the difference between the upper and lower bound of the VRS dependence on temperature for a given QD size is limited to 10% range only. When making a comparison between the calculations and the experimentally observed statistical ensemble data one has to keep in mind that the variations of the light-matter coupling strength that are due to the random positions of the QDs inside the micropillars are not included in the simulations and we therefore have to concentrate on the QDs that are positioned close to the center of the cavity where the coupling strength is maximal, as described previously. To this end we selected the strong coupling cases with a VRS exceeding 80 μeV, which is the minimal VRS that is estimated based on the mode volume and the OS when disregarding all loss channels and assuming perfect spectral and spatial matching of the QD to the cavity mode, and marked them with empty symbols in Fig. 7. For this subset of the experimental data the VRS is increasing with 55.5% probability. The reduction of the probability for an increasing trend is related to the strong scattering of the experimental data and the reduced number of data points which impairs the significance of the statistics. The envelope of the data points shows a behavior similar to the temperature dependence expected from the theory when the temperature dependence of the light-matter coupling constant is included in the calculations.

The underlying effect of the temperature-induced change of the state coupling most efficiently to the CM towards substates with larger wave function extension is an inherent property of large QDs and makes these systems very exceptional and attractive. Not only does it allow for the realization of the strong coupling regime on the single X–single photon level, but also forces back phonon-induced decoherence by compensating their detrimental influence. This effect has been experimentally observed in a solid state system and can pave the way for applications of strongly coupled systems at elevated temperatures.

VI. SUMMARY

We have studied, both theoretically and experimentally, the temperature dependence of the vacuum Rabi splitting. A statistical approach, enabled by the superb sample technology, has been utilized. It allowed for a temperature-dependent study on 89 strongly coupled QD-micropillars in a wide temperature range of (10–50) K. Our experimental results indicate an increase of the vacuum Rabi splitting with temperature. While for strongly confined QDs a decrease of the VRS with temperature due to the dephasing induced by acoustic phonons is expected, the large QDs studied here show a temperature-dependent light-matter coupling strength which seems to overcompensate the phonon effects in the intermediate temperature range. The strong influence of the wave function localization length in the growth direction, the light-matter coupling constant, and the cavity losses on the initial (low-temperature) value of the VRS as well as its renormalization have been addressed theoretically. The positive temperature coefficient of the VRS is an inherent and unique feature of large QDs, which has been proven to maintain the strong coupling in QD-micropillars up to temperatures as high as 50 K. This shows that complex electronic structures, like the large QDs discussed here, combining two-level system behavior with additional properties, can be very advantageous for cQED and possible applications in quantum information technology.

ACKNOWLEDGMENTS

The authors acknowledge financial support from Deutsche Forschungsgemeinschaft (DFG) via projects AX17/7-1 and RE2974/5-1. A.M. appreciates support from the Polish Ministry of Science and Higher Education within the "Mobilność Plus" programme. We thank M. Emmerling and A. Wolf for expert sample preparation.

[1] J. P. Reithmaier, G. Sęk, A. Löffler, C. Hofmann, S. Kuhn, S. Reitzenstein, L. V. Keldysh, V. D. Kulakovskii, T. L. Reinecke, and A. Forchel, Strong coupling in a single quantum dot-semiconductor microcavity system, Nature (London) **432**, 197 (2004).

[2] T. Yoshie, A. Scherer, J. Hendrickson, G. Khitrova, H. M. Gibbs, G. Rupper, C. Ell, O. B. Shchekin, and D. G. Deppe, Vacuum Rabi splitting with a single quantum dot in a photonic crystal nanocavity, Nature (London) **432**, 200 (2004).

[3] S. Haroche and J. Raimond, *Exploring the Quantum* (Oxford University Press, Oxford, 2006).

[4] J. I. Cirac, P. Zoller, H. J. Kimble, and H. Mabuchi, Quantum State Transfer and Entanglement Distribution among Distant Nodes in a Quantum Network, Phys. Rev. Lett. **78**, 3221 (1997).

[5] A. Imamoglu, D. D. Awschalom, G. Burkard, D. P. DiVincenzo, D. Loss, M. Sherwin, and A. Small, Quantum Information Processing Using Quantum Dot Spins and Cavity QED, Phys. Rev. Lett. **83**, 4204 (1999).

[6] M. A. Nielsen and I. L. Chuang, *Quantum Computation and Quantum Information* (Cambridge University Press, Cambridge, 2000).

[7] S. Reitzenstein, C. Hofmann, A. Gorbunov, M. Strauß, S. H. Kwon, C. Schneider, A. Löffler, S. Höfling, M. Kamp, and A. Forchel, AlAs/GaAs micropillar cavities with quality factors exceeding 150.000, Appl. Phys. Lett. **90**, 251109 (2007).

[8] K. Aoki, D. Guimard, M. Nishioka, M. Nomura, S. Iwamoto, and Y. Arakawa, Coupling of quantum-dot light emission with a three-dimensional photonic-crystal nanocavity, Nat. Photon. **2**, 688 (2008).

[9] I. Wilson-Rae and A. Imamoglu, Quantum dot cavity-QED in the presence of strong electron-phonon interactions, Phys. Rev. B **65**, 235311 (2002).

[10] F. Milde, A. Knorr, and S. Hughes, Role of electron-phonon scattering on the vacuum Rabi splitting of a single-quantum dot and a photonic crystal nanocavity, Phys. Rev. B **78**, 035330 (2008).

[11] G. Tarel and V. Savona, Emission spectrum of a quantum dot embedded in a nanocavity, Phys. Status Solidi C **6**, 902 (2009).

[12] M.Glässl, L. Sörgel, A. Vagov, M. D. Croitoru, T. Kuhn, and V. M. Axt, Interaction of a quantum-dot cavity system with acoustic phonons: Stronger light-matter coupling can reduce the visibility of strong coupling effects, Phys. Rev. B **86**, 035319 (2012).

[13] D. P. S. McCutcheon and A. Nazir, Model of the Optical Emission of a Driven Semiconductor Quantum Dot: Phonon-Enhanced Coherent Scattering and Off-Resonant Sideband Narrowing, Phys. Rev. Lett. **110**, 217401 (2013).

[14] P. Kaer and J. Mørk, Decoherence in semiconductor cavity QED systems due to phonon couplings, Phys. Rev. B **90**, 035312 (2014).

[15] C. Roy and S. Hughes, Phonon-Dressed Mollow Triplet in the Regime of Cavity Quantum Electrodynamics: Excitation-Induced Dephasing and Nonperturbative Cavity Feeding Effects, Phys. Rev. Lett. **106**, 247403 (2011).

[16] Z. Harsij, M. Bagheri Harouni, R. Roknizadeh, and M. H. Naderi, Influence of electron-phonon interaction on the optical spectrum and quantum statistics in a quantum-dot–cavity system: Master-equation approach, Phys. Rev. A **86**, 063803 (2012).

[17] Y. Ota, S. Iwamoto, N. Kumagai, and Y. Arakawa, Impact of electron-phonon interactions on quantum-dot cavity quantum electrodynamics, arXiv:0908.0788.

[18] K. Müller, K. A. Fischer, A. Rundquist, C. Dory, K. G. Lagoudakis, T. Sarmiento, Y. A. Kelaita, V. Borish, and J. Vučković, Ultrafast Polariton-Phonon Dynamics of Strongly Coupled Quantum Dot-Nanocavity Systems, Phys. Rev. X **5**, 031006 (2015).

[19] Y.-J. Wei, Y. He, Y.-M. He, C.-Y. Lu, J.-W. Pan, C. Schneider, M. Kamp, S. Höfling, D. P. S. McCutcheon, and A. Nazir, Temperature-Dependent Mollow Triplet Spectra from a Single Quantum Dot: Rabi Frequency Renormalization and Sideband Linewidth Insensitivity, Phys. Rev. Lett. **113**, 097401 (2014).

[20] A. Vagov, M. D. Croitoru, M. Gläßl, V. M. Axt, and T. Kuhn, Real-time path integrals for quantum dots: Quantum dissipative dynamics with superohmic environment coupling, Phys. Rev. B **83**, 094303 (2011).

[21] A. Vagov, M. Gläßl, M. D. Croitoru, V. M. Axt, and T. Kuhn, Competition between pure dephasing and photon losses in the dynamics of a dot-cavity system, Phys. Rev. B **90**, 075309 (2014).

[22] S. Reitzenstein, S. Münch, P. Franeck, A. Rahimi-Iman, A. Löffler, S. Höfling, L. Worschech, and A. Forchel, Control of the Strong Light-Matter Interaction between an Elongated $In_{0.3}Ga_{0.7}As$ Quantum Dot and a Micropillar Cavity Using External Magnetic Fields, Phys. Rev. Lett. **103**, 127401 (2009).

[23] D. Press, S. Götzinger, S. Reitzenstein, C. Hofmann, A. Löffler, M. Kamp, A. Forchel, and Y. Yamamoto, Photon Antibunching from a Single Quantum-Dot-Microcavity System in the Strong Coupling Regime, Phys. Rev. Lett. **98**, 117402 (2007).

[24] J. Kasprzak, S. Reitzenstein, E. A. Muljarov, C. Kistner, C. Schneider, M. Strauss, S. Höfling, A. Forchel, and W. Langbein, Up on the Jaynes-Cummings ladder of a quantum-dot/microcavity system, Nat. Mater. **9**, 304 (2010).

[25] F. Albert, K. Sivalertporn, J. Kasprzak, M. Strauß, C. Schneider, S. Höfling, M. Kamp, A. Forchel, S. Reitzenstein, E.A. Muljarov, and W. Langbein, Microcavity controlled coupling of excitonic qubits, Nat. Commun. **4**, 1747 (2013).

[26] A. Löffler, J. P. Reithmaier, A. Forchel, A. Sauerwald, D. Peskes, T. Kümmell, and G. Bacher, Influence of the strain on the formation of GaInAs/GaAs quantum structures, J. Cryst. Growth **286**, 6 (2006).

[27] M. Syperek, M. Baranowski, G. Sęk, J. Misiewicz, A. Löffler, S. Höfling, S. Reitzenstein, M. Kamp, and A. Forchel, Impact of wetting-layer density of states on the carrier relaxation process in low indium content self-assembled (In,Ga)As/GaAs quantum dots, Phys. Rev. B **87**, 125305 (2013).

[28] L. C. Andreani, G. Panzarini, and J.-M. Gérard, Strong-coupling regime for quantum boxes in pillar microcavities: Theory, Phys. Rev. B **60**, 13276 (1999).

[29] A. Musiał, P. Gold, J. Andrzejewski, A. Löffler, J. Misiewicz, S. Höfling, A. Forchel, M. Kamp, G. Sęk, and S. Reitzenstein, Toward weak confinement regime in epitaxial nanostructures: Interdependence of spatial character of quantum confinement and wave function extension in large and elongated quantum dots, Phys. Rev. B **90**, 045430 (2014).

[30] B. Krummheuer, V. M. Axt, and T. Kuhn, Theory of pure dephasing and the resulting absorption line shape in semiconductor quantum dots, Phys. Rev. B **65**, 195313 (2002).

[31] A. Grodecka, L. Jacak, P. Machnikowski, and K. Roszak, *Quantum Dots: Research Developments*, edited by P. A. Ling (Nova Science, New York, 2005), p. 47.
[32] S. Reitzenstein, C. Böckler, A. Löffler, S. Höfling, L. Worschech, A. Forchel, P. Yao, and S. Hughes, Polarization-dependent strong coupling in elliptical high-Q micropillar cavities, Phys. Rev. B **82**, 235313 (2010).
[33] S. Ohno, S. Adachi, R. Kaji, S. Muto and H. Sasakura, Optical anisotropy and photoluminescence polarization in single InAlAs quantum dots, Appl. Phys. Lett. **98**, 161912 (2011).
[34] S. Reitzenstein and A. Forchel, Quantum dot micropillars, J. Phys. D: Appl. Phys. **43**, 033001 (2010).
[35] M. Bayer and A. Forchel, Temperature dependence of the exciton homogeneous linewidth in $In_{0.60}Ga_{0.40}As/GaAs$ self-assembled quantum dots, Phys. Rev. B **65**, 041308(R) (2002).
[36] L. Besombes, K. Kheng, L. Marsal, and H. Mariette, Acoustic phonon broadening mechanism in single quantum dot emission, Phys. Rev. B **63**, 155307 (2001).
[37] P. Borri, W. Langbein, U. Woggon, V. Stavarache, D. Reuter, and A. D. Wieck, Exciton dephasing via phonon interactions in InAs quantum dots: Dependence on quantum confinement, Phys. Rev. B **71**, 115328 (2005).
[38] E. Peter, P. Senellart, D. Martrou, A. Lemaitre, J. Hours, J. M. Gerard, and J. Bloch, Exciton-Photon Strong-Coupling Regime for a Single Quantum Dot Embedded in a Microcavity, Phys. Rev. Lett. **95**, 067401 (2005).
[39] P. Borri, W. Langbein, S. Schneider, U. Woggon, R. L. Sellin, D. Ouyang, and D. Bimberg, Ultralong Dephasing Time in InGaAs Quantum Dots, Phys. Rev. Lett. **87**, 157401 (2001).
[40] F. Rossi and T. Kuhn, Theory of ultrafast phenomena in photoexcited semiconductors, Rev. Mod. Phys. **74**, 895 (2002).
[41] A. Musiał, P. Kaczmarkiewicz, G. Sęk, P. Podemski, P. Machnikowski, J. Misiewicz, S. Hein, S. Höfling, and A. Forchel, Carrier trapping and luminescence polarization in quantum dashes, Phys. Rev. B **85**, 035314 (2012).
[42] A. Vagov, V. M. Axt, T. Kuhn, W. Langbein, P. Borri, and U. Woggon, Nonmonotonous temperature dependence of the initial decoherence in quantum dots, Phys. Rev. B **70**, 201305(R) (2004).
[43] J. H. Quilter, A. J. Brash, F. Liu, M. Glässl, A. M. Barth, V. M. Axt, A. J. Ramsay, M. S. Skolnick, and A. M. Fox, Phonon-Assisted Population Inversion of a Single InGaAs/GaAs Quantum Dot by Pulsed Laser Excitation, Phys. Rev. Lett. **114**, 137401 (2015).
[44] S. Bounouar, M. Müller, A. M. Barth, M. Glässl, V. M. Axt, and P. Michler, Phonon-assisted robust and deterministic two-photon biexciton preparation in a quantum dot, Phys. Rev. B **91**, 161302(R) (2015).